SYNTHESIS AND CHARACTERIZATION OF NOVEL ORGANIC MATERIALS FOR OPTOELECTRONIC DEVICES

JANEEYA KHUNCHALEE

A THESIS SUBMITTED IN PARTIAL FULFILLMENT OF THE REQUIREMENTS FOR THE DEGREE OF DOCTOR OF PHILOSOPHY

MAJOR IN CHEMISTRY

FACULTY OF SCIENCE

UBON RATCHATHANI UNIVERSITY

YEAR 2012

THESIS APPROVAL

UBON RATCHATHANI UNIVERSITY

DOCTOR OF PHILOSOPHY

MAJOR IN CHEMISTRY FACULTY OF SCIENCE

TITLE SYNTHESIS AND CHARACTERIZATION OF NOVEL ORGANIC MATERIALS FOR OPTOELECTRONIC DEVICES

NAME MS.JANEEYA KHUNCHALEE

THIS THESIS HAS BEEN ACCEPTED BY

..... CHAIR

(ASSOC.PROF.DR.VINICH PROMARAK)

..... COMMITTEE

(ASST.PROF.DR.CHANOKPORN PHAOSIRI)

..... COMMITTEE

(DR.TAWEESAK SUDYOADSUK)

..... COMMITTEE

(DR.TINNAGON KAEWIN)

..... DEAN

(ASST.PROF.DR.JANPEN INTARAPRASERT)

APPROVAL BY UBON RATCHATHANI UNIVERSITY

.....

(ASST.PROF.DR.UTITH INPRASIT)

VICE PRESIDENT FOR ACADEMIC AFFAIRS

FOR THE PRESIDENT OF UBON RATCHATHANI UNIVERSITY

ACADEMIC YEAR 2012

ACKNOWLEDGMENTS

I wish to express my admiration and appreciation to Assoc.Prof.Dr.Vinich Promarak, my advisor, for his excellent suggestions, supervision, and understanding throughout my study.

I would also like to thank the many people who contributed their time, instrumentation, and advice to my project. In particular, Dr.Tinnagon Keawin for NMR experiments, Dr.Taweesak Sudyoadsuk for optoelectronic devices, Asst.Prof.Dr.Siriporn Jungsuttiwong for molecular orbital calculation, Asst.Prof.Dr.Sayant Saengsuwan for TGA and DSC data. Moreover, I would like to thank Ubon Ratchathani Rajabhat University for IR spectroscopy.

I wish to acknowledge Asst.Prof.Dr.Chanokporn Phaosiri for constructive comments and suggestion.

Thanks so much to the Center of excellence for Innovation in Chemistry (PERCH-CIC) and Ubon Ratchathani University for financial support. Gratitude is expressed to all my teachers for showing me a different line in life, as a Chemistry graduate student. My sincere thankful is also express to the Department of Chemistry and Excellent Center for Innovation in Chemistry, Faculty of Science, Ubon Ratchathani University for providing a wonderful academic environment during the course work.

My appreciation is extended to all the staff of the Department of Chemistry. Furthermore, I feel thankful to my friends, sisters, brothers here in Center for Organic Electronics and Polymers.

Most of all, I feel appreciate and grateful to my beloved family for their inculcation and encouragement that found me to be a fortitude person.

(Miss Janeeya Khunchalee)

Reseacher

บทคัดย่อ

ชื่อเรื่อง : การสังเคราะห์และพิสูจน์เอกลักษณ์ของสารอินทรีย์ชนิดใหม่สำหรับใช้ในอุปกรณ์ออปโตอิเล็กทรอนิก

โดย : จาณียา ขันชะลี

ชื่อปริญญา : วิทยาศาสตรดุษฎีบัณฑิต

สาขาวิชา : เคมี

ประธานกรรมการที่ปรึกษา : รองศาสตราจารย์ ดร.วินิช พรมอารักษ์

ศัพท์สำคัญ : หมู่ให้ หมู่รับ ไพ-คอนจูเกต เซลล์แสงอาทิตย์ชนิดสีย้อมไวแสง ไดโอดเรืองแสงสารอินทรีย์

ในงานวิจัยนี้รายงานการสังเคราะห์และพิสูจน์เอกลักษณ์ของสารอินทรีย์ที่ประกอบด้วยไพ-คอนจูเกตชนิดใหม่สำหรับใช้ในอุปกรณ์ออปโตอิเล็กทรอนิกส์ โดยมีหมู่คาร์บาโซลทำหน้าที่เป็นหมู่ให้อิเล็กตรอน หมู่ฟลูออรีน โอลิโกไทโอฟีนทำหน้าที่เป็นไพ-คอนจูเกต อนุกรมชนิดใหม่ที่ประกอบด้วยหมู่ปิดท้ายคือ คาร์บาโซล ฟูออรีน โอลิโกไทโอฟีนที่มีไทโอฟีน หนึ่ง สอง สาม และสี่วง สังเคราะห์ด้วยปฏิกิริยาซูซูกิ คับปลิง วัดการเรืองแสงของโมเลกุลเป้าหมาย พบว่าเรืองแสงในช่วงสีน้ำเงิน-สีส้ม ประสิทธิภาพการเรืองแสงของ **CFTnP** (n = 0-4) อยู่ในช่วง 0.840 ถึง 0.078 และลดลงเมื่อคอนจูเกชันในโมเลกุลเพิ่มขึ้น **CFT3P** เรืองแสงในอุปกรณ์อิเล็กทรอนิกดีที่สุดคือ 31,760 cd/m^2 ที่ศักย์ไฟฟ้า 9.8 V. อนุกรมชนิดใหม่ที่ประกอบด้วยหมู่ปิดท้ายคือ คาร์บาโซล ฟูออรีน โอลิโกไทโอฟีนที่มีไทโอฟีน ศูนย์ สอง สี่ หก และแปดวงสังเคราะห์ด้วยปฏิกิริยาสทิลลี วัดการเรืองแสงของโมเลกุลเป้าหมาย พบว่า เรืองแสงในช่วงสีน้ำเงิน-สีส้ม ประสิทธิภาพการเรืองแสงของ **BCFnT** (n = 0, 2, 4, 6, 8) อยู่ในช่วง 0.158 ถึง 0.023 และลดลงเมื่อคอนจูเกชันในโมเลกุลเพิ่มขึ้น สารอินทรีย์ที่ประกอบด้วยหมู่ให้ (D) หมู่รับอิเล็กตรอน (A) และไพ-คอนจูเกชัน (π) โดยมีคาร์บาโซลที่เป็นหมู่ให้อิเล็กตรอน หมู่ฟูออรีน โอลิโกไทโอฟีนทำหน้าที่เป็นไพ-คอนจูเกตและมีหมู่รับอิเล็กตรอนที่แตกต่างกัน โดยเมื่อใช้หมู่ไซยาโนอะคริลิกแอซิด และอะคริลิก แอซิด ทำหน้าที่เป็นหมู่รับอิเล็กตรอนและหมู่ยึดเกาะสำหรับใช้ในอุปกรณ์เซลล์แสงอาทิตย์ชนิดสีย้อมไวแสง (DSCs) โมเลกุลเป้าหมายที่สังเคราะห์ได้พิสูจน์เอกลักษณ์โดยใช้เทคนิค ^{1}H-NMR, ^{13}C-NMR และ FT-IR ทำการวัดการดูดกลืนแสงด้วยเทคนิคยูวีและวิสิเบิลสเปคโตรสโกปี พบว่าโมเลกุลสารเป้าหมายมีการดูดกลืนแสงในช่วงความยาวคลื่นแสงของยูวีและวิสิเบิล โมเลกุลเป้าหมายทุกตัว พบว่า มีพีคการ

ดูดกลืนแสงเลื่อนไปในทางที่ความยาวคลื่นที่มากขึ้นเมื่อจำนวนไทโอฟีนเพิ่มขึ้น เมื่อทำการทดสอบคุณสมบัติทางความร้อนและทางเคมีไฟฟ้าพบว่า โมเลกุลสารเป้าหมายทุกตัวมีความเสถียรทางความร้อนและทางไฟฟ้าเคมี สำหรับการคำนวณทางทฤษฎีฟังก์ชันความหนาแน่น (DFT) จะมีผลต่อโมเลกุลสีย้อมไวแสง และได้ผลที่แสดงการกระจายอิเล็กตรอนของโมเลกุลสีย้อมไวแสงไปยังหมู่ยึดเกาะที่เกิดขึ้นระหว่างการกระตุ้น HOMO-LUMO โดยหมู่รับอิเล็กตรอนมีความเป็นระนาบกับไทโอฟีน เมื่อนำโมเลกุลสารเป้าหมายมาขึ้นรูปเป็นอุปกรณ์ DSCs พบว่าอุปกรณ์ DSCs ที่ใช้โมเลกุลสีย้อมไวแสง **CA2T** จะให้ค่าประสิทธิภาพการแปลงพลังงานแสงเป็นพลังงานไฟฟ้า (η) ดีที่สุดเท่ากับร้อยละ 3.13 ภายใต้สภาวะมาตรฐานความเข้มแสง 80 mW/cm^2 AM 1.5 G โดยมีค่า V_{oc} = 0.65 V, J_{sc} = 6.70 mA/cm^2 และ ff = 0.72 ภายใต้สภาวะเดียวกันกับโมเลกุลสีย้อมไวแสง **N719** ที่มี η เท่ากับร้อยละ 4.24 โดยมีค่า V_{oc} = 0.67 V, J_{sc} = 9.44 mA/cm^2 และ ff = 0.67 และเมื่อเปลี่ยนหมู่รับอิเล็กตรอนเป็นหมู่มาโลโนไนไตรล์ เมทธิลไซยาโนอะคริเลต หรือเมทธิลีนอินดีน-1,3-ไดโอน เพื่อเพิ่มไพ-คอนจูเกตให้กับโมเลกุลของสารเรืองแสงสำหรับใช้ในอุปกรณ์ไดโอดเรืองแสงการอินทรีย์ (OLEDs) เมื่อทำการศึกษาทางการเรืองแสงของสารเป้าหมายพบว่ามีการเรืองแสงใน ช่วงสีส้มถึงม่วงเข้ม เมื่อทำการศึกษาคุณสมบัติทางความร้อนและทางเคมีไฟฟ้าพบว่าโมเลกุลสารเป้าหมายมีความเสถียรทางความร้อนและทางไฟฟ้าเคมี จึงคาดว่าโมเลกุลเหล่านี้จะสามารถนำไปใช้เป็นสารเรืองแสงในอุปกรณ์ OLEDs ได้อย่างมีประสิทธิภาพ อนุกรมของสารอินทรีย์ที่มีสองขั้วประกอบด้วยหมู่ให้อิเล็กตรอน (D) หมู่เชื่อม (B) และหมู่รับอิเล็กตรอน (A) เป็นโมเลกุล D-B-A ถูกสังเคราะห์ขึ้น โมเลกุลประกอบด้วยหมู่เชื่อมเป็นเอริลลีน เช่น ฟีนิลลีนหรือ ไทโอนิลลีน มีหมู่ให้อิเล็กตรอนเป็นไดฟีนิลเอมีน หมู่รับอิเล็กตรอนเป็นไซยาโนอะคริลิก แอซิด ซึ่งทำหน้าที่เป็นหมู่ยึดเกาะบนผิวของ TiO_2 โมเลกุลเป้าหมายที่ศึกษาเรืองแสงในช่วงสีส้ม การศึกษาในด้านประสิทธิภาพของอุปกรณ์เซลล์แสงอาทิตย์ชนิดสีย้อมไวแสงโดยมีสารที่สังเคราะห์ทำหน้าที่เป็นสีย้อมไวแสงจะมีการศึกษาต่อไปในอนาคต

ABSTRACT

TITLE : SYNTHESIS AND CHARACTERIZATION OF NOVEL ORGANIC MATERIALS FOR OPTOELECTRONIC DEVICES

BY : JANEEYA KHUNCHALEE

DEGREE : DOCTOR OF PHILOSOPHY

MAJOR : CHEMISTRY

CHAIR : ASSOC.PROF.DR.VINICH PROMARAK, D. PHIL.

KEYWORDS : DONOR / ACCEPTOR / π-CONJUGATE / DYE SOLAR CELLS / ORGANIC LIGHT-EMITTING DIODES

This thesis deals with synthesis and characterization of π-conjugated organic materials for using as emitters and dye molecules in optoelectronic devices. π-Conjugated organic materials consist of a carbazole moiety as an electron donor, fluorene-oligothiophene moiety as a conjugated linker. A series of novel carbazole end-caped fluorene-oligothiophenes **CFTnP** (n = 0-4) with one, two, three and four thiophene rings were synthesized using Suzuki coupling reaction. Fluorescence spectra of the target molecules excited at λ_{max} of each molecule show emission peak at blue to orange region. The fluorescence quantum yields (Φ_F) of these fluorescence oligomers range from 0.840 to 0.078 and decrease as the conjugation in molecule increase. The maximum luminance of the organic light emitting diode device using **CFT3P** as emissive layer was about 31,760 cd/m^2 at an operating voltage of 9.8 V with a turn on voltage of 3 V. Novel carbazole end-caped fluorene-oligothiophenes **BCFnT** (n = 0, 2, 4, 6, 8) with zero, two, four, six and eight thiophene ring were synthesized using Stille coupling reaction. Fluorescence spectra of the target molecules excited at λ_{max} of each molecule show emission peak at blue to orange region. The fluorescence quantum yields (Φ_F) of these fluorescence oligomers range from 0.158 to 0.023 and decrease as the conjugation in molecule increase. Novel donor π-conjugated acceptor (D-π-A) organic materials for using as dye molecules in optoelectronic devices were synthesized and characterized. This D-π-A organic materials consist of a carbazole moiety as an electron donor (D), fluorene-thiophene moiety as a conjugated linker (π) and different electron acceptors (A). Cyanoacrylic acid

and acrylic acid groups were applied as the electron-withdrawing part and anchoring groups for the application in dye solar cells (DSCs). The target molecules were characterized by ^{1}H-NMR and ^{13}C-NMR spectroscopy, Mass spectrometry and FT-IR spectroscopy techniques. The target molecules exhibited an adsorption band cover UV and visible region. The absorption maximums of all target molecules were more or less red-shifted with an increase in the number of thiophene units. All compounds show high thermal stability and good electrochemical property. DFT calculations have been performed on these dyes. The results show that electron transfer from the donor part of molecules to the anchoring moieties *via* the π-conjugated bridge occurs during the HOMO-LUMO excitation. The electron-withdrawing groups are coplanar with respect to the thiophene units. A maximum η value of 3.13% is achieved under simulated AM 1.5 irradiation (80 mW/cm^2) with a DSCs based on **CA2T** dye (V_{oc} = 0.65 V, J_{sc} = 6.70 mA/cm^2, ff = 0.72). Under the same conditions, the η value of a DSCs based on N719 dye is 4.24% (V_{oc} = 0.67 V, J_{sc} = 9.44 mA/cm^2, ff = 0.67). By applying the electron-withdrawing parts of methylenemalononitrile, methylcyanoacrylate and methyleneindene-1,3-dione as acceptor groups provide the D-π-A type luminescent organic materials for the application in organic light-emitting diodes (OLEDs). All compounds in this study are fluorescent with the color ranging from orange to violet. All targets have good thermal and electrochemical stabilities and could be used as emissive layers in OLEDs. The performance of OLEDs using these materials as light-emitting layer is under investigation and will be reported in the future. A series of organic dipolar compounds containing a donor (D), a bridge (B), and an acceptor (A), forming a D–B–A type of dyads, were synthesized. The central bridges were made of molecule connected arylene groups, i.e., phenylenes or thiophenylenes. The donor group was a diphenylamine group. The acceptor group was a cyanoacrylic acid, which can be anchored onto the surface of TiO_2. The target molecules in this study are fluorescent with the color orange region. The performance of DSCs using these materials as dyes is under investigation and will be reported in the future.

CONTENTS

CONTENTS (CONTINUED)

CONTENTS (CONTINUED)

LIST OF TABLES

LIST OF TABLES

LIST OF FIGURES

LIST OF FIGURES (CONTINUED)

LIST OF FIGURES (CONTINUED)

LIST OF FIGURES (CONTINUED)

LIST OF FIGURES (CONTINUED)

LIST OF FIGURES (CONTINUED)

LIST OF FIGURES (CONTINUED)

LIST OF FIGURES (CONTINUED)

LIST OF FIGURES (CONTINUED)

LIST OF ABBREVIATIONS

ABBREVIATION	FULL WORD
CH_2Cl_2	Dichloromethane
THF	Tetrahydrofuran
DMSO	Dimethylsulphoxide
RT	Room temperature
d	Doublet
dd	Doublet of doublets
td	Triplet of doublets
ε	Molar absorption
eV	Electron volt
h	Hour/hours
HOMO	Highest occupied molecular orbital
LUMO	Lowest unoccupied molecular orbital
IPCE	Incident photon to current efficiency
η	Overall light-to-electric power conversion efficiency
ITO	Indium-tin oxide
FT-IR	Fourier transform Infrared
J	Coupling constant
M	Molar concentration
MHz	Megahertz
min	Minutes
μA	Microamperes
μm	Micrometers
mol	Moles
mmol	Milimoles
m	Unresolved multiple
N	Normal concentration
nm	Nanometers

LIST OF ABBREVIATIONS (CONTINUED)

ABBREVIATION	FULL WORD
NMR	Nuclear magnetic resonance
δ	Chemical shift in ppm relative to tetramethylsilane
ppm	Parts per million
s	Singlet
t	Triplet
TLC	Thin-layer chromatography
UV	Ultra-violet
n-Bu_4NPF_6	Tetrabutylammonium hexafluorophosphate
TD-DFT	Time-dependent density functional theory
GBL	Gamma-butyrolactone
NMP	*N*-methyl-2-pyrrolidone
S^+	Excited dye
S^o	Original state
AM 1.5	Air Mass 1.5
K	Kilo
W	Watt
V	Voltage (V)
s	second
I	Current (ampere)
V_{oc}	Open circuit voltage
J_{sc}	Short circuit current
ff	Fill factor
J-V	Current density-voltage

CHAPTER 1

INTRODUCTION

1.1 Organic electronics

For a long time it was a matter of fact that polymer and low molar mass organic materials do not conduct electricity. Therefore these materials were used as insulators in the electronic industry. This point of view changed in 1977 when Alan J. Heeger, Alan G. MacDiarmid and Hideki Shirakawa found that the conductivity of the poly(acetylene) can be increased by eleven orders of the magnitude when it is doped with halogen [1, 2]. For the discovery and development of conductive polymers they received the Nobel Prize for Chemistry in 2000 [3, 4]. Since then the possibility of using organic semiconducting materials for applications in opto-electronics and the semiconductor industry has been of great scientific and technological interest [5-7]. Easy processability, i.e. form solution, large area coverage and the possibility to use flexible substrates make organic semiconductors ideal candidates for low cost electronic applications. During the last 15 years rapid progress took place in the field of materials developments, device design, deposition processes and molecular modeling [8]. In the area of organic thin film devices vary active research is going on spanning many subjects such as organic light emitting diode (OLEDs) [9], organic field-effect transistors (OFETs) [10], sensors [11] and organic photovoltaic [12].

1.2 Organic light emitting diodes (OLEDs)

1.2.1 Electroluminescence

The emission of electromagnetic radiation in the UV, visible and infrared region is called luminescence. The different kinds of luminescence can be distinguished by different ways of excitation. If a material is excited optically, an electron form the highest occupied molecular orbital (HOMO, S_0) is excited to the lowest unoccupied molecular orbital (LUMO, S_1). The excited electron rapidly relaxes to the vibrational ground state. Under emission of light the excited electron returns to the S_0 state again. Due to an energy loss in the excited state,

the wavelength of the emitted light is longer than the absorption wavelength. The principle of photoluminescence (PL) is shown in the Jablonski diagram (Figure 1.1).

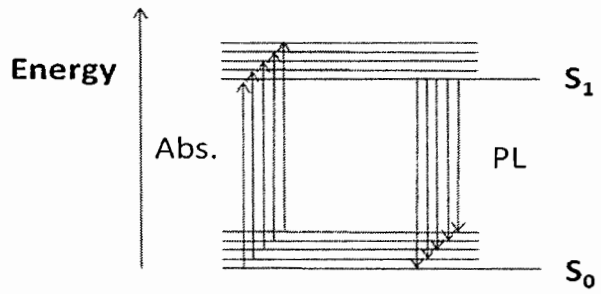

Figure 1.1 Term scheme of optical excitation and photoluminescence (Jablonski diagram).

Applying a voltage to an organic semiconducting material is another possibility to obtain luminescence. This kind of light generation is called electroluminescence (EL) and was discovered by Pope [13] and Helfrich et al. [14]. An emission of blue light was observed by applying voltages around 400 V to an anthracene single crystal. Since Tang and van Slyke found electroluminacence from a thin, evaporated two layer OLED consisting of tris(8-hydroxyquinoline)aluminium (AlQ_3) and an aromatic amine in 1978. At that time Tang et al. used a stable Mg/Al alloy as cathode and reached a brightness of 1000 Cd/m^2 at low operating voltages of about 10 V.

1.2.2 Principle of OLEDs

A single layer device architecture is the simplest OLED structure. In this case the organic emitter is deposited between two metal electrodes. In a single layer setup the organic semiconductor acts as emitter and charge transport material (holes and electrons) at the same time. As material for the anode indium-tinoxide (ITO) is used in most cases. A thin, semitransparent ITO layer is sputtered onto a glass substrate. Afterwards, the emitting layer is deposited either by liquid phase or evaporation techniques onto the ITO anode. Finally, an electropositive metal like Al, Ca and Mg is evaporated on top of the OLED substrate as cathode. A suitable cathode material has a low work function in order to ensure efficient electron injection into the organic semiconductor. A typical single layer OLED setup is shown in Figure 1.2.

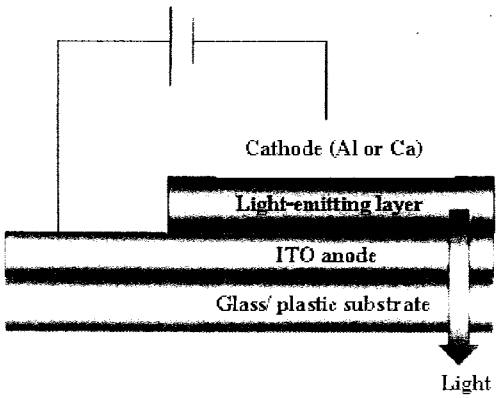

Figure 1.2 Schematic of a single layer OLED setup.

If a voltage is applied to the electrodes of an OLED device as depicted in Figure 1.3, electrons from the cathode and holes form the anode are injected into the organic semiconductor. Due to the electric field between the two electrodes, the positive and negative charge carriers move through the organic layer. As soon as they recombine in the emitting material, light is generated. The energy level diagram of a single layer OLED is shown in Figure 1.3.

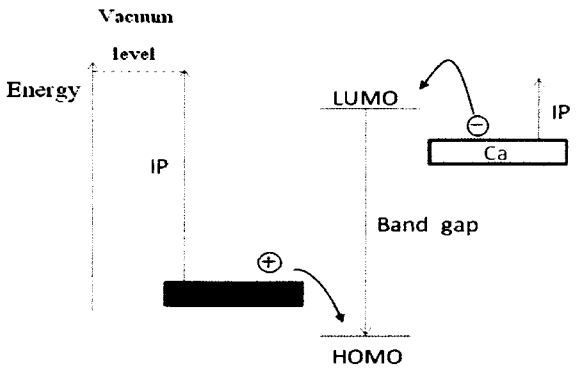

Figure 1.3 Energy level diagram of a single layer OLED device architecture.

The efficiency of an OLED is determined by the number of charge carries that are injected and the number of holes and electrons that actually recombine under emission of light. The materials used in single layer devices are usually better hole than electron conductors. As the hole are moving faster through the emitting layer than the electrons, the recombination zone

is shifted towards the cathode what usually leads to a non-radiative loss of energy [15]. Consequently, the efficiency of the device decrease [16].

In order to improve device efficiency, the multi-layer OLED architecture was introduced which is shown in Figure 1.4 . Additional hole transport layers (HTL) and electron transport layers (ETL) are introduced in order to balance the different charge carrier mobilities. By varying transport properties and thickness of those supporting layers, the recombination zone can be shifted toward the emission layer. The advantages concerning a multi-layer device setup, is the possibility to adapt the HOMO and LUMO levels of the material. A good overlap of the corresponding energy levels is essential to obtain a maximum carrier injection into the different layers [17].

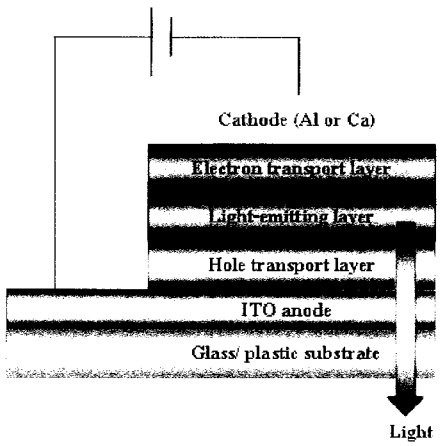

Figure 1.4 Schematic of a multi layer OLED setup.

1.2.3 Material for OLEDs application

Active materials in OLEDs have to fulfill a variety of requirements. First of all they have to emit with suitable color coordinates of the CIE-system (Commission International de L' Eclairang) and have to ensure a sufficient transport of charge carriers. A good chemical and electrochemical stability as well as a high thermal stability are also important prerequisites for OLED materials. Furthermore the compound should exhibit good film forming properties. Crystallization of the thin films may lead to a decrease of the charge carrier mobilities and finally to a short in the device [18, 19]. For this issue small molecules with bulky side groups are well suited. Form low molar mass compounds homogeneous thin films can be prepared by vacuum

deposition. As the bulky substituents prevent crystallization, molecular glasses are formed by these non-polymeric compounds [20]. Material used as HTL have to exhibit HOMO levels in the order of -5.3 eV and therefore low ionization potentials. Aromatic amines like NPD, CBP and TCTA (Figure 1.5) are typical hole conductor materials for applications [21].

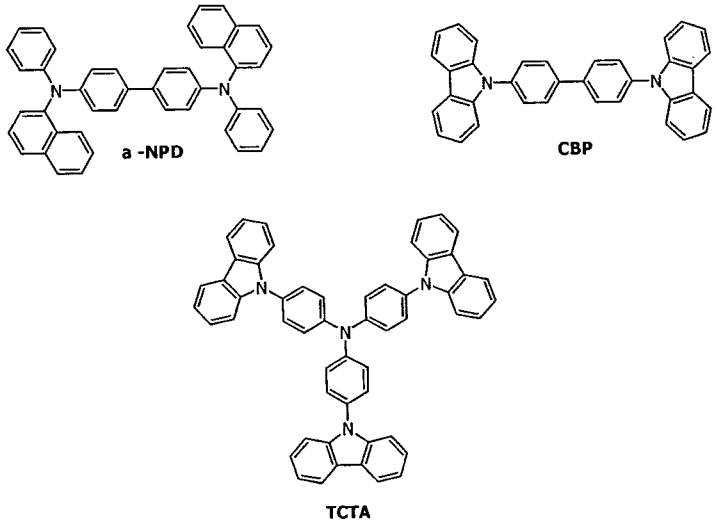

Figure 1.5 Typical aromatic amine that are used for hole transport in OLED device: *N,N'*-di (naphthalene-l-yl)-*N,N'*-diphenyl-biphenyl-4,4'-diamine(α-NPD), bis-(4-carbazol-9-yl)-bi-Phenyl (CBP) and tris-(4-carbazol-9-yl-phenyl)-amine(TCTA).

Substances used for electron transport are often metal complexes like AlQ_3 and BAlQ or electron poor heterocyclics like BPhen (Figure1.6) [22].

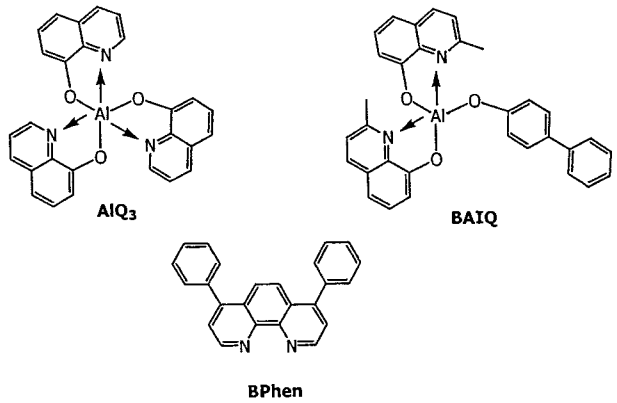

Figure 1.6 Typical examples for ETL materials: tris(8-hydroxyquinoline) aluminium (AlQ_3), bis-(2-dimethyl-8-quinoxalato)-4-(phenyl-phenoxalto) aluminium (III) (BAlQ) and 4,7-Diphenyl-[1,10]phenanthroline (BPhen).

In 1990 the group of Friend was the first who used conjugated polymer as emitter in a solution processed single layer OLED [23]. As the highly fluorescent poly(p-phenylene-vinylene) (PPV, Figure 1.7) is insoluble, they had to work with a precursor material which was converted into PPV by a thermal treatment. A few year later soluble PPV derivatives like MEH-PPV [24] and OC_1C_{10}-PPV were developed (Figure1.7). By the introduction of different alkoxy substituents the solubility of the new polymeric materials can also be influenced by the side chain substitution pattern. PPV for is a green emitter, whereas with MEH-PPV orange light can be generated. OC_1C_{10}-PPV [25] emits red light.

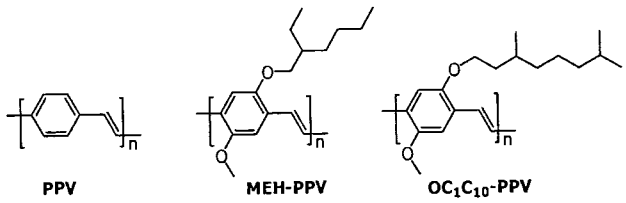

Figure 1.7 Chemical structure of PPV and its soluble derivative.

For the emission of blue light materials with a large energy gap between HOMO and LUMO level are required. Today, 9,9-dialkylated polyfluorenes [26] and so-called ladder-type polymers (LPPP) which are also based on fluorene chromophores are frequently used as blue emitters. The chemical structure of these polymers are shown in Figure 1.8.

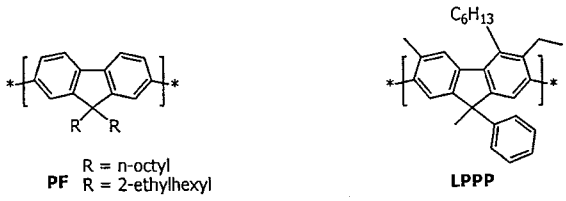

Figure 1.8 Chemical structure of fluorine based blue light emitting polymers for OLED applications: 9,9-dialkylated poly(2,7-fluorene) (PF) and ladder-type poly (p-phenylene) (LPPP).

Due to the large energy gap between HOMO and LUMO level in blue emitters, the term stability of blue OLED devices is still serious problem.

1.3 Organic field-effect transistors (OFETs)

The invention of the first "transistor" (transfer/resistor) in 1947 by John Baedeen, William Shockley and Water Brattain revolutionnized the whole electronic industry [27]. Since then Si-based elctronic devices and their application in microelectronics started to dominate our every day life. Charge carrier mobilities in field-effect transistors made from single crystalline silicon reach values up to 1500 cm^2/Vs [28]. Such high mobilities allow the production of highly integrated circuits requiring vary litle space. In a modern central processing unit (CPU) of a personal computer, 125 million transistors are accommodated in a volumn of only 8 cm^3 the average distance between the single transistors is 65 nm [29].

The first FET for which organic materials were used as semiconducting material was reported in 1986 [30]. Although only low charge carrier mobilities of about 10^{-5} cm^2/Vs were achieved, a lot of research effort was put in the development of new material and processing techniques [31, 32]. The posibilitty to use flexible substrates together with liquid phase deposition methods were the motivation for a number of ambitious reserarch project.

1.3.1 OFET device operation

In principle an OFET consists of three different electrodes: source, drian and gate. Ideally the source and drain contacts should behave as ohic contacts for the majority carrier type in the organic semiconductor. These two contacts can be considered as one plate of a capacitor. The second capacitor plate is the so-called gate contact. These two capacitor plates are

separated by an insulator layer. The semiconducting material is then deposited between the source and drain contacts. Between drain and gate different driving voltages can be applied whereas the source electrode is grounded. The priciple operation modes of an OFET are depicted in Figure 1.9. Usually OFETs are primarily operated as accumulation mode enhancement transistors.

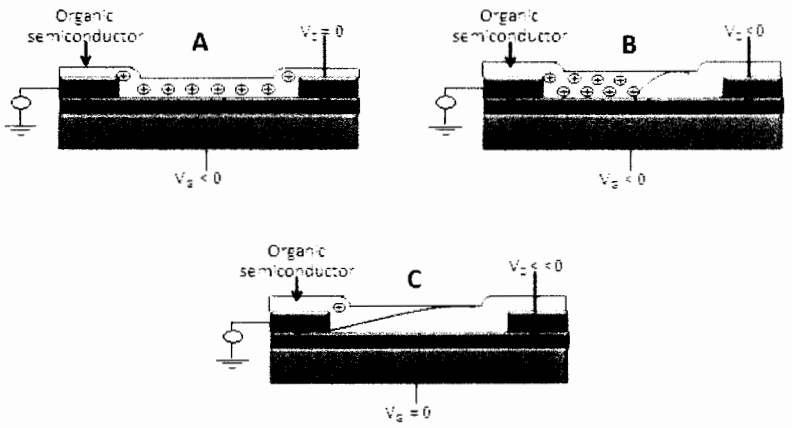

Figure 1.9 Schematic operation modes of a organic field-effect transistor, using a p-type semiconducting material.

In the following paragraph the basic device operation of an OFET will be described for a p-type material, what means that the charge carrier are holes. This operating principle can be adopted for n-type semiconductors with electrons as charge carriers. In Figure 1.9 A, a schematic of the transistor is shown where a negative gate bias but no drain voltage is applied. This leads to an increased concentration of positive charge carrier at the interface between insulator and semiconductor [33] and a conducting channel between the source and drain eletrodes is formed [34]. The additional positive charges accumulated in this region are provided by the ohmic source and drain contacts. When a negative bias is applied to the gate as well as to the drain electrodes (Figure 1.9 B), the charge carrier start to move along the conducting channel. Now a current between source and drain can be measured with the electric field as driving force. If the drain voltage is increased, a depletion zone is formed at the drain electrode. At a sufficiently high drain voltage the depletion zone finally resaches the source electrode what results insatulation current between source and drain. That means that the transistors is driven in the saturation regime what is shown in Figure 1.9 C.

1.3.2 OFET characteristics

The operation modes that were described before can be measured and plotted in two different ways. If a gate voltage sweep is carried out and the source drain voltage is kept constant, a transfer characteristic of the FET device is obtained (Figure 1.10). In this case the source drain current is plotted versus the gate voltage. From this kind of evaluation the turn on voltage and the on/off-ratio of a transistor can be extracted. Turn on voltage of only a few volts are desired to be use batteries as power supply. This is essential when it comes to mobile electronic applications. For integrated circuits, high on/off-ratios of about 10^6 are required in order to distinguish between the on and off status of the transistor. If a gate sweep is carried out in two directions hysteresis effects of the device can be investigated. Hysteresis means that the source drain current of the backward sweep is lower that form the forward sweep. This phenomenon gives information about the semiconducting material and reveals interface effects between semiconductor and insulator. Ideally, no or only little hysteresis effects should be observed. In this contex it is important to mention that the charge carrier transport takes place in the conducting chanel which is only a few monolayers thick [35].

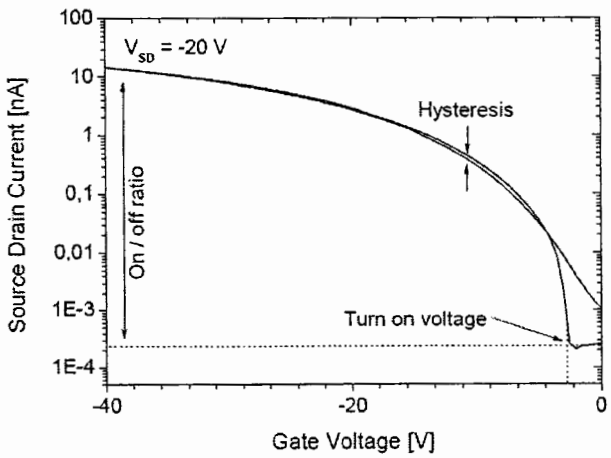

Figure 1.10 Typical transfer characteristic of an OFET: Gate voltage versus source drain current at a constant source drain bias with a star-shaped triphenylamine as semiconductor on a bottom gate FET substante from Philips.

From the transfer characteristics, the field-effectmobility of the semiconducting material (μ_{FET}) can be calculated by Equation 1-1 [36].

$$\mu_{FET} = \left(\frac{L}{WCV_D} \right) \frac{\partial I_{SD}}{\partial V_G}$$

In order to obtain the output characteristics of an OFET, the source drain voltage is plotted versus the source drain current. The measurement are carried out with different (constant) gate voltages. Typical output characteristics are presented in Figure 1.11.

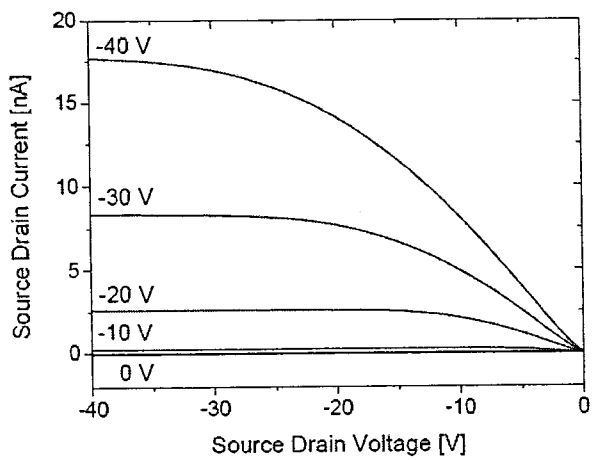

Figure 1.11 Typical output characteristics of an OFET at different gate voltage (0 V, -10 V, -20 V, -30 V, -40 V).

The output characteristics can be divided in two different regimes. If the gate voltage is higher than the source drain bias, the device runs in the linear region. In this region the source drain current should increase linearly. Otherwise the semiconducting material exhibits an homic contact resistance at the source drain electrodes. The saturation regime is reached as soon as the source drain voltage exceeds the gate voltage. At this point the source drain current becomes constant [37].

1.3.3 OFET architectures

For the application of organic materials in FETs, two different device architecture were developed. The bottom gate OFET structure (Figure 1.12 A) is based on a heavily doped n++ silicon wafer that is used as gate constact. Gold is evaporated and photolithographically patterned to from the source and drain contact [38]. Finally the organic semiconductor is deposited, i.e. by spin-coating or drop casting, on top of the substrate. This kind

of setup allows a quick and efficient materail screening. The fact that the non-polar organic material is in direct contact with the highly polar SiO_2 insulator is drawback of this device architecture. A variety of interface effects may occur due to the drastic charge of polarity [39, 40]. In order to reduce the dipole-dipole interactions, different surface treatments can be applied to the SiO_2 [41]. This technique will be described in the following paragraph. Figure 1.12 (B) shows the so-called top gate device architecture. It is deposited on top of the semiconducting layer before the gate electrode is deposited by evaporating gold through a shadow mask. The preparation of these FET substrates is more complex and time consuming but a variety of different organic gate insulators can be utilized [42, 43]. Furthermore the sensitive organic semiconductor is protected by the gate dielectric layer in this FET setup.

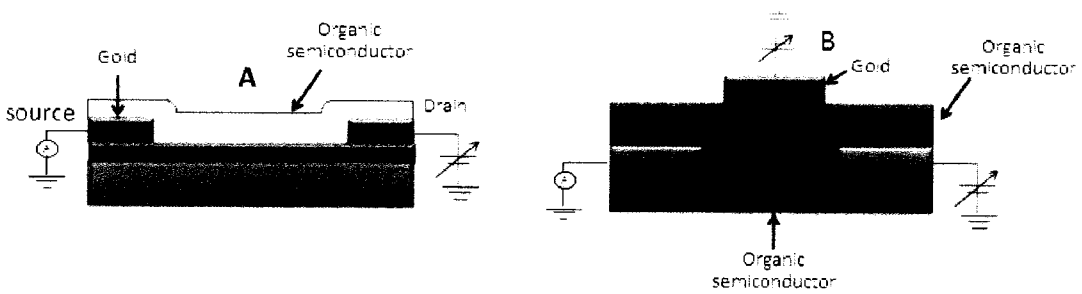

Figure 1.12 Schematic of two different FET device architectures. A: bottom gate setup, B: top gate architecture.

1.3.4 Materials for OFET applications

In the past years, intensive effort has been spent on developing new polymeric or low molar mass semiconducting materials with mibilities approaching the 1 cm^2/Vs of amorphous silicon [44, 45]. It turned out that such high mobilities, which are on the edge of band transport, can only be obtained from organic compounds that show a high degree of molecular order [46, 47]. Consequently, the highest charge carrier mobilities are obtained from single crystalline materials. Acenes like pantacene and rubrene have been investigated intensively during the last years (Figure 1.13). Purification and single crystal growth from these materials is the topic of many publications. With field-effect mobilities of about 15 cm^2/Vs, single crystalline rubrene has set the benchmark among organic semiconductors [48]. The second highest mobility value of about 5 cm^2/Vs was obtained from pectacene single crystals [49].

these acenes show excellent OFET performances, it is very unlikely that theses moleculars will finally be used in organic electronics [50, 51]. In fact, preparation of the single crystal from soft organic materials is an expensive and painstaking process and not suitable for device production in a large scale. Furthermore the acenes are sensitive towards light and suffer from degradation when they are stored under ambient conditions [52, 53].

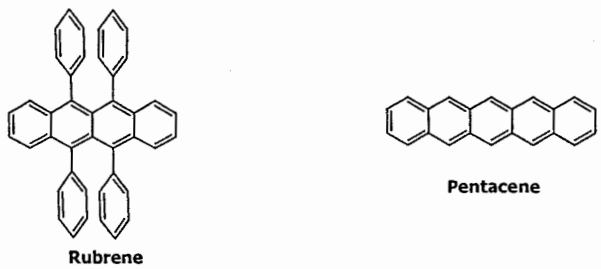

Figure 1.13 Structures of acenes for high mobility single crystalline OFETs.

Vaccum-deposition of small molecule offers a more simplified approch to prepare OFETs exhibiting fairly high carrier mobilities. Espectially with thiophene derivatives impressive improvements have been made. If sexithiophenes [54] (Figure 1.14), mobilities of $2x10^{-3}$ cm^2/Vs have been recorded [56]. If the sexithiophene core is substituted with hexyl side chains (DH6T) field-effect mobilities up to 0.13 cm^2/Vs were reported [55]. The increased mobility of DH6T can be explaned by an improved packing of the single molecules what leads to a smaller intermolecular distance. Bao et al. have reached field-effect mobilities of $2x10^{-2}$ cm^2/Vs [56] by vacum depositing a polycrystalline layer of a bithiophene which is subsituted with two fluorene units (FTTF, DHFTTF, Figure 1.14) the mobility was increased up to 0.14 cm^2/Vs due to a closer packing of the core molecules.

All of low molar mass compounds that were mentioned before can only be processed by vacuum deposition, what makes large scale device fabrication ineffective. For this reason liquid phase processing is the key to low price organic electronics. One possible approach to reach this target is the usage of polymeric compounds. Today, poly(3-hexylthiophene) (P3HT, Figure 1.15) is one of the best investigated polymers concerning its performance in OFETs [57, 58]. Thin films of regioregular P3HT exhibit a highly microcrystalline and

anisotropic lamellar morphology what leads to two-dimentional conjugated layers with strong π-π interchain interactions.

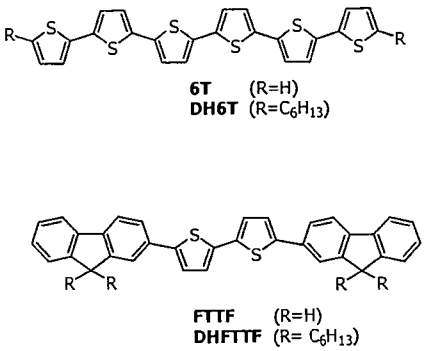

Figure 1.14 Structure of thiophen based materials for OFET applications. Sexithiophen (6T) and α, ϖ -dihexylsexithiophen (DH6T), 5,5'-bis-(*9H*-fluorene-2-yl)-2,2'-bithiophene (FTTF) and 5,5'-bis-(7-hexyl-*9H*-fluorene-2-yl)-2,2'-bithiophene (DHFTTF).

These thiophen layers are separeted from each other by that alkyl side chains which act as a kind of insulating layer. This microstructure allows a fast in-plane charge transport [59]. The charge carrier mobility of P3HT strongly depends on the degree of regioregularity of 81% shows mobilities of about 2x 10^{-4} cm^2/Vs whereas 0.1-0.3 cm^2/Vs can be obtained if the regioregularity is incresed to 96%. Big diyad regioregularity vantages of these thiophen based materials are a poor photostability and the high sensitivity toward oxygen [60]. Explosure to sunlight in the presence of air causes of formation of carbonyl defects in the polymer with an associated loss of conjugation and mobility [61].

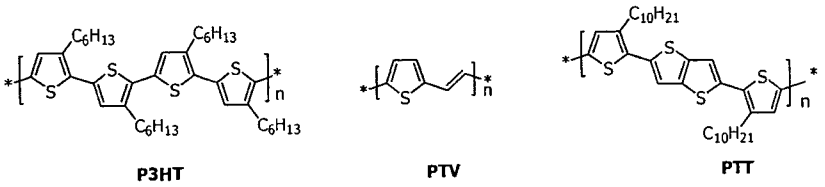

Figure 1.15 Chemical structures of thiophen based polymer: poly(3-hexylthiophene) (P3HT), poly(thiophenvinyllene) (PTV) and poly(2,5-bis(3-decylthiophen-2yl)-thieno-[2,3-b]thiophene (PTT).

A step towards higher environmental stability of thiophene based materials was made by Koezuka et al. who have prepared poly(thiophenvinyllene) (PTV, Figure 1.15) from which mobility values of 0.22 cm^2/Vs were obtained [62]. McCulloch et al. reached 0.15 cm^2/Vs together with a reasonable atmospheric stabiliy from poly(2,5-bis(3-decylthiophen-2yl)-thieno-[2,3-b]thiophene (PTT, Figure 1.15) [63]. An alternative approch to obtain highly ordered thin film are large monodomains fromed by liquid crystal (LC). The molecules can be aligned in the LC-phase at elevated temperatures. The orientation is then frozen in ether by quenching the LC-phase to room temperture or by photopolymerization of liquid crystalline compounds with phoroactive endgroups, which as known as reactive mesogens(RM). de A well estaplished liquid crystalline material from which good charge carrier mobilities can be obtained is poly-(9.9'-dioctylfluorene-2-yl)-co-bithiophene (F8T2, Figure 1.16). Sirringhaus et al. have shown mobilities of about 0.01 cm^2/Vs from solution processed F8T2. Alignment of the F8T2 molecules was carried out in the magnetic phase above 265^0C on rubbed polyimide perpendicular to the FET electrods. The oreintation was frozen in by quenching the sunstrate to room temperature [64]. In such supercooled LC-phase the orientation will fade over the time what is the drawback concerting field-effect mobilities. Broer et al. were the first to solve this problem. They introduced photopolymerizable endgroups to the LC-core molecule in order to fix the orientation of the mesophase by chemically crossliking the mesogens [65]. With this reactive mesogen approach the group of McCulloch reached mobilities of $4x10^{-4}$ cm^2/Vs after photopolymerizing the methacrylate endgroups of a quaterthiophene derivative (Quaterthiophene RM) [66] which is shown in Figure 1.16.

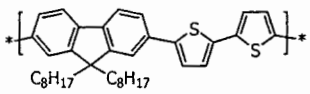

F8T2

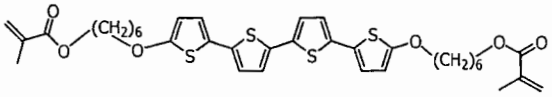

Quartertthiophene RM

Figure 1.16 Chemical structures of thiophen based polymer: poly-(9.9'-dioctylfluorene-2-yl)-co-bithiophene (F8T2) and quaterthiophene derivative (Quaterthiophene RM).

The introduction of aromatic amines as active material in OFETs was an important step towards environment stability. Compounds like poly-(triarylamine) (PTAA, Figure 1.17)

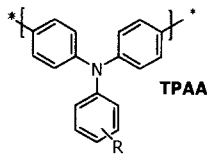

Figure 1.17 Chemical structure of a glass forming poly-(triphenylamine) derivative (**PTAA**).

1.4 The Dye Sensitized Solar Cell (DSC)

The DSC, or the Grazel cell, is a complex system wherein three different components, the semiconductor, the chromophore and the electrolyte are brought together to generate electric power from light with out suffering from any permanence chemical transformation (Figure 1.18) [67].

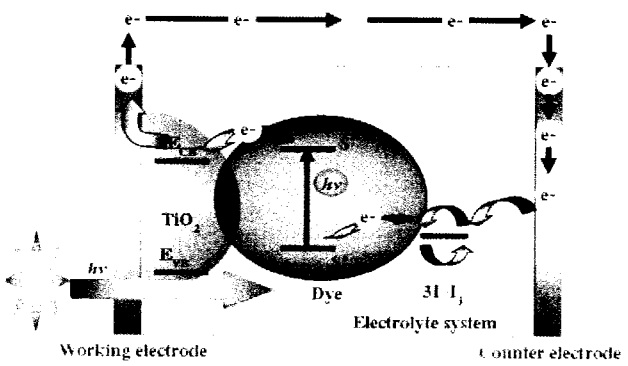

Figure 1.18 Schematic picture of the dye solar cells.

The nanocrystalline semiconductor is usually TiO_2, although alternative wide band gap oxides such as ZnO can be used. A monolayer of the chromophore, i.e. the sensitizer, is attached to the surface of the semiconductor. Photoexcitation of the chromophore results in the injection of an electron into the conduction band of the semiconductor (Figure 1.19). The chromophore is regenerated by the electrolyte, usually an organic solvent containing a redox couple, such as

iodide/triiodide. The electron donation to the chromophore by iodide is compensated by the reduction of triiodide at the counter electrode and the circuit is completed by electron migration through the external load. The overall voltage generated corresponds to the difference between the Fermi level of the semiconductor and the redox potential of the electrolyte.

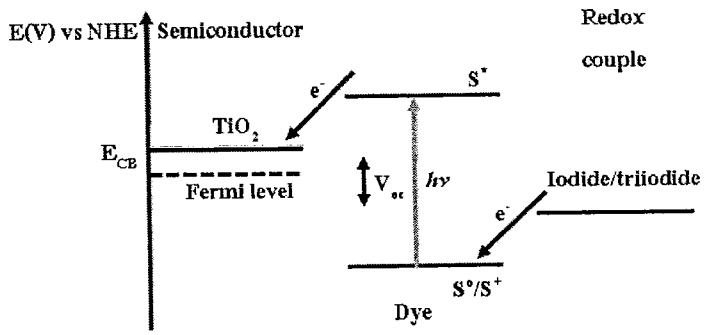

Figure 1.19 Schematic picture of the electron flow in the DSCs.

The performance of the solar cell can be quantified with parameters such as incident photon to current efficiency (IPCE), open circuit photovoltage (V_{oc}) and the overall efficiency of the photovoltaic cell (η_{cell}). The efficiency of the DSCs is related to a large number of parameters. This thesis will only focus on the development of efficient sensitizers and their synthesis, even so, it is important to have the general concepts in mind.

1.4.1 Overall efficiency of the photovoltaic cell (η_{cell})

The solar energy to electricity conversion efficiency under white-light irradiation (e.g., AM1.5G) can be obtained from the following equation:

$$\eta_{cell} = \frac{J_{sc} \cdot V_{oc} \cdot \text{ff}}{I_0} \tag{1}$$

Where I_0 (mW/cm^2) is the photon flux (e.g., ca. 100 mW/cm^2 for AM 1.5 G), J_{sc} (mW/cm^2) is the short-circuit current density under irradiation, V_{oc} (V) is the open-circuit voltage, ff represents the cell fill factor. The fill factor is defined by the ratio of the current and the voltage at the maximum power point to the short circuit current and the open circuit voltage. The fill factor measures the squareness of the *J-V* curve (Figure 1.20).

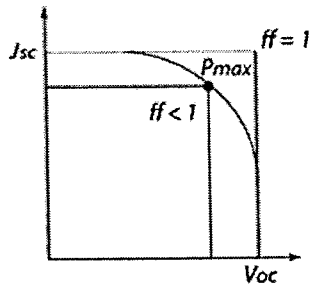

Figure 1.20 *J-V* curve.

1.4.2 Sensitizers

The efficiencies of the sensitizers are related to some basic criteria. The HOMO potential of the dye should be sufficiently positive compared to the electrolyte redox potential for efficient dye regeneration. The LUMO potential of the dye should be sufficiently negative to match the potential of the conduction band edge of the TiO_2 and the light absorption in the visible region should be efficient. However, by broadening the absorption spectra the difference in the potentials of the HOMO and the LUMO energy levels is decreased. If the HOMO and LUMO energy levels are too close in potential, the driving force for electron injection into the semiconductor or regeneration of the dye from the electrolyte could be hindered. The sensitizer should also exhibit small reorganization energy for excited- and ground-state redox processes, in order to minimize free energy losses in primary and secondary electron transfer steps [68].

1.4.2.1 Ruthenium sensitizers

Sensitizer of ruthenium complexes such as the **N3**, **N719** and black dyes have been intensively investigated and show record solar energy-to-electricity conversion efficiencies (η) of 10, 11.2 and 10.8%, respectively (Figure 1.21) [69].

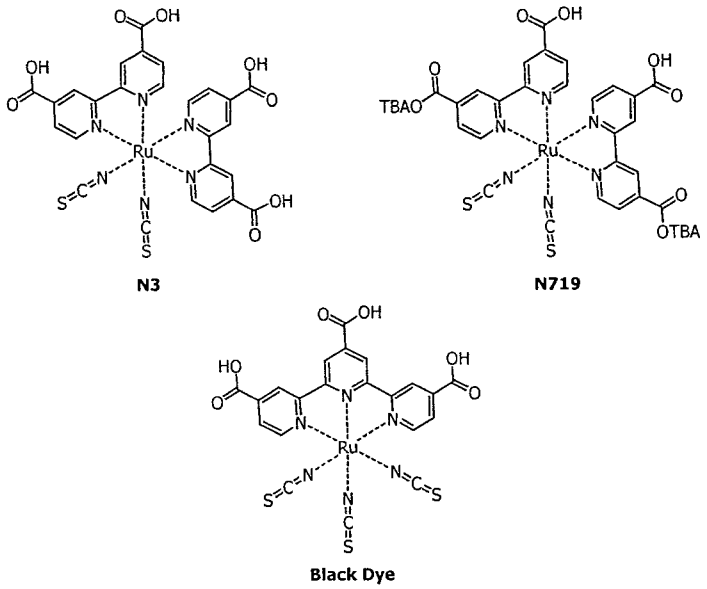

Figure 1.21 Chemical structures of **N3**, **N719** and black dyes.

A large number of different ruthenium based sensitizers have been investigated in order to improve the photovoltaic performance and stability of the DSCs. Amongst them especially four (**K19**, **K73**, **K77** and **Ru-1** [70]) have shown interesting properties in that they are competing in efficiency and have higher molar extinction coefficients than the three former. The enhanced absorption observed is expected from the extended conjugated system.

1.4.2.2 Organic sensitizers

Recently, performances of DSCs based on metal-free organic dyes have been remarkably improved by several groups. The first transient studies on a coumarin dye in DSCs was performed in 1996, when Gratzel et al. found injection rates of 200 fs from **C343** into the conduction band of TiO_2. Since **C343** has a narrow absorption spectrum, the conversion efficiency of this specific compound was low. By introduction of a methine unit, the π-system could be expanded and in 2001 a respectable efficiency of 5.6% was obtained with **NKX-2311** [71]. Adding more methine units (up to three) and introducing bulky substituents to prevent dye-aggregation could push the efficiency to 6.7% in 2005 **(NKX-2753)**. Currently other building blocks like thiophene are tested, which are believed to give a higher stability. First results of 7.4% for **NKX-2677** are encouraging [72].

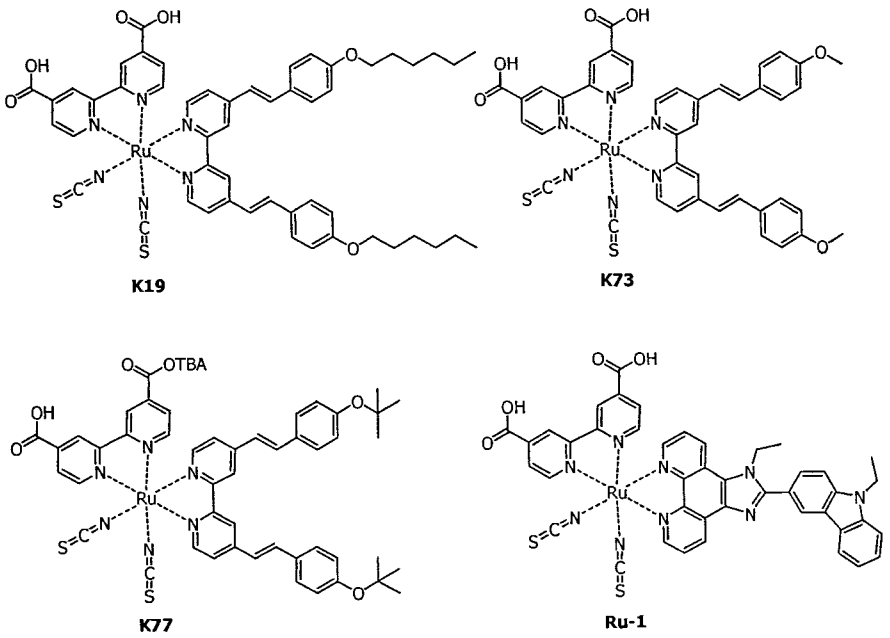

Figure 1.22 Chemical structures of **K19**, **K73**, **K77** and **Ru-1** dyes.

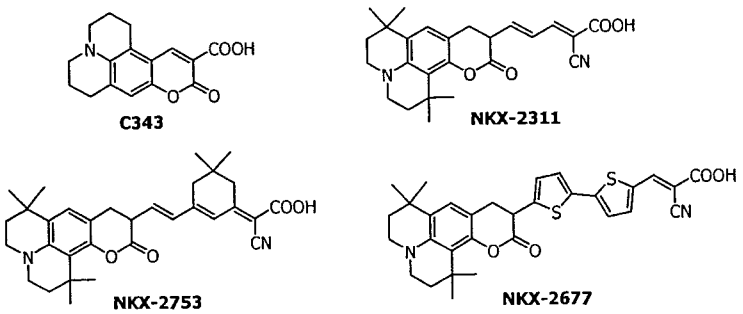

Figure 1.23 Chemical structures of **C343**, **NKX-2311**, **NKX-2753** and **NKX-2677** dyes.

In 2003, an indoline dye **D102** and **D149** discovered by Ito et al. These indoline dyes gave solar-to-electrical energy conversion efficiency of 6.1 and 9%, respectively, in full sunlight. A highest efficiency for organic dyes has been achieved by an indoline dye **D149** [73].

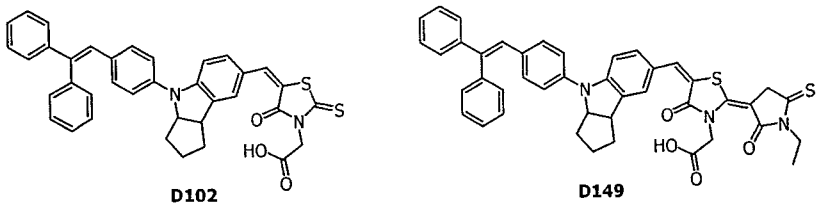

Figure 1.24 Chemical structures of **D102** and **D149** dyes.

In 2007, Yuanzuo Li et al. [74] reported that the highly efficient and stable organic dyes **JK-1** and **JK-2** composed of bis-dimethylfluoreneaniline moiety as the electron donor and cyanoacrylic acid moiety as the electron acceptor with an overall conversion efficiency of 8.01%.

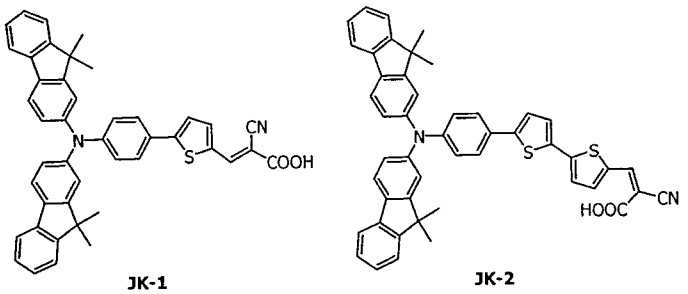

Figure 1.25 Chemical structures of **JK-1** and **JK-2** dyes.

In 2007, Duckhyun Kim et al. [75] investigated that the organic dyes **JK-24** and **JK-25** containing *N*-(9,9-dimethylfluoren-2-yl)carbazole as electron donor and cyanoacrylic acid as electron acceptor bridged by thiophene units, gave an overall conversion efficiency (η) of 5.15%. Although many structure frameworks such as coumarin, aniline, and indoline have been employed as good electron donor unit, the small molecular organic dyes containing the *N*-substituted carbazole structural motif have been little explored for DSCs.

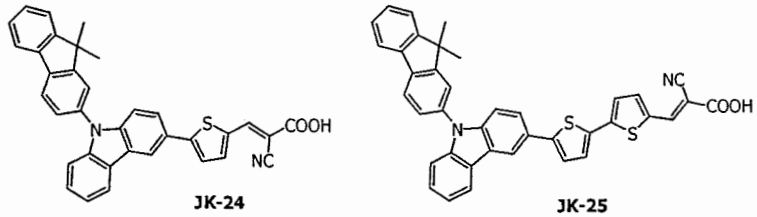

Figure 1.26 Chemical structures of **JK-24** and **JK-25** dyes.

Most of the dyes employed in DSCs have carboxylic acid groups to anchor on the TiO_2-surface. The binding is reversible with high binding equilibrium constants ($K = 10^5\ M^{-1}$). At a pH > 9 the equilibrium is typically shifted to the reactant side and the dye molecules desorb. This somewhat fragile linkage triggered the development of dyes with different anchoring groups. In general the binding strength to a metal oxide surface decreases in the order phosphonic acid > carboxylic acid > ester > acid chloride > carboxylate salts > amides [76] due to its strong electronic withdrawing properties, the most widely used and successful to date being the carboxylic acid and phosphonic acid functionalities. The carboxylic acid groups, while ensuring efficient adsorption of the dye on the surface also promote electronic coupling between the donor levels of the excited chromophores and the acceptor levels of the TiO_2 semiconductor. Some of the possible modes of chelation/derivatization, ranging from chemical bonding (chelating or bridging mode) to H-bonding, are shown in Figure 1.27 [77].

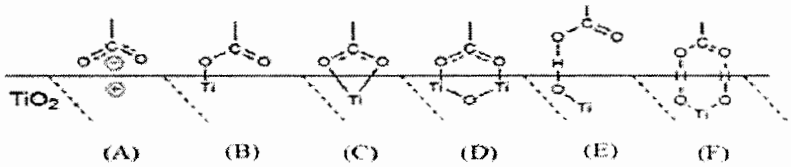

Figure 1.27 Possible binding modes for carboxylic acid groups on TiO_2.

1.5 Aim of the thesis

In the recent year, the development of novel organic materials for optoelectronic applications has attracted a lot of interest both industry and academic. Especially in the area of organic light emitting diodes (OLEDs) and dye solar cells (DSCs) hugs process has been made. One of main technology attractions of organic electronics that the active layers can be deposited at

low temperatures by liquid phase techniques. This makes organic semiconductors ideal candidates for low-cost, large-area electronic applications on flexible substrates.

The aims of this works as follows:

(1) To synthesize of a novel luminescence organic materials for using as emitters in optoelectronic devices. Luminescence materials consist of carbazole moiety as the electron donor group. Chemically, carbazole can be easily functionalized at its 3,6-positions with a bulky group of *tert*-butyl moiety to protect the oxidation coupling at the 3,6-positions of the peripheral carbazole moiety. Fluorene was introduced on *N*-9 of carbazole as electron transport moiety. The *n*-hexyl substituents were introduced on the C-9 position of fluorene ring to increase the solubility, with a thiophene linker and pyrene as photoluminescence moiety to increase the photoluminescence quantum yield of the target molecule as show in Figure 1.28.

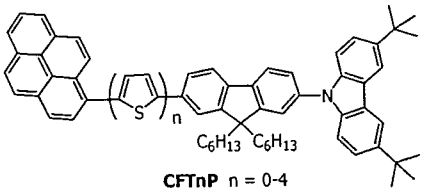

Figure 1.28 Novel luminescence organic materials based on pyrene-oligothiophene.

(2) To synthesize a novel π-conjugate of *N*-carbazole end-capped oligofluorene-thiophene based on carbazole as the donor group, Chemically, carbazole can be easily functionalized at its 3,6-positions with a bulky group of *tert*-butyl moiety to protect the oxidation coupling at the 3,6-positions of the peripheral carbazole moiety. Fluorene was introduced on *N*-9 of carbazole as electron transport moiety. The *n*-hexyl substituents were introduced on the C-9 position of fluorene ring to increase the solubility, with a thiophene linker. The fluorene-substituted oligothiophenes with longer oligothiophene chains still remain to be explored as color turnable light-emitting for OLEDs as show in Figure 1.29.

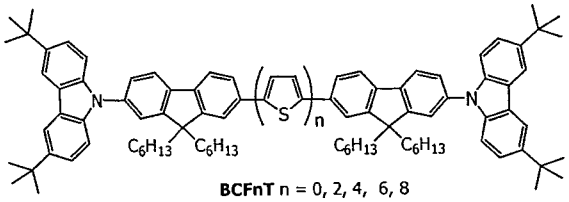

Figure 1.29 Novel organic materials based on oligothiophene.

(3) To synthesize a novel donor π-conjugate acceptor (D-π-A) organic material based on carbazole as the donor group, Chemically, carbazole can be easily functionalized at its 3,6-positions with a bulky group of *tert*-butyl moiety to protect the oxidation coupling at the 3,6-positions of the peripheral carbazole moiety. Fluorene was introduced on *N*-9 of carbazole as electron transport moiety. The *n*-hexyl substituents were introduced on the C-9 position of fluorene ring to increase the solubility, with a thiophene linker, and a acrylic acid and cyanoacrylate moiety as acceptor/anchoring group which would provide an interesting and readily modifiable scaffold. The carbazole was functionalized with *tert*-butyl group to investigate if a bulky substituent would enhance the solar cell performance by suppressing aggregation. The performance of a device with **CAnT** (n = 1-4) as dyes are investigated as show in Figure 1.30.

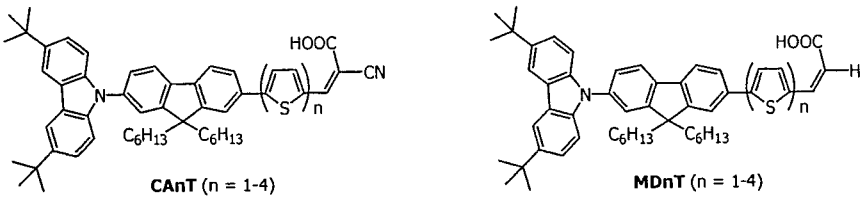

Figure 1.30 Structure of **CAnT** (n = 1-4) and **MDnT** (n = 1-4).

(4) To synthesize a novel π-conjugate of *N*-carbazole end-capped oligofluorene-thiophene based on carbazole as the donor group, Chemically, carbazole can be easily functionalized at its 3,6-positions with a bulky group of *tert*-butyl moiety to protect the oxidation coupling at the 3,6-positions of the peripheral carbazole moiety. Fluorene was introduced on *N*-9 of carbazole as electron transport moiety. The *n*-hexyl substituents were introduced on the C-9 position of fluorene ring to increase the solubility, with a thiophene linker and a methylcyanoacrylate, dimalononitrile and indandione as acceptor units as emitter in OLEDs as show in Figure 1.31.

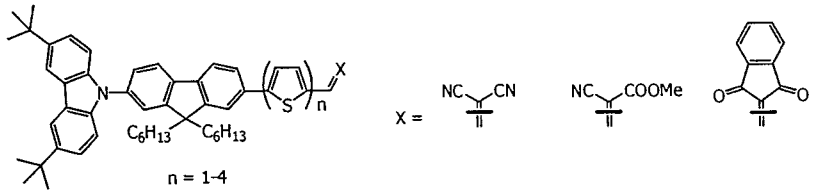

Figure 1.31 Structure of **DMnT** (n = 1-4), **MCnT** (n = 1-4) and **InnT** (n = 1-4).

(5) To synthesis a novel π-conjugate of diphenylamine core oligothiophene based on diphenylamine as the donor group. Chemically, diphenylamine can be easily functionalized at its para-position with variation of the π-conjugate length of the dye molecules, introduced 2-ethylhexyl moiety at N-atom of diphenylamine to increase the solubility in dye sensitized solar cell (DSCs), and a cyanoacrylate moiety as acceptor/anchoring group which would provide an interesting and readily modifiable scaffold. as show in Figure 1.32.

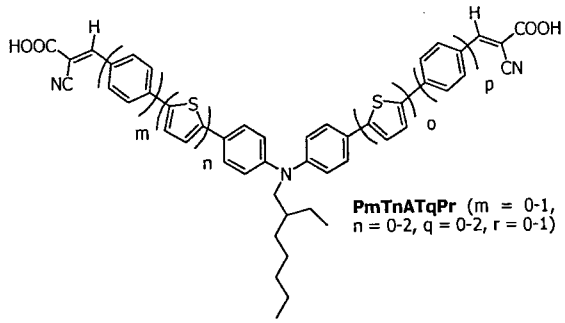

Figure 1.32 Structure of **PmTnATqPr** (m = 0-1, n = 0-2, q = 0-2, r = 0-1).

(6) To characterize and study the electronic, photophysical, electrochemical and thermal properties of the target molecules.

(7) To investigate their potential application as both dye sensitizer and emitters for optoelectronic devices.

CHAPTER 2

SYNTHESIS AND CHARATERIZATION OF LUMINESCENCE MATERIALS BASED ON PYRENE-OLIGOTHIOPHENES

2.1 Introduction

π-Conjugated organic materials have been the subject of great interesting electronic and optical properties have been investigating as advanced molecular electronic materials [78-80]. The simplicity in the modification of chemical structure, solubility, and optical properties of the organic materials makes them superior to those based on inorganic substances in both manufacturing costs of the devices and improving some technological aspects. Advantage of oligotiophenes included cheap precursors, high thermal, excellent conductivity, electroluminescent behavior, photochemical stabilities and characteristics as advanced materials for organic light-emitting diodes (OLEDs) [81]. π-conjugated thiophene oligomer are that their physical properties can be easily tuned to the desired properties by changing the structure e.g. solubilizing chain, end-capping groups, insertion of contain groups, and different oligomer lengths [82, 83].

Fluorene have good stability due to the rigidly planar biphenyl structure in the fluorene unit. The introduction of substituents at the C-9 position makes fluorene soluble, and thus easy to process from organic solvents. One disadvantage, which limits the use of polyfluorenes in blue light-emitting diodes, is the difficulty to inject charges in these materials. To improve the charge injection, different electron donating or accepting units have been incorporated into the structure of fluorenes. In this way, the energies of the highest occupied molecular orbital (HOMO) and the lowest unoccupied molecular orbital (LUMO) can be varied, making it easier to inject charges [84]. Fluorene also has a number of advantages, including its capacity to emit in the blue part of the visible spectrum, chemical and photochemical stability, easy synthesis with high purity, liquid crystalline properties and durability under operation in a LED.

Pyrene has been used as a signaling unit for fluorescent probes, owing to its high photoluminescence efficiency and excimer-formation property [85]. In particular, blue fluorescent emitters based on pyrene units have attracted considerable attention for organic light-emitting

diodes (OLEDs), owing to the advantages of pyrene [86]. The photoluminescence quantum yield, carrier mobility, and hole-injection ability of emitters that consist of pyrene units are higher when compared to those of emitters that consist of oligofluorenes or polyfluorenes.

2.2 Aim of the study

We accomplished the synthesis of novel luminescence organic materials based on pyrene-oligothiophenes for using as emitters in optoelectronic devices. Luminescence materials consist of carbazole moiety as the electron donor group. Chemically, carbazole can be easily functionalized at its 3,6-positions with a bulky group of *tert*-butyl moiety to protect the oxidation coupling at the 3,6-positions of the peripheral carbazole moiety. Fluorene was introduced on *N*-9 of carbazole as electron transport moiety. The *n*-hexyl substituents were introduced on the C-9 position of fluorene ring to increase the solubility, with a thiophene linker and pyrene as photoluminescence moiety to increase the photoluminescence quantum yield of the target molecule, aiming at investigating how their optical, thermal, and electrochemical properties were affected by the molecular structure of the conjugated backbones.

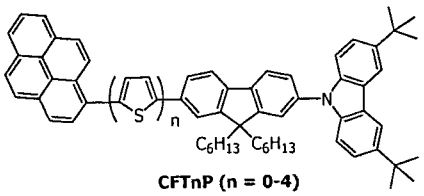

Figure 2.1 Novel luminescence organic materials based on pyrene-oligothiophenes.

2.3 Results and discussion

2.3.1 Synthesis

To synthetic approach to a series of novel luminescence organic materials based on pyrene-oligothiophenes, first dibromofluorene was prepared from bromination of fluorene using bromine as electrophile in the present of $FeCl_3$ as afford dibromofluorene in good yield.

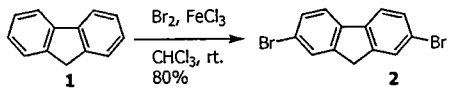

Figure 2.2 Bromination reaction to form dibromofluorene (**2**).

The mechanism of bromination of fluorene is shown in Figure 2.3.

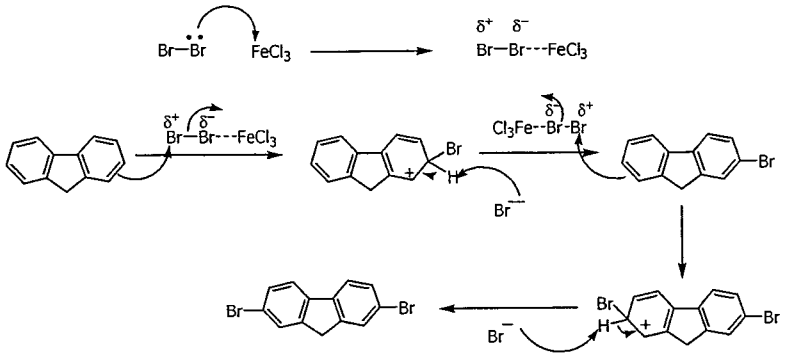

Figure 2.3 The proposed mechanism of bromination of fluorene.

The chemical structure of **2** was confirmed by ^{1}H-NMR analysis. The ^{1}H-NMR spectrum of product **2** shows a singlet signal at chemical shift 7.7 ppm (2H) assigning as 1-H and 8-H position of fluorene ring, a doublet signal at chemical shift 7.65 ppm (2H, J = 7.45 Hz) assigning as 3-H and 4-H of fluorene adduct and a singlet signal at chemical shift 3.9 ppm (2H) assigning as methylene proton of fluorene.

Dialkylation at the C-9 position to increase the solubility of the resultant compound **2** was accomplished by generation of the fluorenyl anion with an aqueous NaOH solution in DMSO and subsequent dihexylation with 1-bromohexane in the presence of n-Bu_4NCl as phase transfer catalyst at room temperature. The desired 2,7-dibromo-9,9-dihexyl-*9H*-fluorene was isolated by silica-gel column chromatography as brown solid in 86% yield.

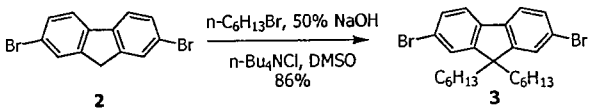

Figure 2.4 Alkylation reaction to form 2,7-dibromo-9,9-dihexyl-*9H*-fluorene.

The mechanism of alkylation with phase transfer catalyst to explain the critical role of tetraalkylammonium salts (Q^+X^-) in the reactions between two substances located in different immiscible phase is shown in Figure 2.5. Key to this tremendous enhancement in reactivity is the generation of a quaternary ammonium hydroxide, which makes the hydroxide anion soluble in organic solvents and sufficiently nucleophilic. The high rate of displacement is mainly due to two of the three characteristic features of the pairing cation (Q^+): high lipophilicity and the large ionic radius [87].

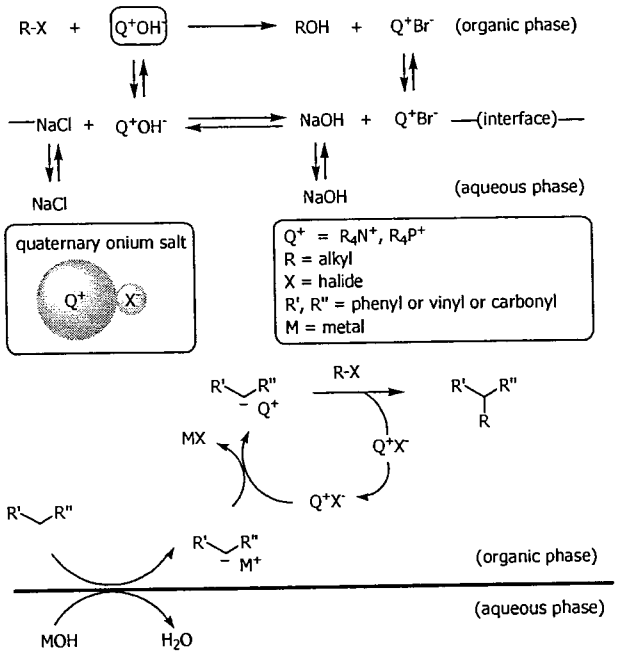

Figure 2.5 The proposed mechanism of alkylation.

The chemical structure of **3** was confirmed by ^{1}H-NMR analysis. The ^{1}H-NMR spectrum of product **3** shows a singlet signal at chemical shift 7.60 ppm (2H) assigning as 1-H and 8-H position of fluorene ring, a doublet signal at chemical shift 7.55 ppm (4H, J = 7.45 Hz) assigning as 3-H and 4-H of fluorene adduct, a triplet signal at chemical shift 2.0 ppm (4H) assigning as methylene proton of hexyl unit.

Subsequently, the key intermediate *N*-carbazole fluorene was synthesized by using Ullmann coupling of 2,7-dibromo-9,9-bis-*n*-hexylfluorene with 1 equivalent of 3,6-di-*tert*-carbazole in the presence of copper(I)iodide as catalyst, potassium phosphate as base and (±)-*trans*-diaminocyclohexane as co-catalyst in toluene at 170°C under N_2 in moderate yield.

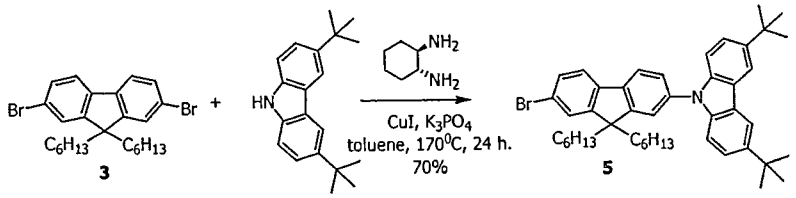

Figure 2.6 Ullmann coupling reaction to form 9-(7-bromo-9,9-dihexyl-*9H*-fluoren-2-yl)-3,6-di-*tert*-butyl-*9H*-cabazole (**5**).

The proposed mechanism of Ullmann coupling reaction is shown in Figure 2.7. The active species is a copper(I)iodide which undergoes oxidative addition with the second equivalent of halide, followed by reductive elimination and the formation of the fluorene-carbazole carbon bond.

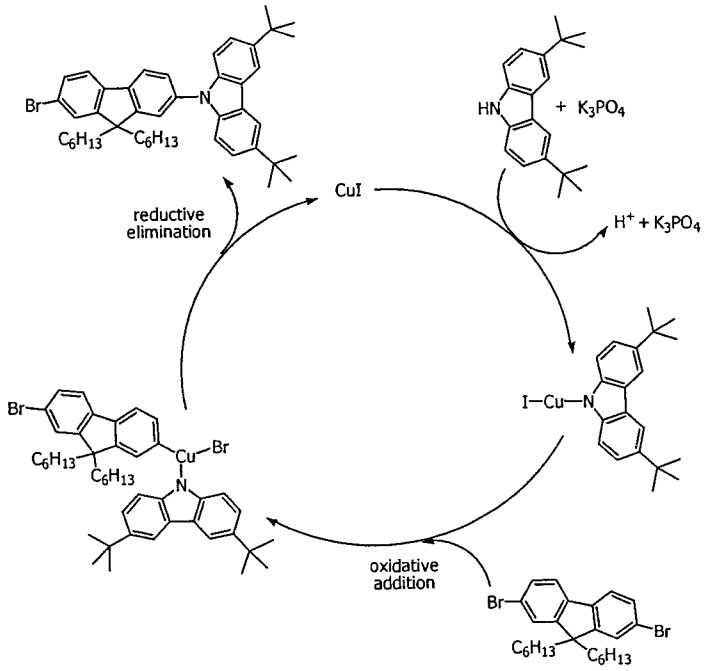

Figure 2.7 The proposed mechanism of Ullmann coupling reaction.

The chemical structure of **5** was confirmed by ^{1}H-NMR analysis. The ^{1}H-NMR spectrum of product **5** shows a singlet signal at chemical shift 8.18 ppm (2H) assigning as 4-H and 5-H of carbazole, a doublet signal at chemical shift 7.68 ppm (1H, J = 7.77 Hz) assigning as 3-H, a doublet signal at chemical shift 7.63 ppm (1H, J = 8.48 Hz) 4-H of carbazole adduct, a multiplet signal at chemical shift 7.51 ppm (4H) assigning as proton of fluorene unit, a doublet signal at chemical shift 7.39 ppm (2H, J = 8.59 Hz) assigning as proton of fluorene adduct. Moreover, IR spectrum reveals the absorption at 1364 cm^{-1} which is consistent with the presence of C-N bond.

Suzuki cross-coupling reaction of pyreneboronic acid and 9-(7-bromo-9,9-dihexyl-*9H*-fluoren-2-yl)-3,6-di-*tert*-butyl-*9H*-cabazole (**5**) were prepared by using $Pd(PPh_3)_4$ as catalyst in the presence of aqueous sodium carbonate solution in THF at refluxing temperature afforded 3,6-di-*tert*-butyl-9-(9,9-dihexyl-7-(pyren-1-yl)-*9H*-fluoene-2-yl)-*9H*-carbazole (**CFP**) in low yield as shown in Figure 2.8.

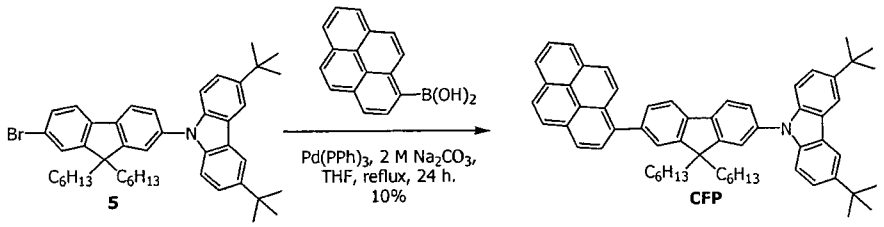

Figure 2.8 Suzuki cross-coupling reaction to form 3,6-di-*tert*-butyl-9-(9,9-dihexyl-7-(pyren-1-yl)-*9H*-fluoene-2-yl)-*9H*-carbazole (**CFP**).

The proposed mechanism of Suzuki cross-coupling reaction is shown in Figure 2.9. The Suzuki reaction is the coupling of an aryl or vinyl boronic acid with an aryl or vinyl halide using a palladium catalyst to form C-C bond. Thus, base activation of organoboron reagents as boronate intermediates facilitated the transfer of the organic group from boron to palladium (transmetallation). The reaction has later been extended to also include couplings with alkyl groups [88].

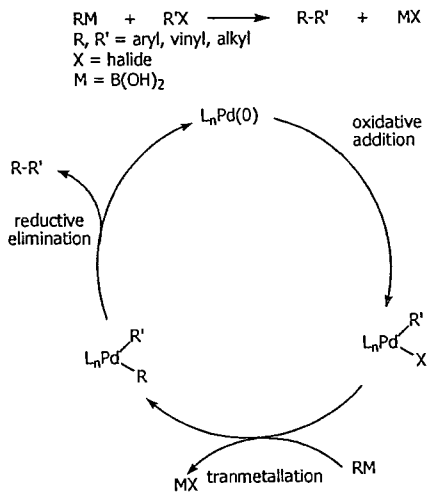

Figure 2.9 The proposed mechanism of Suzuki cross-coupling.

The chemical structure of **CFP** was confirmed by ^{1}H-NMR analysis. The ^{1}H-NMR spectrum of product **CFP** shows a multiplet signal at chemical shift 8.30-8.24 ppm (3H) assigning as the proton of pyrene group, a multiplet signal at chemical shift 8.18-8.09 ppm (8H) assigning as the proton of pyrene group and 4-H, 5-H of carbazole, a multiplet signal at chemical shift 8.07-7.94 ppm (4H) of carbazole adduct, a doublet signal at chemical shift 7.66 ppm (2H) assigning as proton of fluorene unit, a multiplet signal at chemical shift 7.63-7.59 ppm (2H) assigning as proton of fluorene unit, a multiplet signal at chemical shift 7.53-7.49 ppm (2H) assigning as proton of adduct.

Suzuki cross-coupling reaction of 2-thiophenboronic acid and the corresponding bromo-compound employed in order to increase the number of thiophene units in the molecules. The thiophene intermediates were prepared by using $Pd(PPh_3)_4$ as catalyst in the presence of aqueous sodium carbonate solution in THF at refluxing temperature afforded the thiophene adduct in range 62-81 % yield. The bromination reaction was carried out in THF as solvent with NBS. The reaction mixture was stirred at room temperature for 30 min to directly yield bromocompound as show in Figure 2.10.

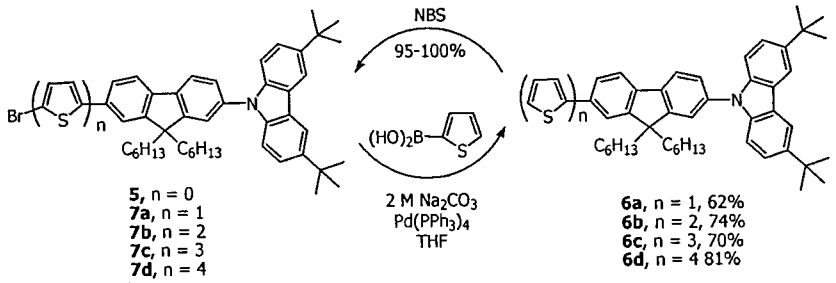

Figure 2.10 Suzuki cross-coupling reaction and bromination reaction to form bromocompounds.

Suzuki cross-coupling mechanism of thiophene intermediate (**6**) as described in Figure 2.9. The mechanism of bromination reaction by NBS as show in Figure 2.12.

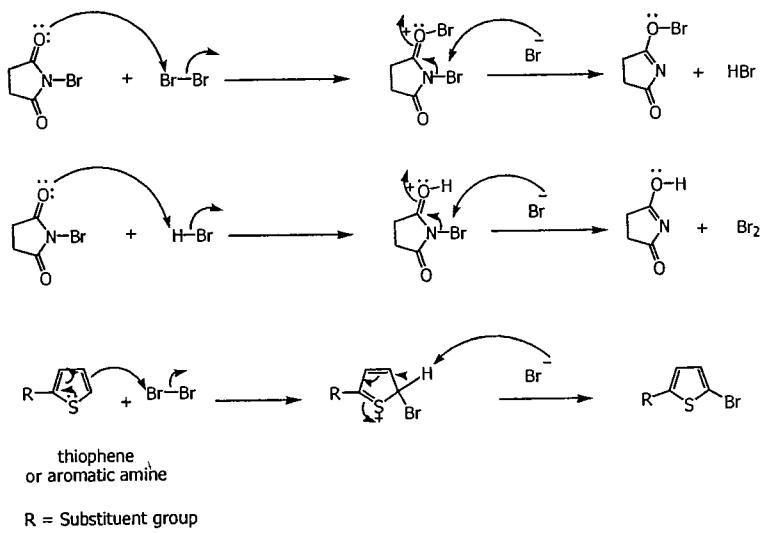

Figure 2.11 The proposed mechanism of bromination reaction by NBS.

To form the target oligomers **CFTnP** (n = 1-4) coupling each of the bromo-compound was treated with pyreneboronic acid under Suzuki cross-coupling reaction conditions.

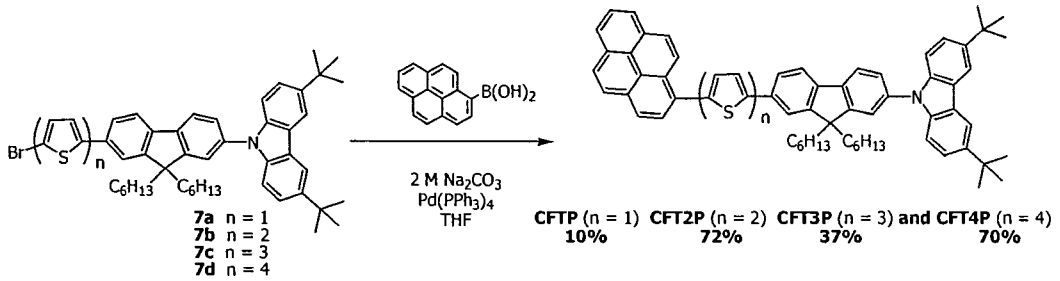

Figure 2.12 Suzuki cross-coupling reaction to form pyrene compound **CFTP, CFT2P, CFT3P** and **CFT4P.**

The chemical structures of **CFTP, CFT2P, CFT3P** and **CFT4P** were confirmed by ^{1}H-NMR and IR analysis. The ^{1}H-NMR spectra of the **CFTP, CFT2P, CFT3P** and **CFT4P** show doublet chemical shift 8.65 ppm assigning as the proton of 6-H of pyrene adduct. Moreover, IR spectrum reveal the adsorption at 2312 cm^{-1} whish is consistent with the presence of C-S bond and 1581 and 1487 cm^{-1} whish is consistent with the presence of C-C bond of aromatic.

2.3.2 Optical properties

The UV-vis and fluorescence spectra of dyes in CH_2Cl_2 and film spin coated on a quartz substrate are depicted in Table 2.1. The target molecule **CFP CFTP** and **CFT2P**, exhibited two absorption bands, covering from 298 to 349 nm and **CF3TP** and **CFT4P** exhibited three absorption band, covering from 298 to 435 nm as shown in Figure 2.13. The former absorption bands were assigned in terms of the strong absorption band as at longer wavelength corresponding to the π-π^* electron transition of the entire conjugated backbone and absorption band at 298 nm assigned to the π-π^* local electron transition of the end-capped carbazole units. The peak about 310-350 nm comes from the pyrene unit [89]. Peaks at longer wavelength were due to the absorption from pyrene-thiophene functioned fluorine at 349, 379, 401, 422 and 436 nm, respectively, which were considerably red-shift when increasing the number of thiophen ring. Such red-shift may due to the incorporation of the strong donating carbazole group at end. In the thin film, all compounds showed as expected, the intensity and absorption maxima of

the former bands of **CFTnP** (n = 0-4) progressively increased and were red-shifted with increasing number of thiophene unit. The fluorescence spectra of **CFTnP** (n = 0-4) solution and solid thin film shows red-shift about 8-35 nm compared to solution absorption, which can be attributed to the π-π^* transition of conjugation main chains. The phenomena indicated strong intermolecular aggregation existed film come from conjugated backbone. In solution, all of emission spectra range from 435 to 526 nm and increase as the conjugation in molecule increase, which located in the blue-orange region. The fluorescence quantum yields (Φ_F) of the fluorescence oligomers **CFTnP** (n = 0-4) in dilute dichloromethane solution range from 0.840 to 0.078 (Table 2.1). The result indicate that the fluorescence quantum yield of the oligomers decrease with the increasing number of thiophene units. As the number of thiophene ring increases, the molecule comeback large, planar π-conjugated structure and they are particularly vulnerable to π-stacking.

Table 2.1 Summary of the physical data of **CFTnP** (n = 0-4).

Compound	λ_{max} **(nm)**	λ_{max} **in thin film (nm)**	λ_{max} **of emission (nm)**		Φ_F
			Solution	**Thin film**	
CFP	349	351	407	443	0.840
CFTP	379	382	471	484	0.359
CFT2P	401	493	493	518	0.385
CFT3P	422	416	510	546	0.083
CFT4P	436	435	526	556	0.078

However, DSC curves of **CFT4P** behave totally different. In both first and second heating cycles, and endothermic phenomenon (T_g) at 113 °C was observed followed by an exothermic peak due to crystallization around 271 °C to give a crystal, which endothermically melted at 163 °C. There results indicate that the **CFT3P** and **CFT4P** is a semi-crystalline and **CFT4P** is a crystalline, with T_g increasing as the number of thiophene unit increase. The abilities of **CFP, CFTP** and **CFT2P** to form stable amorphous glasses, whereas **CFTnP** (n = 0-4) showed good thermal stability T_{dec} = 405, 420, 412, 443 and 388 °C, respectively, in nitrogen and the possibility and by solution casting are highly desirable for applications in OLEDs.

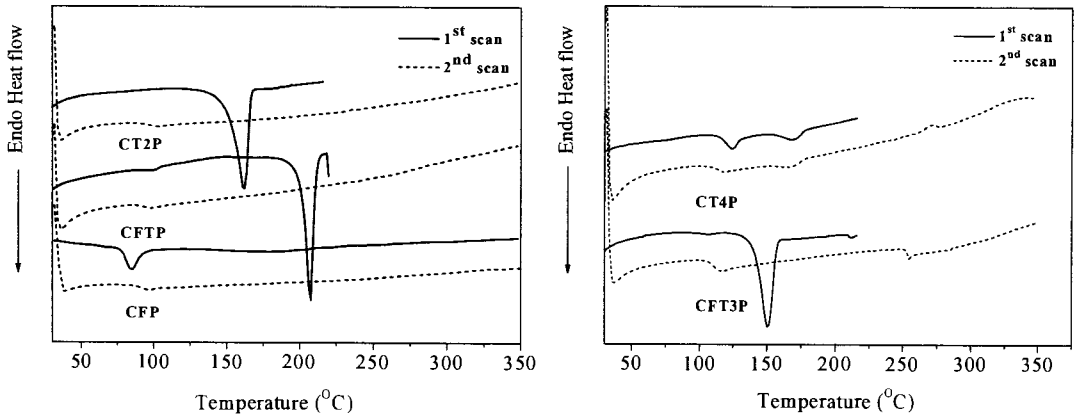

Figure 2.15 DSC thermograms of **CFTnP** (n = 0-4) measured at a heating rate of 10 °C/min under N_2.

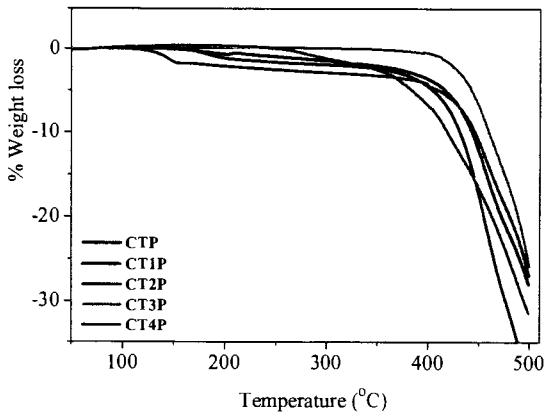

Figure 2.16 TGA thermograms of **CFTnP** (n = 0-4) measured at a heating rate of 10 °C/min under N_2.

Table 2.2 Thermal properties of **CFTnP** (n = 0-4).

Compound	Temperature (°C)			
	T_g	T_C	T_m	T_d
CFP	92	-	-	405
CFTP	93	-	-	420
CFT2P	94	-	-	415
CFT3P	110	-	253	443
CFT4P	113	163	271	388

2.3.3 Electrochemical properties

The redox properties and HOMO-LUMO energy levels of the target molecules **CTnP** (n = 0-4) were investigated using cyclic voltammetry (CV). The measurement was performed with a 1.0 mM solution of **CFTnP** (n = 0-4) in CH_2Cl_2 with the presence of tetrabutylammonium hexafluoro-phosphate (n-Bu_4NPF_6) as supporting electrolyte. The results are summarized in Table 2.3.

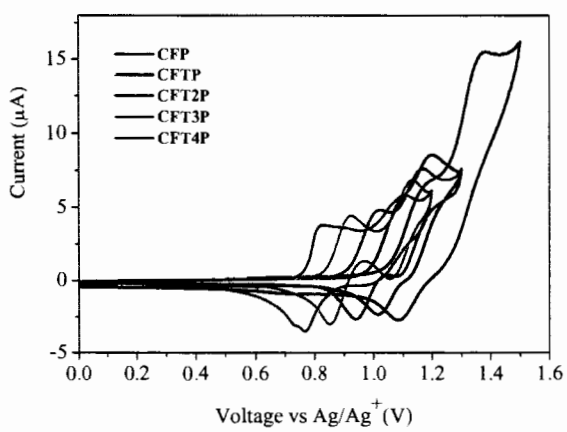

Figure 2.17 Cyclic voltammograms of **CFTnP** (n = 0-4) in dry CH_2Cl_2 with scan rate of 0.05 V/s and 0.1M n-Bu_4NPF_6 as electrolyte.

Cyclic voltammograms of **CFTnP** (n = 0-4) are shown in Figure 2.17. It shows two oxidation waves with half-wave potential ($E_{1/2}$) yielding cations and dications at 1.09 and 1.26 V, 1.01 and 1.15 V, 0.94 and 1.09 V , 0.85 and 1.06 V, 0.76 and 1.00 V, respectively.

However, under these experimental conditions no reduction process was observed in all cases. All the pyrene-oligothiophenes gave well defined CV curves with stable formation of both the radical cations and the dication, indicating as expected, the first oxidation process can be attributed to the removeal of electron from the peripheral of the carbazole unit and other reversible process corresponds to removal of electrons from the thiophene at the α and α' positions block the reactivity. It also shows similar wave in different scans, no distinct a slight shift of the CV curves was observed indicate *tert*-butyl group to protect a oxidation coupling at the 3, 6-positions peripheral carbazole moiety. which it has a good electrochemical property. During in order oxidation cycle of all compounds, the oxidation progressively shifted to lower energy with increasing the number of thiophene unit. The onset oxidation potentials (E_{ox}) of **CTnP** (n = 0-4) were estimated from the first anodic oxidation wave to be 1.01, 0.96, 0.89, 0.81 and 0.73, respectively. The HOMOs of all compounds were calculated, according to the following equation: HOMO = -(4.44 + E_{ox}) (eV), to be -5.52, -5.40, -5.33, -5.25 and -5.17 eV, respectively. The LUMOs of all compounds were calculated from the value of the energy gap and HOMO energy to be -2.35, -2.75, -2.82, -2.74 and -2.76 eV, respectively.

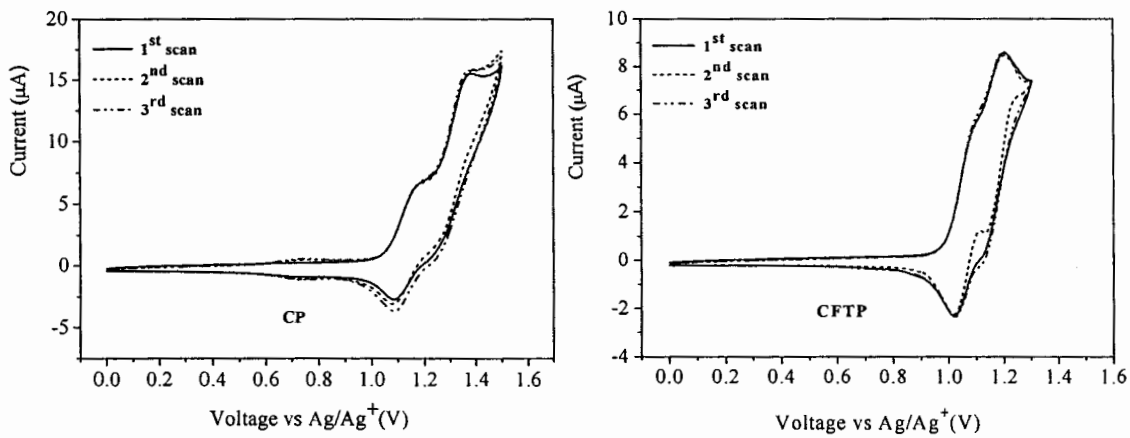

Figure 2.18 Cyclic voltammograms of **CFP** and **CFTP** in dry CH_2Cl_2 with scan rate of 0.05 V/s and 0.1 M *n*-Bu_4NPF_6 as electrolyte.

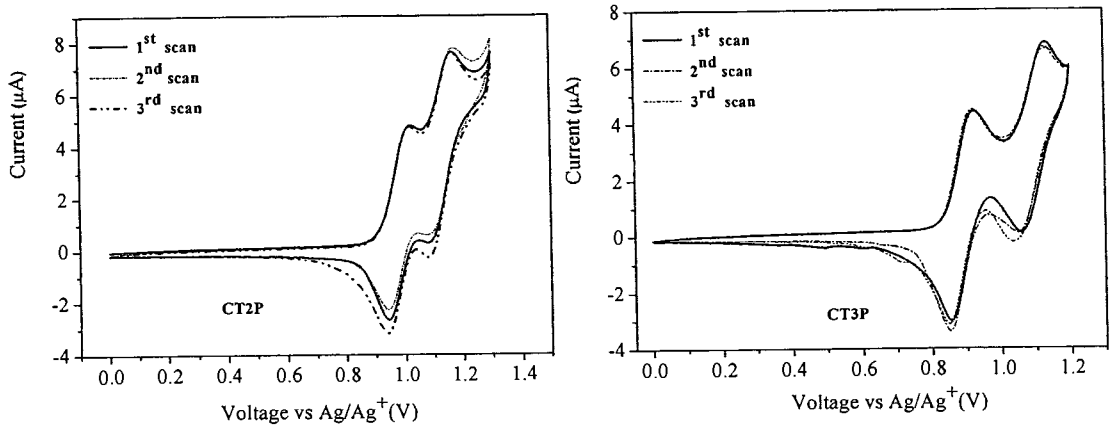

Figure 2.19 Cyclic voltammograms of **CFT2P** and **CFT3P** in dry CH_2Cl_2 with scan rate of 0.05 V/s and 0.1 M n-Bu_4NPF_6 as electrolyte.

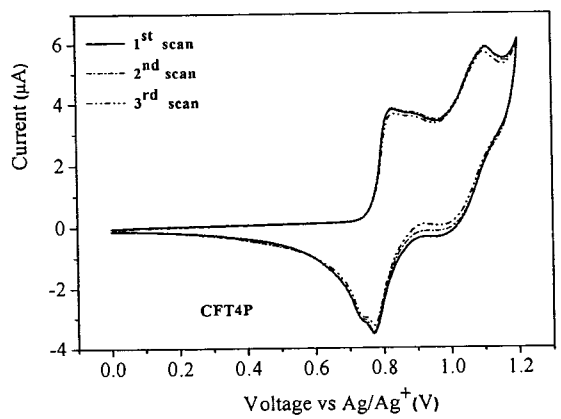

Figure 2.20 Cyclic voltammogram of **CFT4P** in dry CH_2Cl_2 with scan rate of 0.05 V/s and 0.1 M *n*-Bu_4NPF_6 as electrolyte.

2.3.4 Molecular orbital calculation

To get an insight into the molecular structure and electron distribution of the synthesized organic molecule, the **CFTnP** (n = 0-4) geometrics have been optimized using DFT calculations with Gaussian functional order 6-31G (d, p) basis set. Computed HOMO and LUMO distributions of **CFTnP** (n = 0-4) are depicted in Figure 2.20 and summary in Table 2.4. The HOMO is π-electrons delocalized over the entire conjugated backbone through the lone pair electron at the nitrogen atom of the carbazole, which is attributed to the asymmetric destabilization of the HOMO and LUMO energy levels leading to a decrease energy gap. In addition, the optimized geometries of **CFTnP** (n = 0-4) indicate that the carbazole moiety at the end of

the molecule are in 3-D spatal arrangement, which makes the molecular structure nonplanar structure due to the twist conformation around the carbazole-fluorene C-N bond. The nonplanar structures of **CFTnP** (n = 0-4) could be beneficial to solution-processability to form amorphous film. **CFTnP** (n = 0-4) are soluble in common organic solvents such as CH_3CN, CH_2Cl_2 and $CHCl_3$. High-quality amorphous film can be obtained by spin-coating its solution.

Table 2.3 The highest occupied molecular orbital (HOMO), lowest unoccupied molecular orbital (LUMO), and wave length at maximum adsorption (λ_{max}), for **CFTnP** (n = 0-4).

Compound	λ_{max}	Δ_{H-L} (eV)	**HOMO**[e] (eV)	**LUMO**[f] (eV)
CFP	393	3.45	-5.32	-1.87
CFTP	434	3.17	-5.22	-2.05
CFT2P	466	2.99	-5.13	-2.14
CFT3P	498	2.81	-5.04	-2.23
CFT4P	520	2.70	-4.99	-2.83

[e]Calculated using the empirical equation from HOMO = $-(4.44 + E_{onset})$, [f]Calculated from LUMO = HOMO + E_g

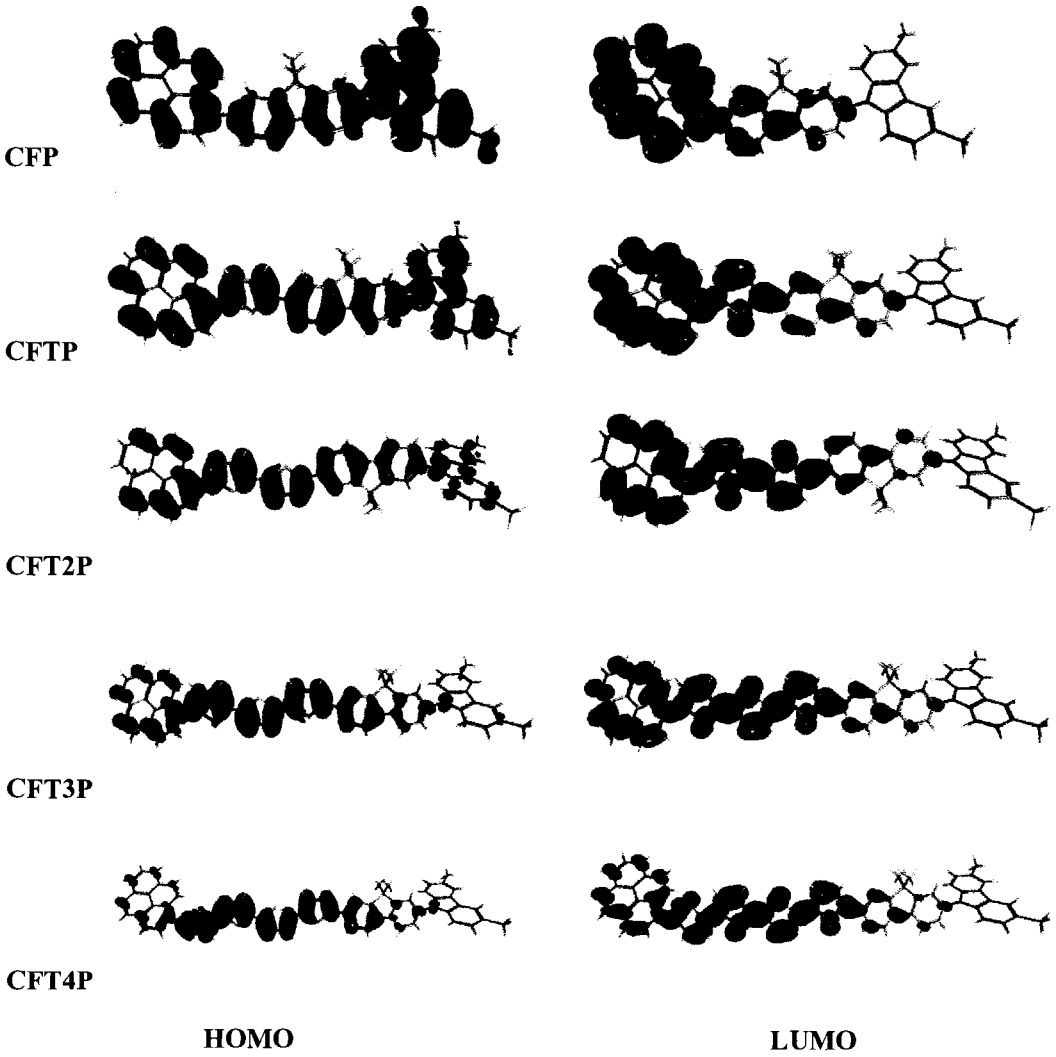

Figure 2.21 HOMO and LUMO distribution of the **CFTnP** (n = 0-4) calculated with DFT on a BTLYP/6-31G (d, p) level (Cont.).

2.3.5 Device performance of OLEDs based on CFTnP (n = 0-4)

In order to investigate their luminance properties, the double-layer OLED devices of ITO/PEDOT:PSS (50 nm)/**CFTnP** (13 nm) /BCP (7 nm)/LiF (0.5 nm):Al (200 nm) were fabricated using PEDOT:PSS as the hole-transporting layer (HTL), **CFTnP** (n = 0-4) as the light emitting and electron-transporting layer, indium tin oxide (ITO) as the anode and LiF:Al as the cathode. When a bias potential was applied to the electrode, the ITO/PEDOT:PSS/**CFTnP**/ BCP/LiF:Al devices were emitted in the blue to orange region as shown in Figure 2.22. The voltage-luminance and voltage-current density characteristic of the device are shown in Figure

2.23 and summarized in Table 2.5. The maximum luminance of the device was 31,760 cd/m^2 at an operating voltage of 9.8 V with a turn on voltage of 3 V.

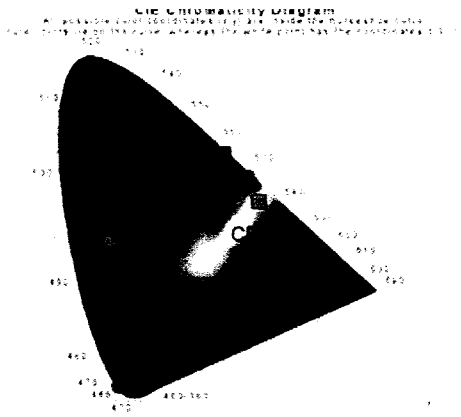

Figure 2.22 CIE coordinates of **CFTnP** (n = 1-4) devices.

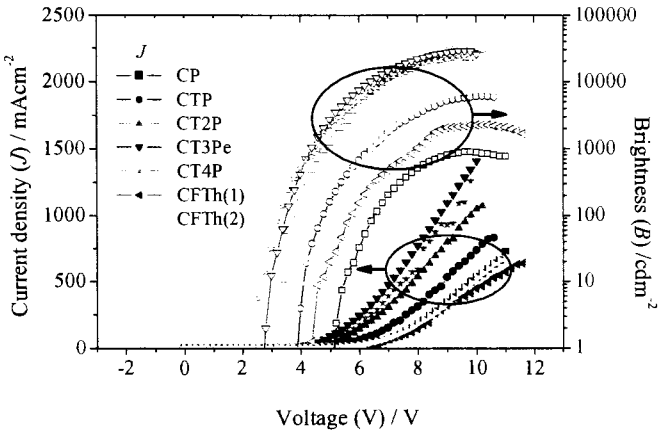

Figure 2.23 *J-V-L* curves of **CFTnP** (n = 1-4) devices.

Table 2.4 Physical datas of **CFTnP** (n = 0-4)[a].

Compound	E_{1o} (V)	E_{2o} (V)	E_g[d] (eV)	*HOMO*[e] (eV)	*LUMO*[f] (eV)
CFP	0.76	1.09	3.07	-5.42	-2.35
CFTP	1.00	1.01	2.65	-5.40	-2.75
CFT2P	0.85	1.15	2.51	-5.33	-2.82
CFT3P	1.06	1.09	2.51	-5.25	-2.74
CFT4P	0.94	1.26	2.41	-5.17	-2.76

[a]Measured using a platinum rod couter electrode, a glassy carbon electrode and a SCE reference electrode in CH_2Cl_2 containing *n*-Bu_4NPF_6 as a supporting electrolyte with scan rate of 0.05 V/s under argon atmosphere, [b]Peak potential, [c]Half-wave potential, [d]Estimated form the onset of the absorption spectra ($E_g = 1240/\lambda_{onset}$), [e]Calculated using the empirical equation from HOMO = -(4.44 + E_{onset}), [f]Calculated from LUMO = HOMO + E_g

Table 2.5 Photovoltaic performance of OLEDs base on **CFTnP** (n = 1-4).

Device	λ_{pl} film (nm)	λ_{el} (nm), $CIE_{x,y}$	Turn on (V)	V at max L. (V)	max. L (cd/m^2)	Cur. at max. L (*J*) (mA/cm^2)	Eff. at max. L (cd/A)	Ext. at max. L (%)	Max Eff. (cd/A)	Max Ext. (%)
CP	405	433m, 465 0.161, 0.148	5	9.6	898	455	0.20	0.04	0.32 (7V)	0.07 (7V)
CTP	473	479m, 497 0.159, 0.360	4	10.2	6033	781	0.77	0.08	1.14 (7V)	0.12 (7V)
CT2P	493	513m, 540 0.285, 0.609	3	9.8	31760	1004	3.16	0.13	3.73 (7.6)	0.16 (7.6)
CT3P	513	531 0.374, 0.591	2.8	9.6	28722	1285	2.24	0.09	3.11 (5.8V)	0.13 (5.8V)
CT4P	527	549m, 581 0.448, 0.539	2.6	9.4	24096	1090	2.21	0.09	3.06 (4.6V)	0.13 (4.6V)
CFTh1	443, 470	443, 470m 0.145, 0.190	4.4	9.8	2248	411	0.55	0.09	0.72 (7.2)	0.12 (7.2)
CFTh2	484, 512	484, 512 0.194, 0.516	3.8	10.2	7277	564	1.29	0.08	2.48 (6.4V)	0.16 (6.4V)

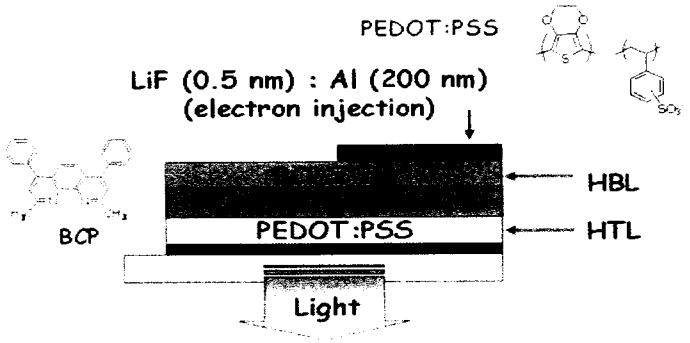

Figure 2.24 Structure of multi-layer OLED devices.

2.4 Conclusion

Pyrene-oligothiophenes were synthesized by using Suzuki cross-coupling reaction of pyrene boronic acid and corresponding bromo-compounds to give **CFTnP** (n = 0-4). Pyrene-oligothiophenes have good electrochemical stability and thermal stability. Their electronic properties are variable depending on a number of thiophene units. The fluorescence quantum yields (Φ_F) of the fluorescence oligomer **CFTnP** (n = 0-4) in dilute CH_2Cl_2 solution range from 0.84 to 0.078 and decrease as the conjugation in molecule increase. The OLED devices using **CFTnP** (n = 0-4) as emissive layers were fabricated. In the device work, the **CFTnP** (n = 0-4) show blue-orange emission with high brightness and efficiency.

CHAPTER 3

SYNTHESIS AND CHARACTERIZATION OF A NOVEL CARBAZOLE END-CAPPED-α,α′-BIS(9,9-BIS-*n*-HEXYLFLUORENYL)-SUBSTITUTED OLIGOTHIOPHENES

3.1 Introduction

π-Conjugated small molecules have attracted much attention in area of organic chemistry and material science. They have some very interesting electronic and optical properties and have been interested as advanced molecular electronic materials [89-91]. π-Conjugated thiophene-based oligomers are that their physical properties can be easily tuned to the desired properties by changing the structure such as solubilizing chain, end capping groups, insertion of contain groups, and different oligomer length. Oligothiophenes with different terminal α, α′ substituents such as aldehyde, diphenylamine, cyclophane, pyrene, bis(4-methylphenyl)-aminophenyl, cyclohexene, ethylenedithio, and phenyl groups are a growing synthetic interest. Recently, a series of oligothiophenes terminated with fluorene moieties have also been synthesized using Suzuki cross coupling reaction and Stille coupling reaction or nickel-catalyzed reductive dimerization. These materials exhibited interesting optical and electrochemical properties and have been shown to act as potential light-emitting materials in OLEDs [92] and active components in OFETs [93]. Carbazole has strong absorption in the near-UV region and a low redox potential. The electrochemical and spectroscopic properties of carbazole and its derivative have been extensively investigated. Chemically, carbazole can be easily functionalized at its 3-, 6- or 9-positions and covalently linked to other molecular moieties. Due to its unique optical, electrical, and chemical properties, carbazole has been used widely as a functional building block or substituent in the construction of organic molecules for use as light-emitting and hole-transporting layers in OLED devices, as host materials for electrophosphorescent applications, and as active components in solar cells. Moreover, the thermal stability and glassy state durability of the organic molecules were found to be significantly improved upon incorporation of a carbazole moiety into the structure.

3.2 Aim of the study

We designed a novel π-conjugate of *N*-carbazole end-capped oligofluorene-thiophene based on carbazole as the donor group, Chemically, carbazole can be easily functionalized at its 3,6-positions with a bulky group of *tert*-butyl moiety to protect the oxidation coupling at the 3, 6-positions of the peripheral carbazole moiety. Fluorene was introduced on *N*-9 of carbazole as electron transport moiety. The *n*-hexyl substituents were introduced on the C-9 position of fluorene ring to increase the solubility, with a thiophene linker, with zero, two, four, six and eight thiophene ring were synthesized using stille coupling reaction. The fluorene-substituted oligothiophenes with longer oligothiophene chains still remain to be explored as color turnable light-emitting for OLEDs Their basic optical, electrochemical, and thermal properties have been investigated.

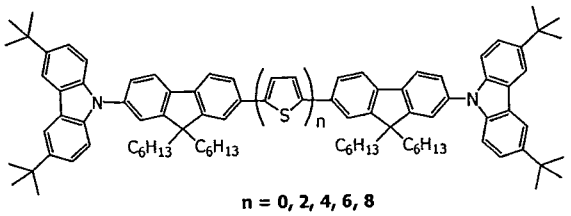

Figure 3.1 Chemical structures of **BCFnT** (n = 0, 2, 4, 6, 8).

3.3 Results and discussion

3.3.1 Synthesis

Suzuki cross-coupling reaction of 2-thiophenboronic acid and 9-(7-bromo-9, 9-dihexyl-*9H*-fluoren-2-yl)-3,6-di-tert-butyl-*9H*-carbazole (7) employed in order to increase the number of thiophene units in the molecules. **BCF**, were prepared by using $Pd(PPh_3)_4$ as catalyst in the presence of aqueous sodium carbonate solution in THF at refluxing temperature afforded the thiophene adduct in 15 % yield as show in Figure 3.2.

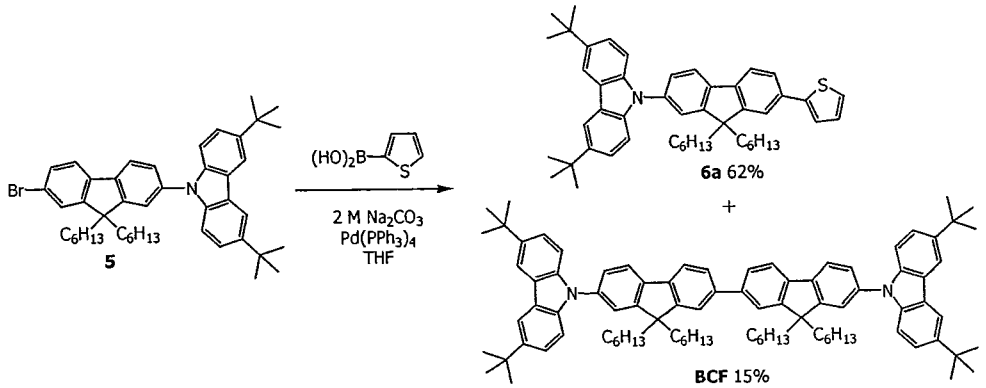

Figure 3.2 Suzuki cross-coupling reaction to form **6a** and **BCF**.

The chemical structure of **BCF** was confirm by ^{1}H-NMR analysis. The ^{1}H-NMR spectrum of the product **BCF** shows a singlet signal at chemical shift 8.19 pm (4H) assigning as 4-H and 5-H of carbazole adduct, a doublet signal at chemical shift 7.45-7.42 ppm (4H, J= 8.7 Hz) assigning as 1-H and 8-H of fluorene .

Stille coupling reaction of 3,6-di-*tert*-butyl-9-(2-(5-bromothiophen-2-yl)-9, 9-dihexyl-*9H*-fluoren-7-yl)-*9H*-carbazole is a versatile C-C bond forming reaction between stannanes and halide, with very few limitations on the aryl group. Well-elaborated methods allow the preparation of different products from all of the combination of halides and stannanes depicted below.

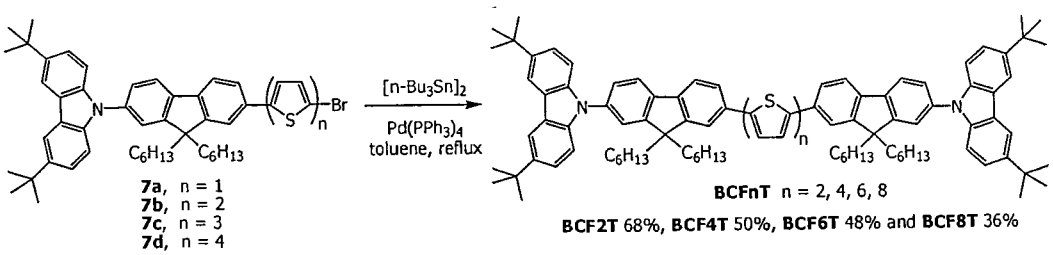

Figure 3.3 Stille coupling reaction to form **BCFnT** (n = 0, 2, 4, 6, 8).

The proposed mechanism of Stille coupling reaction is shown in Figure 3.4.

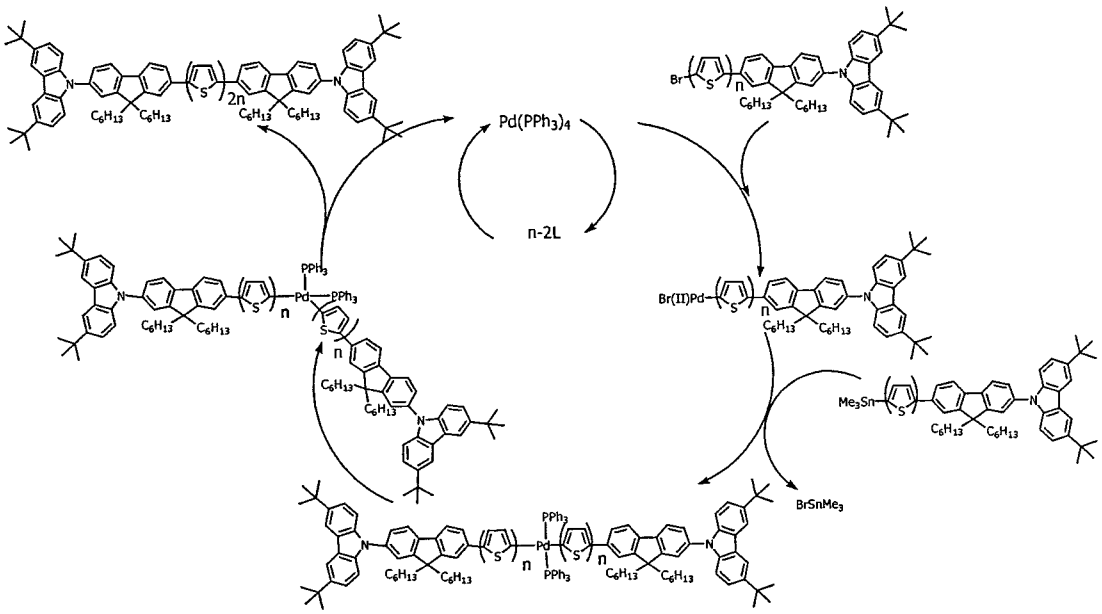

Figure 3.4 The proposed mechanism of Stille coupling reaction of **BCFnT** (n = 0, 2, 4, 6, 8).

The chemical structures of **BCFnT** (n = 2, 4, 6, 8) were confirm by ^{1}H-NMR, and Mass analysis. The ^{1}H-NMR spectrum of the product **BCFnT** (n = 2, 4, 6, 8) shows a singlet signal at chemical shift 8.17 ppm (4H) assigning as 4-H and 5-H of carbazole adduct, a doublet signal at chemical shift 7.89-7.74 ppm (4H, J = 8.4 Hz) assigning as 1-H and 8-H of fluorene and a multiplet at chemical shift 7.26-7.11 ppm assigning as a proton of thiophene unit. HRMS-ESI calcd for **BCF2T**, **BCF4T**, **BCF6T** and **BCF8T** : *m/z* 1368.113, 1550.3604, 1714.6078 and 1878.8551 founds 1386.036, 1551.1836, 1716.016 and 1879.867, respectively.

3.3.2 Optical properties

The optical properties of the **BCFnT** (n = 0, 2, 4, 6, 8) were investigated using UV-vis absorption and photoluminescence (PL) spectroscopy in dilute CH_2Cl_2 solution. The result are depicted in Figure 3.5 and summarized in Table 3.1. The absorption spectra of all the compounds showed two major absorption bands, an absorption band at 298 nm assigned to the π-π^* local electron transition of the end-capped carbazole unit, the medium intense absorption band originating from the π-π^* local electron transition of the individual fluorene unit and a broader absorption band at longer wavelength corresponding to the π-π^* electron transition of

the entire π-conjugated backbone. The absorption maxima of the latter band of **BCFnT** (n = 0, 2, 4, 6, 8) are progressively red-shift with the increasing number of thiophene ring as the extent of the π-conjugated system in the oligomer increases. Compounds **BCFnT** (n = 0, 2, 4, 6, 8) exhibited the longest wavelength absorption at 356, 407, 444, 460 and 466 nm, respectively. In the thin film, **BCFnT** (n = 0, 2, 4, 6, 8) show red-shift peak compared with solution, with can be attributed to the π-π^* of conjugated main chains. However, the absorption maxima were considerably red-shifted in comparison to those of the parent unend-capped bithiophene (405 nm), quaterthiophene (442 nm), sexithiophene (462 nm) [94] and eightthiophene (484nm) [95] indicating the formation of a highly extended π-electron delocalization system through the fluorene carbazole end-capped. The energy band gap of **BCFnT** (n = 0, 2, 4, 6, 8) were estimated to be 3.11, 2.58, 2.36, 2.28 and 2.21 eV, respectively, from the absorption edge of the solution, decrease with the increase of the π-conjugation length of the oligothiophene segments. All compounds **BCFnT** (n = 0, 2, 4, 6, 8) in this study are highly fluorescent with the color of fluorescence ranging from bright blue to bright red. The fluorescence quantum yields (Φ_F) of the fluorescence oligomer **BCFnT** (n = 0, 2, 4, 6, 8) in dilute dichloromethane solution range from 0.158 to 0.023 (Table 3.1). The result indicate that the fluorescence quantum yields of the oligomer decrease with the increasing number of thiophene units. As the number of thiophene ring increases, π-conjugated structure are particularly vulnerable to π-stacking. Thus that molecule can form π-stack there is a strong tendency toward reduced fluorescence quantum yields. The photoluminescence (PL) spectra of **BCFnT** (n = 0, 2, 4, 6, 8) showed an increasing red-shift of the maxima emission peak with an increase in the number of thiophene rings. The PL spectrum of **BCF** is characterized by one well-defined emission peak at 406 nm. The PL spectrum of **BCF2T** is characterized by two well-defined emission peak at 475 and 502 nm. However, these appeared as a shoulder for compound **BCF4T**, **BCF6T** and **BCF8T** shows well- defined emission peak at 519, 538 and 549 nm. This indicates the existence of a broad distribution of the ground and excited state molecular conformations for both compounds.

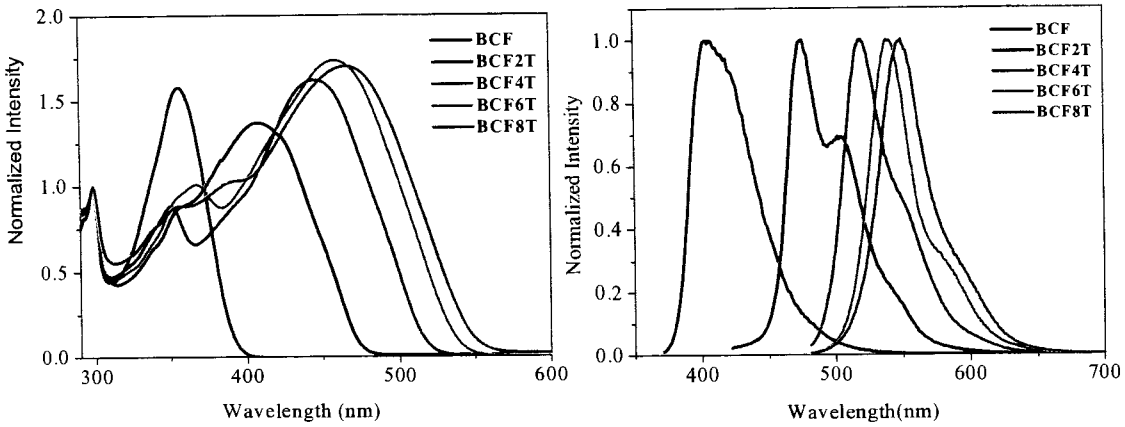

Figure 3.5 Absorption spectra and PL spectra of **BCFnT** (n = 0, 2, 4, 6, 8) in dry CH_2Cl_2 solution.

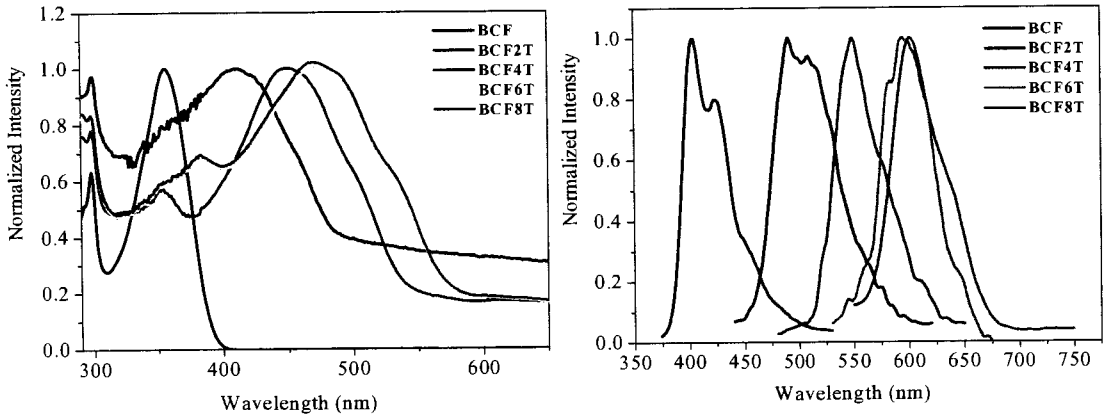

Figure 3.6 Absorption spectra and PL spectra of **BCFnT** (n = 0, 2, 4, 6, 8) on thin film.

Table 3.1 The absorption and fluorescence data of **BCFnT** (n = 0, 2, 4, 6, 8).

Compound	λ_{max} (nm)	λ_{max} in thin film (nm)	λ_{max} of emission in CH_2Cl_2 (nm)		Φ_F
			Solution	Thin film	
BCF	298, 356	298, 356	404	404, 423	0.130
BCF2T	298, 407	298, 411	475, 502	491	0.158
BCF4T	298, 350, 444	298, 448	519	549	0.156
BCF6T	298, 367, 459	298, 470	538	595	0.078
BCF8T	298, 356, 392, 465	298, 482	549	601	0.023

3.3.2 Thermal properties

For OLED application, thermal stability of organic materials is crucial for device stability and lifetime. The thermal instability or low glass transition temperature (T_g) of the amorphous organic layer may result in the degradation of organic devices due to morphological changes. The thermal properties of the **BCFnT** (n = 0, 2, 4, 6, 8) were determinate by DSC and TGA analysis (Figure 3.7) with a heating rate of 10 °C/min under a nitrogen atmosphere. DSC curves of all compound **BCFnT** (n = 0, 2, 4, 6, 8) show T_g at 156, 140, 136, 139 and 159 °C, respectively, in first and second heating cycles. There results indicate that the **BCFnT** (n = 0, 2, 4, 6, 8) are sem-crystalline with T_g increasing as the number of thiophene unit increase. The ability of **BCFnT** (n = 0, 2, 4, 6, 8) to form stable amorphous glasses, whereas **BCFnT** (n = 0, 2, 4, 6, 8) showed good thermal stability T_{dec} of 372, 371, 288, 217 and 362 °C, respectively, in nitrogen and the possibility and by solution casting are highly desirable for applications in OLEDs.

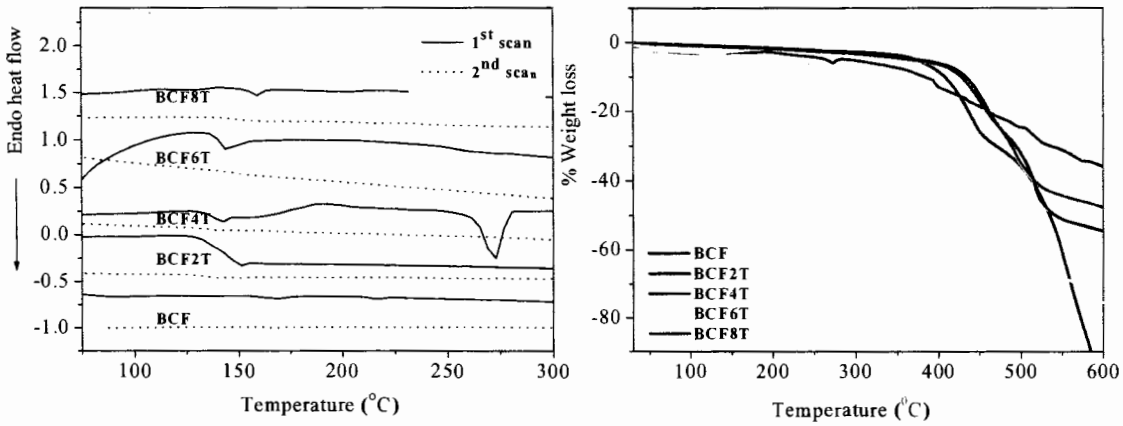

Figure 3.7 DSC and TGA of **CFnTFC** (n = 0, 2, 4, 6, 8) measured at a heating rate of 10°C/min uder N_2.

Table 3.2 Thermal properties of **BCFnT** (n = 0, 2, 4, 6, 8).

Compound	Temperature (°C)			
	T_g	T_C	T_m	T_d
BCF	**156**	**-**	**-**	**372**
BCF2T	**140**	**-**	**151**	**371**
BCF4T	**136**	**-**	**273**	**288**
BCF6T	**139**	**-**	**331**	**217**
BCF8T	**159**	**-**	**305**	**362**

3.3.3 Electrochemical properties

In order to investigate the electrochemical behavior of **BCFnT** (n = 0, 2, 4, 6, 8) cyclic voltammetry (CV) measurements were performed in dichloromethane containing 0.1 M *n*-Bu_4NPF_6 as a supporting electrolyte. The results are shown in Figure 3.8 and summarized in Table 3.3. The CV curves of **BCF** demonstrated one oxidation waves with half-wave potential ($E_{1/2}$) yielding radical cation and dications at 1.13 V. The CV curve of **BCF4T** and **BCF8T** demonstrated three oxidation waves with half-wave potential ($E_{1/2}$) yielding radical cation and dications at 0.80, 1.01 and 1.71 V, 0.69, 1.19 and 1.48 V, respectively. The CV curve of **BCF2T** and **BCF6T** demonstrated four oxidation waves with half-wave potential ($E_{1/2}$) yielding radical cation and dications at 0.95, 1.10, 1.22 and 1.56 V, 0.71, 0.95, 1.16 and 1.46 V, respectively.

However, under these experimental conditions no reduction process was observed in all case. All the carbazole-oligothiophene gave well defined CV curves with stable formation of both the radical cations and the dication, indicating as expected, the first oxidation process can be attributed to the removeal of electron from the peripheral of the carbazole unit and other reversible process corresponds to removal of electrons from the thiophene at the α and α' positions block the reactivity. It also shows similar wave in different scan no distinct a slight shift of the CV curves was observed indicate *tert*-butyl group to protect a oxidation coupling at the 3,6-positions peripheral carbazole moiety, which it has a good electrochemical property. During in order oxidation cycle of all compounds, the oxidation progressively shifted to lower energy with increasing the number of thiophene unit. The onset oxidation potentials (E_{ox}) of **BCFnT** (n = 0, 2, 4, 6, 8) were estimated from the first anodic oxidation wave to be 1.07, 0.91, 0.75, 0.71 and 0.65, respectively. The HOMO of all compound were calculated, according to the following equation: HOMOs = -(4.44 + E_{ox}) (eV), to be -5.51, -5.35, -5.19, -5.11 and -5.09 eV, respectively. The LUMO of all compound were calculated from the value of the energy gap and HOMO energy to be -2.40, -2.77, -2.83, -2.83 and -2.88 eV, respectively.

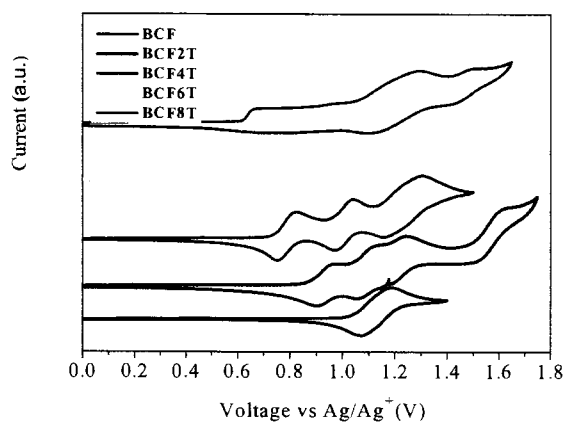

Figure 3.8 Cyclic voltammograms of **BCFnT** (n = 0, 2, 4, 6, 8) in dry CH_2Cl_2 with scan rate of 0.05 V/s and 0.1M *n*-Bu_4NPF_6 as electrolyte.

Cyclic voltammogram of **BCF** was analyzed in CH_2Cl_2 with scan rate of 0.05 V/s and 0.1 M *n*-Bu_4NPF_6 as electrolyte, detected one oxidation peaks as show in Figure 3.9. It shows one oxidation with half-wave potentials ($E_{1/2}$) of 1.13 V, which are assigned as the formation 3,6-di-(*tert*-butyl)carbazole cation. **BCF** gave well defined CV curves with stable

formation of both the radical cations and the dication. It also shows a similar wave in difference scans no distinct a slight shift of the CV curves was observed indicate *tert*-butyl group to protect a oxidation coupling at the 3,6-positions peripheral carbazole moiety, indicating a good and electrochemical property. However, under these experimental conditions no reduction process was observed. At first anodic scan, oxidation wave at lower potential 1.07 V was observed. The HOMO calculated, according to the following equation: HOMO = -(4.44 + E_{ox}) (eV), to be -5.51 eV. The LUMO was calculated from the value of the energy gap (3.11 eV) and HOMO energy level to be -2.40 eV.

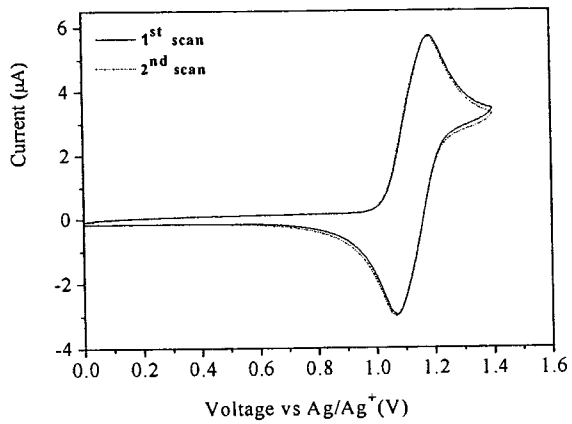

Figure 3.9 Cyclic voltammogram of **BCF** in dry CH_2Cl_2 with scan rate of 0.05 V/s and 0.1 M *n*-Bu_4NPF_6 as electrolyte.

Cyclic voltammogram of **BCF2T** was analyzed in CH_2Cl_2 with scan rate of 0.05 V/s and 0.1 M *n*-Bu_4NPF_6 as electrolyte, detected one oxidation peaks as show in Figure 3.10. It shows four oxidation with half-wave potentials ($E_{1/2}$) of 0.95, 1.10, 1.22 and 1.56 V, which are assigned as the formation 3,6-di-(*tert*-butyl)carbazole cation. **BCF2T** gave well defined CV curves with stable formation of both the radical cations and the dication, indicating as expected, that the thiophene at the α and α′ positions block the reactivity. It also shows a similar wave in difference no distinct a slight shift of the CV curves was observed indicate *tert*-butyl group to protect a oxidation coupling at the 3,6-positions peripheral carbazole moiety, indicating a good and electrochemical property. However, under these experimental conditions no reduction process was observed. At first anodic scan, oxidation wave at lower potential 0.91 V was observed. The HOMO calculated, according to the following equation: HOMO = -(4.44 + E_{ox})

(eV), to be -5.35 eV. The LUMO was calculated from the value of the energy gap (2.58 eV) and HOMO energy level to be -2.77 eV.

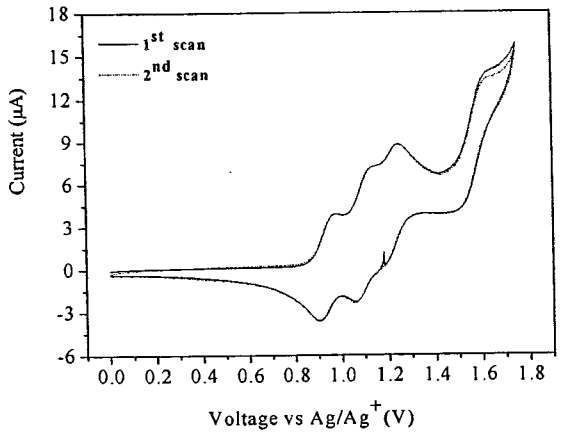

Figure 3.10 Cyclic voltammogram of **BCF2T** in dry CH_2Cl_2 with scan rate of 0.05 V/s and 0.1 M *n*-Bu_4NPF_6 as electrolyte.

Cyclic voltammogram of **BCF4T** was analyzed in CH_2Cl_2 with scan rate of 0.05 V/s and 0.1 M *n*-Bu_4NPF_6 as electrolyte, detected one oxidation peaks as show in Figure 3.11. It shows one oxidation with half-wave potentials ($E_{1/2}$) of 0.80, 1.01 and 1.71 V, which are assigned as the formation 3,6-di-(*tert*-butyl)carbazole cation. **BCF4T** gave well defined CV curves with stable formation of both the radical cations and the dication, indicating as expected, that the thiophene at the α and α' positions block the reactivity. The proposed oxidation mechanism for π-conjugated thiophene system was illustrated in Figure 3.12 It also shows a similar wave in difference scans no distinct a slight shift of the CV curves was observed indicate *tert*-butyl group to protect a oxidation coupling at the 3,6-positions peripheral carbazole moiety, indicating a good and electrochemical property. However, under these experimental conditions no reduction process was observed. At first anodic scan, oxidation wave at lower potential 0.75 V was observed. The HOMO calculated, according to the following equation: HOMO = -(4.44 + E_{ox}) (eV), to be -5.19 eV. The LUMO was calculated from the value of the energy gap (2.36 eV) and HOMO energy level to be -2.83 eV.

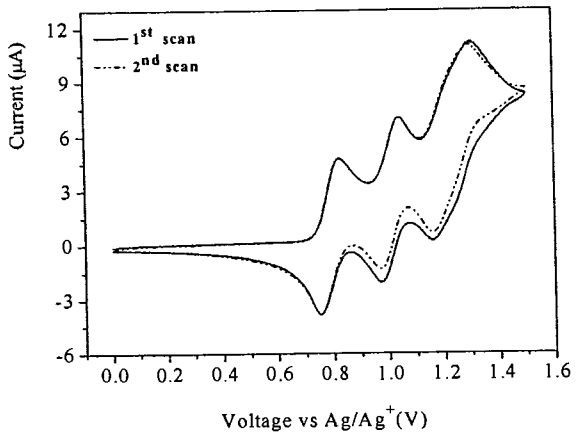

Figure 3.11 Cyclic voltammogram of **BCF4T** in dry CH_2Cl_2 with scan rate of 0.05 V/s and 0.1 M n-Bu_4NPF_6 as electrolyte.

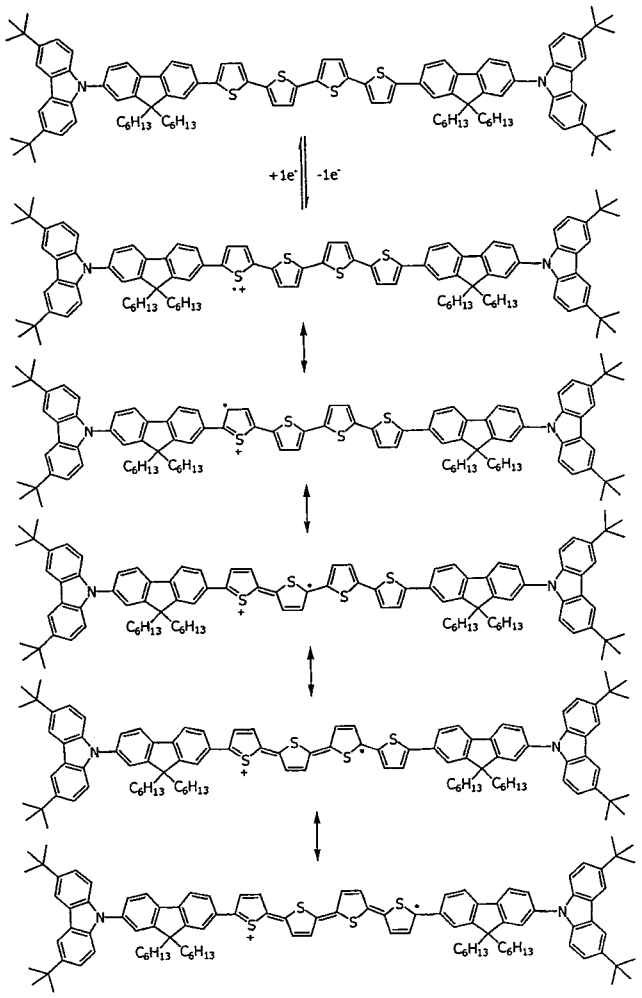

Figure 3.12 The proposed oxidation mechanism for π-conjugated thiophene system.

Cyclic voltammogram of **BCF6T** was analyzed in CH_2Cl_2 with scan rate of 0.05 V/s and 0.1 M n-Bu_4NPF_6 as electrolyte, detected one oxidation peaks as show in Figure 3.12. It shows one oxidation with half-wave potentials ($E_{1/2}$) of 0.71, 0.95, 1.16 and 1.46 V, which are assigned as the formation 3,6-di-(*tert*-butyl)carbazole cation. **BCF6T** gave well defined CV curves with stable formation of both the radical cations and the dication, indicating as expected, that the thiophene at the α and α' positions block the reactivity. The proposed oxidation mechanism oxidation mechanism for π-conjugated thiophene system was described for **BCF4T.** It also shows a similar wave in difference scans no distinct a slight shift of the CV curves was observed indicate *tert*-butyl group to protect a oxidation coupling at the 3,6-positions peripheral carbazole moiety, indicating a good and electrochemical property. However, under these experimental conditions no reduction process was observed. At first anodic scan, oxidation wave at lower potential 0.67 V was observed. The HOMO calculated, according to the following equation: HOMO = -(4.44 + E_{ox}) (eV), to be -5.11 eV. The LUMO was calculated from the value of the energy gap (2.28 eV) and HOMO energy level to be -2.83 eV.

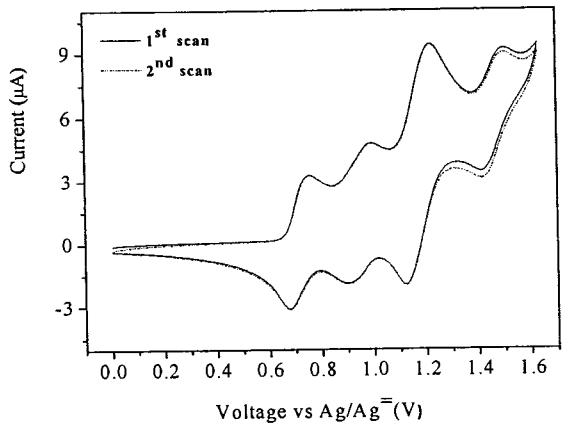

Figure 3.13 Cyclic voltammogram of **BCF6T** in dry CH_2Cl_2 with scan rate of 0.05 V/s and 0.1 M n-Bu_4NPF_6 as electrolyte.

Table 3.3 Physical datas of **BCFnT** (n = 0, 2, 4, 6, 8)[a].

Compound	E_{1o} (V)	E_{2o} (V)	E_{3o} (V)	E_{4o} (V)	E_g[d] (eV)	HOMO[e] (eV)	LUMO[f] (eV)
BCF	1.07	-	-	-	3.11	-5.51	-2.40
BCF2T	0.91	1.06	1.19	1.49	2.58	-5.35	-2.77
BCF4T	0.75	0.98	1.16	-	2.36	-5.19	-2.83
BCF6T	0.67	0.90	1.11	1.42	2.28	-5.11	-2.83
BCF8T	0.65	1.09	1.42	-	2.21	-5.09	-2.88

[a]Measured using a platinum rod couter electrode, a glassy carbon electrode and a SCE reference electrode in CH_2Cl_2 containing *n*-Bu_4NPF_6 as a supporting electrolyte with scan rate of 0.05 V/s under argon atmosphere, [b]Peak potential, [c]Half-wave potential, [d]Estimated form the onset of the absorption spectra ($E_g = 1240/\lambda_{onset}$), [e]Calculated using the empirical equation from HOMO = -(4.44 + E_{onset}), [f]Calculated from LUMO = HOMO + E_g

Cyclic voltammogram of **BCF8T** was analyzed in CH_2Cl_2 with scan rate of 0.05 V/s and 0.1 M *n*-Bu_4NPF_6 as electrolyte, detected one oxidation peaks as show in Figure 3.13. It shows one oxidation with half-wave potentials ($E_{1/2}$) of 0.69, 1.19 and 1.48 V, which are assigned as the formation 3,6-di-(*tert*-butyl)carbazole cation. **BCF8T** gave well defined CV curves with stable formation of both the radical cations and the dication, indicating as expected, that the thiophene at the α and α' positions block the reactivity. The proposed oxidation mechanism oxidation mechanism for π-conjugated thiophene system was described for **BCF4T.** It also shows a similar wave in difference scans, indicating a good and electrochemical property. However, under these experimental conditions no reduction process was observed. At first anodic scan, oxidation wave at lower potential 0.65 V was observed. The HOMO calculated, according to the following equation: HOMO = -(4.44 + E_{ox}) (eV), to be -5.09 eV. The LUMO was calculated from the value of the energy gap (2.21 eV) and HOMO energy level to be -2.88 eV.

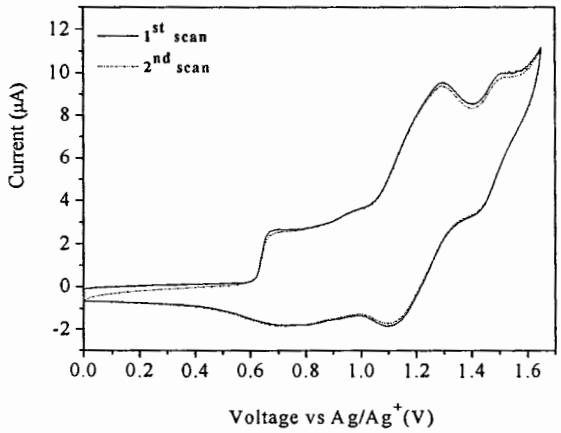

Figure 3.14 Cyclic voltammogram of **BCF8T** in dry CH_2Cl_2 with scan rate of 0.05 V/s and 0.1 M *n*-Bu_4NPF_6 as electrolyte.

3.3.4 Molecular orbital calculation

The optimum geometrires and electron-state-density distributions of the HOMO and LUMO of **BCFnT** (n = 0, 2, 4, 6, 8) were calculated by using DFT calculation with Gaussian 03 program. The calculations were performed with the BTLYP exchange correlation functional under 6-31D(d,p) basic set. Figure 3.15 shows the optimum geometries and the electron-state-density distributed of the HOMO and LUMO of **BCFnT** (n = 0, 2, 4, 6, 8) molecules. The HOMO state density mainly distributed on the carbazole moiety with some extending to the fluorene unit of the molecule.

The electron density of LUMO was mainly localized at the thiophene moiety. Besides, the optimized geometry of the **BCFnT** (n = 0, 2, 4, 6, 8) indicates that the carbazole moiety at the end of molecule are in 3-D spatial arrangement, which makes the molecular structure nonplanar. The nonplanar molecule structure of **BCFnT** (n = 0, 2, 4, 6, 8) could be beneficial to solution processability to form amorphous film. **BCFnT** (n = 0, 2, 4, 6, 8) are soluble in common organic solvents such as CH_2Cl_2, $CHCl_3$ and acetonitrile. High-quality amorphous film can be obtained by spin-coating its solution. The HOMO-LUMO energy gaps (E_g) of **BCFnT** (n = 0, 2, 4, 6, 8) (Table 3.3), estimated from the onset absorption edge, decrease with the increase of the π-conjugated length of the oligothio-phene segments.

All of the oligothiophenes **BCFnT** (n = 0, 2, 4, 6, 8) in this study are highly fluorescent with the color of the fluorescence ranging from bright blue to bright orange. The fluorescence quantum yields (Φ_F) of the fluoresce oligomers **BCFnT** (n = 0, 2, 4, 6, 8) in dilute CH_2Cl_2 solution range from 0.03-0.15. The results indicate that the fluorescence quantum yields of the oligomers decrease with the increasing number of thiophene units, as commonly observed in most case with oligothiophene derivatives.

Table 3.4 The Highest occupied molecular orbital (HOMO), lowest unoccupied molecular orbital (LUMO),and wave length at maximum absorption (λ_{max}) for **BCFnT** (n = 0, 2, 4, 6, 8).

Compound	λ_{max} **(nm)**	Δ_{H-L} **(eV)**	HOMO[e] **(eV)**	LUMO[f] **(eV)**
BCF2T	465	3.01	-5.12	-2.11
BCF4T	539	2.61	-4.96	-2.35
BCF6T	581	2.45	-4.89	-2.44
BCF8T	613	2.35	-4.85	-2.50

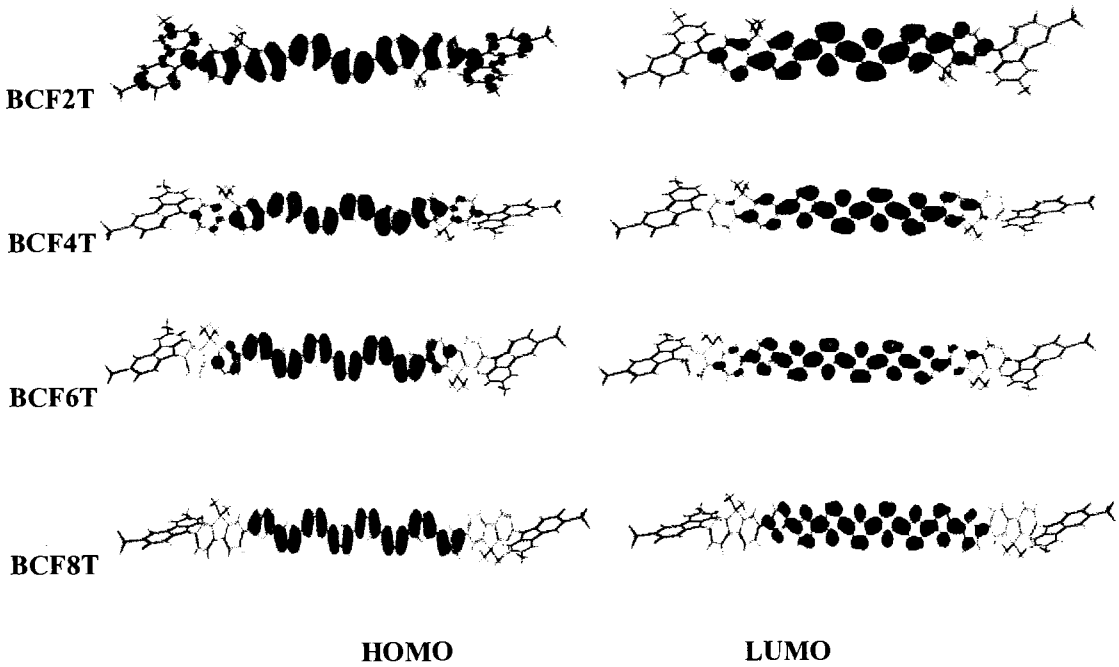

Figure 3.15 HOMO and LUMO distribution of the **BCFnT** (n = 0, 2, 4, 6, 8) dyes calculated with DFT on a BTLYP/6-31G (d,p) level.

3.4 Conclusion

A series of new α,α'-bis(9,9-bis-n-hexylfluorenyl)-substituted oligothiophenes were synthesized by using Stille coupling reaction of bromo-oligothiophenes with 0-, 2-, 4-, 6- and 8-thiophene units and their physical properties were investigated. The presence of 9,9-bis-n-hexylfluorene rings at both ends of the oligothiophenes had significant effects on the solubility allowing longer oligomers, up to the hexamer, to be prepared and blocking the reactive α,α'-positions of the thiophene moieties. The optical and electrochemical investigations revealed an electronic interaction between the carbazole-fluorene moieties and the oligothiophene chains. The fluorescence quantum yields (Φ_F) of the fluorescence oligomer **BCFnT** (n = 0, 2, 4, 6, 8) in dilute CH_2Cl_2 solution range from 0.023 to 0.158 and decrease as the conjugation in molecule increase. The thermal properties of these materials are enhanced with the increasing number of thiophene rings. These oligothiophene derivatives display strong fluorescence and should be promising materials for OLED devices.

CHAPTER 4

SYNTHESIS AND CHARACTERIZATION OF NOVEL ORGANIC DYE FOR DYE SENSITIZER SOLAR CELLS

4.1 Introduction

The division of the organic sensitizer into three components, donor, linker and acceptor, is a convenient method to systematize the sensitizer. There are several basic that an efficient sensitizer should fulfill, and there criteria can be used when designing a new chromophore. First of all, light excitation should be associated with vectorial electron flow from the light harvesting moiety of the dye i.e. the donor and the linker, towards the proximity of the semiconductor, i.e. the acceptor/anchoring group of the dye. This can be seen as the HOMO is located over the donor and the linker, while the LUMO is locates over the acceptor, i.e. a pronounced push-pull effect. Secondly, the HOMO potential of the dye should be sufficiently positive compared to the electrolyte redox potential for efficient dye regeneration [96]. Thirdly, the LUMO potential of the dye should be sufficiently negative to match the potential of the conducting band edge of the TiO_2. Fourthly, a strong conjugation and electron coupling across the donor and the acceptor is necessary to ensure high electron transfer rates. Finally, to obtain the dye with efficient photocurrent generation, π-stacked aggregation on the semiconductor should be avoided [97].

4.1.1 Carbazole as donating group

Due to the electron-donating nature of carbazole, they have been widely used as hole-transporting materials for a number of applications, organic field-effect transistors, light emitting diodes, organic photovoltaic devices etc. The carbazole moiety can be easily functionalized or covalently linked to other molecule. Numerous ways are known for enhancement of its conjugated π-electron system. For instance, 3,6- or 2,7-linking of carbazole molecule into dimers, trimers or oligomers, and addition of enamine, hydrazone or diarylamino fragment [98]. Moreover, arylation at the 9-position of carbazoles leads to a shift in its highest occupied molecular

orbital (HOMO) level to lower energy and this is helpful to obtain a wider range of band gaps when associated with proper acceptor groups [99].

4.1.2 Thiophene as π-conjugated linker

Expansion of the π-conjugated C=C backbone to extend the absorption spectra and broaden it to red region, is one way to decrease the HOMO and LUMO energy level band gap and there by increase the solar cell performance. This would, however, complicat the synthetic procedure and affect the stability of the dye due to photoinduced *trans* to *cis* isomerisation [100]. The introduction of different π-conjugated ring moiety, such as thiophene, benzene or pyrole is an elegant way of extending the π-conjugated system without affecting the stability of the dye [101]. By introducing a thiophene in the linker, the absorption spectra is indeed broadened toward the red region when the dyes are adsorbed on the surface of TiO_2, leading to an increase of the photocurrent.

4.1.3 Cyanoacrylic acid as acceptor/anchoring group

The carboxylic acid group is by far the most employed group for attachment of the sensitizers to the semiconductor surface. The binding modes (Figure 4.1) for dye sensitizers with carboxylic acid anchoring groups have been investigated by Galoppini [76]. Phosphonic acid also binding strongly to metal oxide but are not frequently used, derivative of carboxylic acids has also been employed, such as esters and carboxylic salts [102].

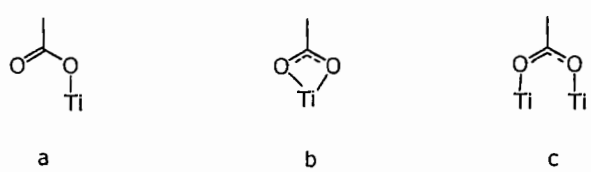

Figure 4.1 Main binding modes of carboxylate group to TiO_2, a) unidentate, b) bidentate chelating, c) bridging bidentate.

When it comes to the term of acceptor groups, cyanoacrylic acid is by far most commonly used due to its strong electronic withdrawing properties. The electronic withdrawing properties of the nitrile group will affect the acidity of the carboxylic acid, which will give a negative influence on the binding to the semiconductor [103]. Hence for a stronger binding to the TiO_2 a less acidic carboxylic acid would be preferable, this would however affect the push-pull

system of the chromophore. There is a number of different acceptor groups reported and some show promising results (Figure4.2) [104].

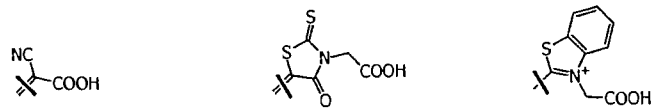

Figure 4.2 Examples of different acceptor groups.

4.2 Aim of the study

We designed To synthesize a novel donor π-conjugate acceptor (D-π-A) organic material based on carbazole as the donor group, Chemically, carbazole can be easily functionalized at its 3,6-positions with a bulky group of *tert*-butyl moiety to protect the oxidation coupling at the 3,6-positions of the peripheral carbazole moiety. Fluorene was introduced on *N*-9 of carbazole as electron transport moiety. The *n*-hexyl substituents were introduced on the C-9 position of fluorene ring to increase the solubility, with a thiophene linker, and a acrylic acid and cyanoacrylate moiety as acceptor/anchoring group which would provide an interesting and readily modifiable scaffold. The carbazole was functionalized with *tert*-butyl group to investigate if a bulky substituent would enhance the solar cell performance by suppressing aggregation. The performance of a device with **CAnT** (n = 1-4) as dyes are investigated The synthesis strategy included well-known methodology, such as Ullmann coupling, Suzuki cross coupling and Knoevenagel reactions.

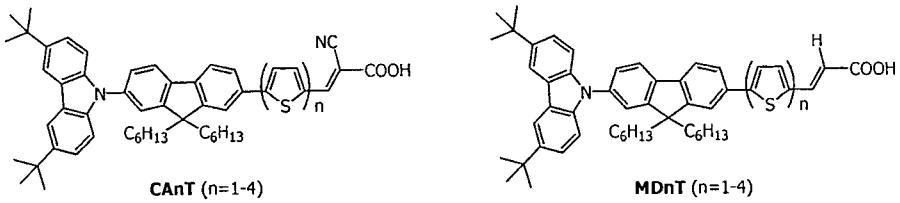

Figure 4.3 Structures of **CAnT** (n = 1-4) and **MDnT** (n = 1-4).

4.3 Results and discussion

4.3.1 Synthesis

The synthesis of oligothiophene-based dyes, **CAnT** (n = 1-4) started with coupling of bromo-intermediate with 5-formyl-2-thiopheneboronic acid under Suzuki cross coupling conditions using $Pd(PPh_3)_4$ as catalyst and Na_2CO_3 as base to afford aldehyde intermediate yielded the aldehyde intermediates (n = 1-4) as yellow to orange solids in range 34-83% yields as shown in Figure 4.4.

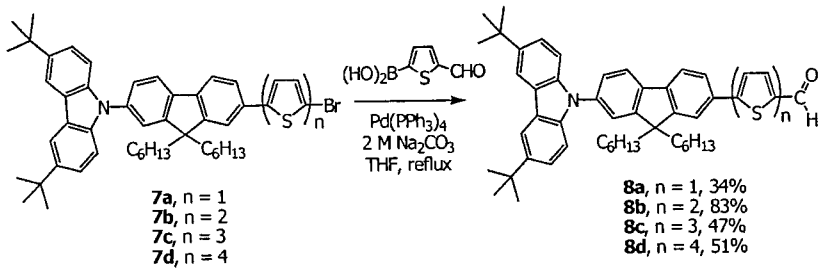

Figure 4.4 Suzuki cross coupling reaction to form aldehyde compounds.

The proposed mechanism of Suzuki cross coupling reaction is shown in Figure 2.9. The chemical structures of aldehyde compounds were confirmed by ^{1}H-NMR, ^{13}C-NMR and IR analysis. The ^{1}H-NMR spectra of the aldehyde compounds show a singlet signals at chemical shift 9.94-9.84 ppm (1H) assigning as the proton of aldehyde group, a singlet signals at chemical shift 8.19 ppm (2H) assigning of unequivalent 4-H and 5-H protons of carbazole adduct and a doublet signal at chemical shift 7.87 ppm (1H) assigning as 1-H of fluorene unit. The ^{13}C-NMR spectra of aldehyde compounds show a single peak for chemical shift atom of aldehyde group in range 182.70-182.32 ppm. In addition, IR spectra reveal the absorption at 1726 cm^{-1} which the present of aldehyde group.

The dyes with cyanoacetic acid as an acceptor were synthesized. Knoevenagel condensation reaction of aldehyde compounds with cyanoacetic acid in a present of piperidine as a base and catalyst in mixture of THF and acetonitrile as solvent at reflux for 6 h gave the target **CAnT** (n = 1-4) as orange solid in range 52-87% yield as shows in Figure 4.6.

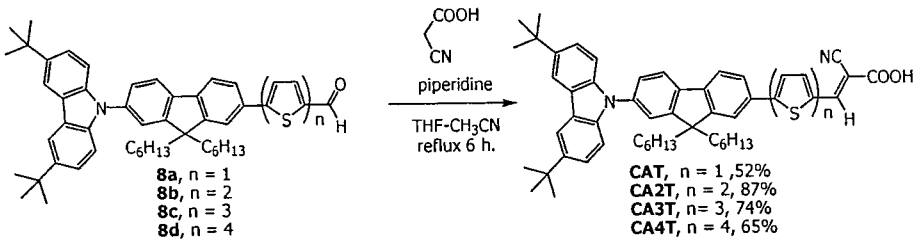

Figure 4.5 Knoevenagel condensation reaction to form **CAnT** (n = 1-4).

Knoevenagel condensation is addition reaction of the methylene components, activated with two electronwithdrawing groups, to aldehydes can be performed with secondary amines. A reasonable variation of the mechanism, in which piperidine acts as organocatalyst, involves the corresponding iminium intermediate as the acceptor is shown in Figure 4.7. [105]

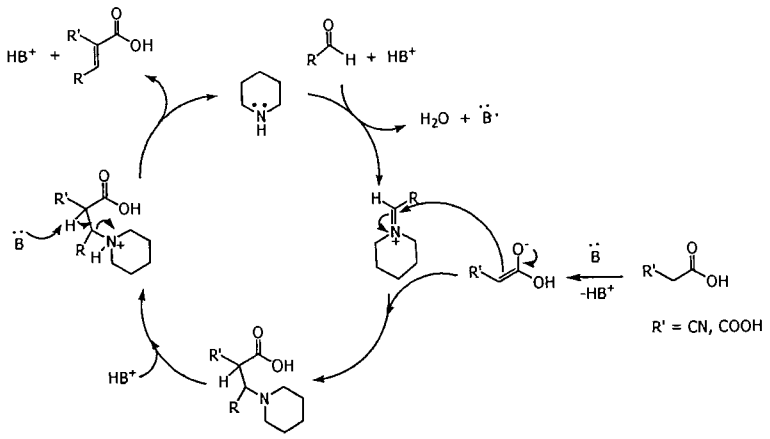

Figure 4.6 The proposed mechanism of Knoevenagel condensation reaction.

The chemical structures of **CAnT** (n = 1-4) were confirmed by ^{1}H-NMR, ^{13}C-NMR and IR analysis. The ^{1}H-NMR spectra of the final product **CAnT** (n = 1-4) show a singlet at chemical shift in rang 6.97 ppm (1H) assigning as the proton of vinyl double bond. The ^{13}C-NMR spectrum of **CAnT** (n = 1-4) show a single peak for chemically carbon atom of cyano at 116.27 ppm indicating **CAnT** (n = 1-4) exists *E* isomer which has higher photostability properties. Moreover IR spectra reveal the adsorption at 3429 cm^{-1} which is consistent with the presence of of hydroxyl group, at 2212 cm^{-1} which is consistent with the presence of of cyano group and at 1613 cm^{-1} which is consistent with the presence of of carbonyl group.

MDnT (n = 1-4) dyes having the vinyl acetic acid acceptor were prepared from reaction of aldehyde compounds with malonic acid under conditions according to the procedure above and obtained as orange solid in range 40-62% yield as shown in Figure 4.8.

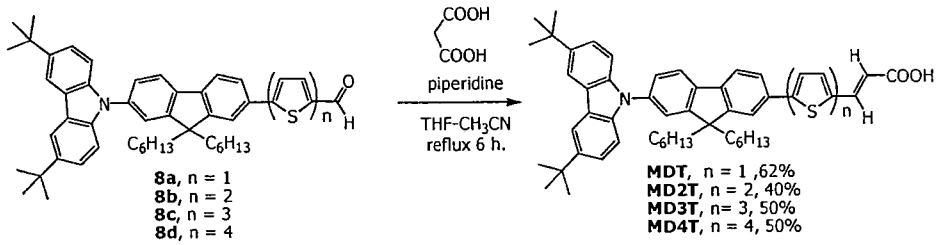

Figure 4.7 Knoevenagel condensation reaction to form **MDnT** (n = 1-4).

The Doebner-Modification in refluxing pyridine effects concerted decarboxylation and elimination in acrylic acid with malonic acid as active methylene [106].

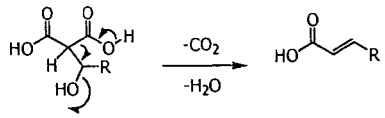

Figure 4.8 The proposed mechanism of decarboxylation and elimination in acrylic acid.

The chemical structures of **MDnT** (n = 1-4) were confirmed by ^{1}H-NMR, ^{13}C-NMR, Mass and IR analysis. The ^{1}H-NMR spectra of the final product **MDnT** (n = 1-4) show a singlet at chemical shift in rang 6.25-6.03 ppm (1H) assigning as the proton of vinyl double bond indicating **MDnT** (n = 1-4) exists *E* isomer which has higher photostability properties. The ^{13}C-NMR spectra of **MDnT** (n = 1-4) show a single peak for chemically carbon atom of carbonyl at 168.02 ppm. Moreover IR spectra reveal the adsorption at 3446 cm^{-1} which is consistent with the presence of of hydroxyl group and at 1618 cm^{-1} which is consistent with the presence of of carbonyl group.

4.3.2 Optical properties

The absorption spectra of the dyes in CH_2Cl_2 solution are displayed in Figure 4.9 and listed in Table 4.1, together with the UV-vis spectra of the corresponding dyes absorbed on TiO_2 film. All of dyes exhibit π-π* transition band at 294 nm assigned to the π-π^* local electron

transition of the end-capped carbazole units. The more congested π-π^* transition band in **CA2T**, **CA3T** and **CA4T** than in **CAT** may be attributed to the additional π-π^* transition upon the oligothiophene. As depicted in Figure 4.9, compound **CAnT** (n = 1-4) have a similar extinction coefficient of in the π-π^* transition band, while the extinction coefficient of the chart transfer transition band increases in the order of **CA2T** > **CA3T** > **CA4T** > **CAT**. The absorption spectra of **CAnT** (n = 1-4) are progressively red shift with increasing number of thiophene unit as the extent of the π-conjugation system in the oligomer increases. The energy band gaps of the **CAnT** (n = 1-4) dyes were estimated to be 2.37, 2.18, 2.08 and 1.99 eV, respectively, from the absorption edge of the solution spectra.

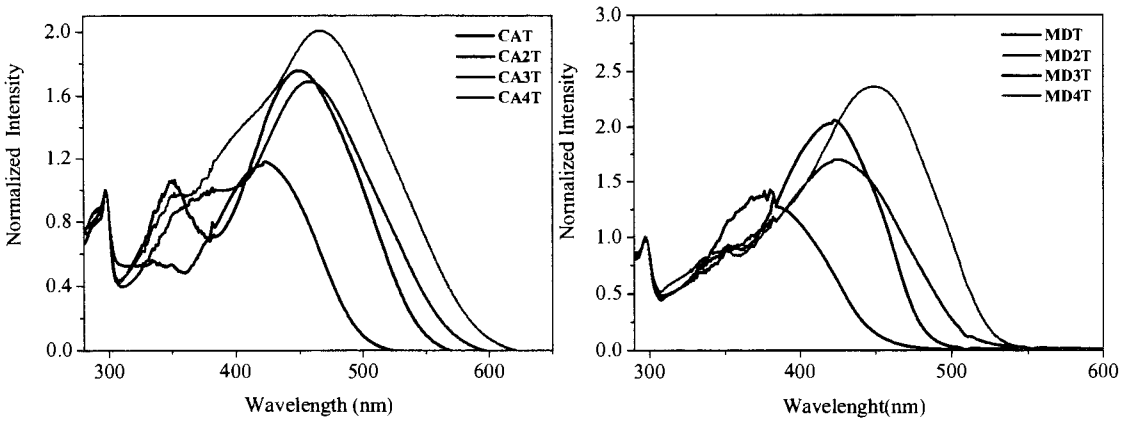

Figure 4.9 Absorption spectra of **CAnT** (n = 1-4) and **MDnT** (n = 1-4) in CH_2Cl_2 solution.

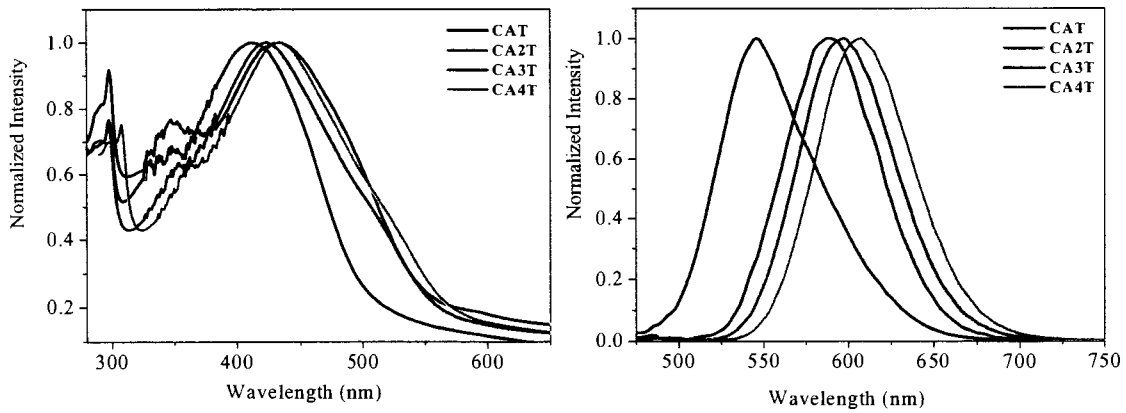

Figure 4.10 Absorption spectra and PL spectrum of **CAnT** (n = 0-4) in thin film.

UV-vis and fluorescence spectra of dyes in dry CH_2Cl_2 are shown in Figure 4.10 and listed in Table 4.1, together with the UV-vis spectrum of the corresponding dyes absorbed on TiO_2 film. The absorption spectrum of **MDnT** (n = 1-4) displayed absorption bands with absorption maximum at 298 and 373-460 nm, which corresponding to carbazole, fluorene and π-conjugation system of dyes through the thiophene ring into acrylic acid acceptor, which is due to the Intermolecular change change transfer transition (ICT) of the D-π-A molecule. The absorption spectra of **MDnT** (n = 1-4) on TiO_2 film are broadened when compared to solution due to interaction of the anchoring group with the titanium ions. Similar broadening has been reported in several organic dyes on TiO_2 electrodes. We observed that the dyes **MDnT** (n = 1-4) exhibited strong luminescence maxima of 369-420 nm when it is excited within its π-π^* band in solution. The energy band gaps of the **MDnT** (n = 1-4) dyes were estimated to be 2.66, 2.51, 2.43 and 2.37 eV, respectively, from the absorption edge of the solution spectra.

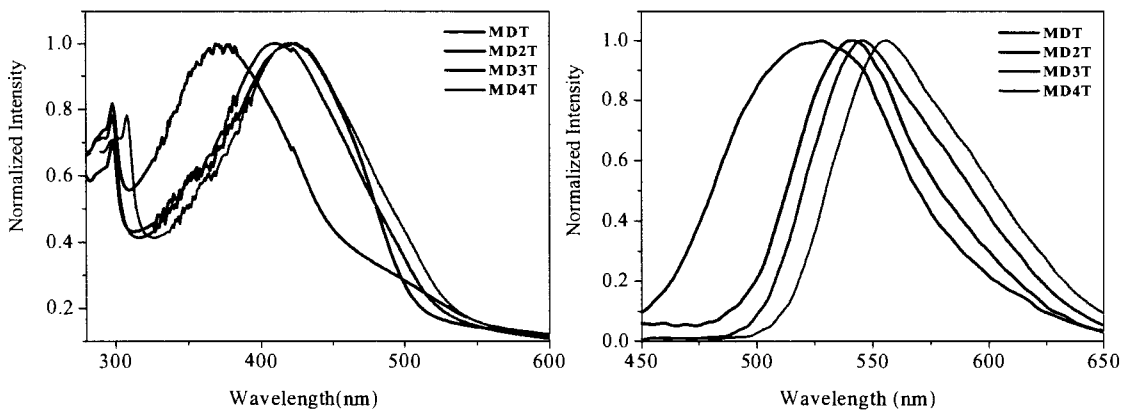

Figure 4.11 Absorption spectra and PL spectrum of **MDnT** (n = 0-4) in thin film.

Absorption band of **CAnT** (n = 1-4) and **MDnT** (n = 1-4) in thin film is similar to that of the corresponding solution spectrum. However, the **CAnT** (n = 1-4) and **MDnT** (n = 1-4) in thin film have blue-shifted band compared to the corresponding solution spectrum. When **CAnT** (n = 1-4) and **MDnT** (n = 1-4) sensitizers were coated in thin film, a slight blue shifts were found probably due to the H-aggregation.

Table 4.1 The absorption and fluorescence data of **CAnT** (n = 1-4) and **MDnT** (n = 1-4).

Compound	λ_{max} (nm) and	λ_{max} on thin film (nm)	λ_{em} of emission in CH_2Cl_2 (nm)
CAT	426	412	546
CA2T	450	434	589
CA3T	456	424	598
CA4T	465	435	608
MDT	380	369	528
MD2T	423	423	541
MD3T	424	410	546
MD4T	448	420	556

4.3.3 Thermal properties

For DSCs applications, thermal properties of **CAnT** (n = 1-4) and **MDnT** (n = 1-4) were determined by TGA and DSC measurements as show in Figure 4.11 The thermal instability or low glass transition temperature (T_g) of the amorphous organic layer may result in the degradation of organic devices due to morphological changes. The thermal property of **CAnT** (n = 1-4) and **MDnT** (n = 1-4) were determinated by DSC analysis with a heating rate of 10 °C/min under a nitrogen atmosphere.

In the first heating cycle, DSC curves of **CA2T, CA3T** and **CA4T** display only an endothermic phenomenon (T_g) at 145, 166 and 204 °C, respectively. However, DSC curves of **CAT** behave totally different. In first heating cycle, an endothermic phenomenon (T_g) at 148 °C was observed followed by an endothermically melted at 159 ° C. The results indicate that the **CA2T, CA3T** and **CA4T** are amorphous state, and CAT is semi-crystalline properties. The degradation temperature at 5% weight loss (T_d) of **CAT, CA2T, CA3T** and **CA4T** were measured to be 130, 185, 173 and 135 °C, respectively. The ability of **CAT, CA2T, CA3T** and **CA4T** to form stable amorphous glasses and the possibility to prepare thin films form **CAT, CA2T, CA3T** and **CA4T** both by evaporation and by solution casting are highly desirable for application in DSCs.

Table 4.2 Thermal properties of **CAnT** (n = 1-4) and **MDnT** (n = 1-4).

Compound	Temperature (°C)			
	T_g	T_C	T_m	T_d
CAT	148	-	159	130
CA2T	146	-	-	185
CA3T	166	-	-	173
CA4T	204	-	-	135
MDT	150	-	-	149
MD2T	70	173	254	268
MD3T	90	-	-	202
MD4T	157	-	-	118

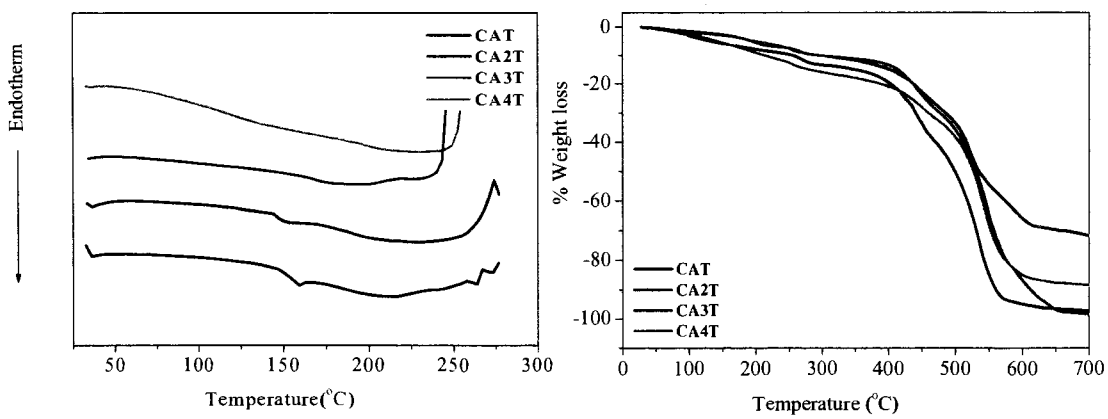

Figure 4.12 DSC and TGA curves of **CAnT** (n = 1-4) N_2 at heating rate of 10 °C/min.

DSC curves of **MDT, MD3T** and **MDA4T** display only an endothermic phenomenon (T_g) at 150, 90 and 157 °C, respectively. However, DSC curves of **MD2T** behave totally different. In first heating cycle, an endothermic phenomenon (T_g) at 70 °C was observed followed by an exothermic peak due to crystalline around 173 °C, to give crystal, which endothermically melted at 254 °C. The results indicate that the **MDT, MD3T** and **MDA4T** are amorphous state. The ability of **MDT, MD3T** and **MDA4T** to form stable amorphous glasses and the possibility to prepare thin films form **MDT, MD3T** and **MDA4T** both by evaporation and by solution casting are highly desirable for application in DSCs.

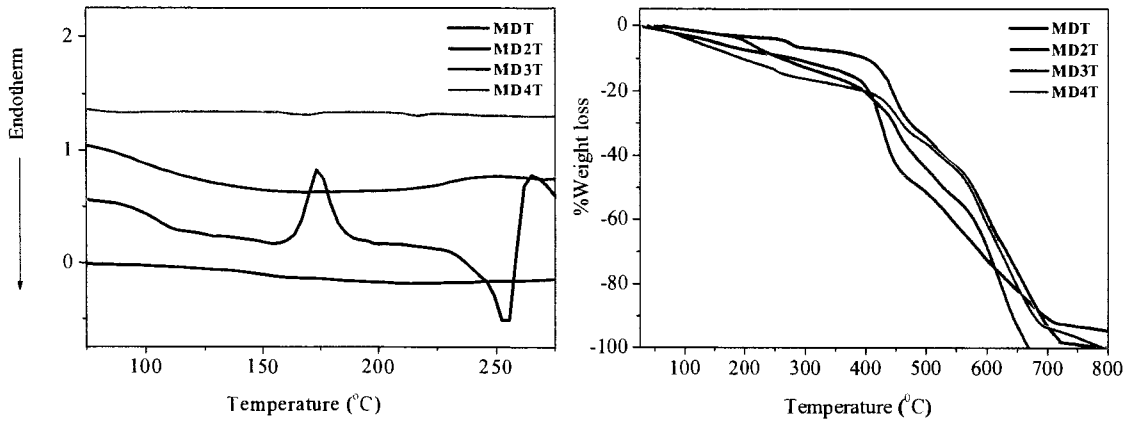

Figure 4.13 DSC and TGA curves of **MDnT** (n = 1-4) N_2 at heating rate of 10 °C/min.

The TGA data revealed that all the materials **MDnT** (n = 1-4) were thermally stable materials, with the onset of decomposition temperatures above 118 °C under N_2. The temperatures corresponding to 5% weight loss (T_{5d}) of **MDT, MD2T, MD3T** and **MD4T** were measured to be 149, 268, 202 and 118 °C, respectively.

4.3.4 Electrochemical properties

In order to investigate the electrochemical properties of the target molecule, cyclic voltametry (CV) measurements were performed in CH_2Cl_2 containing 0.1 M n-Bu_4NPF_6 as a supporting electrolyte. The results are shown in Figure 4.13 and summarized in Table 4.3. Compounds **CAT** detected one reversible oxidation and one irreversible reduction, **CA2T** and **CA3T** demonstrated two quasi-reversible oxidation- processes, while compound **CA4T** showed three quasi-reversible oxidation processes. All the **CAnT** (n = 1-4) gave well defined CV curves with stable formation of both the radical cations and the dication, indicating indicating as expected, the first oxidation process can be attributed to the removeal of electron from the peripheral of the carbazole unit and other reversible process corresponds to removal of electrons from the thiophene at the α and α' positions block the reactivity.

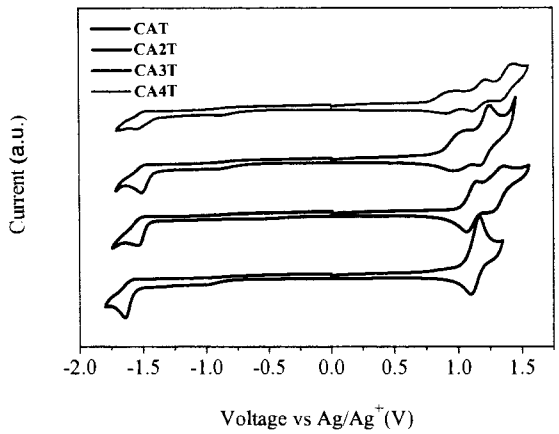

Figure 4.14 Cyclic voltammograms of **CAnT** (n = 1-4) in CH_2Cl_2 with scan rate of 0.05 V/s and 0.1 M *n*-Bu_4NPF_6 as electroly.

Cyclic voltammogram of **CAT** (Figure 4.14) was analyzed in CH_2Cl_2 solution with scan rate of 0.05 V/s and *n*-Bu_4NPF_6 as electrolyte, detected one reversible oxidation (one electron oxidation) and one irreversible reduction (one electron transfer) peaks. It shows one oxidation waves with half-wave potential ($E_{1/2}$) yielding cations at 1.08 V, which is assigned as the formation 3,6-di-(*tert*-butyl)carbazole cation is show in Figure 4.15. It also shows a similar wave in difference scans no distinct a slight shift of the CV curves was observed indicate *tert*-butyl group to protect a oxidation coupling at the 3,6-positions peripheral carbazole moiety, indicating a good and electrochemical property. It shows one irreversible reduction with half-wave potential ($E_{1/2}$) of -1.62 V, which are assigned as the reduction process of cyanoacrylate acceptor. The propose reduction mechanism for the cyanoacrylate system is shown in Figure 4.16, which one electron transfer process lead to the formation of radical anion. It is reasonable to assume that the major portion of electron density resides on the carbonyl oxygen due to the electron-withdrawing nature of the oxygen atom as indicated in possible resonance. The HOMO calculated, according to the following equation: HOMO = -(4.44 + E_{ox}) (eV), to be -5.46 eV. The LUMO was calculated from the value of the energy gap (2.37 eV) and HOMO energy level to be -3.09 eV.

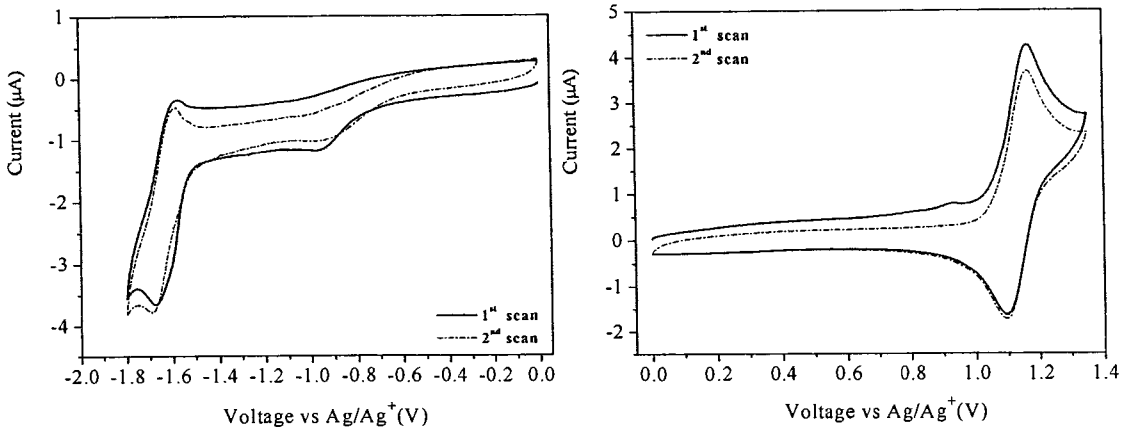

Figure 4.15 Cyclic voltammograms of **CAT** in CH_2Cl_2 with scan rate of 0.05 V/s and 0.1 M n-Bu_4NPF_6 electroly.

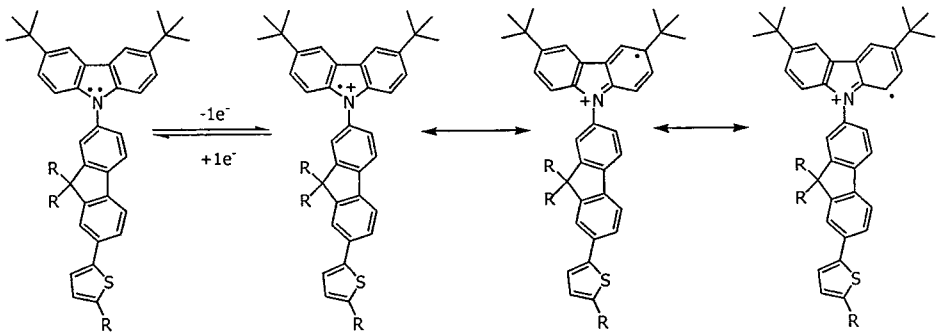

Figure 4.16 The oxidation propose of 3,6-di(*tert*-butyl)carbazole.

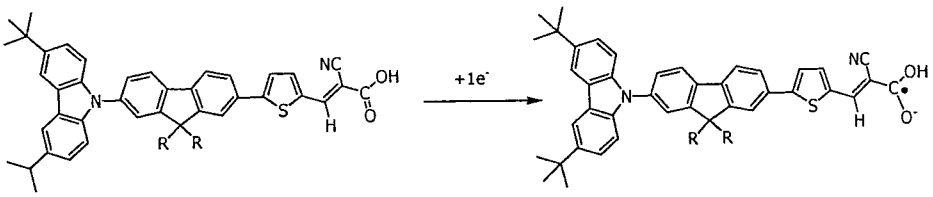

Figure 4.17 Proposed one reduction mechanism for the cyanoacrylic acid.

Cyclic voltammogram of **CA2T** (Figure 4.17) was analyzed in CH_2Cl_2 with scan rate of 0.05 V/s and 0.1 M n-Bu_4NPF_6 as electrolyte, detected two irreversible oxidation (two electron oxidation) and one irreversible reduction (one electron transfer) peaks. It shows one irreversible reduction with half-wave potential ($E_{1/2}$) of -1.55 V, which is assigned as the reduction process of cyanoacrylate acceptor, the formation of the cyanoacrylate radical anion. The proposed

reduction mechanism for the cyanoacrylate system is the same as **CAT**, when the one electron transfer process lead to the formation of radical anion. It is reasonable to assume that the major portion of electron density resides on the carbonyl oxygen due to the electron-withdrawing nature of the oxygen atom as indicated in possible resonance. It shows two oxidation wave with half-wave potential ($E_{1/2}$) of 1.10 and 1.30, respectively, which are assigned as the formation 3,6-di-(*tert*-butyl)carbazole cation. It also shows a similar wave in difference scans no distinct a slight shift of the CV curves was observed indicate *tert*-butyl group at the 3,6-positions peripheral carbazole moiety to protect oxidation coupling, indicating a good and electrochemical property. The onset oxidation potential (E_{ox}) of **CA2T** was estimated from the first anodic oxidation wave to be 1.00 V. The HOMO calculated, according to the following equation: HOMO = -(4.44 + E_{ox}) (eV), to be -5.54 eV. The LUMO was calculated from the value of the energy gap (2.18 eV) and HOMO energy level to be -3.26 eV.

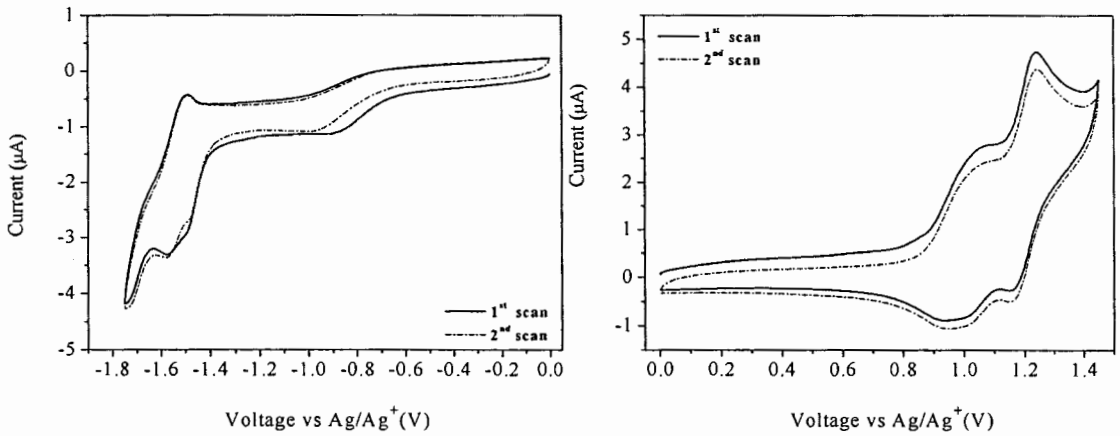

Figure 4.18 Cyclic voltammograms of **CA2T** in CH_2Cl_2 with scan rate of 0.05 V/s and 0.1 M *n*-Bu_4NPF_6 as electroly.

Cyclic voltammogram of **CA3T** (Figure 4.18) was analyzed in CH_2Cl_2 with scan rate of 0.05 V/s and 0.1 M *n*-Bu_4NPF_6 as electrolyte, detected two irreversible oxidation (two electron oxidation) and one irreversible reduction (one electron transfer) peaks. It shows one irreversible reduction with half-wave potential ($E_{1/2}$) of -1.52 V, which is assigned as the reduction process of cyanoacrylate acceptor, the formation of the cyanoacrylate radical anion. It shows two oxidations with half-wave potential of 1.01 and 1.19, respectively, which are assigned as the formation 3,6-di-(*tert*-butyl)carbazole cation and dication, respectively. It also shows a similar

wave in difference scans no distinct a slight shift of the CV curves was observed indicate *tert*-butyl group at the 3,6-positions peripheral carbazole moiety to protect oxidation coupling, indicating a good and electrochemical property. The onset oxidation potential (E_{ox}) of **CA3T** was estimated from the first anodic oxidation wave to be 0.84 V. The HOMO calculated, according to the following equation: HOMO = -(4.44 + E_{ox}) (eV), to be -5.28 eV. The LUMO was calculated from the value of the energy gap (2.08 eV) and HOMO energy level to be 3.20 eV.

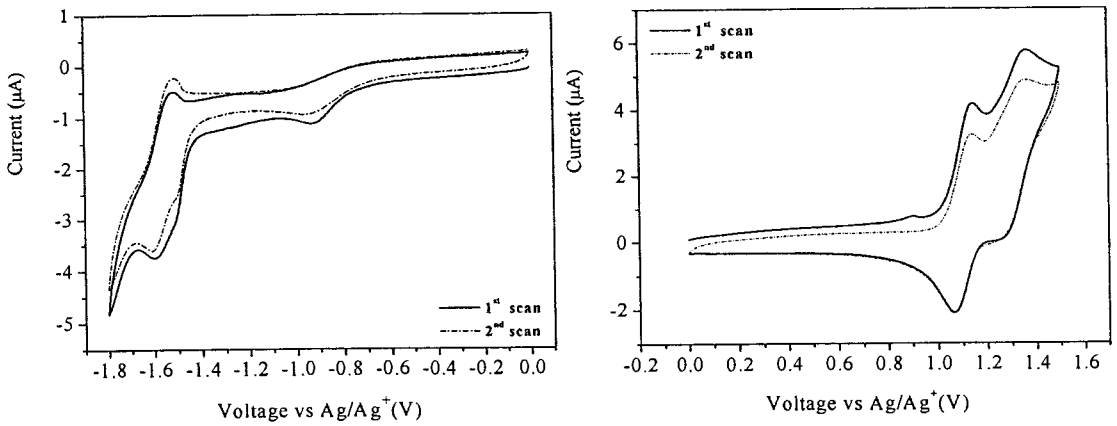

Figure 4.19 Cyclic voltammograms of **CA3T** in CH_2Cl_2 with scan rate of 0.05 V/s and 0.1 M *n*-Bu_4NPF_6 as electrolyte.

Cyclic voltammogram of **CA4T** is shown in Figure 4.19. It shows three oxidation waves with half-wave potential ($E_{1/2}$) of 0.91, 1.16 and 1.38, respectively, which are assigning as the formation 3,6-di-(*tert*-butyl)carbazole cation, dication and formation of both the radical cations, the dication and indicating as expected, that the thiophene at the α and α′ positions block the reactivity. The proposed oxidation mechanism for π-conjugated thiophene system was illustrated in Figure 4.20. It shows one irreversible reduction with half-wave potential ($E_{1/2}$) of -1.51 V, which is assigned as the reduction process of cyanoacrylate acceptor, the formation of the cyanoacrylate radical anion. It also shows similar wave in different scans no distinct a slight shift of the CV curves was observed indicate *tert*-butyl group at the 3,6-positions peripheral carbazole moiety to protect oxidation coupling, indicating a good and stable electrochemical property. The onset oxidation potential (E_{ox}) of **CA4T** was estimated from the first anodic oxidation wave to be 0.76V. The HOMO calculated, according to the following equation:

HOMO = -(4.44 + E_{ox}) (eV), to be -5.20 eV. The LUMO was calculated from the value of the energy gap (1.99 eV) and HOMO energy level to be -3.21 eV.

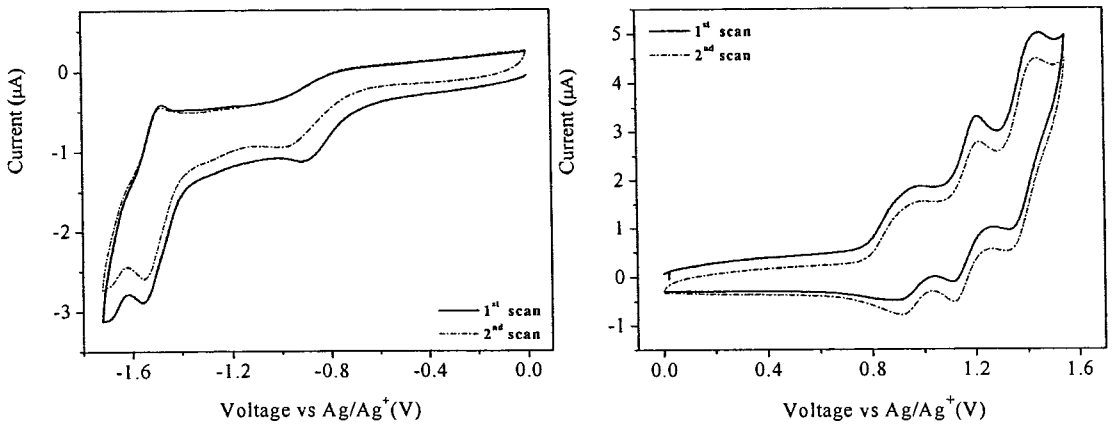

Figure 4.20 Cyclic voltammograms of **CA4T** in CH_2Cl_2 with scan rate of 0.05 V/s and 0.1 M *n*-Bu_4NPF_6 as electroly.

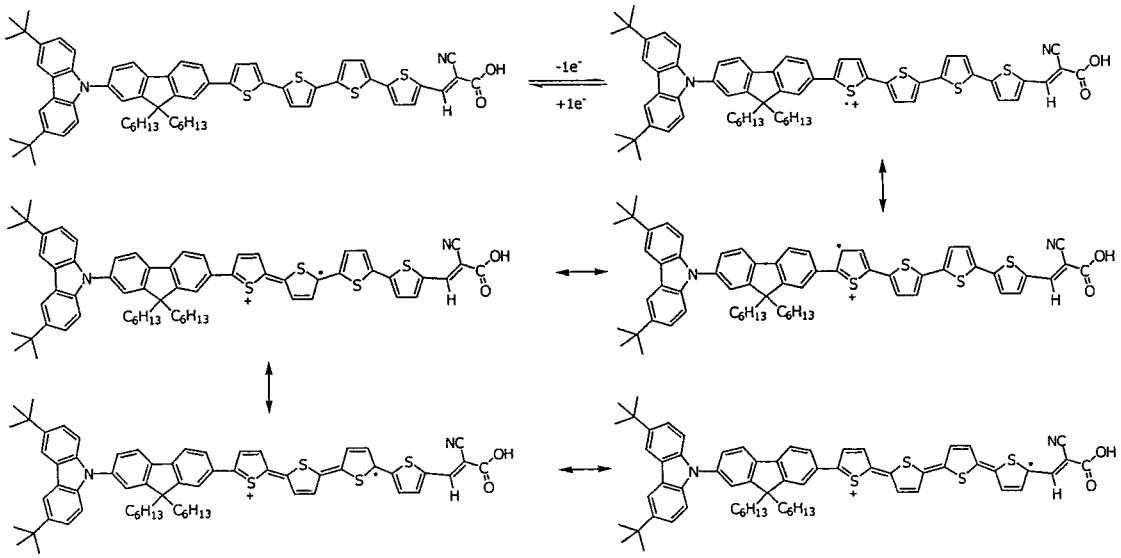

Figure 4.21 The proposed oxidation mechanism for π-conjugated thiophene system.

Electrochemistry of **MDT** detected only one oxidation peaks as show in Figure 4.21 and listed in Table 4.3. It shows one oxidation with half-wave potentials ($E_{1/2}$) of 1.13 V, which is assigning as the formation 3,6-di(*tert*-butyl)carbazole cation. The proposed oxidation mechanism for tert-butyl substituented carbazole system was described for **CAT**. It also shows a similar wave in different scans no distinct a slight shift of the CV curves was observed

indicate *tert*-butyl group at the 3,6-positions peripheral carbazole moiety to protect oxidation coupling, indicating a good and stable lectrochemical property. It does not show reduction peak. The onset oxidation potential (E_{ox}) of **MDT** was estimated from the first anodic oxidation wave to be 1.01 V. the HOMO was calculated, according to the following equation: HOMO = -(4.44+E_{ox}) (eV), to be -5.45 eV. The LUMO was calculated from the value of the energy gap (2.66 eV) and HOMO energy level to be -2.79 eV.

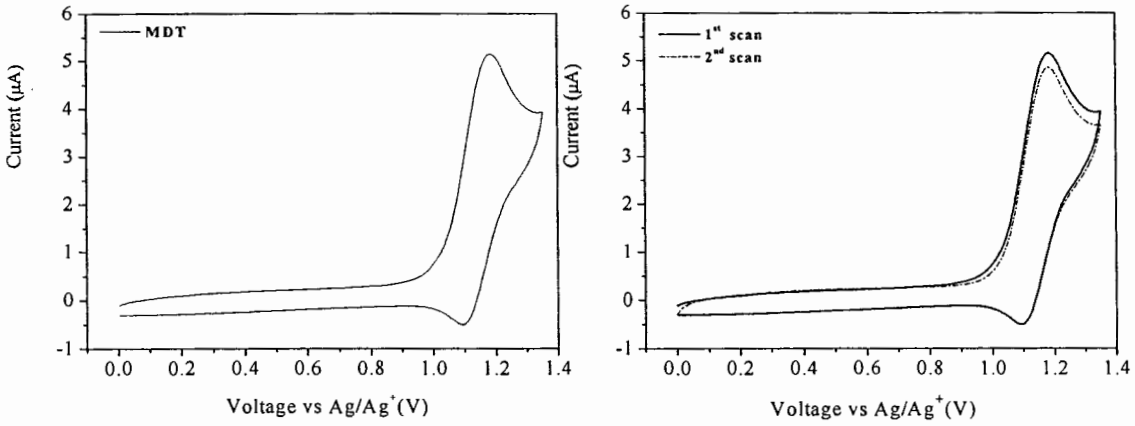

Figure 4.22 Cyclic voltammograms of **MDT** in CH_2Cl_2 with scan rate of 0.05 V/s and 0.1 M *n*-Bu_4NPF_6 as electroly.

Cyclic voltammogram of **MD2T** (Figure 4.22) was analyzed in CH_2Cl_2 with scan rate of 0.05 V/s and 0.1 M *n*-Bu_4NPF_6 as electrolyte, detected one oxidation peaks as show in Figure 4.21. It shows one oxidation with half-wave potentials ($E_{1/2}$) of 1.18 V, which is assigning as the formation 3,6-di(*tert*-butyl)carbazole cation. The proposed oxidation mechanism for *tert*-butyl substituented carbazole system was described for **CAT.** It also shows a similar wave in different scans no distinct a slight shift of the CV curves was observed indicate *tert*-butyl group at the 3,6-positions peripheral carbazole moiety to protect oxidation coupling, indicating a good and stable electrochemical property. It does not show reduction peak. The onset oxidation potential (E_{ox}) of **MD2T** was estimated from the first anodic oxidation wave to be 1.00 V. the HOMO was calculated, according to the following equation: HOMO = -(4.44+E_{ox}) (eV), to be -5.44 eV. The LUMO was calculated from the value of the energy gap (2.51 eV) and HOMO energy level to be -2.93 eV.

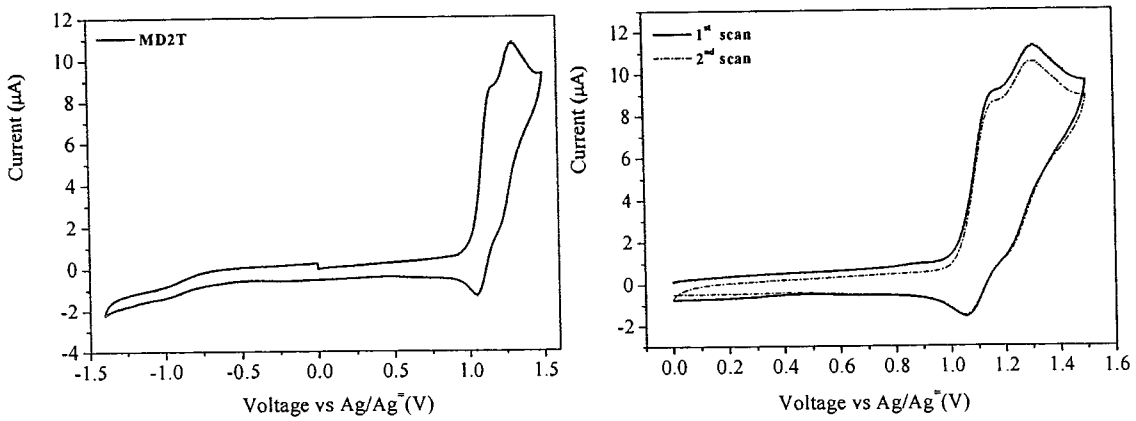

Figure 4.23 Cyclic voltammograms of **MD2T** in CH_2Cl_2 with scan rate of 0.05 V/s and 0.1 M *n*-Bu_4NPF_6 as electroly.

Cyclic voltammogram of **MD3T** was analyzed in CH_2Cl_2 with scan rate of 0.05 V/s and 0.1 M *n*-Bu_4NPF_6 as electrolyte, detected two oxidation and one irreversible reduction peaks as show in Figure 4.24. It shows two oxidation with half-wave potentials ($E_{1/2}$) of 1.00 and 1.16 V, respectively, which are assigning as the formation 3,6-di(*tert*-butyl)carbazole cation and dication. The proposed oxidation mechanism for *tert*-butyl substituented carbazole system was described for **CAT**. It shows one irreversible process with half-wave potential ($E_{1/2}$) of -0.99 V, which is assigning as the reduction process of acrylic acceptor, the formation of the acrylic radical anion. The proposed reduction mechanism for acrylic system is show in Figure 4.22. It also shows a similar wave in different scans no distinct a slight shift of the CV curves was observed indicate *tert*-butyl group at the 3,6-positions peripheral carbazole moiety to protect oxidation coupling, indicating a good and stable electrochemical property. The onset oxidation potential (E_{ox}) of **MD3T** was estimated from the first anodic oxidation wave to be 0.80 V. the HOMO was calculated, according to the following equation: HOMO = -(4.44+E_{ox}) (eV), to be -5.23 eV. The LUMO was calculated from the value of the energy gap (2.51 eV) and HOMO energy level to be -2.80 eV.

Table 4.3 Physical datas of **CAnT** (n = 1-4)[a] and **MDnT** (n = 1-4)[a].

Compound	E_{1o} V	E_{2o} V	E_{3o} V	E_{1r} V	ΔE^0_{or} V	E_g[d] eV	HOMO[e] eV	LUMO[f] eV
CAT	1.10	-	-	-1.52	2.62	2.37	-5.46	-3.09
CA2T	1.05	1.26	-	-1.52	2.57	2.18	-5.44	-3.26
CA3T	0.96	1.16	-	-1.53	2.49	2.08	-5.28	-3.20
CA4T	0.90	1.11	1.34	-1.64	2.54	1.99	-5.20	-3.21
MDT	1.09	-	-	-	-	2.66	-5.45	-2.79
MD2T	1.04	-	-	-	-	2.51	-5.44	-2.93
MD3T	0.96	-	-	-0.99	1.95	2.43	-5.23	-2.80
MD4T	0.84	2.37	1.32	-1.52	2.36	2.37	-5.19	-2.82

[a]Measured using a platinum rod couter electrode, a glassy carbon electrode and a SCE reference electrode in CH_2Cl_2 containing *n*-Bu_4NPF_6 as a supporting electrolyte with scan rate of 0.05 V/s under argon atmosphere, [b]Peak potential, [c]Half-wave potential, [d]Estimated form the onset of the absorption spectra ($E_g = 1240/\lambda_{onset}$), [e]Calculated using the empirical equation from HOMO = -(4.44 + E_{onset}), [f]Calculated from LUMO = HOMO + E_g

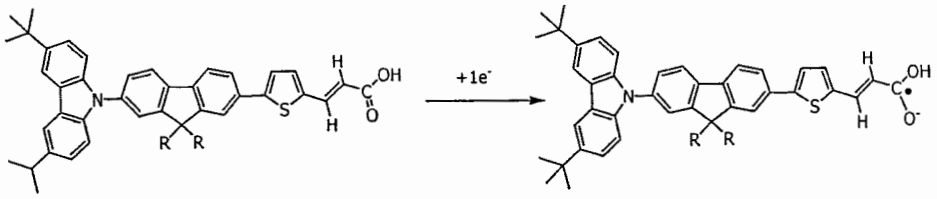

Figure 4.24 Proposed one reduction mechanism for the acrylic acid.

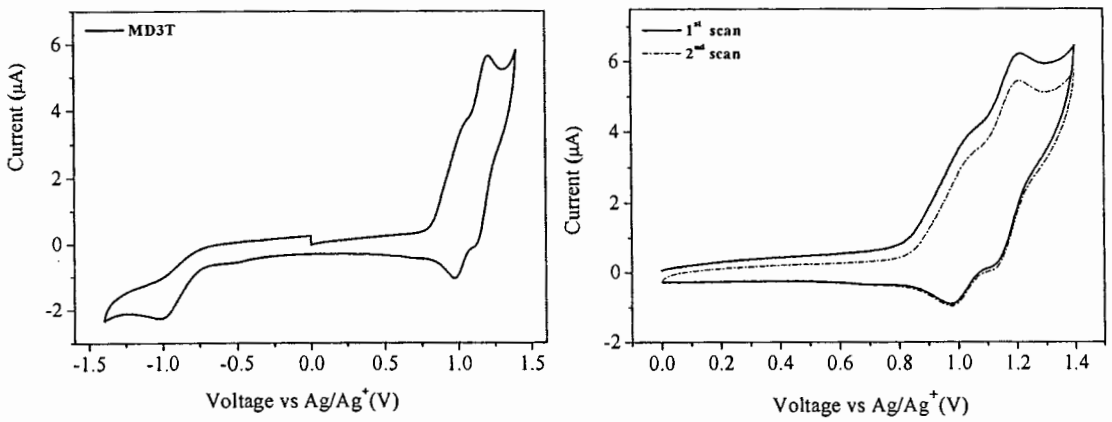

Figure 4.25 Cyclic voltammograms of **MD3T** in CH_2Cl_2 with scan rate of 0.05 V/s and 0.1 M *n*-Bu_4NPF_6 as electroly.

Cyclic voltammogram of **MD4T** was analyzed in CH_2Cl_2 with scan rate of 0.05 V/s and 0.1 M *n*-Bu_4NPF_6 as electrolyte, detected three oxidation and one irreversible reduction peaks as show in Figure 4.25. It shows three oxidation with half-wave potentials ($E_{1/2}$) of 0.90, 1.16 and 1.37 V, respectively, which are assigning as the formation 3,6-di(*tert*-butyl)carbazole cation, the dication and indicating as expected, that the thiophene at the α and α' positions block the reactivity. The proposed oxidation mechanism for *tert*-butyl substituented carbazole and π-conjugated thiophene system were described for **CAT** and **CA4T**, respecrively . It shows one irreversible process with half-wave potential ($E_{1/2}$) of -0.97 V, which is assigning as the reduction process of acrylic acceptor, the formation of the acrylic radical anion. The proposed reduction mechanism for acrylic system was described for MD3T. It also shows a similar wave in different scans no distinct a slight shift of the CV curves was observed indicate *tert*-butyl group at the 3,6-positions peripheral carbazole moiety to protect oxidation coupling, indicating a good and stable electrochemical property. The onset oxidation potential (E_{ox}) of **MD4T** was estimated from the first anodic oxidation wave to be 0.75 V. the HOMO was calculated, according to the following

equation: HOMO = -(4.44+E_{ox}) (eV), to be -5.19 eV. The LUMO was calculated from the value of the energy gap (2.37 eV) and HOMO energy level to be -2.82 eV.

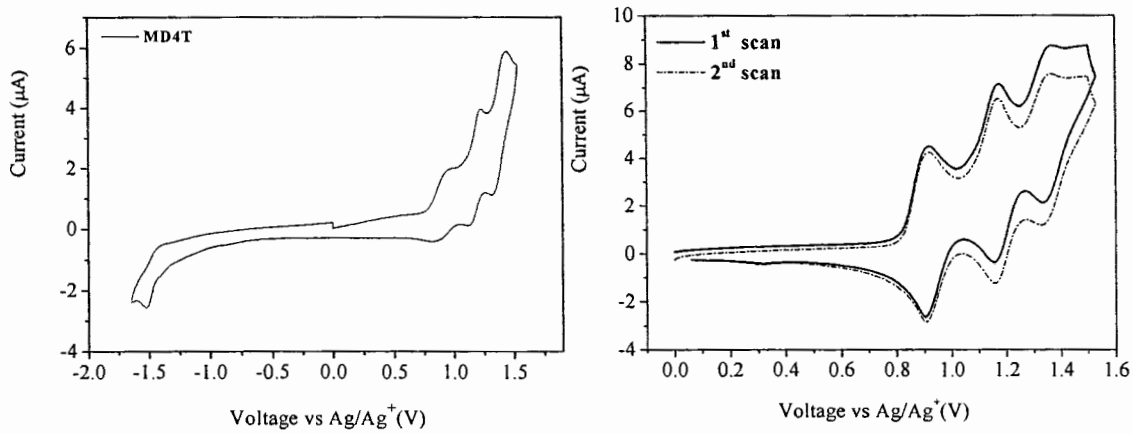

Figure 4.26 Cyclic voltammograms of **MD4T** in CH_2Cl_2 with scan rate of 0.05 V/s and 0.1 M *n*-Bu_4NPF_6 as electroly.

4.3.5 Molecular orbital calculation

To get an insight the molecular structure and electron distribution of the organic dye, the **CAnT** (n = 1-4) dyes geometries have been optimized using DFT calculations with DFT calculations with Gaussian 03 program. The calculations were performed with the BTLYP exchange correlation functional under 6-31G(d,p) basis set. Computed HOMO and LUMO distribution of **CAnT** (n = 1-4) are depicted in Figure 4.26. The general characters of the orbital are independent of the number of thiophen unit. The HOMO is of π-characteristics and is delocalized over the entries molecule, including the carbazole groups. In the LUMO, which also has π-character, there is essentially no contribution from the carbazole groups, and the electron density has been shifted towards the acceptor group of the sensitizer. This supports the supposed push-pull characteristics of these sensitizer as shown in Figure 4.27. In addition, the optimized geometries of **CAnT** (n = 1-4) indicate that the carbazole moiety at the end of the molecule are in 3-D spatial arrangement, which makes the molecular structure nonplanar structure of due to the twist conformation around the carbazole-fluorene C-N bond. The nonplanar molecular structure of **CAnT** (n = 1-4) could be beneficial to solution-processability to from amorphous film. **CAnT** (n = 1-4) are soluble in common rganic solvents such as CH_2Cl_2, $CHCl_3$, THF and acetone. Hight-quality amorphous film can be obtained by spin-coasting its solution.

By comparing the HOMO and LUMO energy levels of four dyes **CAnT** (n = 1-4) with linker variation is shown in Figure 4.26

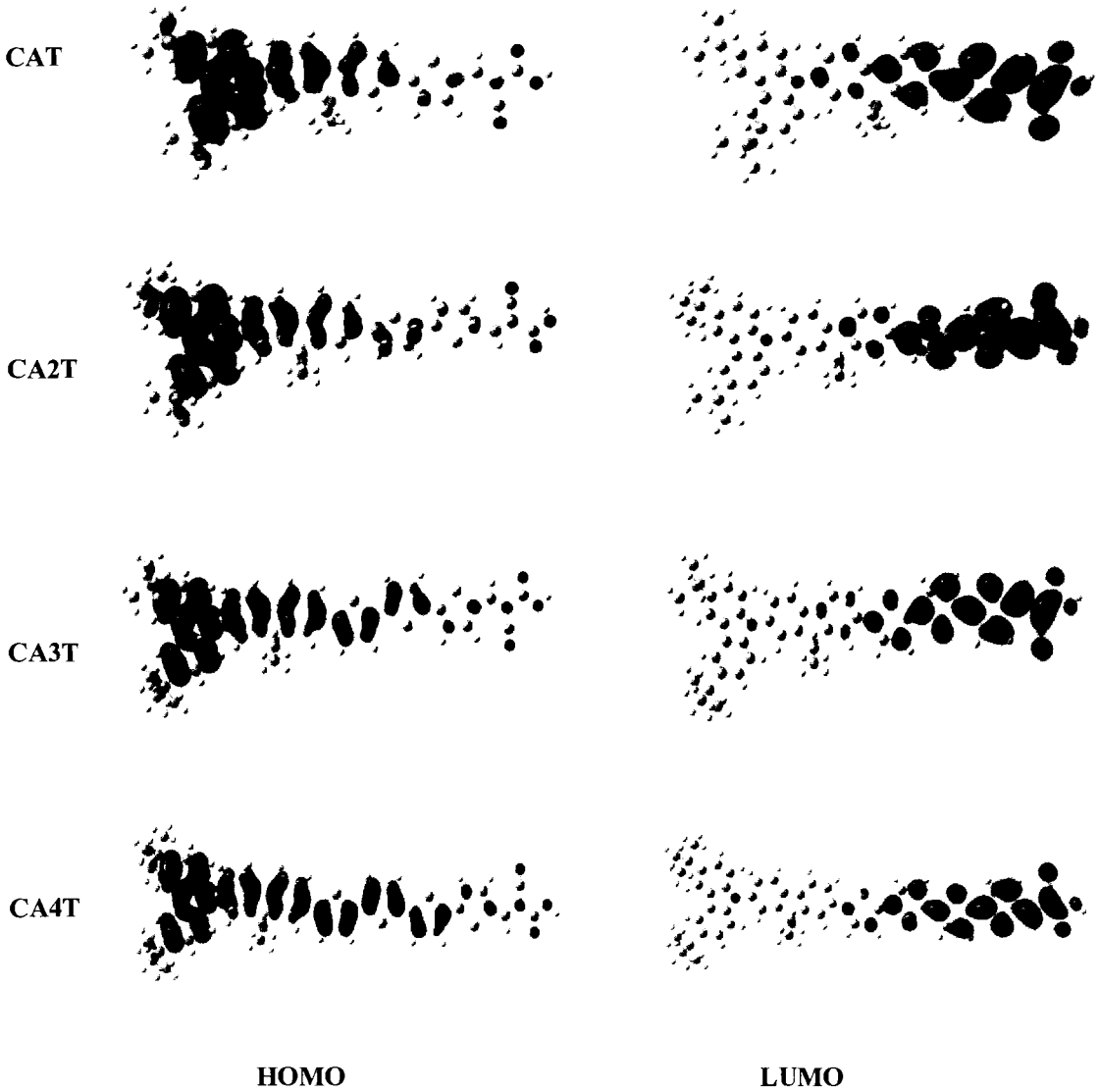

Figure 4.27 HOMO and LUMO distributions of the **CAnT** (n = 1-4) dyes calculated with DFT on a BTLYP/6-31G(d,p) level.

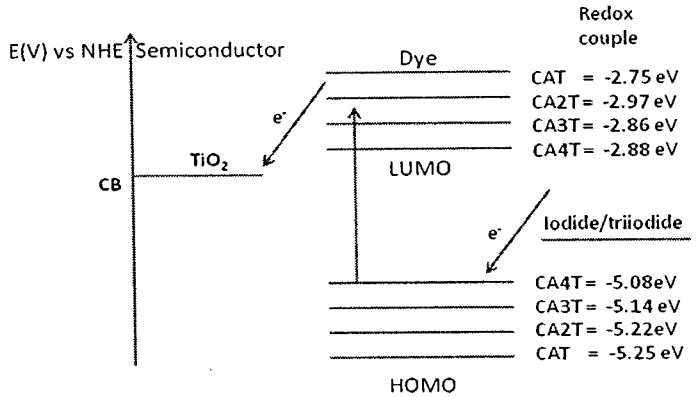

Figure 4.28 Schematic energy level diagram of **CAnT** (n = 1-4).

The optimum geometries and electron-state-density distribution of the HOMO and LUMO of **MDnT** (n = 1-4) were calculated by using DFT calculated with Gaussian 03 program. The calculations were performed with the BTLYP exchange correlation functional under 6-31G9d,p0 basis set. Figure 4.29 shows the optimum geometry and the electron-state-density distribution of the HOMO and LUMO of **MDnT** (n = 1-4) molecules.

The general characters of the orbital are independent of the number of thiophen unit. The HOMO is of π-characteristics and is delocalized over the entries molecule, including the carbazole groups. In the LUMO, which also has π-character, there is essentially no contribution from the carbazole groups, and the electron density has been shifted towards the acceptor group of the sensitizer. This supports the supposed push-pull characteristics of these sensitizer as shown in Figure 4.28. In addition, the optimized geometry of **MDnT** (n = 1-4) indicates that the carbazole moiety at the end of the molecule are in 3-D spatial arrangement, which makes the molecular structure nonplanar structure of due to the twist conformation around the carbazole-fluorene C-N bond. The nonplanar molecular structure of **MDnT** (n = 1-4) could be beneficial to solution-processability to from amorphous film. **MDnT** (n = 1-4) are soluble in common organic solvents such as CH_2Cl_2, $CHCl_3$, THF and acetone. Hight-quality amorphous film can be obtained by spin-coating its solution.

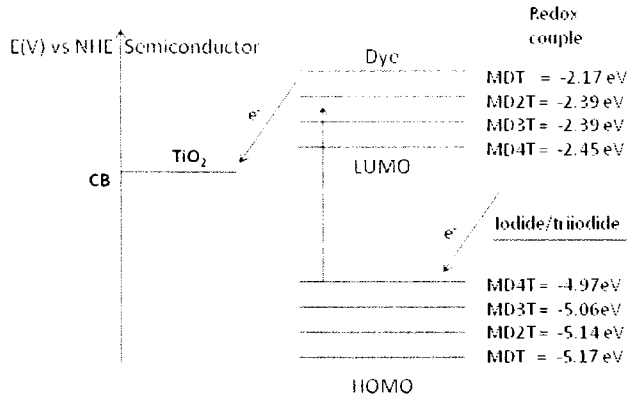

Figure 4.29 Schematic energy level diagram of **MDnT** (n = 1-4).

By comparing the HOMO and LUMO energy levels of four dyes **CAnT** (n = 1-4) with linker variation is shown in Figure 4.29.

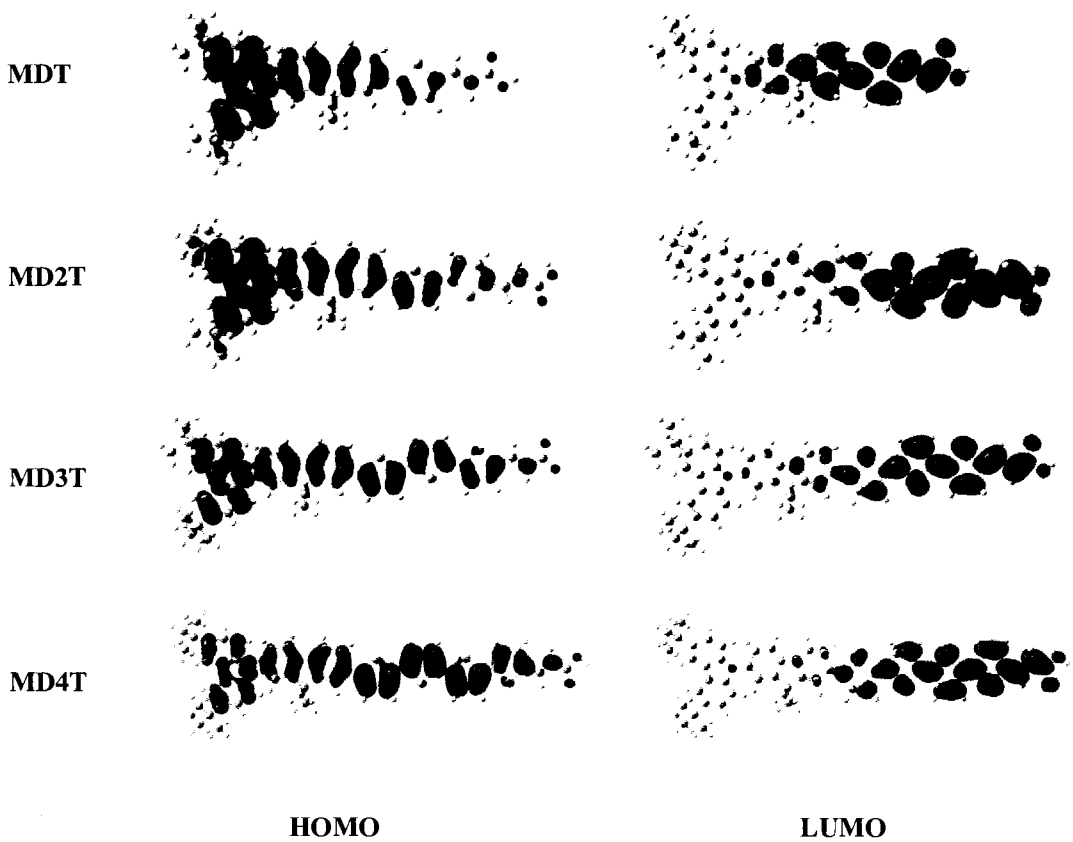

Figure 4.30 HOMO and LUMO distributions of the **MDnT** (n = 1-4) dyes calculated with DFT on a BTLYP/6-31G(d,p) level.

4.3.6 Photovoltaic performance of DSCs band on the dyes

The photovoltaic properties of the solar cell constructed from the **CAnT** (n = 1-4) dye-sensitized TiO_2 electrodes were measured under simulated AM 1.5 G irradiation (80 mW/cm^2). The open circuit photovoltage (V_{oc}), short circuit (J_{sc}), fill factor (ff), and solar-to-electrical energy conversion efficient (η) are list in table 4.4. The optimized evaluation condition for **CAnT** (n = 1-4) dye is determined to be 5 x 10^{-5} M of dye in chloroform solution and the electrolyte compose of 70 v% GBL, 30 v% NMP, 0.5 M LiI, 0.05 M I_2 and 0.4M PY.

Table 4.4 Photovoltaic performance of DSCs base on **CAnT** (n = 1-4) dye.

Dye	V_{oc}(V)	J_{sc}(mA/cm^2)	fill factor (ff)	η (%)
N 719	0.67	9.44	0.67	4.24
CAT	0.60	4.28	0.69	
CA2T	0.65	6.70	0.72	1.81
CA3T	0.61	6.89	0.63	3.13
CA4T	0.54	3.66	0.64	2.58
				1.25

Current-density-voltage (*J-V*) characteristics of device based on the **CAnT** (n = 1-4) dye are shown in Figure 4.30. The photovoltaic performance of **CAnT** (n = 1-4) were promising with an overall solar-to-electric conversion efficiency (η) of 1.81% (V_{oc} = 0.60 V, J_{sc} = 4.28 mA/cm^2, ff = 0.69), 3.13% (V_{oc} = 0.65 V, J_{sc} = 6.70 mA/cm^2, ff = 0.72), 2.58% (V_{oc} = 0.61 V, J_{sc} = 46.89 mA/cm^2, ff = 0.63) and 1.25% (V_{oc} = 0.54 V, J_{sc} = 3.66 mA/cm^2, ff = 0.64), respectively, compared to **N 719** which under the same conditions gave η = 4.24% (V_{oc} = 0.67 V, J_{sc} = 9.44 mA/cm^2, ff = 0.67). The *J-V* curves obtained under dark conditions for **CAnT** (n = 1-4) on shown in Figure 4.30. It is found that the onsets for **CAnT** (n = 1-4) in range 0.53-0.65 V compared with **N719** dyes. This indicates that the back-electron-transfer process corresponding to the reaction between the conduction-band electrons in the TiO_2 and I_3^- in the electrolyte under dark conditions occurs more easily in DSCs base on **N719** dyes [106].

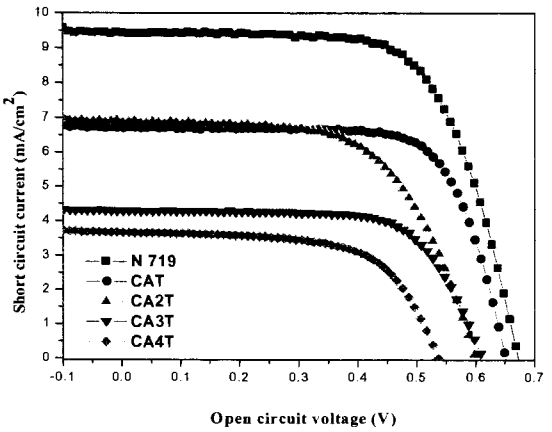

Figure 4.31 *J-V* curves of DSCs based on **CAnT** (n = 1-4) and **N719**.

4.4 Conclusion

Novel D-π-A organic dye, **CAnT** (n = 1-4) and **MDnT** (n = 1-4) have synthesized as dye sensitizers for DSCs applications by using Ullmann coupling, Suzuki coupling and Knoevenagel condensation reaction. Different number of thiophene unit is introduced to the molecule and serve as linker. The electron-withdrawing part are cyanoacrylic acid and acrylic acid groups. The target molecules were characterized by using NMR, IR, Mass, UV-vis and fluorescence techniques. The target molecules exhibit a absorption band cover UV and visible region. Fluorescence spectra of the target molecules show emission peak at yellow-orange region, exited at λ_{max} of each molecule. **CAnT** (n = 1-4) and **MDnT** (n = 1-4) show a good electrochemical and thermal properties. The overall solar-to-electric conversion efficiency of **CAnT** (n = 1-4) were 1.81%, 3.13%, 2.58% and 1.25% , respectively, compared to the conversional **N719** dye which gave 4.24 under the same conditions. DFT calculations have been performed on the dyes, and the results show the electron distribution from the whole molecules to the anchoring moieties occurred during the HOMO-LUMO excitation. The cyanoacrylic acid and acrylic acid are coplanar with respect to the thiophene units.

CHAPTER 5

SYNTHESIS AND CHARACTERIZATION OF NOVEL DONOR π-CONJUGATE ACCEPTOR ORGANIC MATERIALS FOR ORGANIC LIGHT-EMITTING DIODES: π-CONJUGATE VARIATION

5.1 Introduction

Carbazole has strong absorption in the near-UV region and a low redox potential. The electrochemical and spectroscopic properties of carbazole and its derivative have been extensively investigated. Chemically, carbazole can be easily functionalized at its 3-,6- or 9-positions and covalently linked to other molecular moieties [108]. Due to its unique optical, electrical, and chemical properties, carbazole has been used widely as a functional building block or substituent in the construction of organic molecules for use as light-emitting and hole-transporting layers in OLED devices [109, 110], as host materials for electrophosphorescent applications [111], and as active components in solar cells. Moreover, the thermal stability and glassy state durability of the organic molecules were found to be significantly improved upon incorporation of a carbazole moiety into the structure [112, 113].

Fluorene is a polycyclic aromatic compound, which received its name due to strong violet fluorescence arising from its highly conjugated planar π-electron system. 2- and 7-Positions in fluorene are the most reactive sites toward electrophilic attack, which allows construction of a fully conjugated rigid-rod polymer chain by substitution reactions, whereas the methylene bridge provides an opportunity to modify the processability of the polymer by substituents without perturbing the electronic structure of the backbone. Polyfluorenes (PFs) are the most promising class of blue-emitting materials. Small-molecule fluorenes have a number of advantages, such as ease of purification and characterization, well-defined structures, and easily tunable luminescence and thermal properties. However, small-molecule fluorene derivatives used as practical blue emitters in OLEDs are still rare [114-117].

Malononitrile, methyl cyanoacetate and 1,3-indandione is a versatile compound of exceptional reactivity. It is used extensively as a reactant or reaction intermediate since

the methylene group and cyano groups or can take part in condensation reaction to give a variety of addition products [118]. They are known to be strongly electron accepting group. The advantages of including these group might be indicated. Firstly, it creates intramolecular charge transfer effect and secondly, its presence may lead to the reduction of the energy gap in the molecule. On the other hand due to the size of the substituent it may cause steric interactions [119].

5.2 Aim of the study

We designed a novel π-conjugate of *N*-carbazole end-capped oligofluorene-thiophene based on carbazole as the donor group, Chemically, carbazole can be easily functionalized at its 3,6-positions with a bulky group of *tert*-butyl moiety to protect the oxidation coupling at the 3,6-positions of the peripheral carbazole moiety. Fluorene was introduced on *N*-9 of carbazole as electron transport moiety. The *n*-hexyl substituents were introduced on the C-9 position of fluorene ring to increase the solubility, with a thiophene linker and a methylcyanoacrylate, dimalononitrile and indandione as acceptor units as emitter in OLEDs. Their basic optical, electrochemical, and thermal properties have been investigated. Their basic optical, electrochemical, and thermal properties have been investigated.

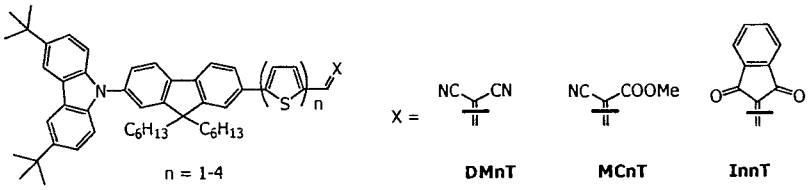

Figure 5.1 Chemical structures of **DMnT** (n = 1-4), **MCnT** (n = 1-4) and **InnT** (n = 1-4).

5.3 Results and discussion

5.3.1 Synthesis

The synthesis of oligothiophene-based dyes, **DMnT** (n = 1-4) with molononirile, as an acceptor was synthesized. Knoevenagel condensation reaction of aldehyde compounds with molononirile in a present of piperidine as a base and catalyst in mixture of THF and acetonitrile as solvent at reflux for 6 h gave the targets **DMnT** (n = 1-4) as orange solid to red solid in range 14-30% yield as shows in Figure 5.2.

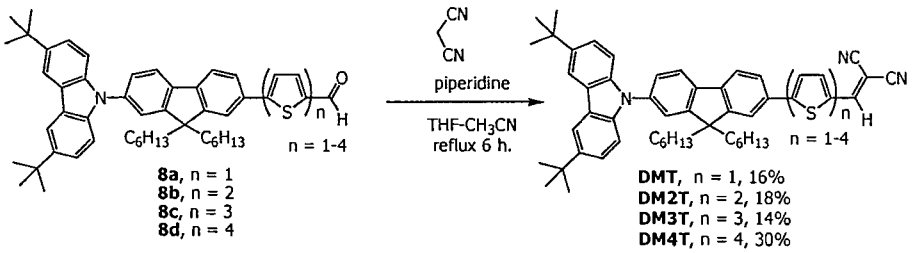

Figure 5.2 Knoevenagel condensation reaction to form **DMnT** (n = 1-4).

The chemical structures of **DMnT** (n = 1-4) were confirm by ^{1}H-NMR, ^{13}C-NMR and IR analysis. The ^{1}H-NMR spectra of the products **DMnT** (n = 1-4) shows a singlet signal at chemical shift 8.19-8.13 ppm (2H) assigning of 4-H and 5-H of 3,6-di-tert-butylcarbazole and a singlet signal at chemical shift 7.33-7.21 ppm (1H) is ascribed to vinyl double bond. The ^{13}C-NMR spectra of **DMnT** (n = 1-4) show a single peak for chemically carbon atom of of cyano group at 116.35 ppm. Furthermore, IR spectra display the absorption peak at 2222 cm^{-1} which is consistent with the present of cyano group of malononitrile group.

MCnT (n = 1-4) dyes with methylcyanoacetic acid, as an acceptor were synthesized. Knoevenagel condensation reaction of aldehyde compounds with methylcyanoacetic acid in a present of piperidine as a base and catalyst in mixture of THF and acetonitrile as solvent at reflux for 6 h gave the targets **MCnT** (n = 1-4) as orange solid to red solid in range 57-85% yield as shows in Figure 5.3.

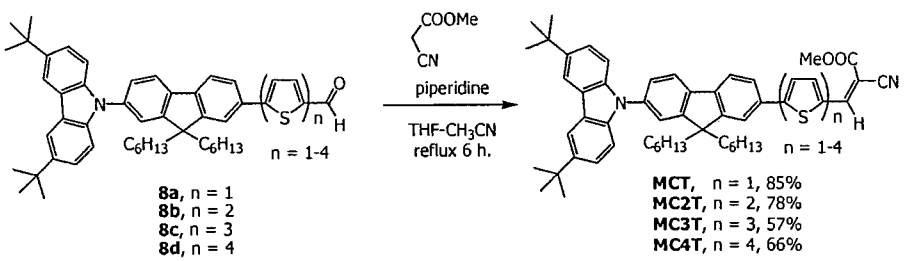

Figure 5.3 Knoevenagel condensation reaction to form **MCnT** (n = 1-4).

The chemical structures of **MCnT** (n = 1-4) were confirm by ^{1}H-NMR, ^{13}C-NMR, Mass and IR analysis. The ^{1}H-NMR spectrum of the products **MCnT** (n = 1-4) show a singlet signal at chemical shift in range 7.31 ppm (1H) is ascribed to vinyl double bond of

methyl-2-cyanoacrylate moiety, a singlet signal at chemical shift in range 8.19-8.17 ppm (2H) assigning of 4-H and 5-H of 3,6-di-*tert*-butylcarbazole, and a singlet signal at chemical shift in range 3.92-3.94 ppm (3H) is assigned to 3 protons of methyl group of methyl-2-cyanoacrylate moiety. The ^{13}C-NMR spectra of **MCnT** (n= 1-4) show a single peak for chemically carbon atom of carbonyl group at 163.54-163.48 ppm and a singlet peak for carbon atom of cyano group at 116.34-116.09 ppm. Furthermore, IR spectra display the absorption peak at 2217-2222 cm^{-1} and 1721-1724 cm^{-1} which is consistent with the present of cyano group and the present of carbonyl group of the methyl-2-cyanoacrylate moiety, respectively.

For **InnT** (n = 1-4) dyes having the indandione as an acceptor were synthesized by Knoevenagel condensation reaction of aldehyde compound with 1,3-indandione in the same condition as **DMnT** (n = 1-4) and afforded as orange to dark violet in range 59-69% as shows in Figure 5.4.

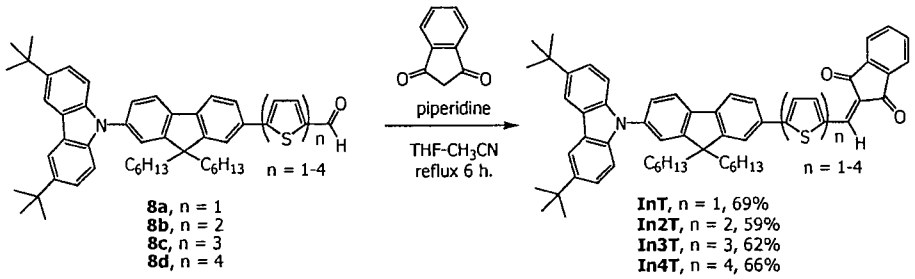

Figure 5.4 Knoevenagel condensation reaction to form **InnT** (n = 1-4).

The chemical structures of **InnT** (n = 1-4) were confirmed by ^{1}H-NMR, ^{13}C-NMR and IR analysis. The ^{1}H-NMR spectra of the final products **InnT** (n = 1-4) show singlet signal at chemical shift 8.18-8.17 ppm (2H) is assigned 4-H and 5-H of 3,6-di-*tert*-butylcarbazole, multiplet signal at chemical shift 8.01-7.97 ppm (2H) assigned 4-H and 7-H of methyleneindanedione meoity, doublet signal at chemical shift 7.20 ppm (1H) ascribed to vinyl double bond of methyleneindanedione meoity. The ^{13}C-NMR spectra of **InnT** (n = 1-4) show two singlet peaks for chemically carbon atom of carbonyl group at 190.42-190.26 and 189.92-189.71 ppm. Furthermore, IR spectra display the absorption peak at 1678-1681 cm^{-1} which is consistent with the present of carbonyl group of the methyleneindanedione meoity.

5.3.2 Optical properties

The UV-vis and fluorescence spectra of dyes in CH_2Cl_2 and film spin-coated on a quartz substrate are listed in Table 5.1. The target molecules **DMnT** (n = 1-4), exhibited three UV-visible absorption band cover from 280-600 nm as shown in Figure 5.5 The absorption peak around 298 and 336-402 nm corresponds of absorption peak of carbazole and fluorene unit, respectively. The absorption band is shifted depending on molecular structure of the end-capping groups. While the later absorption band assigned as the absorption of ICT band from D-π-A at 454-520 nm. In the thin film, **DMnT** (n = 1-4) show red-shift and broader absorption peak compared with solution, which have a similar extinction coefficient of in the π-π^* transition band, while the extinction coefficient of the chart transfer transition band increases in the order of **DM3T** > **DMT** > **DM2T** > **DM4T**. The energy band gaps of **DMnT** (n = 1-4) were estimated to be 2.33, 2.15, 2.05 and 2.03 eV, respectively, from the absorption edge of the solution. The fluorescence spectra of **DMnT** (n = 1-4) solution and solid film exhibit a fluorescence peaked at 592-627 nm, which are red shifted with increasing number of thiophene unit as the extent of the π-conjugation system in the oligomers increases.

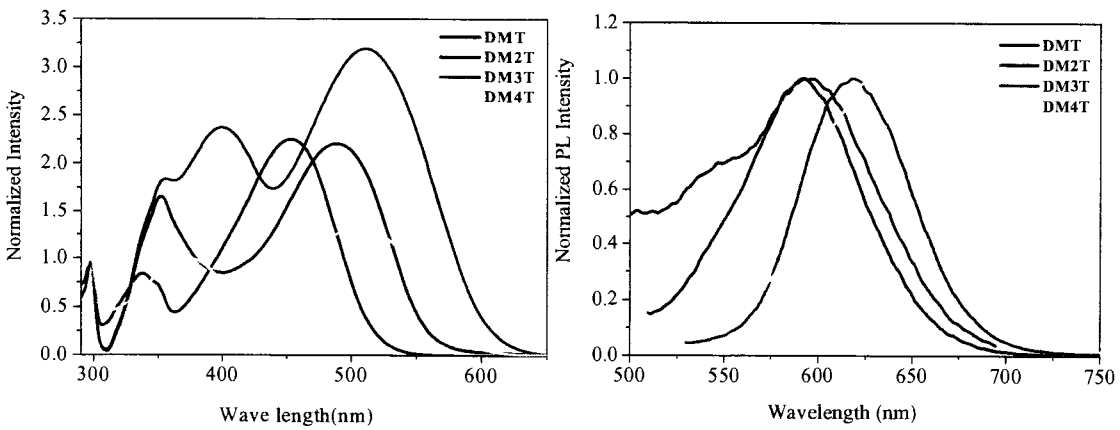

Figure 5.5 Absorption spectra and PL spectra of **DMnT** (n = 1-4) in dry CH_2Cl_2 solution.

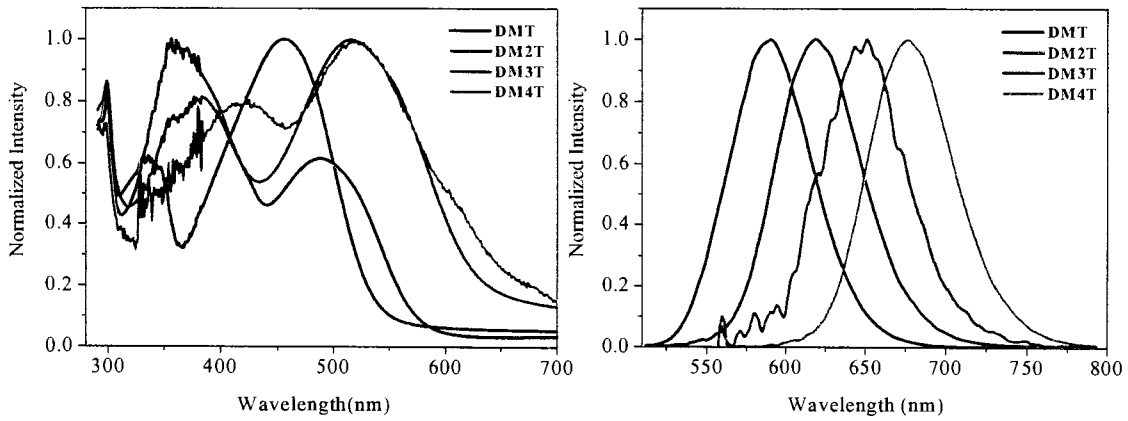

Figure 5.6 Absorption spectra and PL spectra in thin films of **DMnT** (n = 1-4).

The UV-vis and fluorescence spectra of dyes in CH_2Cl_2 and film spin-coated on a quartz substrate are listed in Table 5.1. The target molecules **MCnT** (n = 1-4), exhibited three UV-visible absorption band cover from 280-600 nm as shown in Figure 5.7. The former absorption band corresponds to the absorptions of fluorene and carbazole groups. The absorption band is shifted depending on molecular structure of the end-capping groups. The absorption peak around 298 and 325-402 nm corresponds of absorption peak of carbazole and fluorene unit, respectively. While the later absorption band assigned as the absorption of the methyl cyanoacrylate core at 434-495 nm. In the thin film, **MCnT** (n = 1-4) shows red-shift and broader absorption peak compared with solution, which can be attributed to the π-π^* transition of conjugated main chains, while the extinction coefficient of the chart transfer transition band increases in the order of **MC2T** > **MC4T** > **MCT** > **MC3T**. The energy band gap of **MCnT** (n = 1-4) were estimated to be 2.40, 2.21, 2.12 and 2.05 eV, respectively, from the absorption edge of the solution. The fluorescence spectra of **MCnT** (n = 1-4) solution and solid film exhibit a fluorescence peaked at 550-615 nm, which are red shifted with increasing number of thiophene unit as the extent of the π-conjugation system in the oligomers increases.

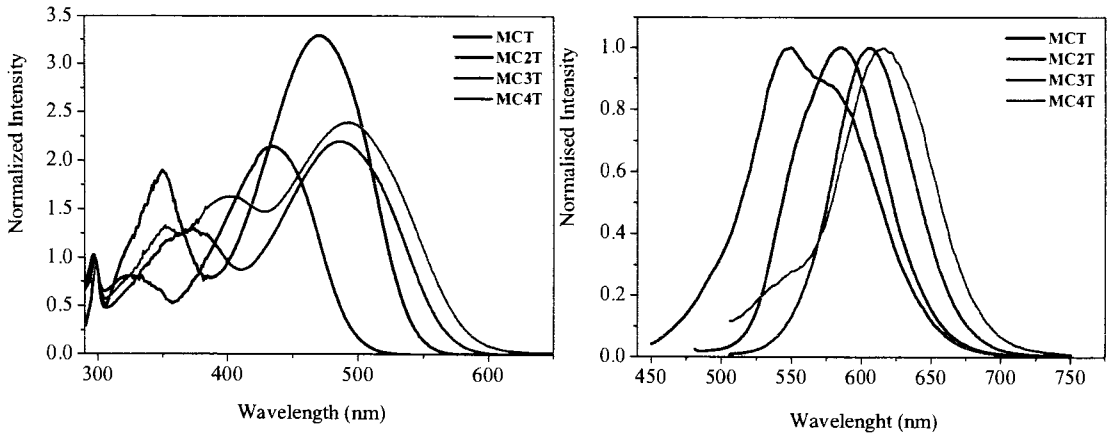

Figure 5.7 Absorption spectra and PL spectra of **MCnT** (n = 1-4) in dry CH_2Cl_2 solution.

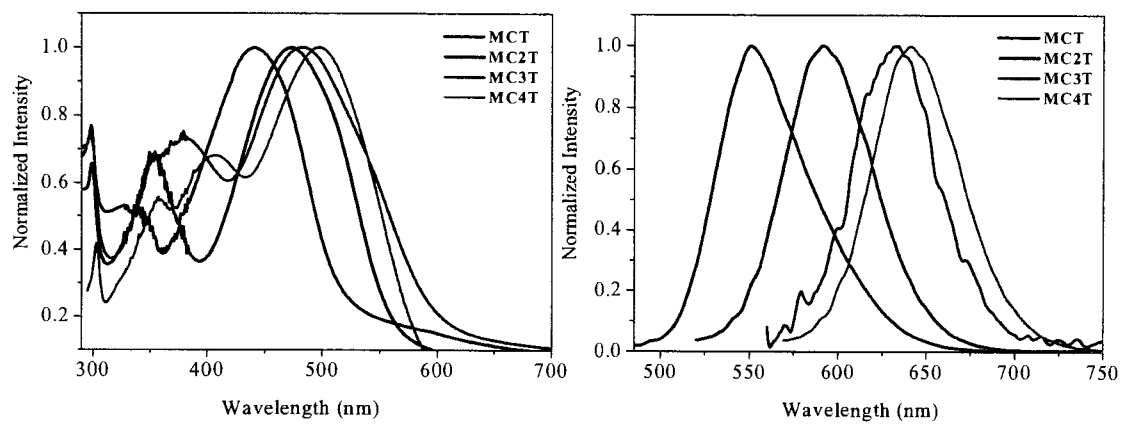

Figure 5.8 Absorption spectra and PL spectra in thin film of **MCnT** (n = 1-4).

The UV-vis and fluorescence spectra of dyes in CH_2Cl_2 and film spin-coated on a quartz substrate are listed in Table 5.1. The target molecules **InnT** (n = 1-4), exhibited three UV-visible absorption band cover from 280-650 nm as shown in Figure 5.9. The former absorption band corresponds to the absorptions of fluorene and carbazole groups. The absorption band is shifted depending on molecular structure of the end-capping groups. The absorption peak around 298 and 336-407 nm corresponds of absorption peak of carbazole and fluorene unit, respectively. While the later absorption band assigned as the absorption of the methyl cyanoacrylate core at 483-532 nm. In the thin film, **InnT** (n = 1-4) shows red-shift and broader absorption peak compared with solution, which can be attributed to the π-π^* transition of conjugated main chains, while the extinction coefficient of the chart transfer transition band increases in the order of **In2T** > **In4T** > **In3T** > **InT**. The energy band gap of **InnT** (n = 1-4) were estimated to be 2.18,

1.99, 1.94 and 1.89 eV, respectively, from the absorption edge of the solution. The fluorescence spectra of **InnT** (n = 1-4) solution and solid film exhibit a fluorescence peaked at 550-615 nm, which are red shifted with increasing number of thiophene unit as the extent of the π-conjugation system in the oligomers increases.

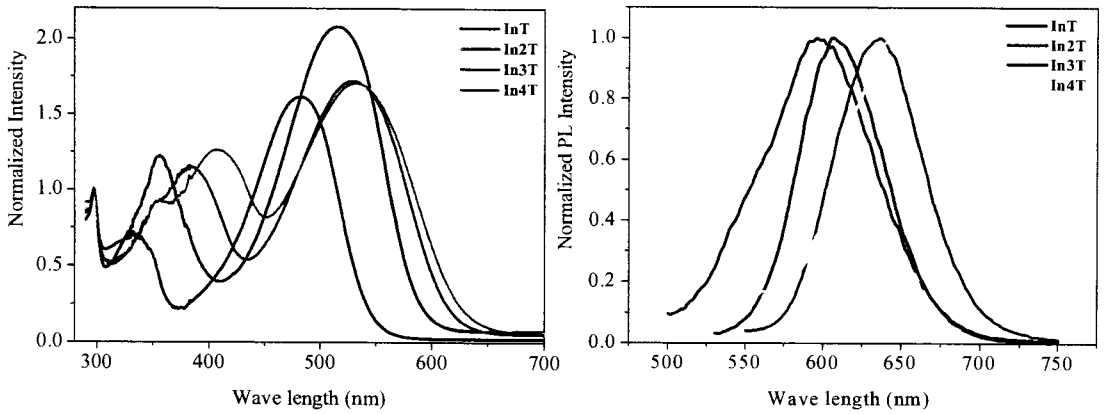

Figure 5.9 Absorption spectra and PL spectra of **InnT** (n = 1-4) in dry CH_2Cl_2 solution.

A series of oligothiophens with different acceptor as dimalononitrile, methylcyanoacrylate and 1,3-indandione, exhibited the former absorption band corresponds to the absorptions of π-conjugate linker connected to acceptor moiety. **InnT** (n = 1-4) shows longer red-shift and broader absorption peak compared with **DMnT** (n = 1-4) and **MCnT** (n = 1-4), which can be tributed to the π-π^* transition of longer conjugated main chains, its presence may lead to the reduction of the energy gap in the molecule.

Table 5.1 The absorption and fluorescence data of **DMnT** (n = 1-4), **MCnT** (n = 1-4) and **InnT** (n = 1-4).

Compound	λ_{max} (nm)	λ_{max} in thin film (nm)	λ_{max} of emission in CH_2Cl_2 (nm)
DMT	298, 337, 453	455	592
DM2T	298, 352, 490	488	593
DM3T	298, 399, 511	515	618
DM4T	298, 375, 506	519	627
MCT	298, 326, 434	441	550
MC2T	298, 349, 470	472	584
MC3T	298, 372, 486	482	605
MC4T	298, 402, 492	482	615
InT	298, 336, 483	475	596
In2T	298, 356, 514	507	605
In3T	298, 386, 529	512	635
In4T	298, 407, 532	527	643

5.3.3 Thermal Properties

For OLED application, thermal stability of organic materials is crucial for device stability and lifetime. The thermal instability or low glass transition temperature (T_g) of the amorphous organic layer may result in the degradation of organic devices due to morphological changes. The thermal properties of the **DMnT** (n = 1-4) were determinated by DSC analysis (Figure 5.11) with a heating rate of 10 °C/min under a nitrogen atmosphere. DSC curves of **DM2T** shows T_g at 86 °C, in first heating cycles. DSC curves of **DM3T** and **DM4T** displays in the first heating an endothermic peak due to melting is observed at 164 and 226 °C, respectively. These results indicate that the **DM2T** is amorphous material, **DM3T** and **DM4T** are semi-crystalline material. However, DSC curve of **DMT** behave totally different. In first heating cycle, an endothermic phenomena (T_g) at 79 °C was observed followed by an exothermic peak due to crystallization around 189 °C to give a crystal, which endothermically melted at 200 °C. The ability of **DM2T**, **DM3T** and **DM4T** to form stable amorphous glasses and the possibility to prepare thin

films form **DM2T, DM3T** and **DM4T** both by evaporation and by solution casting are highly desirable for application in OLEDs.

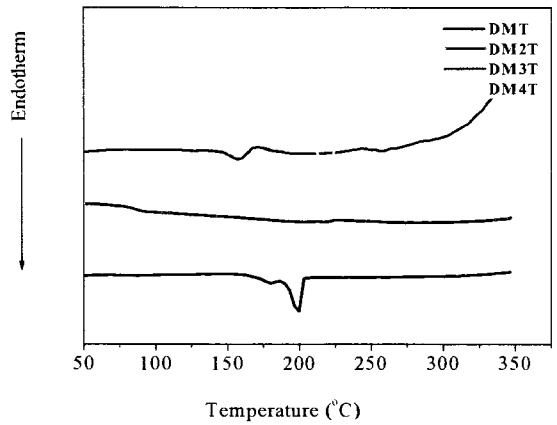

Figure 5.10 DSC curves of **DMnT** (n = 1-4) measured at a heating rate of 10 min/ °C under N_2.

The thermal properties of the **MCnT** (n = 1-4) were determinated by DSC and TGA analysis (Figure 5.12) with a heating rate of 10 °C /min under a nitrogen atmosphere. In first heating cycle, DSC curves of **MCT** display only an endothermic phenomenon (T_g) at 186 °C. These results indicate that the **MCT** is amorphous material. DSC curves of **MC3T** shows only T_m at 204 °C in first heating scan. DSC curves of **MC4T** displays in the first heating scan an endothermic peak due to melting is observed at 253 °C and exothermic peak due to crystallization around 172 °C to give crystal. These results indicate that the **MC4T** is crystalline. However, DSC curves of **MC2T** behave totally different. In first heating cycle, an endothermic phenomenon (T_g) at 158 °C was observed followed by an exothermic peak due to crystalline around 179 °C to give a crystal, which endothermically melted at 184 °C. The degradation temperature at 5% weight loss (T_d) of **MCT, MC2T, MC3T** and **MC4T** were measured to be 170, 303, 311 and 292 °C, respectively. The ability of **MCT, MC2T** and **MC3T** to form stable amorphous glasses and the possibility to prepare thin films form **MCT, MC2T** and **MC3T** both by evaporation and by solution casting are highly desirable for application in OLEDs.

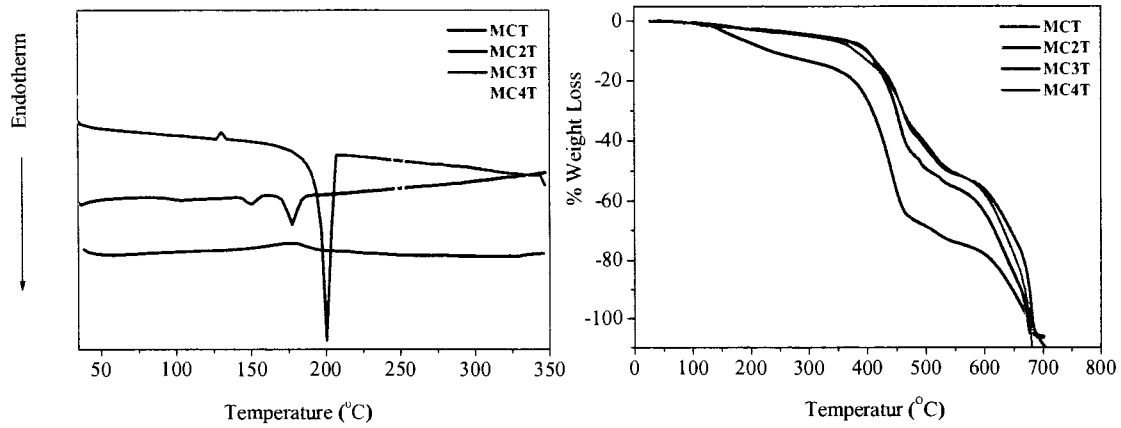

Figure 5.11 DSC and TGA curves of **MCnT** (n = 1-4) measured at a heating rate of 10 min/ °C under N_2.

The thermal properties of the **InnT** (n = 1-4) were determinated by DSC and TGA analysis (Figure 5.13) with a heating rate of 10^0C/min under a nitrogen atmosphere. DSC curves of **InT** show only T_g at 103 °C. The result indicate that the **InT** is amorphous property. DSC curves of **In2T** displays in the first heating scan an endothermic peak due to melting is observed at 160 °C and T_g around 113 °C to give semi-crystal. However, DSC curves of **In3T** and **IN4T** behave totally different. In first heating cycle, an endothermic phenomenon (T_g) at 96 °C was observed followed by an exothermic peak due to crystalline around 197 and 179 °C to give a crystal, which endothermically melted at 230 and 219 °C, respectively. The degradation temperature at 5% weight loss (T_d) of **InT, In2T, In3T** and **In4T** were measured to be 223, 242, 232 and 239 °C, respectively. The ability of **InT** and **In2T** to form stable amorphous glasses and the possibility to prepare thin films form **InT** and **In2T** both by evaporation and by solution casting are highly desirable for application in OLEDs.

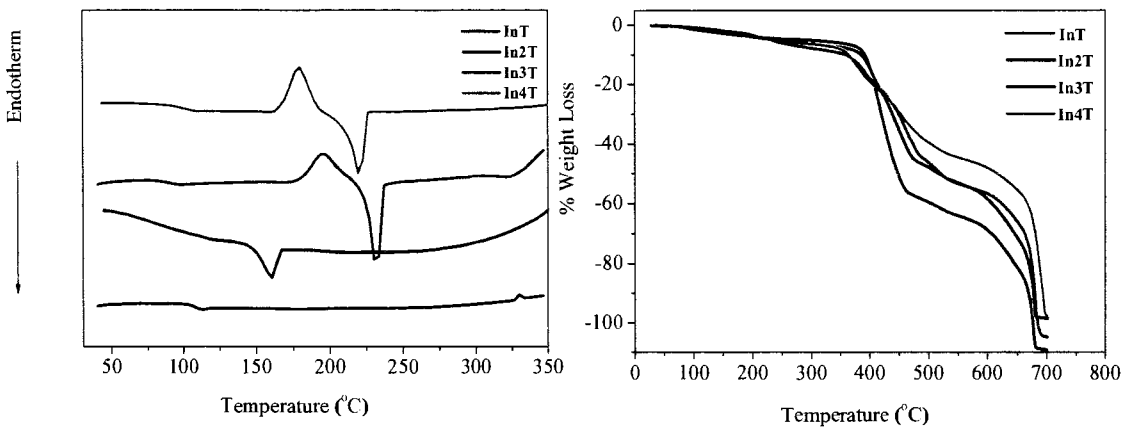

Figure 5.12 DSC and TGA curves of **InnT** (n = 1-4) measured at a heating rate of 10 min/ °C under N_2.

5.3.4 Electrochemical properties

In order to investigate the electrochemical properties of the target molecule, cyclic voltametry (CV) measurements were performed in CH_2Cl_2 containing 0.1 M *n*-Bu_4NPF_6 as a supporting electrolyte. The results are shown in Figure 5.14 and summarized in Table 5.3. Compounds **DMT** detected one reversible oxidation and one irreversible reduction, **DM2T** and **DM3T** demonstrated two quasi-reversible oxidation- processes and one irreversible reduction, while compound **DM4T** showed three quasi-reversible oxidation processes and one irreversible reduction.

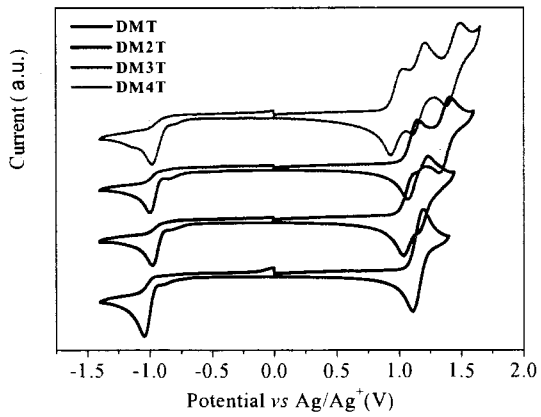

Figure 5.13 Cyclic voltammograms of **DMnT** (n = 1-4) in CH_2Cl_2 with scan rate of 0.05 V/s and 0.1 M *n*-Bu_4NPF_6 as electrolyte.

Cyclic voltammograms of **DMT** (Figure 5.15) was analyzed in CH_2Cl_2 solution with scan rate of 0.05 V/s and n-Bu_4NPF_6 as electrolyte, detected one reversible oxidation (one electron oxidation) and one irreversible reduction (one electron transfer) peaks. It shows one oxidation waves with half-wave potential ($E_{1/2}$) yielding cations at 1.16 V, which is assigned as the formation 3,6-di-(*tert*-butyl)carbazole cation. The proposed oxidation mechanism for *tert*-butyl substituented carbazole system were described for **CAT**. It also shows a similar wave in difference scans, indicating a good and electrochemical property. It shows one irreversible reduction with half-wave potential ($E_{1/2}$) of -1.00 V, which are assigned as the reduction process of malononitrile acceptor. The propose reduction mechanism for the malononitrile system is shown in Figure 5.15, which one electron transfer process lead to the formation of radical anion. It is reasonable to assume that the major portion of electron density resides on the carbonyl oxygen due to the electron-withdrawing nature of the oxygen atom as indicated in possible resonance. The HOMO calculated, according to the following equation: HOMO = -(4.44 + E_{ox}) (eV), to be -5.49 eV. The LUMO was calculated from the value of the energy gap (2.33 eV) and HOMO energy level to be -3.16 eV.

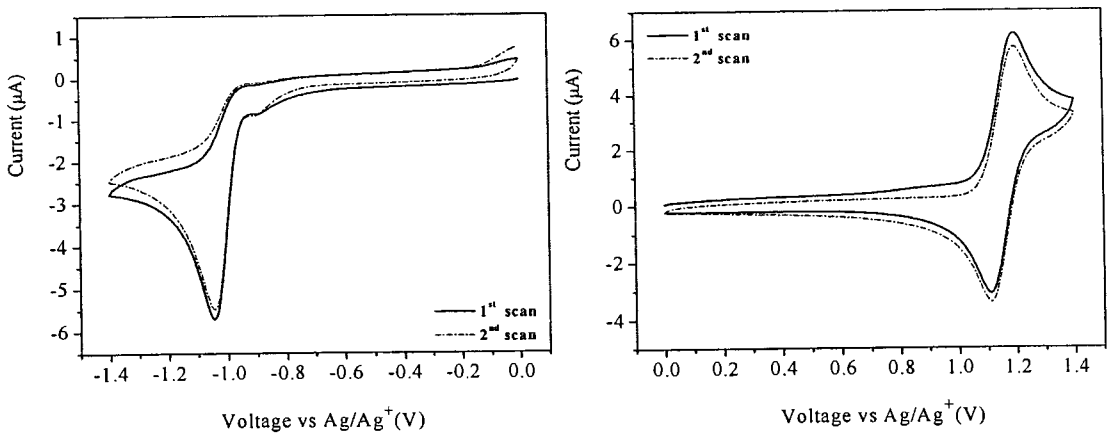

Figure 5.14 Cyclic voltammograms of **DMT** in CH_2Cl_2 with scan rate of 0.05 V/s and 0.1 M n-Bu_4NPF_6 as electrolyte.

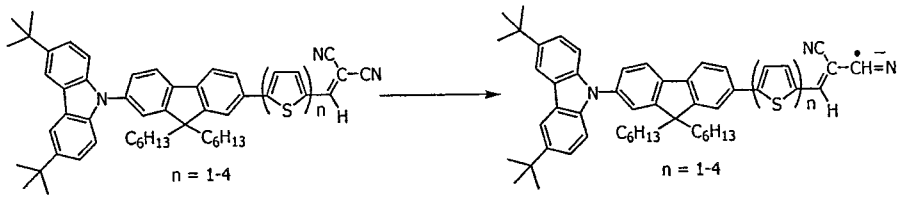

Figure 5.15 Proposed one reduction mechanism for the malononitrile.

Cyclic voltammogram of **DM2T** (Figure 5.17) was analyzed in CH_2Cl_2 solution with scan rate of 0.05 V/s and *n*-Bu_4NPF_6 as electrolyte, detected two reversible oxidation (two electron oxidation) and one irreversible reduction (one electron transfer) peaks. It shows two oxidation waves with half-wave potential ($E_{1/2}$) yielding cation and dication at 1.08 and 1.2 V, respectively, which are assigned as the formation 3,6-di-(*tert*-butyl)carbazole cation and dication. The proposed oxidation mechanism for *tert*-butyl substituented carbazole system were described for **CAT**. It also shows a similar wave in different scans no distinct a slight shift of the CV curves was observed indicate *tert*-butyl group at the 3,6-positions peripheral carbazole moiety to protect oxidation coupling, indicating a good and stable electrochemical property. It shows one irreversible reduction with half-wave potential ($E_{1/2}$) of -1.00 V, which is assigned as the reduction process of malononitrile acceptor. The propose reduction mechanism for the malononitrile system is the same as **DMT**, when the one electron transfer process lead to the formation of radical anion. It is reasonable to assume that the major portion of electron density resides on the carbonyl oxygen due to the electron-withdrawing nature of the oxygen atom as indicated in possible resonance. The HOMO calculated, according to the following equation: HOMO = -(4.44 + E_{ox}) (eV), to be -5.41 eV. The LUMO was calculated from the value of the energy gap (2.15 eV) and HOMO energy level to be -3.26 eV.

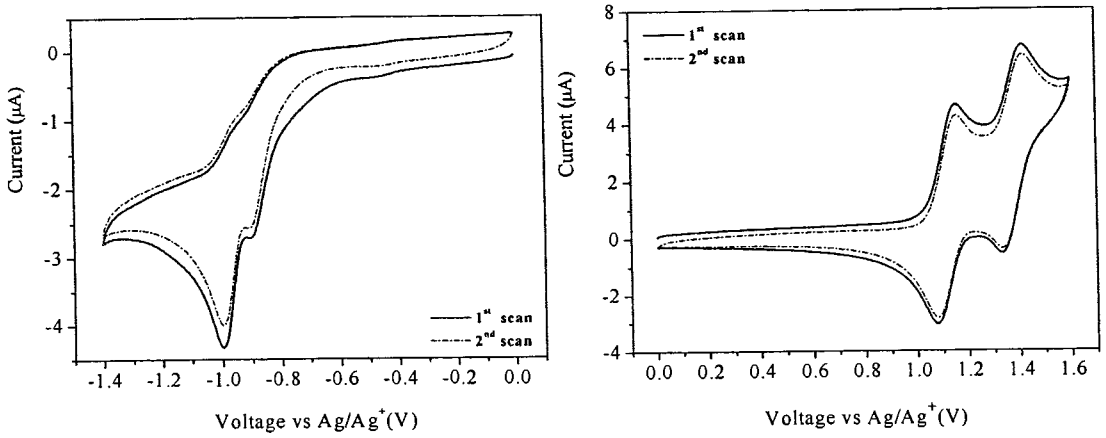

Figure 5.16 Cyclic voltammograms of **DM2T** in CH_2Cl_2 with scan rate of 0.05 V/s and 0.1 M *n*-Bu_4NPF_6 as electrolyte.

Cyclic voltammogram of **DM3T** is shown in Figure 5.18. It shows two oxidation waves with half-wave potential ($E_{1/2}$) of 1.10 and 1.36 V, respectively, which are assigned as the formation formation 3,6-di-(*tert*-butyl)carbazole cation and dication. The proposed oxidation mechanism for *tert*-butyl substituented carbazole system were described for **CAT**. It also shows a similar wave in difference scans, indicating a good and electrochemical property. It shows one irreversible reduction with half-wave potential ($E_{1/2}$) of -1.00 V, which is assigned as the reduction process of malononitrile acceptor. The onset oxidation potential (E_{ox}) of **DM3T** was estimated from the first anodic oxidation wave to be 1.07 V. The HOMO was calculated, according to the following equation: HOMO = -(4.44 + E_{ox}) (eV), to be -5.44 eV. The LUMO was calculated from the value of the energy gap (2.05 eV) and HOMO energy level to be -3.39 eV.

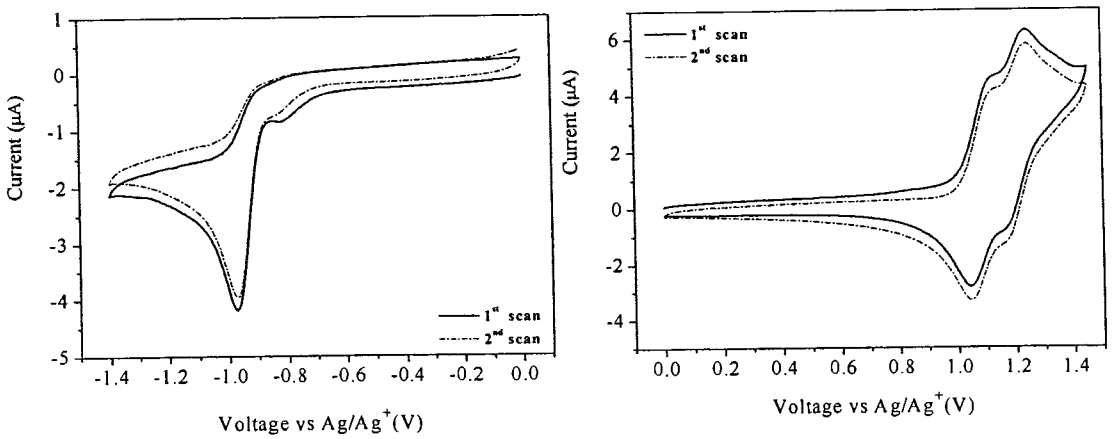

Figure 5.17 Cyclic voltammograms of **DM3T** in CH_2Cl_2 with scan rate of 0.05 V/s and 0.1 M *n*-Bu_4NPF_6 as electrolyte.

Cyclic voltammogram of **DM4T** is shown in Figure 5.19. It shows three oxidation waves with half-wave potential ($E_{1/2}$) of 0.98, 1.15 and 1.43 V, respectively, which are assigned as the formation formation 3,6-di-(*tert*-butyl)carbazole cation, dication and formation of both the radical cations the dication and indicating as expected, that the thiophene at the α and α′ positions block the reactivity. The proposed oxidation mechanism for *tert*-butyl substituented carbazole and π-conjugated thiophene system were described for **CAT** and **CA4T.** It also shows a similar wave in different scans no distinct a slight shift of the CV curves was observed indicate *tert*-butyl group at the 3,6-positions peripheral carbazole moiety to protect oxidation coupling, indicating a good and stable electrochemical property. It shows one irreversible reduction with half-wave potential ($E_{1/2}$) of -1.00 V, which are assigned as the reduction process of malononitrile acceptor. The onset oxidation potential (E_{ox}) of **DM4T** was estimated from the first anodic oxidation wave to be 0.93 V. The HOMO was calculated, according to the following equation: HOMO = -(4.44 + E_{ox}) (eV), to be -5.32 eV. The LUMO was calculated from the value of the energy gap (2.03 eV) and HOMO energy level to be -3.29 eV.

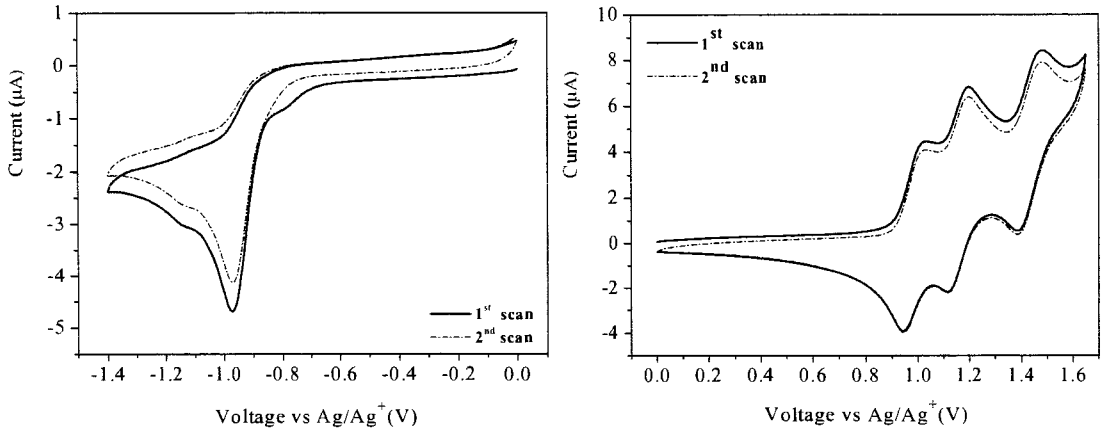

Figure 5.18 Cyclic voltammograms of **DM4T** in CH_2Cl_2 with scan rate of 0.05 V/s and 0.1 M *n*-Bu_4NPF_6 as electrolyte.

The redox property and HOMO-LUMO energy levels of the target molecules **MCnT** (n=1-4) were investigated using cyclic voltammetry (CV). The measurement was performed with a 1.0 mM solution of **MCnT** (n = 1-4) in CH_2Cl_2 with the present of *n*-Bu_4NPF_6 as a supporting electrolyte. The results are shown in Figure 5.20 and summarized in Table 5.3.

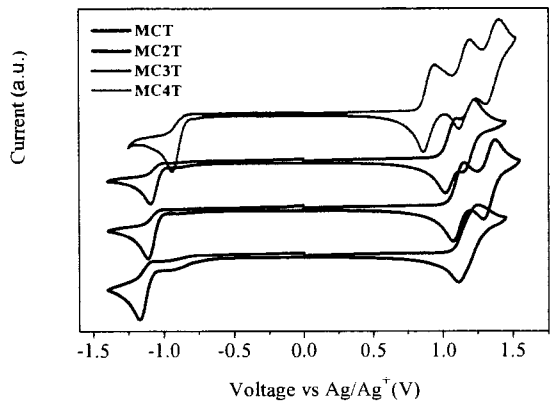

Figure 5.19 Cyclic voltammograms of **MCnT** (n = 1-4) in CH_2Cl_2 with scan rate of 0.05 V/s and 0.1 M *n*-Bu_4NPF_6 as electrolyte.

Cyclic voltammogram of **MCT** (Figure 5.22) was analyzed in CH_2Cl_2 solution with scan rate of 0.05 V/s and *n*-Bu_4NPF_6 as electrolyte, detected one reversible oxidation and one irreversible oxidation (one electron oxidation) and one irreversible reduction (one electron transfer) peaks. It shows one irreversible reduction with half-wave potential ($E_{1/2}$) of -1.28 V, which is

assigned as the reduction process of methylcyanoacetate acceptor, the formation of the methylcyanoacetate radical anion. The proposed reduction mechanism for the methylcyanoacetate system is show in Figure 5.21, when the one electron transfer process lead to the formation of radical anion. It is reasonable to assume that the major portion of the electron density resides on the carbonyl oxygen due to the electron-withdrawing nature of the oxygen atom as indicated in possible resonance.

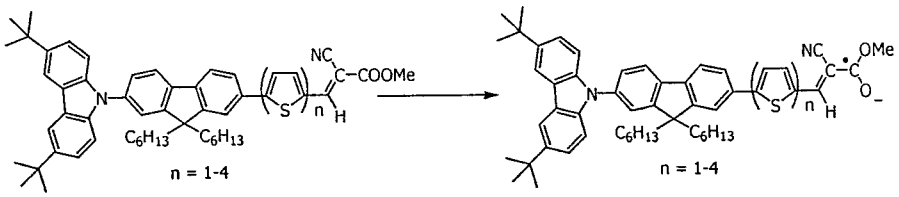

Figure 5.20 Proposed one reduction mechanism of the methylcyanoacetate.

Furthermore, It shows one oxidation waves with half-wave potential ($E_{1/2}$) of 1.18 V, which is assigned as the formation 3,6-di(*tert*-butyl)carbazole cation and dication, respectively. The proposed oxidation mechanism for *tert*-butyl substituented carbazole system was described in Chapter 4. It also shows a similar wave in different scans no distinct a slight shift of the CV curves was observed indicate *tert*-butyl group at the 3,6-positions peripheral carbazole moiety to protect oxidation coupling, indicating a good and stable electrochemical property. The onset oxidation potential (E_{ox}) of **MCT** was estimated from the first anodic oxidation wave to be 1.06 V. The HOMO was calculated, according to the following equation: HOMO = -(4.44 + E_{ox}) (eV), to be -5.50 eV. The LUMO was calculated from the value of the energy gap (2.40 eV) and HOMO energy level to be -3.10 eV.

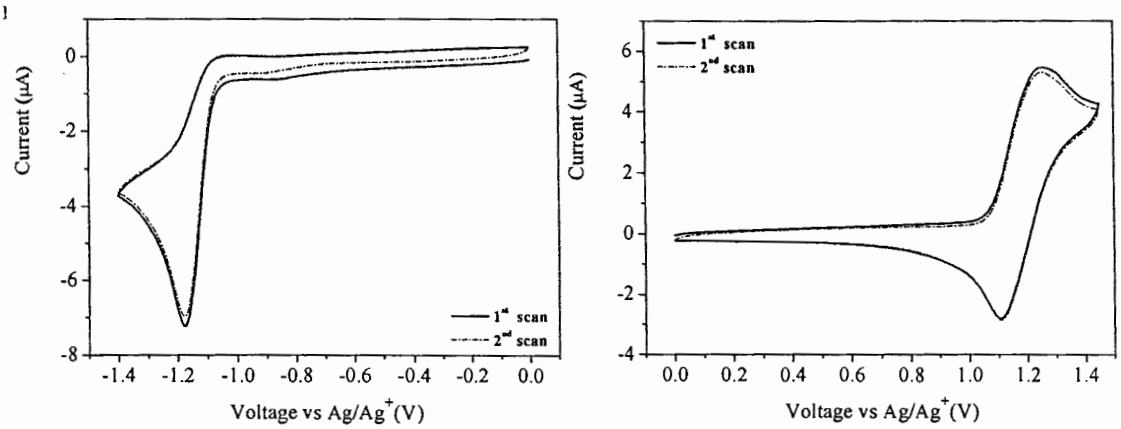

Figure 5.21 Cyclic voltammograms of **MCT** in CH_2Cl_2 with scan rate of 0.05 V/s and 0.1 M *n*-Bu_4NPF_6 as electrolyte.

Cyclic voltammogram of **MC2T** (Figure 5.23) was analyzed in CH_2Cl_2 solution with scan rate of 0.05 V/s and *n*-Bu_4NPF_6 as electrolyte, detected two reversible oxidation and one irreversible reduction (one electron transfer) peaks. It shows one irreversible reduction with half-wave potential ($E_{1/2}$) of -1.26 V, which is assigned as the reduction process of methylcyanoacetate acceptor, the formation of the methylcyanoacetate radical anion. The proposed reduction mechanism for the methylcyanoacetate system is show in Figure 5.23, when the one electron transfer process lead to the formation of radical anion. It is reasonable to assume that the major portion of the electron density resides on the carbonyl oxygen due to the electron-withdrawing nature of the oxygen atom as indicated in possible resonance.

In addition, it shows two oxidation waves with half-wave potential ($E_{1/2}$) of 1.08 and 1.20 V, respectively, which are assigned as the formation 3,6-di(*tert*-butyl)carbazole cation and dication, respectively. The proposed oxidation mechanism for *tert*-butyl substituented carbazole system were described for **CAT**. It also shows a similar wave in different scans no distinct a slight shift of the CV curves was observed indicate *tert*-butyl group at the 3,6-positions peripheral carbazole moiety to protect oxidation coupling, indicating a good and stable electrochemical property. The onset oxidation potential (E_{ox}) of **MC2T** was estimated from the first anodic oxidation wave to be 1.11 and 1.33 V. The HOMO was calculated, according to the following equation: HOMO = -(4.44 + E_{ox}) (eV), to be -5.45 eV. The LUMO was calculated from the value of the energy gap (2.21 eV) and HOMO energy level to be -3.24 eV.

Table 5.2 Physical datas of **DMnT** (n = 1-4)[a].

Compound	E_{1o} V	E_{2o} V	E_{3o} V	E_{1r} V	ΔE^0_{or} V	E_g[d] eV	HOMO[e] eV	LUMO[f] eV
DMT	1.10[b]	-	-	-1.05	2.15	2.33	-5.49	-3.16
	(1.16)[c]	-	-					
DM2T	1.04	1.17	-	-0.97	2.01	2.15	-5.41	-3.26
	(1.08)	(1.20)	-					
DM3T	1.07	1.33	-	-0.99	2.06	2.05	-5.44	-3.39
	(1.10)	(1.36)	-					
DM4T	0.92	1.10	1.36	-0.98	1.90	2.03	-5.32	-3.29
	(0.98)	(1.15)	(1.43)					

[a]Measured using a platinum rod couter electrode, a glassy carbon electrode and a SCE reference electrode in CH_2Cl_2 containing *n*-Bu_4NPF_6as a supporting electrolyte with scan rate of 0.05 V/s under argon atmosphere, [b]Peak potential, [c]Half-wave potential, [d]Estimated form the onset of the absorption spectra ($E_g = 1240/\lambda_{onset}$), [e]Calculated using the empirical equation from HOMO = -(4.44 + E_{onset}), [f]Calculated from LUMO = HOMO + E_g

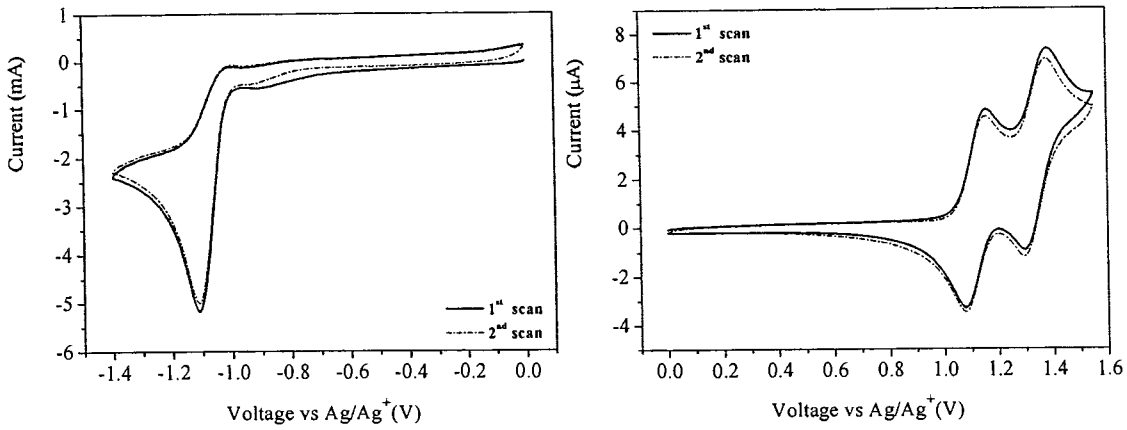

Figure 5.22 Cyclic voltammograms of **MC2T** in CH_2Cl_2 with scan rate of 0.05 V/s and 0.1 M *n*-Bu_4NPF_6 as electrolyte.

Cyclic voltammogram of **MC3T** (Figure 5.24) was analyzed in CH_2Cl_2 solution with scan rate of 0.05 V/s and *n*-Bu_4NPF_6 as electrolyte, detected two reversible oxidation (two electron oxidation) and one irreversible reduction (one electron transfer) peaks. It shows one irreversible reduction with half-wave potential ($E_{1/2}$) of -1.25 V, which is assigned as the reduction process of methylcyanoacetate system is the same as **MCT**. Its shows two reversible oxidation waves with half-wave potential ($E_{1/2}$) of 1.10 and 1.36 V, respectively, The proposed oxidation mechanism for *tert*-butyl substituented carbazole system were described for **CAT**. It also shows a similar wave in different scans no distinct a slight shift of the CV curves was observed indicate *tert*-butyl group at the 3,6-positions peripheral carbazole moiety to protect oxidation coupling, indicating a good and stable electrochemical property. The onset oxidation potential (E_{ox}) of **MC3T** was estimated from the first anodic oxidation wave to be 1.01 V The HOMO was calculated, according to the following equation: HOMO = -(4.44 + E_{ox})(eV), to be -5.43 eV. The LUMO was calculated from the value of the energy gap (2.12 eV) and HOMO energy level to be -3.31 eV.

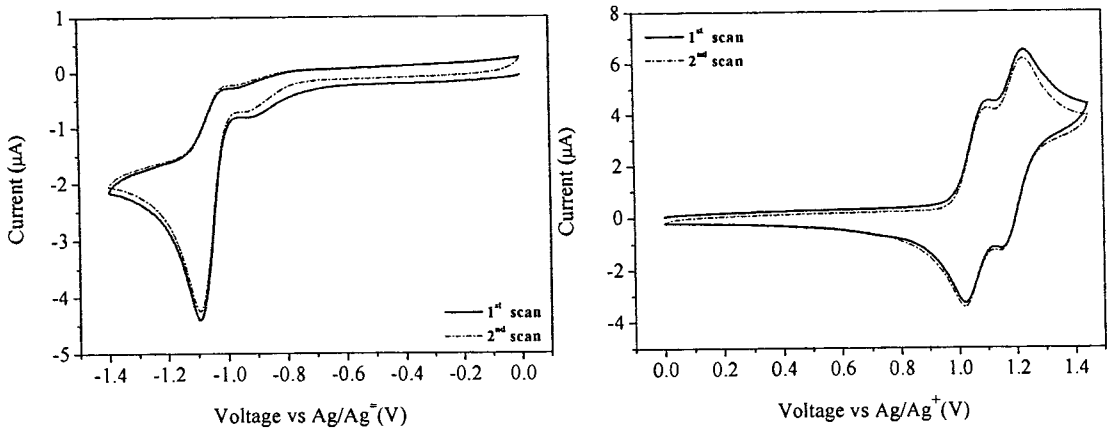

Figure 5.23 Cyclic voltammograms of **MC3T** in CH_2Cl_2 with scan rate of 0.05 V/s and 0.1 M *n*-Bu_4NPF_6 as electrolyte.

Cyclic voltammogram of **MC4T** (Figure 5.25) was analyzed in CH_2Cl_2 solution with scan rate of 0.05 V/s and *n*-Bu_4NPF_6 as electrolyte, detected three reversible oxidation (three electron oxidation) and one irreversible reduction (one electron transfer) peaks. It shows one reversible reduction with half-wave potential ($E_{1/2}$) of -1.25 V, which is assigned as the reduction process of methylcyanoacetate system is the same as **MCT**. Its shows two reversible oxidation waves with half-wave potential ($E_{1/2}$) of 1.11 and 1.33 V, respectively, The proposed oxidation mechanism for *tert*-butyl substituented carbazole and π-conjugated thiophene system were described for **CAT** and **CA4T.** It also shows a similar wave in different scans no distinct a slight shift of the CV curves was observed indicate *tert*-butyl group at the 3,6-positions peripheral carbazole moiety to protect oxidation coupling, indicating a good and stable electrochemical property. The onset oxidation potential (E_{ox}) of **MC4T** was estimated from the first anodic oxidation wave to be 1.06 V. The HOMO was calculated, according to the following equation: HOMO = -(4.44 + E_{ox}) (eV), to be -5.29 eV. The LUMO was calculated from the value of the energy gap (2.05 eV) and HOMO energy level to be -3.24 eV.

Table 5.3 Physical datas of **MCnT** (n = 1-4)[a].

Compound	E_{1o} V	E_{2o} V	E_{3o} V	E_{1r} V	ΔE^0_{or} V	E_g[d] eV	HOMO[e] eV	LUMO[f] eV
MCT	1.10[b]	-	-	-1.17	2.27	2.40	-5.50	-3.10
	(1.18)[c]	-		(-1.28)				
MC2T	1.07	1.30	-	-1.11	2.18	2.21	-5.45	-3.24
	(1.18)	1.33		(-1.25)				
MC3T	1.06	1.20	-	-1.08	2.14	2.12	-5.37	-3.31
	(1.06)	1.19		(-1.25)				
MC4T	0.89	1.11	1.33	-0.93	1.82	2.05	-5.29	-3.24
	(0.93)	1.13	1.37	(-1.25)				

[a]Measured using a platinum rod couter electrode, a glassy carbon electrode and a SCE reference electrode in CH_2Cl_2 containing *n*-Bu_4NPF_6 as a supporting electrolyte with scan rate of 0.05 V/s under argon atmosphere, [b]Peak potential, [c]Half-wave potential, [d]Estimated form the onset of the absorption spectra ($E_g = 1240/\lambda_{onset}$), [e]Calculated using the empirical equation from HOMO = -(4.44 + E_{onset}), [f]Calculated from LUMO = HOMO + E_g

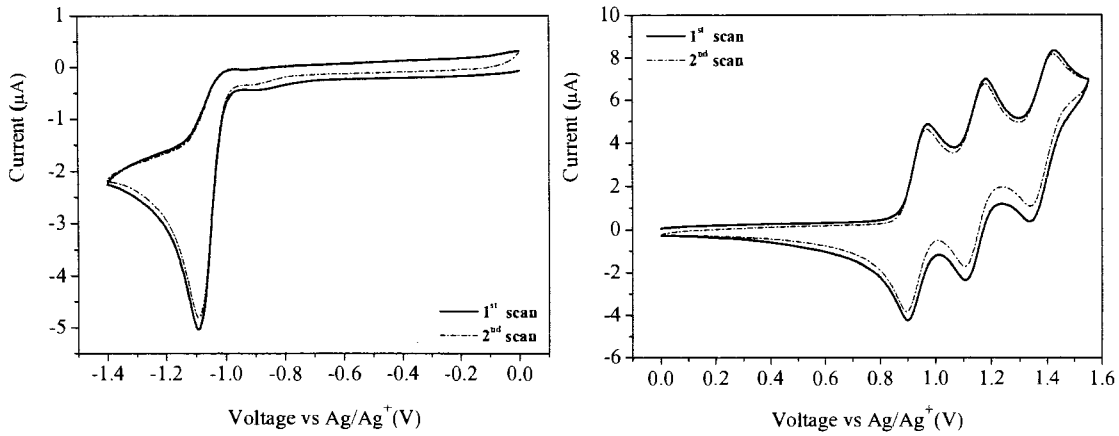

Figure 5.24 Cyclic voltammograms of **MC4T** in CH_2Cl_2 with scan rate of 0.05 V/s and 0.1 M *n*-Bu_4NPF_6 as electrolyte.

The redox property and HOMO-LUMO energy levels of the target molecules **InnT** (n = 1-4) were investigated using cyclic voltammetry (CV). The measurement was performed with a 1.0 mM solution of **InnT** (n = 1-4) in CH_2Cl_2 with the present of *n*-Bu_4NPF_6 as a supporting electrolyte. The results are shown in Figure 5.26 and summarized in Table 5.3.

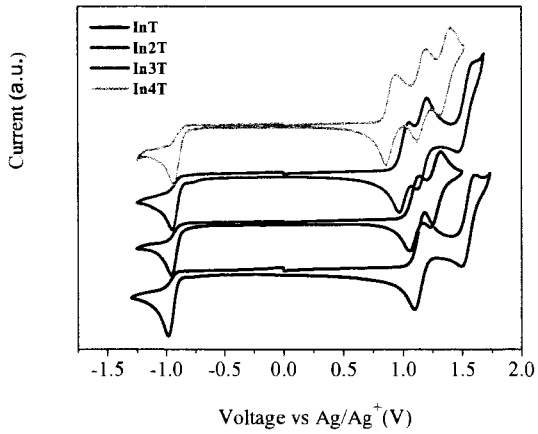

Figure 5.25 Cyclic voltammograms of **InnT** (n = 1-4) in CH_2Cl_2 with scan rate of 0.05 V/s and 0.1 M *n*-Bu_4NPF_6 as electrolyte.

Cyclic voltammogram of **InT** (Figure 5.27) was analyzed in CH_2Cl_2 solution with scan rate of 0.05 V/s and *n*-Bu_4NPF_6 as electrolyte, detected two reversible oxidation (two electron oxidation) and one irreversible reduction (one electron transfer) peaks. It shows one reversible reduction with half-wave potential ($E_{1/2}$) of -1.14 V, which is assigned as the reduction

process of methyleneindene1,3-dion acceptor, the formation of the methyleneindene-1,3-dion radical anion. The proposed reduction mechanism for the methyleneindene 1,3-dion system is show in Figure 5.28, when the one electron transfer process lead to formation of radical anion. It is reasonable to assume that the major portion of the electron density resides on the carbonyl oxygen due to the electron-withdrawing nature of the oxygen atom as indicated in possible resonance.

In addition, it shows two oxidation waves with half-wave potential ($E_{1/2}$) of 1.14 and 1.55 V, respectively, which are assigned as the formation 3,6-di(*tert*-butyl)carbazole cation and dication, respectively. The proposed oxidation mechanism for *tert*-butyl substituented carbazole system was described in Chapter 4. It also shows a similar wave in different scans no distinct a slight shift of the CV curves was observed indicate *tert*-butyl group at the 3,6-positions peripheral carbazole moiety to protect oxidation coupling, indicating a good and stable electrochemical property. The onset oxidation potential (E_{ox}) of **InT** was estimated from the first anodic oxidation wave to be 1.05 V. The HOMO was calculated, according to the following equation: HOMO = -(4.44 + E_{ox}) (eV), to be -5.49 eV. The LUMO was calculated from the value of the energy gap (2.18 eV) and HOMO energy level to be -3.31 eV.

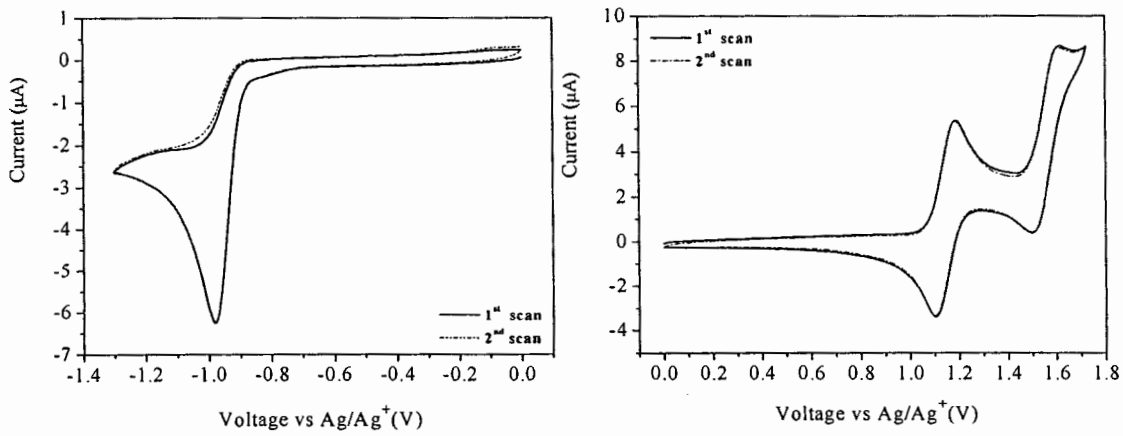

Figure 5.26 Cyclic voltammograms of **InT** in CH_2Cl_2 with scan rate of 0.05 V/s and 0.1 M *n*-Bu_4NPF_6 as electrolyte.

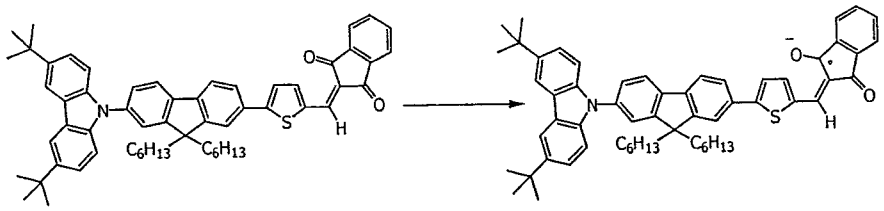

Figure 5.27 Proposed one reduction mechanism for the methyleneindene 1,3-dion.

Cyclic voltammogram of **In2T** (Figure 5.29) was analyzed in CH_2Cl_2 solution with scan rate of 0.05 V/s and *n*-Bu_4NPF_6 as electrolyte, detected two reversible oxidation (two electron oxidation) and one irreversible reduction (one electron transfer) peaks. It shows one reversible reduction with half-wave potential ($E_{1/2}$) of -1.10 V, which is assigned as the reduction process of methyleneindene-1,3-dion acceptor, the proposed reduction mechanism for the methyleneindene-1,3-dion system is the same as **InT**. It shows two oxidation waves with half-wave potential ($E_{1/2}$) of 1.09 and 1.27 V, respectively, which are assigned as the formation 3,6-di(*tert*-butyl)carbazole cation and dication, respectively. The proposed oxidation mechanism for *tert*-butyl substituented carbazole system was described in Chapter 4. It also shows a similar wave in different scans no distinct a slight shift of the CV curves was observed indicate *tert*-butyl group at the 3,6-positions peripheral carbazole moiety to protect oxidation coupling, indicating a good and stable electrochemical property. The onset oxidation potential (E_{ox}) of **In2T** was estimated from the first anodic oxidation wave to be 1.02 V. The HOMO was calculated, according to the following equation: HOMO = -(4.44 + E_{ox}) (eV), to be -5.46 eV. The LUMO was calculated from the value of the energy gap (1.99 eV) and HOMO energy level to be -3.47 eV.

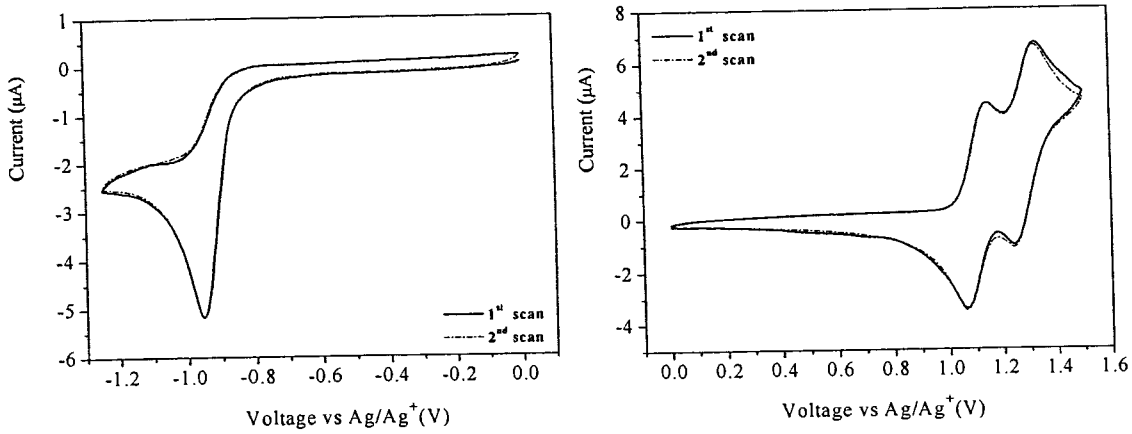

Figure 5.28 Cyclic voltammograms of **In2T** in CH_2Cl_2 with scan rate of 0.05 V/s and 0.1 M *n*-Bu_4NPF_6 as electrolyte.

Cyclic voltammogram of **In3T** (Figure 5.30) was analyzed in CH_2Cl_2 solution with scan rate of 0.05 V/s and *n*-Bu_4NPF_6 as electrolyte, detected three reversible oxidation (three electron oxidation) and one irreversible reduction (one electron transfer) peaks. It shows one reversible reduction with half-wave potential ($E_{1/2}$) of -1.10 V, which is assigned as the reduction process of methyleneindene 1,3-dion acceptor, the proposed reduction mechanism for the methyleneindene 1,3-dion system is the same as **InT**. It shows three oxidation waves with half-wave potential ($E_{1/2}$) of 1.01, 1.16 and 1.53 V, respectively, which are assigned as the formation 3,6-di(*tert*-butyl)carbazole action and dication, respectively. The proposed oxidation mechanism for *tert*-butyl substituented carbazole system was described in Chapter 4. It also shows a similar wave in different scan, which it has a good electrochemical property. The onset oxidation potential (E_{ox}) of **In3T** was estimated from the first anodic oxidation wave to be 0.93 V. The HOMO was calculated, according to the following equation: HOMO = -(4.44 + E_{ox}) (eV), to be -5.37 eV. The LUMO was calculated from the value of the energy gap (1.99 eV) and HOMO energy level to be -3.43 eV.

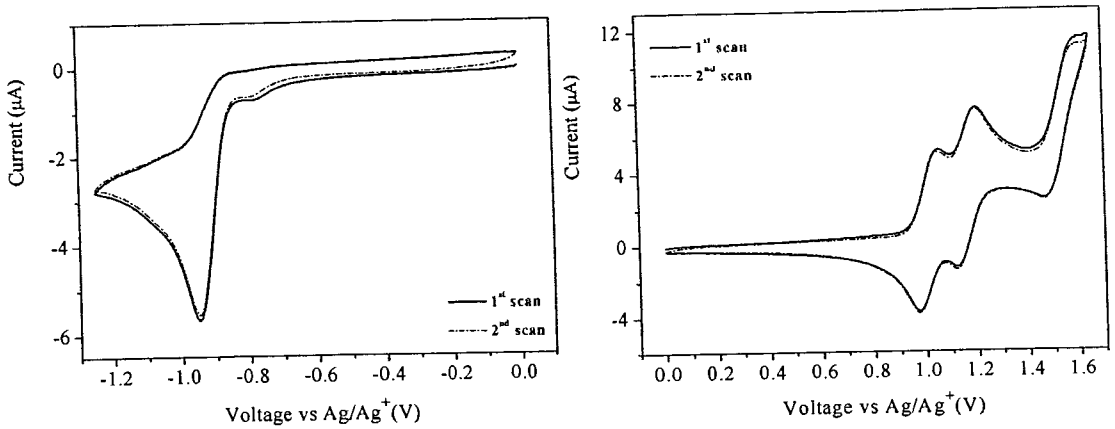

Figure 5.29 Cyclic voltammograms of **In3T** in CH_2Cl_2 with scan rate of 0.05 V/s and 0.1 M *n*-Bu_4NPF_6 as electrolyte.

Cyclic voltammograms of **In4T** (Figure 5.31) was analyzed in CH_2Cl_2 solution with scan rate of 0.05 V/s and *n*-Bu_4NPF_6 as electrolyte, detected three reversible oxidation (three electron oxidation) and one irreversible reduction (one electron transfer) peaks. It shows one reversible reduction with half-wave potential ($E_{1/2}$) of -1.09 V, which is assigned as the reduction process of methyleneindene 1,3-dion acceptor, the proposed reduction mechanism for the methyleneindene 1,3-dion system is the same as **InT**. It shows two oxidation waves with half-wave potential ($E_{1/2}$) of 0.91, 1.15 and 1.36 V, respectively, which are assigned as the formation 3,6-di(*tert*-butyl)carbazole cation and dication, respectively. The proposed oxidation mechanism for *tert*-butyl substituented carbazole and π-conjugated thiophene system were described in Chapter 4. It also shows a similar wave in different scan, which it has a good electrochemical property.The onset oxidation potential (E_{ox}) of **In4T** was estimated from the first anodic oxidation wave to be 0.85 V. The HOMO was calculated, according to the oxidation potential (E_{ox}) of **In4T** was estimated from the first anodic oxidation wave to be 0.85 V. The HOMO was calculated, according to the following equation: HOMO = -(4.44 + E_{ox}) (eV), to be -5.29 eV. The LUMO was calculated from the value of the energy gap (1.99 eV) and HOMO energy level to be -3.40 eV.

Table 5.4 Physical datas of **InnT** (n = 1-4)[a].

Compound	E_{1o} V	E_{2o} V	E_{3o} V	E_{1r} V	ΔE^0_{or} V	E_g[d] eV	HOMO[e] eV	LUMO[f] eV
InT	1.10[b]	1.50	-	-0.98	2.08	2.18	-5.49	-3.31
	(1.14)[c]	(1.55)		(-1.14)	(2.28)			
In2T	1.06	1.25	-	-0.95	2.01	1.99	-5.46	-3.47
	(1.09)	(1.27)		(-1.10)	(2.19)			
In3T	0.97	1.14	1.47	-0.95	1.92	1.94	-5.37	-3.43
	(1.01)	(1.16)	(1.53)	(-1.10)	(2.11)			
In4T	0.86	1.12	1.31	-0.94	1.80	1.89	-5.29	-3.24
	(0.91)	(1.15)	(1.46)	(-1.10)	(2.01)			

[a]Measured using a platinum rod couter electrode, a glassy carbon electrode and a SCE reference electrode in CH_2Cl_2 containing *n*-Bu_4NPF_6 as a supporting electrolyte with scan rate of 0.05 V/s under argon atmosphere, [b]Peak potential, [c]Half-wave potential, [d]Estimated form the onset of the absorption spectra ($E_g = 1240/\lambda_{onset}$), [e]Calculated using the empirical equation from HOMO = -(4.44 + E_{onset}), [f]Calculated from LUMO = HOMO + E_g

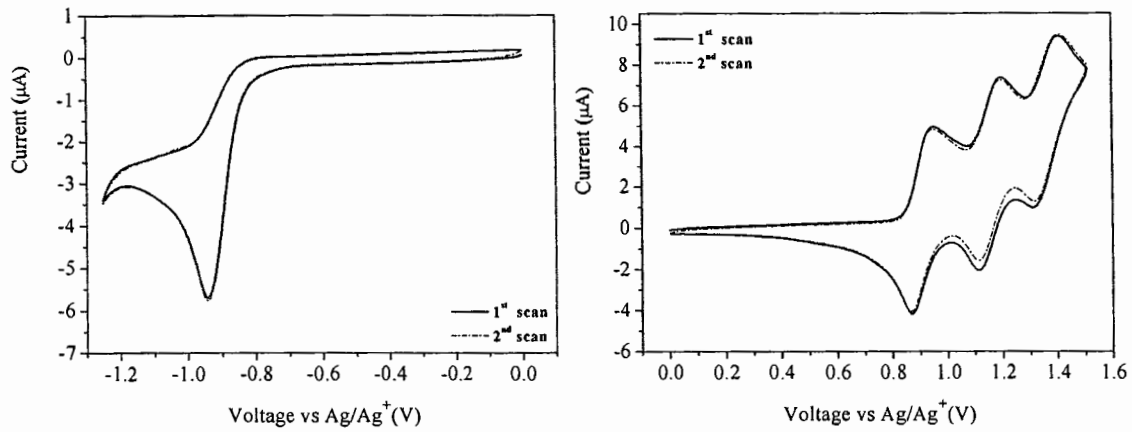

Figure 5.30 Cyclic voltammograms of **In4T** in CH_2Cl_2 with scan rate of 0.05 V/s and 0.1 M *n*-Bu_4NPF_6 as electrolyte.

5.3.5 Molecular orbital calculation

To get an insight into the molecular structure and electron distribution of the organic dye, the **InnT** (n = 1-4) were calculated by using DFT calculation with Gaussian 03 program. The calculations were performed with the BTLYP exchange correlation functional under 6-31D(d,p) basic set. Figure 5.32 shows the optimum geometry and the electron-state-density distributed of the HOMO and LUMO of **InnT** (n = 1-4) molecules. The general characters of the orbitals are independent of the linker length and electron acceptor. The HOMO is of π-characteristics and is delocalized over the entire molecule, including the carbazole groups. In the LUMO, which also has π-character, there is essentially no contribution from the carbazole groups, this supports the push-pull characteristics of these sensitizers. In addition, the optimized geometry of **InnT** (n = 1-4) indicates that the carbazole moiety at the end of the molecule are in 3-D spatial arrangement, which makes the molecular structure nonplanar due to the twist conformation **InnT** (n = 1-4) ion around the carbazoe-fluorene C-N bond. The nonplanar molecular structure **InnT** (n = 1-4) could be beneficial to solution-processability to form amorphous film. **InnT** (n = 1-4) are soluble in common organic solvents such as THF, CH_2Cl_2, $CHCl_3$ and acetone. High-quality amorphous film can be obtained by spin-coating its solution.

Table 5.5 The Highest occupied molecular orbital (HOMO), lowest unoccupied molecular orbital (LUMO), and wave length at maximum absorption (λ_{max}), for **InnT** (n = 1-4).

Compound	E_g (eV)	Δ_{H-L} (eV)	HOMO[e] (eV)	LUMO[f] (eV)
InT	**2.88**	**2.55**	**-5.17**	**-2.61**
In2T	**2.55**	**2.39**	**-5.14**	**-2.74**
In3T	**2.13**	**2.31**	**-5.08**	**-2.77**
In4T	**2.03**	**2.23**	**-5.03**	**-2.80**

[e]Calculated using the empirical equation from HOMO = -(4.44 + E_{onset}), [f]Calculated from LUMO = HOMO + E_g

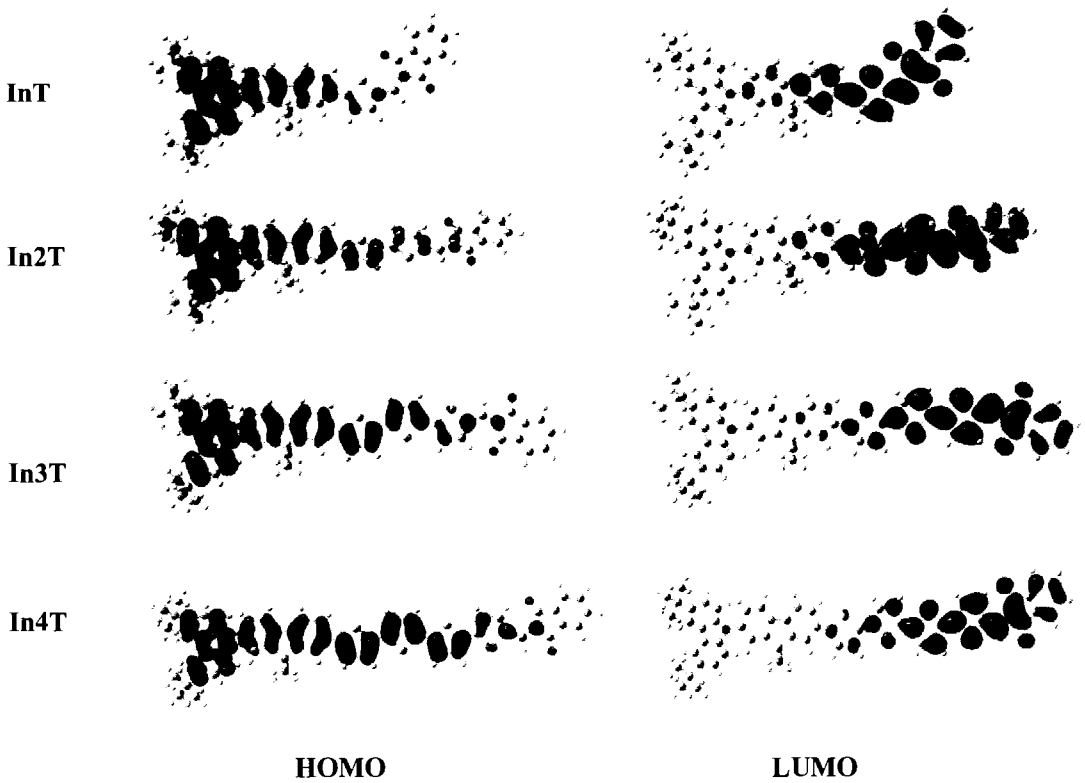

Figure 5.31 HOMO and LUMO distributions of the **InnT** (n = 1-4) dyes calculated with DFT on a BTLYP/6-31G (d,p) level .

5.4 Conclusion

Novel D-π-A organic materials **DMnT** (n = 1-4), **MCnT** (n = 1-4) and **InnT** (n = 1-4) containing one donor unit and one acceptor unit were successfully synthesis by using Knovenagel condensation reaction of active methylene compounds and corresponding formyl-compounds. They fully characterized by standard spectroscopy methods. The absorption maximum of **DMnT** (n = 1-4), **MCnT** (n = 1-4) and **InnT** (n = 1-4) were red-shift with an increase in the number of thiophene units. Compounds **DMnT** (n = 1-4), **MCnT** (n = 1-4) and **InnT** (n = 1-4) in this study are fluorescent with the color ranging from orange to dark-violet. All of Novel D-π-A **DMnT** (n = 1-4), **MCnT** (n = 1-4) and **InnT** (n = 1-4) have good electrochemical and thermal stabilities and could be used as emissive layers in OLEDs. In the HOMO level, electrons locate on the carbazole-fluorene unit, while in the LUMO level electron locate on the methelenemalononitrile, methylcyanoacrylate and metheleneindene-1,3-dione units indicating push-pull property.

CHAPTER 6

SYNTHESIS AND CHARACTERIZATION OF NOVEL DONOR π-CONJUGATE ACCEPTOR ORGANIC MATERIALS BASED ON DIPHENYLAMINE FOR DYE SENSITIZED SOLAR CELL

6.1 Introduction

Organic dipolar compounds containing an electron donor (D) and an electron acceptor (A), separated by a bridge group (B), have found wide applications on the new generation of optoelectronic devices [120]. Electron transfer from D to A happens rapidly upon photoexcitation to generate a charge-separated species [121]. Subsequent charge recombination may proceed within the molecule to generate a charge-transfer (CT) emission in certain cases, or it may be guided to proceed through an external circuit such as the design in dye-sensitized solar cells (DSCs). Because the efficiency of the solar cell competes with the internal charge recombination, the lifetime of the CT state becomes a major concern for designing the dyes. In previous reports, organic dyes using aryl amine as a donor and cyanoacrylic acid as an acceptor have exhibited promising results. For the donor group, a wide choice of aryl amines have been used such as coumarin, indoline, cyanine, merocyanine, hemicyanine, porphyrin, etc., while most of them exhibited satisfactory performances. The function of a bridge group is twofold, i.e., acting both as a part of the light absorbing chromophore and also as a channel for transporting charges. A good bridge group should promote the absorption of light over a wide wavelength region, yet retards the rate of internal charge recombination.

Diphenylamine units are well known for their ease in oxidation of the nitrogen center and the ability to transport charge carriers via radical cation species with high stability. Diphenylamine is a parent compound of many derivatives used for the production of dyes, pharmaceuticals, red electroluminescent materials, photography applications, and other small-scale applications [122].

6.2 Aim of the study

We designed To synthesis a novel π-conjugate of diphenylamine core oligothiophene based on diphenylamine as the donor group. Chemically, diphenylamine can be easily functionalized at its para-position with variation of the π-conjugate length of the dye molecules, introduced 2-ethylhexyl moiety at N-atom of diphenylamine to increase the solubility in dye sensitized solar cell (DSCs), and a cyanoacrylate moiety as acceptor/anchoring group which would provide an interesting and readily modifiable scaffold. Their basic optical properties have been investigated with the aim of understanding the structure–physical property relationships and developing novel molecular organic materials.

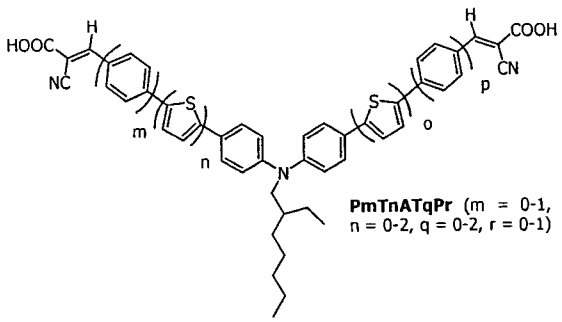

Figure 6.1 Chemical structures of **PmTnATqPr** (m = 0-1, n = 0-2, q = 0-2, r = 0-1).

6.3 Results and Discussion

6.3.1 Synthesis

To synthetic approach to a series of novel organic materials based on diphenylamine, first **A2** was accomplished by generation of the diphenylamine anion with an aqueous NaOH solution in DMSO and subsequent dihexylation with 2-ethylhexylbromide at room temperature. The desired **A2** was isolated by silica-gel column chromatography as colorless viscous in 36% yield.

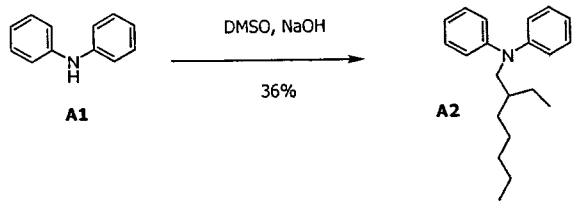

Figure 6.2 Alkylation reaction to form *N*-(2-ethylhexyl)-*N*-phenylbenzenenamine (**A2**).

The reaction involves base-catalyzed of diphenylamine is shown in Figure 6.3.

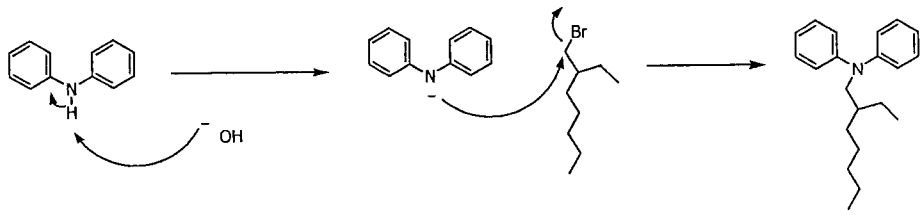

Figure 6.3 The proposed mechanism of alkylation of diphenylamine.

The chemical structure of **A2** was confirmed by ^{1}H-NMR, ^{13}C-NMR and IR analysis. The ^{1}H-NMR spectrum of product **A2** shows a doublet signal at chemical shift 3.66 ppm (2H, J = 7.2 Hz) assigning as methylene proton of 2-ethylhexyl unit. Subsequently, bromination of A2 was carried out in THF as solvent with NBS. The reaction mixture was stirred at room temperature for 30 min. to directly yield bromocompound as show in Figure 6.4.

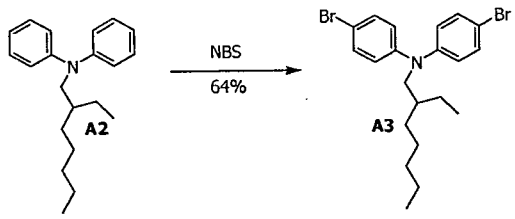

Figure 6.4 Bromination of *N*-(2-ethylhexyl)-*N*-phenylbenzenenamine (**A2**).

The chemical structure of **A3** was confirmed by ^{1}H-NMR analysis. The ^{1}H-NMR spectrum of product **A3** shows a doublet signal at chemical shift 7.26 ppm (4H, J = 8.1 Hz) assigning as 3-H and 5-H of diphenylamine, a doublet signal at chemical shift 6.08 ppm (4H,

J = 8.1 Hz) assigning as proton of 2-H and 6-H of diphenylamine and a doublet signal at chemical shift 3.48 ppm (2H, J = 6.9 Hz) assigning as methylene proton of 2-ethylhexyl unit.

Suzuki cross-coupling reaction of 2-thiopheneboronic acid and the **A3** employed in order to increase the number of thiophene units in the molecules. The thiophene intermediates **A4** and **A5** were prepared by $Pd(PPh_3)_4$ as catalyst in the presence of aqueous sodium carbonate solution in THF at refluxing temperature afforded the thiophene adduct in 36 and 14% yield, respectively. Suzuki cross-coupling reaction of **A3** as show in Figure 6.5.

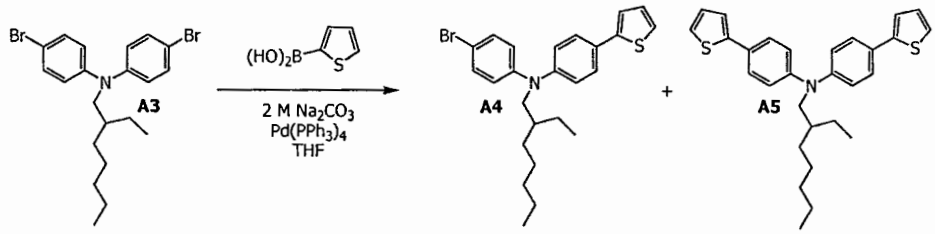

Figure 6.5 Suzuki cross-coupling reaction to form **A4** and **A5**.

Suzuki cross-coupling mechanism as described in Figure 2.9. The chemical structure of **A4** was confirmed by ^{1}H-NMR analysis. The ^{1}H-NMR spectrum of the **A4** shows a doublet signal at chemical shift 7.51 ppm (2H, J = 8.1 Hz) assigning as 3-H and 5-H and a doublet signal at chemical shift 6.99 ppm (2H, J = 8.7 Hz) assigning as 2-H and 6-H of phenyl ring connected to thiophene ring, a multiplet signal at chemical 7.22 ppm (2H) assigning as proton of 3-H and 5-H of thiophen ring and a multiplet signal at chemical shift 7.08 ppm (1H, Hz) assigning as proton of 4-H of thiophen ring and a doublet signal at chemical shift 3.60 ppm (2H, J = 6.9 Hz) assigning as methylene proton of 2-ethylhexyl unit

The chemical structure of **A5** was also confirmed by ^{1}H-NMR analysis. The ^{1}H-NMR spectrum of the **A5** shows a double doublet signal at chemical shift 7.60 ppm (4H, J = 3.6 Hz) assigning as 3-H and 5-H of phenyl ring and a multiplet signal at chemical shift 7.28 ppm (4H) assigning as 2-H and 6-H of phenyl ring, a multiplet signal at chemical 7.16 ppm (6H) assigning as proton of thiophen ring and a doublet signal at chemical shift 3.73 ppm (2H, J = 6.9 Hz) assigning as methylene proton of 2-ethylhexyl unit.

Bromination at C-5 position of thiophene ring of **A4** was carried out in THF as solvent with NBS. The reaction mixture was stirred at room temperature for 30 min. The desired

A4 was isolated by silica-gel column chromatography as yellow viscous in quantitative yield as show in Figure 6.8. Bromination mechanism of **A4** as shown in Figure 6.6.

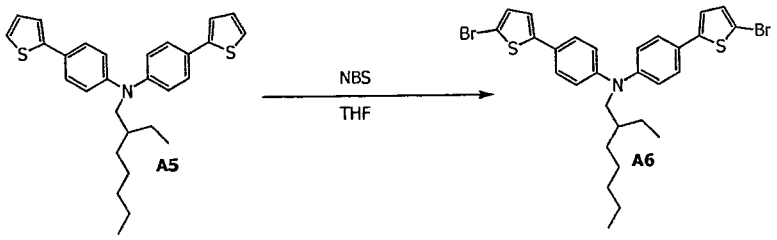

Figure 6.6 Bromination of *N*-(2-ethylhexyl)-4-(thiophene-2-yl)-*N*--4-(thiophene-2-yl)benzene-namine (**A5**).

The chemical structure of **A6** was also confirmed by ^{1}H-NMR analysis. The ^{1}H-NMR spectrum of the **A6** shows a doublet signal at chemical shift 7.40 ppm (4H, J = 8.4 Hz) assigning as 3-H and 5-H of phenyl ring and a triplet signal at chemical shift 7.04-7.01 ppm (6H) assigning as 2-H of phenyl ring and 4-H of thiophene ring, a doublet signal at chemical shift 6.97 ppm (2H, J = 3.6 Hz) assigning as assigning as 6-H of phenyl ring and a doublet signal at chemical shift 3.63 ppm (2H, J = 7.5 Hz) methylene proton of 2-ethylhexyl unit.

Suzuki cross-coupling reaction of 2-thiopheneboronic acid and the **A6** employed in order to increase the number of thiophene units in the molecules. The thiophene intermediates **A7** and **A8** were prepared using $Pd(PPh_3)_4$ as catalyst in the presence of aqueous sodium carbonate solution in THF at refluxing temperature afforded the thiophene adduct in 36 and 14% yield, respectively. Suzuki cross-coupling reaction of **A6** as show in Figure 6.7, Suzuki cross-coupling mechanism of **A6** as described for **A4**.

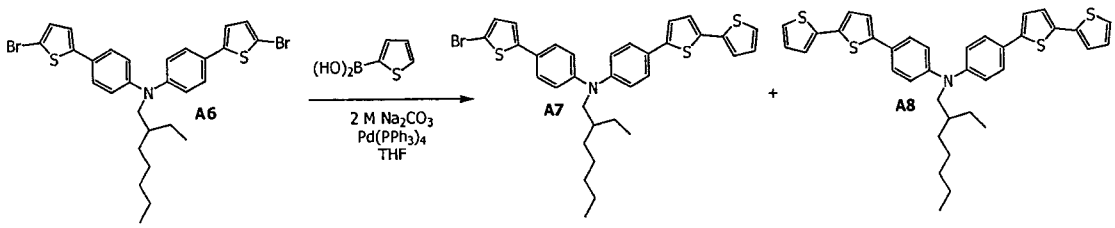

Figure 6.7 Suzuki cross-coupling reaction to form **A7** and **A8**.

The chemical structure of **A7** was also confirmed by ^{1}H-NMR analysis. The ^{1}H-NMR spectrum of the **A7** shows a doublet signal at chemical shift 7.53 ppm (2H, J = 8.4 Hz) assigning as 5-H of phenyl ring, a doublet signal at chemical shift 7.42 ppm (2H) assigning as 3-H of phenyl ring with connected to one thiophene ring, a doublet signal at chemical 6.97 ppm (1H, J = 3.6 Hz) assigning as 4-H of thiophen ring with terminal bromine and a doublet signal at chemical shift 3.67 ppm (2H, J = 6.9 Hz) assigning as methylene proton of 2-ethylhexyl unit.

The chemical structure of **A8** was confirmed by ^{1}H-NMR analysis. The ^{1}H-NMR spectrum of the **A8** shows a doublet signal at chemical shift 7.48 ppm (2H, J = 8.4 Hz) assigning as 5-H of phenyl ring, a doublet signal at chemical shift 7.38 ppm (2H) assigning as 3-H of phenyl ring, a multiplet signal at chemical 7.03-6.94 ppm (7H) assigning as 2-H and 6-H of phenyl ring and proton of thiophen ring and a doublet signal at chemical shift 3.67 ppm (2H, J = 6.9 Hz) assigning as methylene proton of 2-ethylhexyl unit.

Bromination at C-5 position of thiophene ring of **A7** was carried out in THF as solvent with NBS. The reaction mixture was stirred at room temperature for 30 min. The desired **A9** was isolated by silica-gel column chromatography as yellow viscous in quantitative yield as show in Figure 2.11. Bromination mechanism was described for **A4**.

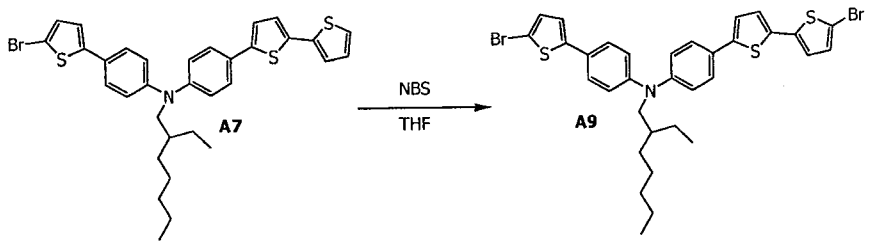

Figure 6.8 Bromination of *N*-(4-(5-bromothiophen-2-yl)phenyl)-*N*-(2-ethylhexyl)-4-thiophene-2-yl)thiophene-2-yl)benzenenamine (**A7**).

The chemical structure of **A9** was confirmed by ^{1}H-NMR analysis. The ^{1}H-NMR spectrum of the **A9** shows a doublet signal at chemical shift 7.54 ppm (2H, J = 8.4 Hz) assigning as 5-H of phenyl ring, a doublet signal at chemical shift 7.44 ppm (2H) assigning as 3-H of phenyl ring, a doublet signal at chemical 6.98 ppm (1H, J = 3.6 Hz) assigning as 4-H of thiophen ring with

one unit and a doublet signal at chemical shift 3.68 ppm (2H, J = 6.9 Hz) assigning as methylene proton of 2-ethylhexyl unit.

Suzuki cross-coupling reaction of 4-formylphenylboronic acid and the thiophene intermediates **A9** employed in order to increase the number of phenyl ring in the molecules. The aldehyde intermediates **A10** were prepared by $Pd(PPh_3)_4$ as catalyst in the presence of aqueous sodium carbonate solution in THF at refluxing temperature afforded the thiophene adduct in 87% yield, respectively. Suzuki cross-coupling reaction of **A9** as show in Figure 6.9, Suzuki cross-coupling mechanism of **A9** as described for **A4**.

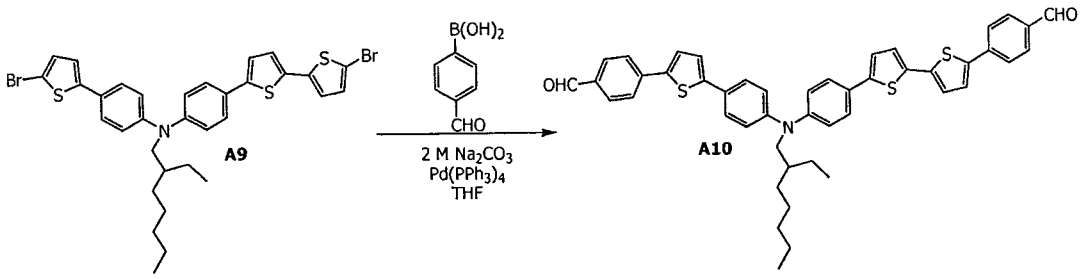

Figure 6.9 Suzuki cross-coupling reaction to form aldehyde compound **A10**.

The chemical structure of **A10** was confirmed by ^{1}H-NMR analysis. The ^{1}H-NMR spectrum of the **A10** shows a singlet signal at chemical shift 9.95 ppm (2H) assigning as proton of aldehyde, a doublet signal at chemical shift 7.89 ppm (2H, J = 8.4 Hz) assigning as 3-H and 5-H of phenyl ring with connected to two thiophene ring, a doublet signal at chemical 7.59 ppm (2H, J = 8.4 Hz) assigning as 3-H and 5-H of phenyl ring with connected to one thiophene ring, and a doublet signal at chemical shift 3.68 ppm (2H, J = 6.9 Hz) assigning as methylene proton of 2-ethylhexyl unit.

The dye with cyanoacetic acid as an acceptor was synthesized. Knoevenagel condensation reaction of aldehyde compounds with cyanoacetic acid in a present of piperidine as a base and catalyst in mixture of THF and acetonitrile as solvent at reflux for 6 h gave the target **PTA2TP** as orange solid in range 60% yield as shows in Figure 6.10. The reaction mechanism involves base-catalyzed of the active methylene to the enolate anion is shown in Chapter 4.

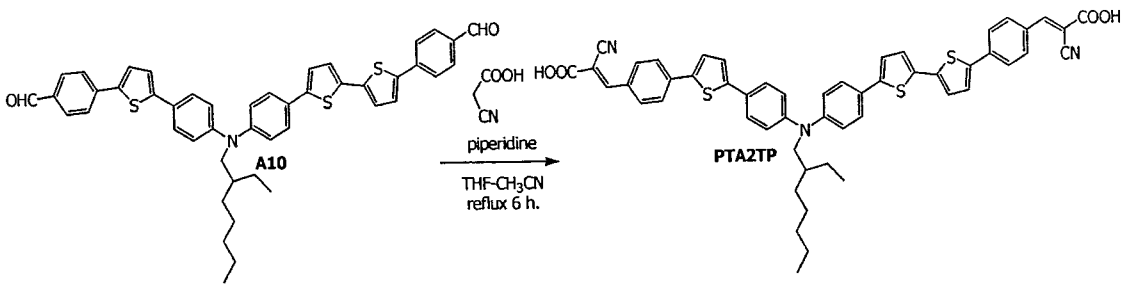

Figure 6.10 Knoevenagel condensation reaction to form **PTA2TP.**

The chemical structure of **PTA2TP** was confirmed by ^{1}H-NMR analysis. The ^{1}H-NMR spectrum of the **PTA2TP** shows a doublet signal at chemical shift 8.14 ppm (2H) assigning as the proton of double bond indicating **PTA2TP** is *E* isomer and a doublet signal at chemical shift 3.68 ppm (2H, J = 6.9 Hz) assigning as methylene proton of 2-ethylhexyl unit.

Bromination at C-5 position of thiophene ring of **A8** was carried out in THF as solvent with NBS. The reaction mixture was stirred at room temperature for 30 min. The desired **A11** was isolated by silica-gel column chromatography as yellow viscous in quantitative yield as show in Figure 6.11. Bromination mechanism was described for **A4.**

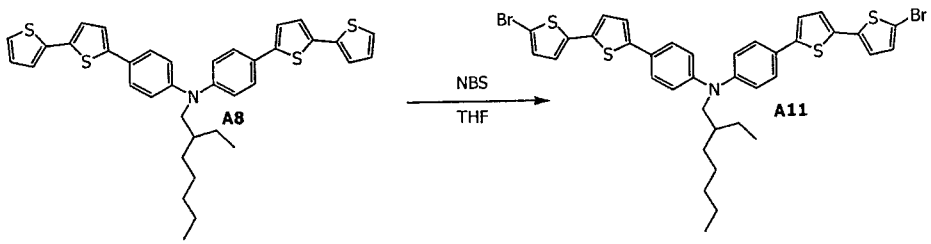

Figure 6.11 Bromination of **A8.**

The chemical structure of **A11** was confirmed by ^{1}H-NMR analysis. The ^{1}H-NMR spectrum of the **A11** shows a doublet signal at chemical shift 7.50 ppm (4H, J = 8.4 Hz) assigning as 3- H and 5-H of phenyl ring of diphenylamine core, a doublet signal at chemical shift 7.04 ppm (4H, J = 8.7 Hz) assigning as 2-H and 6-H of phenyl ring of diphenylamine core, and a doublet signal at chemical shift 3.66 ppm (2H, J = 7.5 Hz) assigning as methylene proton of 2-ethylhexyl unit.

Suzuki cross-coupling reaction of 4-formylphenylboronic acid and the thiophene intermediate **A11** employed in order to increase the number of phenyl ring in the molecules. The aldehyde intermediates **A12** were prepared by $Pd(PPh_3)_4$ as catalyst in the presence of aqueous sodium carbonate solution in THF at refluxing temperature afforded the aldehyde adduct in 60% yield, respectively. Suzuki cross-coupling reaction of **A11** as show in Figure 6.12, Suzuki cross-coupling mechanism of **A11** as described for **A4**.

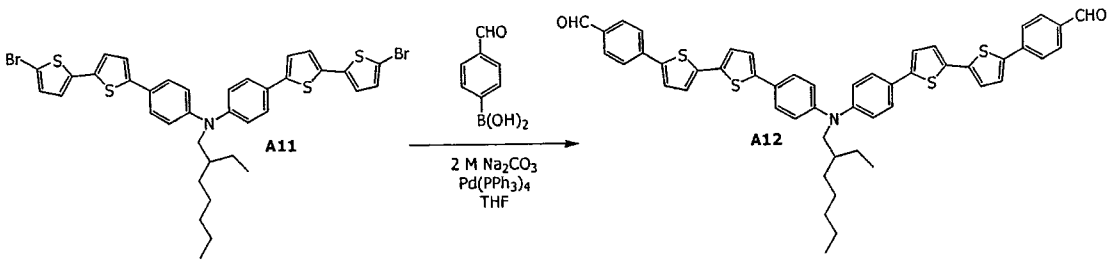

Figure 6.12 Suzuki cross-coupling reaction to form aldehyde compound **A12**.

The chemical structure of **A12** was confirmed by ^{1}H-NMR analysis. The ^{1}H-NMR spectrum of the **A12** shows a singlet signal at chemical shift 10.00 ppm (2H) assigning as proton of aldehyde, a doublet signal at chemical shift 7.88 ppm (2H, J = 8.4 Hz) assigning as 3-H of phenyl ring, a doublet signal at chemical shift 7.74 ppm (2H, J = 8.4 Hz) assigning as 5-H of phenyl ring and a doublet signal at chemical shift 3.66 ppm (2H, J = 6.9 Hz) assigning as methylene proton of 2-ethylhexyl unit.

Knoevenagel condensation reaction of aldehyde compounds **A12** with cyanoacetic acid in a present of piperidine as a base and catalyst in mixture of THF and acetonitrile as solvent at reflux for 6 h gave the target **P2TA2TP** as orange solid in range 60% yield as shows in Figure 6.13. The reaction mechanism involves base-catalyzed of the active methylene to the enolate anion is shown in Figure 4.9.

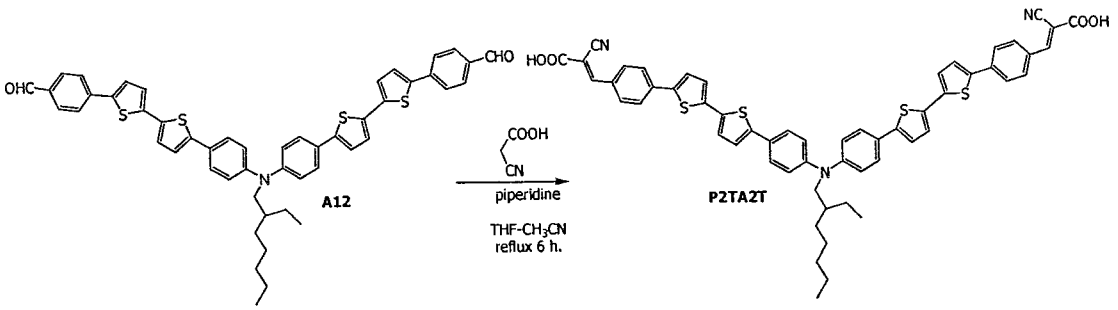

Figure 6.13 Knoevenagel condensation reaction to form **P2TA2TP**.

The chemical structure of **P2TA2TP** was confirmed by ^{1}H-NMR. The ^{1}H-NMR spectrum of the **P2TA2TP** shows a triplet signal at chemical shift 7.91-7.85 ppm (6H, J = 8.4 Hz, J = 9.9 Hz) assigning as two proton of double bond and 2-H and 6-H of phenyl ring with connected to cyanoacrylic acid and a doublet signal at chemical shift 3.66 ppm (2H, J = 7.5 Hz) assigning as methylene proton of 2-ethylhexyl unit.

Suzuki cross-coupling reaction of 4-formylphenylboronic acid and the thiophene compound **A6** employed in order to increase the number of phenyl ring in the molecules. The aldehyde intermediates **A13** were prepared by $Pd(PPh_3)_4$ as catalyst in the presence of aqueous sodium carbonate solution in THF at refluxing temperature afforded the aldehyde adduct in 60% yield, respectively. Suzuki cross-coupling reaction of **A6** as show in Figure 6.14, Suzuki cross-coupling mechanism of **A6** as described for **A4**.

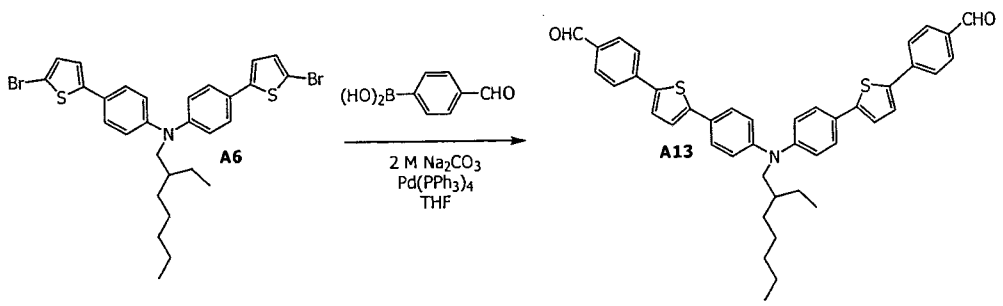

Figure 6.14 Suzuki cross-coupling reaction to form aldehyde compound **A13**.

The chemical structure of **A13** was confirmed by ^{1}H-NMR analysis. The ^{1}H-NMR spectrum of the **A13** shows a singlet signal at chemical shift 9.99 ppm (2H)

assigning as proton of aldehyde and a doublet signal at chemical shift 3.66 ppm (2H, J = 6.9 Hz) assigning as methylene proton of 2-ethylhexyl unit.

Knoevenagel condensation reaction of aldehyde compounds **A13** with cyanoacetic acid in a present of piperidine as a base and catalyst in mixture of THF and acetonitrile as solvent at reflux for 6 h gave the target **PTATP** as orange solid in range 52% yield as shown in Figure 6.15. The reaction mechanism involves base-catalyzed of the active methylene to the enolate anion is shown in Figure 4.9.

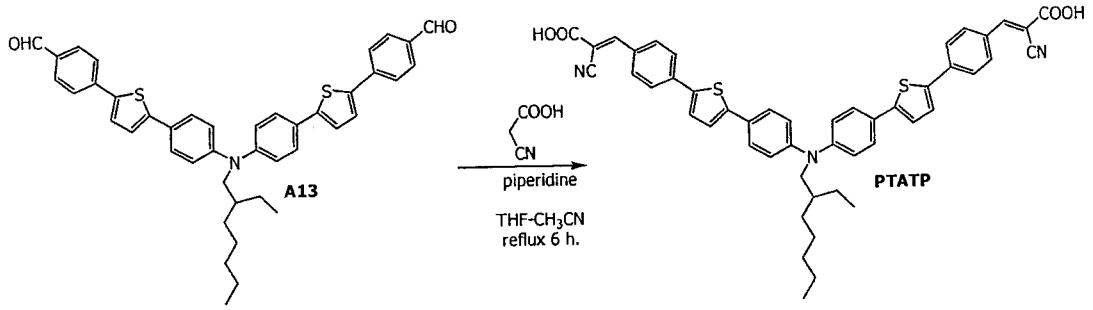

Figure 6.15 Knoevenagel condensation reaction to form **PTATP.**

The chemical structure of **PTATP** was confirmed by ^{1}H-NMR analysis. The ^{1}H-NMR spectrum of the **PTATP** shows a singlet signal at chemical shift 8.01 ppm (2H) assigning as proton of double bond indicating **PTATP** is *E* isomer and a doublet signal at chemical shift 3.67 ppm (2H, J = 6.9 Hz) assigning as methylene proton of 2-ethylhexyl unit.

Suzuki cross-coupling reaction of 5-formyl-2-thiopheneboronic acid and the thiophene compound **A3** employed in order to increase the number of thiophene ring in the molecules. The aldehyde intermediates **A14** and **A15** were prepared by using $Pd(PPh_3)_4$ as catalyst in the presence of aqueous sodium carbonate solution in THF at refluxing temperature afforded the aldehyde adduct in 15% yield, respectively. Suzuki cross-coupling reaction of **A3** as show in Figure 6.16, Suzuki cross-coupling mechanism of **A3** as described for **A4**.

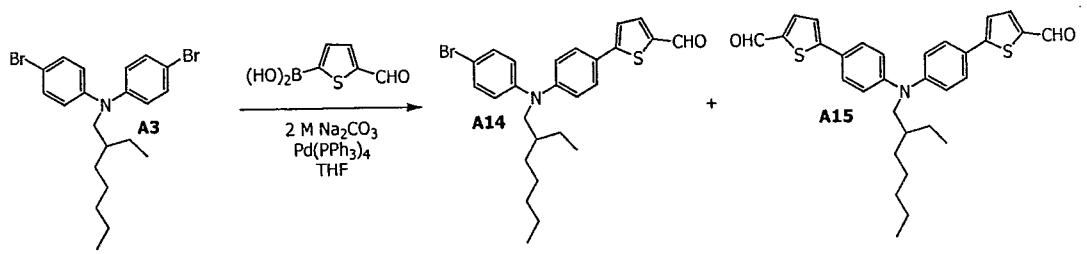

Figure 6.16 Suzuki cross-coupling reaction to form aldehyde compounds **A14** and **A15**.

The chemical structure of **A14** was confirmed by ^{1}H-NMR, ^{13}C-NMR and IR analysis. The ^{1}H-NMR spectrum of the **A14** shows a singlet signal at chemical shift 9.83 ppm (1H) assigning as proton of aldehyde, a singlet signal at chemical shift 7.68 ppm (1H) assigning as 4-H of thiophene ring, a singlet signal at chemical shift 7.27 ppm (1H) assigning as 3-H of thiophene ring and a doublet signal at chemical shift 3.39 ppm (2H, J = 6.9 Hz) assigning as methylene proton of 2-ethylhexyl unit.

The chemical structure of **A15** was confirmed by ^{1}H-NMR, ^{13}C-NMR and IR analysis. The ^{1}H-NMR spectrum of the **A15** shows a singlet signal at chemical shift 9.8 ppm (2H) assigning as proton of aldehyde, a doublet signal at chemical shift 7.70 ppm (2H, J = 3.9 Hz) assigning as 4-H of thiophene ring, a doublet signal at chemical shift 7.32 ppm (2H, J = 3.9 Hz) assigning as 3-H of thiophene ring and a doublet signal at chemical shift 3.68 ppm (2H, J = 7.2 Hz) assigning as methylene proton of 2-ethylhexyl unit.

Knoevenagel condensation reaction of aldehyde compounds **A15** with cyanoacetic acid in a present of piperidine as a base and catalyst in mixture of THF and acetonitrile as solvent at reflux for 6 h gave the target **TAT** as orange solid in range 74% yield as shows in Figure 6.17. The reaction mechanism involves base-catalyzed of the active methylene to the enolate anion is shown in Figure 4.9.

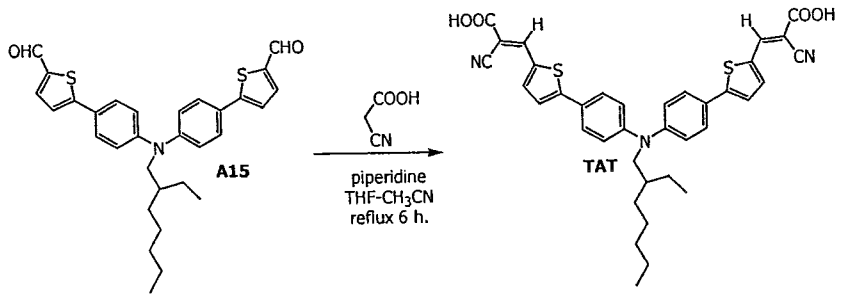

Figure 6.17 Knoevenagel condensation reaction to form **TAT.**

The chemical structure of **TAT** was confirmed by ^{1}H-NMR analysis. The ^{1}H-NMR spectrum of the **TAT** shows a singlet signal at chemical shift 8.06 ppm (1H) assigning as proton of double bond indicating **TAT** is *E* isomer, a singlet signal at chemical shift 7.49 ppm (6H) assigning as of thiophene ring and 3-H of phenyl ring and a singlet signal at chemical shift 3.59 ppm (2H) assigning as methylene proton of 2-ethylhexyl unit.

Suzuki cross-coupling reaction of 4-formylphenylboronic acid and the aldehyde compound **A14** employed in order to increase the number of phenyl ring in the molecules. The aldehyde intermediates **A16** was prepared by using $Pd(PPh_3)_4$ as catalyst in the presence of aqueous sodium carbonate solution in THF at refluxing temperature afforded the aldehyde adduct in 15% yield, respectively. Suzuki cross-coupling reaction of **A14** as show in Figure 6.18, Suzuki cross-coupling mechanism of **A14** as described for **A4**.

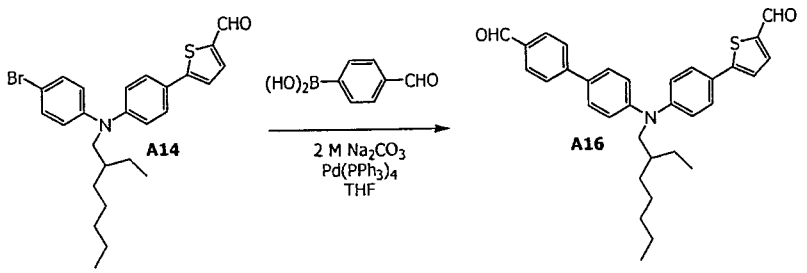

Figure 6.18 Suzuki cross-coupling reaction to form aldehyde compound **A16.**

The chemical structure of **A16** was confirmed by ^{1}H-NMR analysis. The ^{1}H-NMR spectrum of the **A16** shows a singlet signal at chemical shift 10.50 ppm (1H) assigning as proton of aldehyde of phenyl ring, a singlet signal at chemical shift 9.85 ppm (1H)

assigning as proton of aldehyde of thiophene ring and a doublet signal at chemical shift 3.75 ppm (2H) assigning as methylene proton of 2-ethylhexyl unit.

Knoevenagel condensation reaction of aldehyde compounds **A16** with cyanoacetic acid in a present of piperidine as a base and catalyst in mixture of THF and acetonitrile as solvent at reflux for 6 h gave the target **PAT** as orange solid in range 54% yield as shows in Figure 6.19. The reaction mechanism involves base-catalyzed of the active methylene to the enolate anion is shown in Figure 4.9.

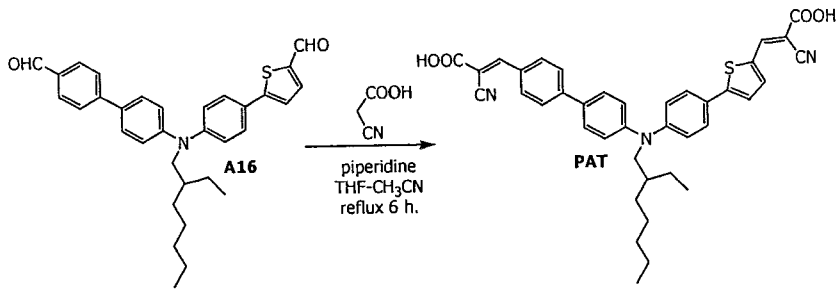

Figure 6.19 Knoevenagel condensation reaction to form **PAT.**

The chemical structure of **PAT** was confirmed by ^{1}H-NMR analysis. The ^{1}H-NMR spectrum of the **PAT** shows a multiplet signal at chemical shift 8.05-7.86 ppm (4H) assigning as proton of double bond and 2-H and 6-H of phenyl ring with connected to cyanoacrylic acid and a singlet signal at chemical shift 3.63 ppm (2H) assigning as methylene proton of 2-ethylhexyl unit.

6.3.2 Optical properties

The absorption spectra of organic dyes in CH_2Cl_2 solution are displayed in Figure 6.20. Each of these compounds exhibits a major absorption band on the long wavelength edge λ_{max} 409-441 nm. Upon photo excitation, the high-lying electron mostly localized on the diphenylamine (D) moiety, migrate to cyanoacrylic acid (A) on other side of the molecule. The electron movement is heavily coupled with π-orbital of the diphenylamine linkage (B). The linkage containing more thiophene moiety displayed a grater bathochromic shift, e.g. P2TA2TP>TAT>PTA2TP>PTATP>PAT in both series. The high-lying π-orbital in the thiophene is located at the high potential level than that the phenyl ring, therefore is delocalized more extensively than that later. Additionally, **P2TA2TP** dyes, has larger red-shift values as

compared **PTA2TP** dye with increasing number of thiophene unit as the extent of the π-conjugation system in the oligomer increases. However, absorption bands of **TAT** and **PAT** behave different. The target molecule **TAT** has larger blue-shift values as comparison to the maximum absorption of compound **PAT**. This bathochomic shift is a consequence of degree of free rotation of phenyl ring of **TAT**, which enforces a nonplanar and generated a blue-shift. The absorption spectra of **PAT**, **TAT**, **PTATP**, **PTA2TP** and **PTA2TP** solution exhibit a absorption peaks at 409, 440, 417, 431 and 441 nm which is blue-shifted about 25, 40, 60, 41 and 37 nm, respectively, compared to absorb on solid films. It may result from H-aggregation in the conjugated main chain. The stronger aggregation of all compound caused its absorption shifted to lower energy. In addition, 1P-PSP contain triphenylamin as dornor group with the same π-conjugated linkage as PTATP exhibits a major absorption band at 422 nm [122]. In solution, all target molecule show emission peak at orange region. When the dyes are attached to TiO_2 surface, the absorption spectra of these dyes are blue-shifted more or less as compared to that in solutions, indicating strong interactions between the dyes and the semiconductor surface. Also, the strong interaction between the surface and the adsorbed molecules often lead to aggregation effect. The blue-shifted values of different dyes are change obviously depending on different electron spacer. These values may be results of aggregation of the dyes on TiO_2 surface. Phenyl moieties and acceptor unit in the molecules could increase the aggregation effect of adsorbed dyes. Its seems that cyanoacrylate moiety in these dye molecules could lead to higher aggregation, and maybe have a negative effect for DSCs application. The energy band gaps of the of **PAT**, **TAT**, **PTATP**, **PTA2TP** and **P2TA2TP** dyes were estimated to be 2.35, 2.12, 2.09, 2.02 and 2.06 eV, respectively, from the absorption edge of the solution spectra.

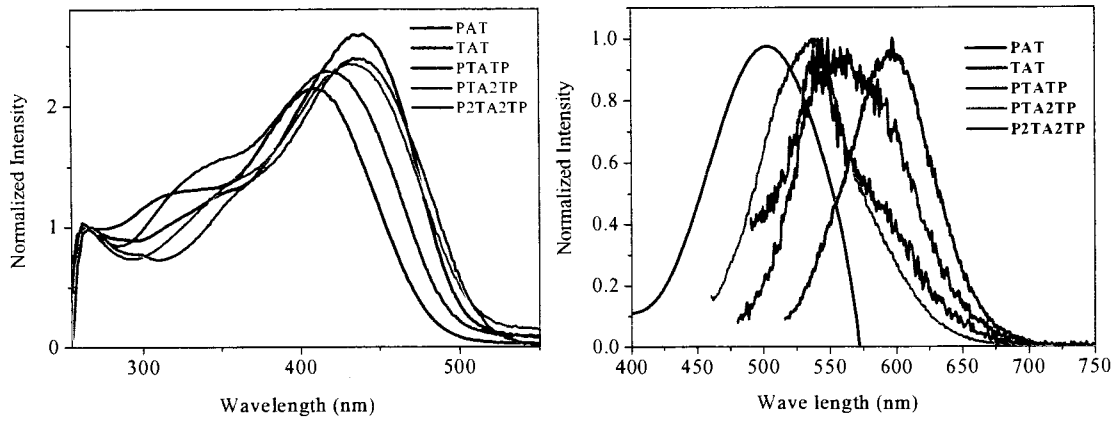

Figure 6.20 Absorption spectra and PL spectra of **PmTnATqPr** (m = 0-1, n = 0-2, q = 0-2, r = 1) in CH_2Cl_2 solution.

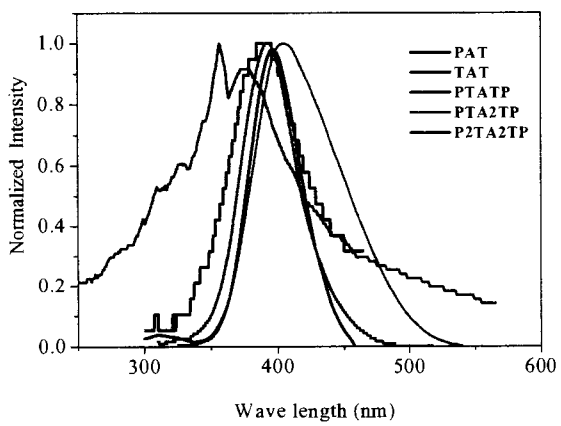

Figure 6.22 Absorption spectra of **PmTnATqPr** (m = 0-1, n = 0-2, q = 0-2, r = 0-1) on TiO_2.

Table 6.1 The absorption and fluorescence data of **PmTnATqPr** (m = 0-1, n = 0-2, q = 0-2, r = 0-1).

Compound	λ_{max} (nm)	λ_{max} **on** TiO_2 (nm)	λ_{max} **of emission in** CH_2Cl_2 (nm)
PAT	409	384	504
TAT	440	396	596
PTATP	417	357	548
PTA2T	431	390	539
P2TA2TP	441	404	544

6.4 Conclusion

A series of organic dipolar compounds containing a donor (D), a bridge (B), and an acceptor (A), forming a D–B–A type of dyads, were synthesized by convenient. The central bridges were made of molecule connected arylene groups, i.e., phenylenes or thiophenylenes. The donor groups were aromatic amines, i.e., either a diphenylamine group. The acceptor group was a cyanoacrylic acid, which can be anchored onto the surface of TiO_2. The target molecules in this study are fluorescent with the color orange region. Electrochemical properties, thermal stabilities and the performance of DSCs using these materials as dyes is under investigation and will be reported in the future.

CHAPTER 7

SUMMARY

π-Conjugated thiophene oligomers using as emissive molecules in optoelectronic devices were successfully synthesized from Suzuki coupling reaction of bromo-compounds and pyreneboronic acid. Different numbers of thiophene unit are introduced to the molecules and serve as linker. The target molecules were characterized by using ^{1}H-NMR and ^{13}C-NMR spectroscopy, Mass spectrometry and FT-IR spectroscopy techniques. The target molecules were soluble in chlorinated solvents, tetrahydrofuran and acetone, which are helpful for separation and purification. The target molecules exhibit a adsorption band cover UV and visible region. All compounds show thermal and good electrochemical properties. The target molecules geometrics have been optimized using DFT calculations with Gaussian functional order 6-31G (d, p) basis set and the results show that electron distribution from the whole molecules to the pyrene moieties occurred during the HOMO-LUMO excitation. The fluorescence quantum yields (Φ_F) of the fluorescence oligomers **CFTnP** (n = 1, 2, 3, 4) range from 0.840 to 0.078 and decrease as the conjugation in molecule increase. The maximum luminance of the device of **CFT3P** was about 31,760 cd/m^2 at an operating voltage of 9.8 V with a turn on voltage of 3 V. π-Conjugated thiophene-based oligomers using as emissive molecules in optoelectronic devices were successfully synthesized from Stille coupling reaction with different number of thiophene unit. The optical and electrochemical investigations revealed an electronic interaction between the carbazole-fluorene moieties and the oligothiophene chains. The fluorescence quantum yields (Φ_F) of the fluorescence oligomer **BCFnT** (n = 0, 2, 4, 6, 8) range from 0.158 to 0.023 and decrease as the conjugation in molecule increase. The thermal properties of these materials are enhanced with the increasing number of thiophene rings. These oligothiophene derivatives display strong fluorescence and should be promising materials for OLED devices. Novel D-π-A organic materials containing different linker and acceptor unit for using as dye molecules in optoelectronic devices were successfully synthesized from Knoevenagel condensation reaction of donor-containing aldehydes and acceptor-containing activated methylene. Different number of thiophene unit is introduced to the molecules and serve as linker. The electron-withdrawing parts

and anchoring group are cyanoacrylic acid or acrylic acid groups for DSCs. The target molecules were characterized by using ^{1}H-NMR and ^{13}C-NMR spectroscopy, Mass spectrometry and FT-IR spectroscopy techniques. The target molecules were soluble in chlorinated solvent, tetrahydrofuran and acetone, which are helpful for separation and purification. The target molecules exhibit a adsorption band cover UV and visible region. All compounds show thermal and good electrochemical properties. DFT calculations have been performed on the dyes, and the results show that electron distribution from the whole molecules to the anchoring moieties occurred during the HOMO-LUMO excitation. The electron-withdrawing groups are coplanar with respect to the phenyl units. A maximum η value of 3.13% is achieved under simulated AM 1.5 irradiation (80 mW/cm^2) with a DSCs based on **CA2T** dye (V_{oc} = 0.65 V, J_{sc} = 6.70 mA/cm^2, ff = 0.72). Under the same conditions, the η value of a DSCs based on N719 dye is 4.24% (V_{oc} = 0.67 V, J_{sc} = 9.44 mA/cm^2, ff = 0.67). The electron-withdrawing parts are methylenemalononitrile, methylcyanoacrylate and methyleneindene-1,3-dione groups for OLEDs. The absorption maximums of the target molecules were red-shifted with an increase in the number of thiophene units. All compounds in this study are fluorescent with the color ranging from orange to violet. All targets have good electrochemical and thermal stabilities and could be used as emissive layers in OLEDs. The performance of OLEDs using these materials as light-emitting layer is under investigation and will be reported in the future. A series of organic dipolar compounds containing a donor (D), a bridge (B), and an acceptor (A), forming a D–B–A type of dyads, were synthesized by convenient. The central bridges were made of V shape molecule connected arylene groups, i.e., phenylenes or thiophenylenes. The donor groups were aromatic amines, i.e., either a diphenylamine group. The acceptor group was a cyanoacrylic acid, which can be anchored onto the surface of TiO_2. The target molecules in this study are fluorescent with the color orange region. Electrochemical properties, thermal stabilities and the performance of DSCs using these materials as dyes is under investigation and will be reported in the future.

CHAPTER 8

EXPERIMENT

8.1 General procedures and instruments

^{1}H-NMR spectra were recorded on Brüker AVANCE (300 MHz) spectrometer. ^{13}C NMR spectra were recorded on Brüker AVANCE (75 MHz) spectrometer and were fully decoupled. Chemical shifts (δ) are reported relative to the residual solvent peak in part per million (ppm). Coupling constants (*J*) are given in Hertz (Hz). Multiplicities are quoted as singlet (s), broad (br), doublet (d), triplet (t), quartet (q), AA′BB′ quartet system (AA′B B′), AB quartet (ABq) and multiplet (m).

The IR spectra were recorded on a Perkin-Elmer FT-IR spectroscopy as KBr disks or neat liquid between two NaCl plates. The absorption peaks are quoted in wavenumber (cm^{-1}). UV-visible spectra were measured in spectrometric grade dichloromethane on a Perkin-Elmer UV Lambda 25 spectrometer. The absorption peaks are reported as in wavelength (nm) (log ε /$dm^3mol^{-1}cm^{-1}$) and sh refers to shoulder. Fluorescence spectra were recorded solid dilute solution in spectroscopic grade dichloromethane on a Perkin-Elmer LS 50B Luminescence Spectrometer.

Dichloromethane was washed with conc. H_2SO_4 and distilled twice from calcium hydride. Tetrahydrofuran (THF) was heated at reflux under nitrogen over sodium wire and benzophenone until the solution became blue and freshly distilled before use. All reagents and solvents were purchased from Aldrich, Acros, Fluka or Thai Supplies and received unless otherwise stated.

Analytical thin-layer chromatography (TLC) was performed with Merck aluminium plates coated with silica gel 60 F_{254}. Column chromatography was carried out using gravity feed chromatography with Merck silica gel mesh, 60 Å. Where solvent mixtures are used, the portions are given by volume.

The electrochemistry was performed using a AUTOLAB spectrometer. All measurements were made at room temperature on sample dissolved in freshly distilled dichloromethane, 0.1 M tetra-*n*-butylammonium hexafluorophosphate as electrolyte. The solutions

were degassed by bubbling with argon. Dichloromethane was washed with concentrated sulfuric acid and distilled from calcium hydride. A glassy carbon working electrode, platinum wire counter electrode, and a Ag/AgCl/NaCl (Sat.) reference electrode were used. The ferrocenium/ferrocene couple was used as standard, and the ferrocene was purified by recrystallisation from ethanol and then dried under high vacuum and stored over P_2O_5.

Differential scanning calorimetric (DSC) analysis was performed on a METTLER DSC823e thermal analyzer using a heating rate of 10 °C/min and a cooling rate of 50 °C/min under a nitrogen flow. Samples were scanned from 25 to 350 °C and then rapidly cooled to 25 °C and scanned for the second time at the same heating rate to 350 °C.

Thermal gravimetric analysis (TGA) was performed on a TG8120 thermoPlus, Rigaku, Japan thermal analyzer using a heating rate of 10 °C/min and a cooling rate of 70 °C/min under a nitrogen flow. Samples were scanned from 25 to 700 °C and then rapidly cooled to 25 °C and scanned for the second time at the same heating rate to 700 °C.

Melting points was measured by BIBBY Stuart Scientific melting point apparatus SMP3 in open capillary method and are uncorrected and reported in degree Celsius.

8.2 Synthesis and characterization

Chapter 2:

2,7-Dibromofluorene (2)

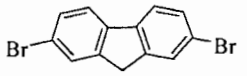

To a solution of fluorine (15 g, 90.24 mmol) in chloroform (100 ml), was cooled to 0 °C then added $FeCl_3$ (80 mg, 0.694 mmol) with stirring Br_2 in chloroform was slowly added the mixture and stirred at room temperature for 3 h. The reaction mixture was poured into water and washed with aqueous sodium thiosulfate solution until red color of bromine disappeared. The organic layer was dried over sodium sulfate anhydrous, filtered and evaporate to dryness. The residue was purified by crystallization by dichloromethane gave **2** as white solid (23 g, 80%); ^{1}H-NMR (300 MHz, $CDCl_3$) δ 7.75 (2H, s), 7.65 (2H, d, J = 9.0 Hz), 7.55 (2H, d, J = 9.0 Hz) and 3.85 (2H, s) ppm.

2,7-Dibromo-9,9-dihexyl-9H-fluorene (3)

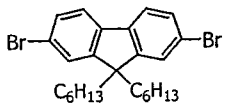

To a mixture of 2,7-dibromofluorene (10g, 30.86 mmol) and tetrabutyl ammonium bromide (1 g, 3 mmol) in DMSO (100 ml) was added an aqueous NaOH solution (50% wt/V, 6 ml) follow by 1-brromohexane (15 ml). After being stirred at room temperature for 3 h, the reaction mixture was extracted with ethyl acetate (100 mlx3). The combined organic phase was washed with water (100 ml), HCl solution (1 M, 50 ml), brine solution (100 ml), dried over sodium sulfate anhydrous, filtered and the organic phase was removed in vacuum. Purification by column chromatography using silica gel eluent with hexane gave **3** solid colorless viscous (12.7 g, 86%); ^{1}H-NMR (300 MHz, $CDCl_3$) δ 7.50 (6H, m), 1.95 (4H, t, J = 8.4 Hz), 1.00-1.40 (16H, m) and 0.95 (6H, m) ppm.

3,6-Di-*tert*-butylcarbazole

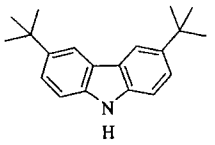

Carbazole (10 g, 59.80 mmol) and $ZnCl_2$ (24.45 g, 179.41 mmol) were dissolved in nitromethane (150 ml), then *tert*–butyl chloride was slowly added to the mixture. The reaction mixture was stirred at room temperature under N_2 for 5 h. The reaction mixture was poured into water and extracted with dichloromethane (100 ml x 3). The combined organic phase was washed with water (100 ml), brine solution (100 ml), dried over sodium sulfate anhydrous, filtered and the solvent was remove in vacuum. The residue was purified by recrystallization with hexane, gave 3,6-di-*tert*-butylcarbazole as white powder (15.370 g, 92%); m.p. 222-224 °C; ^{1}H-NMR (300 MHz, $CDCl_3$) δ 8.09 (2H, s), 7.85 (1H, s), 7.48 (2H, dd, J = 8.5 Hz, J = 1.6 Hz), 7.34 (2H, d, J = 8.5 Hz), and 1.47 (18H, s) ppm; FT-IR (KBr) 3411, 3059, 2959, 2903, 2864, 1628, 1577, 1492, 1466, 880, and 815 cm^{-1}.

9-(7-Bromo-9,9-dihexyl-*9H*-fluoren-2-yl)-3,6-di-*tert*-butyl-*9H*-carbazole (5)

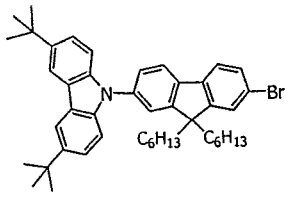

A stirred mixture of 2,7-dibromo-9,9-dihexyl-*9H*-fluorene (7.5 g,. 23.18 mmol), 3,6-di-*tert*-butyl-*9H*-carbazole (2.16 g, 7.33 mmol), copper iodide (0.736 g, 3.86 mmol), potassium phosphate (4.1 g, 19.3 mmol) and *trans*-diaminocyclohexane in toluene (70 ml) was refluxed for 24 h under N_2 atmosphere. After cooling, the reaction mixture was extracted with dichloromethane (50 ml x 3). The combined organic phase was washed with water (100 ml), brine solution (100 ml), dried over sodium sulfate anhydrous, filtered and the solvent was remove in vacuum. The product was obtain by silica gel chromatography (eluent hexane, $R_f = 0.5$) to afforded **5** as light yellow viscous (3.530 g, 70%); m.p. 87-89 °C; ^{1}H-NMR (300 MHz, $CDCl_3$) δ 8.18 (2H, s), 7.86 (1H, d, $J = 7.77$ Hz), 7.63 (1H, d, $J = 8.48$ Hz), 7.51 (6H, m), 7.39 (2H, d, $J = 8.59$ Hz), 1.98 (4H, m), 1.53 (16H, m), and 0.95 (6H, m) ppm; ^{13}C-NMR (75 MHz, $CDCl_3$) δ 153.24, 152.14, 142.91, 139.51, 137.35, 130.22, 126.29, 125.52, 123.62, 123.62, 121.42, 121.16, 120.87, 116.36, 109.19, 55.71, 40.36, 40.25, 32.06, 31.86, 29.96, 29.74, 29.27, 23.91, 22.64 and 14.10 ppm; FT-IR (KBr) 3028, 2954, 2926, 2853, 1617, 1560, 1489, 1474, 1364, 876, 811, and 614 cm^{-1}; HRMS-ESI m/z: [MH^+] calcd for $C_{45}H_{56}BrN$, 689.3596 found 689.2210.

3,6-Di-*tert*-butyl-9-(7-(8,10-dihydropyren-1-yl)-9,9-dihexyl-*9H*-fluoren-2-yl)-*9H*-carbazole (CFP)

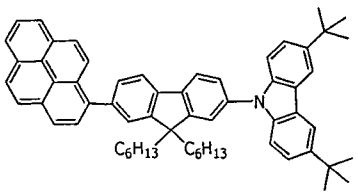

A mixture of 9-(7-bromo-9,9-dihexyl-*9H*-fluoren-2-yl)-3,6-di-*tert*-butyl-*9H*-carbazole (1.5 g, 2.2 mmol), pyreneboronic acid (0.584 g, 2.37 mmol), $Pd(PPh_3)_4$ (0.653 g, 2.656 mmol) solid catalyst in the present of 2 M sodium carbonate solution (6.5 ml, 13.1mmol) in THF as

solvent was degas in with N_2 at 2 min. The mixture was heated at reflux under N_2 atmosphere for 24 h. After cooled to room temperature, water (50 ml) was added. The reaction mixture was extracted with dichloromethane (50 ml x 3). The combined organic phase was washed with water (50 ml), brine solution (50 ml), dried over sodium sulfate anhydrous, filtered and the solvent was remove in vacuum. The product was obtain by silica gel chromatography (eluent dichloromethane:hexane = 5:95, R_f = 0.5) to afforded **CFP** as yellow solid (1.500 g, 10%); m.p. 152-154 °C; ^{1}H-NMR (300 MHz, $CDCl_3$) δ 8.30-8.24 (3H, m), 8.20-8.07 (8H, m), 8.04-7.94 (4H, m), 7.68 (2H, d, J = 8.4 Hz), 7.63-7.59 (2H, m), 7.54-7.49 (2H, m), 2.10-2.05 (4H, m), 1.51 (18H, m), 1.18 (12H, m) and 0.86-0.81 (10H, m) ppm; ^{13}C-NMR (75 MHz, $CDCl_3$) δ 152.83, 151.19, 142.86, 140.17, 139.69, 139.65, 139.42, 138.22, 137.02, 131.58, 131.04, 130.63, 129.61, 128.87, 128.67, 127.73, 127.65, 127.51, 126.10, 125.83, 125.66, 125.43, 125.36, 125.21, 125.01, 124.87, 124.73, 123.65, 123.43, 123.28, 123.19, 121.61, 121.51, 120.90, 119.82, 117.83, 116.38, 109.32, 55.57, 40.37, 34.82, 32.11, 31.6, 29.76, 24.11, 22.68 and 14.16 ppm; FT-IR (KBr) 3042, 2951, 2925, 2854, 1613, 1581, 1478, 1365, 1324, 1293, 1260, 1232, 877, 845, 808, 757, 719, 685 and 613 cm^{-1}.; HRMS-ESI calcd for $C_{61}H_{65}N$: *m/z* 811.5117 found 812.1358 [MH^+].

3,6-Di-*tert*-butyl-9-(9,9-dihexyl-7-(thiophen-2-yl)-*9H*-fluoren-2-yl)-*9H*-carbazole (6a)

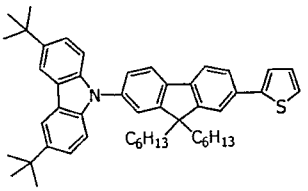

A mixture of 9-(7-bromo-9,9-dihexyl-*9H*-fluoren-2-yl)-3,6-di-*tert*-butyl-*9H*-carbazole (3.5 g, 5.16 mmol), $Pd(PPh_3)_4$ (0.042 g, 0.036 mmol) and an aqueous Na_2CO_3 solution (2 M, 25.8 ml) in THF (30 ml) was degas in with N_2 at 2 min. The mixture was heated at reflux under N_2 atmosphere for 24 h. After the mixture cooled to room temperature water (50 ml) was added. The mixture was extracted with dichloromethane (50 ml x 3). The combined organic phase was washed with water (50 ml), brine solution (50 ml) dried over anhydrous sodium sulfate, filtered and the organic solvent was remove in vacuum. Purification by column chromatography using silica gel eluting with hexane afforded **6a** as light yellow viscous (2.220 g, 62%); m.p. 156-158 °C;

^{1}H-NMR (300 MHz, $CDCl_3$) δ 8.26 (2H, s), 8.10 (1H, d, J = 8.7 Hz), 7.81 (1H, d, J = 7.8 Hz), 7.73-7.69 (2H, m), 7.62-7.55 (4H, m), 7.49-7.46 (3H, m), 7.37-7.36 (1H, m), 7.19-7.17 (1H, m), 2.13-2.07 (4H, m), 1.56-1.50 (18H, m),1.89 (12H, m) and 0.96-0.84 (10H, m) ppm; ^{13}C-NMR (75 MHz, $CDCl_3$) δ 152.67, 151.84, 145.10, 142.85, 140.02, 139.48, 139.39, 136.97, 133.48, 128.15, 125.43, 125.16, 124.69, 123.63, 123.42, 123.05, 121.43, 120.79, 120.25, 116.37, 109.29, 55.52, 40.43, 34.81, 32.10, 31.60, 29.72, 23.94, 22.66 and 14.12 ppm; FT-IR (KBr) 2950, 2925, 2854, 1608, 1583, 1488, 1473, 1453, 1390, 1376, 1358, 1294, 1259, 1229, 1172, 1148, 1103, 1078, 1030, 922, 875, 854, 837, 808, 757,691, 672, 652 and 614 cm^{-1}; HRMS-ESI m/z: calcd for $C_{49}H_{59}NS$, 693.4368 found 693.3612 [MH^+].

9-(7-(5-Bromothiophen-2-yl)-9,9-dihexyl-*9H*-fluoren-2-yl)-3,6-di-*tert*-butyl-*9H*-carbazole (7a)

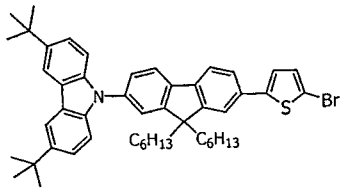

NBS (0.165 g, 0.927 mmol) was added in small portions to a stirred solution of 3,6-di-*tert*-butyl-9-(9,9-dihexyl-7-(thiophen-2-yl)-*9H*-fluoren-2-yl)-*9H*-carbazole (0.63 g, 0.9mmol) in THF (20 ml). After being stirred at room temperature for 30 min, water was added. The mixture was extracted with dichloromethane (30 ml x 3). The combined organic phase was washed with water (50 ml), brine solution (50 ml), dried over anhydrous sodium sulfate, filtered and the solvent was remove in vacuum. Purification by short column chromatography using silica gel eluting with dichloromethane : hexane, 5:95 gave **7a** as light yellow viscous (0.650 g, 94%); m.p. 77-80 °C; ^{1}H-NMR (300 MHz, $CDCl_3$) δ 8.18 (2H, s), 7.87 (1H, d, J = 8.7 Hz), 7.74 (1H, d, J = 7.8 Hz), 7.56-7.47 (6H, m), 7.39 (2H, d, J = 8.7 Hz), 7.15 (1H, d, J = 3.6 Hz), 7.07 (1H, d, J = 3.9 Hz), 2.04-21.98 (4H, m), 1.52 (18H, m), 1.19-1.11 (12H, m) and 0.82-0.77 (10H, m) ppm; ^{13}C-NMR (75 MHz, $CDCl_3$) δ 152.64, 151.94, 146.54, 142.85, 140.41, 139.33, 139.22, 137.14, 132.63, 130.88, 125.44, 124.79, 123.56, 123.40, 123.09, 121.41, 120.81, 120.28, 119.91, 116.31, 111.14, 109.20, 55.50, 40.32, 34.75, 32.03, 31.51, 29.63, 23.88, 22.56 and 14.00 ppm; FT-IR (KBr) 3042, 2954, 2926, 2855, 1610, 1584, 1490, 1474, 1362, 1324, 1294, 1262, 1233,

1201, 877, 809, 790, 714 and 614 cm^{-1}; HRMS-ESI calcd for $C_{49}H_{58}BrNS$: *m/z* 771.3473 found 772.3613 [MH^+].

3,6-Di-*tert*-butyl-9-(7-(5-(4,6-dihydropyren-1-yl)thiophen-2-yl)-9,9-dihexyl-9H-fluoren-2-yl)-9H-carbazole (CFTP)

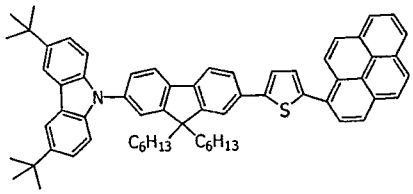

A mixture of 9-(7-(5-bromothiophen-2-yl)-9,9-dihexyl-*9H*-fluoren-2-yl)-3,6-di-*tert*-butyl-*9H*-carbazole (0.5 g, 0.65 mmol), pyreneboronic acid (0.173 g, 0.70 mmol), $Pd(PPh_3)_4$ (0.195 g, 0.776 mmol) solid catalyst in the present of sodium carbonate solution in THF as solvent was degas in with N_2 at 2 min. The mixture was heated at reflux under N_2 atmosphere for 24 h. After cooled to room temperature, water (50 ml) was added. The reaction mixture was extracted with dichloromethane (50 ml x 3). The combined organic phase was washed with water (50 ml), brine solution (50 ml), dried over sodium sulfate anhydrous, filtered and the solvent was remove in vacuum. The product was obtain by silica gel chromatography eluent 5% dichloromethane : hexane afforded **CFTP** as yellow-orange solid (0.410 g, 70%); m.p. 216-218 °C; ^{1}H-NMR (300 MHz, $CDCl_3$) δ 8.69 (1H, d, J = 9.3 Hz), 8.24-8.05 (10H, m), 7.94 (1H, d, J = 8.1 Hz), 7.86-7.78 (3H, m), 7.61-7.54 (5H, m), 7.47 (1H, d, J = 8.7 Hz), 2.12-2.10 (4H, m), 1.55 (18H, m), 1.19 (12H, m) and 0.88-0.84 (10H, m) ppm; ^{13}C-NMR (75 MHz, $CDCl_3$) δ 152.69, 151.96, 145.82, 142.86, 141.85, 140.18, 139.48, 139.38, 137.01, 133.38, 131.52, 131.08, 131.01, 129.75, 129.08, 129.01, 128.28, 128.07, 127.88, 127.40, 126.23, 125.45, 125.14, 125.01, 124.93, 124.85, 124.73, 123.63, 123.53, 123.42, 121.43, 120.81, 120.36, 119.99, 116.37, 109.29, 55.56, 40.46, 34.81, 32.09, 31.63, 29.74, 23.98, 22.67 and 14.13 ppm; FT-IR (KBr) 3040, 2952, 2925, 2854, 1609, 1583, 1478, 1363, 1324, 1294, 1262, 1233, 877, 845, 808, 757, 718, 684 and 614 cm^{-1}; HRMS-ESI calcd for $C_{65}H_{67}NS$: *m/z* 893.4994 found 893.6961 [M^+].

3,6-Di-*tert*-butyl-9-(9,9-dihexyl-7-(5-thiophen-2-yl)(thiophene-2-yl)-*9H*-fluorene-2-yl)-*9H*-carbazole (6b)

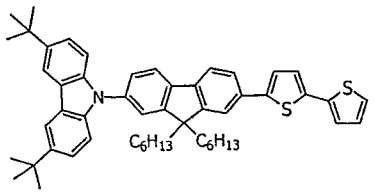

A mixture of 9-(7-(5-bromothiophen-2-yl)-9,9-dihexyl-*9H*-fluoren-2-yl)-3,6-di-*tert*-butyl-*9H*-carbazole (4.3 g, 5.56 mmol), 2-thiopheneboronic acid (0.77 g, 5.92 mmol), $Pd(PPh_3)_4$ (0.045 g, 0.038 mmol) and an aqueous sodium carbonate solution in THF as solvent was degassed with N_2 for 5 min. The mixture was heated at reflux under N_2 atmosphere for 24 h. After the mixture was cooled to room temperature, water (50 ml) was added. The reaction mixture was extracted with dichloromethane (100 ml x 3). The combined organic phase was washed with water (100 ml), brine solution (50 ml), dried over sodium sulfate anhydrous, filtered and the solvent was remove in vacuum. The product was purified by silica gel chromatography to afford **6b** as light yellow viscous (3.190 g, 74%); m.p. 70-72 °C; ^{1}H-NMR (300 MHz, $CDCl_3$) δ 8.28 (2H, s), 7.93 (1H, d, J = 7.5 Hz), 7.80 (1H, d, J = 7.5 Hz), 7.70 (2H, d, J = 7.2 Hz), 7.63-7.57 (4H, m) 7.50 (2H, d, J = 8.4 Hz), 7.38 (1H, s), 7.26 (3H, d, J = 9 Hz, J = 6 Hz), 7.11-7.08 (1H, m), 2.02 (4H, m), 1.58 (18H, m), 1.12 (12H, m) and 0.87 (10H, m) ppm; ^{13}C-NMR (75 MHz, $CDCl_3$) δ 152.73, 151.96, 143.82, 142.91, 140.20, 139.45, 137.59, 137.09, 136.62, 133.17, 127.96, 125.50, 124.86, 124.73, 124.42, 123.71, 123.66, 123.50, 121.49, 120.84, 120.34, 119.93, 116.40, 109.34, 55.57, 40.45, 34.84, 32.13, 31.63, 29.76, 27.02, 24.00, 22.68 and 14.22 ppm; FT-IR (KBr) 3044, 2952, 2925, 2855, 1612, 1480, 1362, 1324, 1290, 1261, 1233, 1033, 877, 837, 794, 691 and 613 cm^{-1}; HRMS-ESI calcd for $C_{53}H_{61}NS_2$: *m/z* 775.4245 found 774.8981 [M^+].

9-(7-(5-(5-Bromothiophene-2-yl)thiophene-2-yl)-9,9-dihexyl-*9H*-fluoren-2-yl)-3,6-di-*tert*-butyl-*9H*-carbazole (7b)

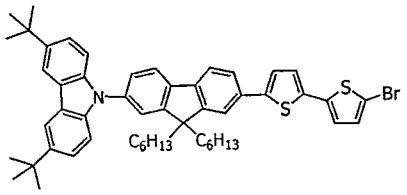

NBS (0.744 g, 4.18 mmol) was added in small portion to a stirred solution of 3,6-di-*tert*-butyl-9-(9,9-dihexyl-7-(5-thiophen-2-yl)(thiophene-2-yl)-*9H*-fluorene-2-yl)-*9H*-carbazole (2.95g, 0.8 mmol) in THF (50 ml). After being stirred at room temperature for 30 min, water (50 ml) was added. The mixture was extracted with dichloromethane (70 ml x 3). The combined organic phase was washed with water (70 ml), brine solution (50 ml), dried over sodium sulfate anhydrous, filtered and the solvent was remove in vacuum. Purification by short column chromatography using silica gel eluting with recycle solvent gave **7b** as light yellow viscous (0.680 g, 100%); m.p. 87-89 °C; ^{1}H-NMR (300 MHz, $CDCl_3$) δ 8.17 (2H, s), 7.88 (1H, d, J = 8.4 Hz), 7.75 (1H, d, J = 8.4 Hz), 7.64-7.58 (6H, m), 7.39 (2H, d, J = 8.7 Hz), 7.30 (1H, d, J = 3.9 Hz), 7.13 (1H, d, J = 3.6 Hz), 7.02-6.97 (2H, m), 2.06-2.04 (4H, m), 1.49 (18H, m), 1.27-1.12 (12H, m) and 0.82-0.77 (10H, m) ppm; ^{13}C-NMR (75 MHz, $CDCl_3$) δ 152.65, 151.91, 144.33, 142.84, 140.33, 139.33, 139.29, 139.00, 137.09, 135.39, 132.83, 130.71, 125.43, 124.92, 124.84, 123.65, 123.62, 123.56, 123.40, 121.41, 120.78, 120.26, 119.92, 116.31, 110.92, 109.22, 55.50, 40.35, 34.75, 31.93, 31.53, 29.65, 23.89, 22.57 and 14.02 ppm; FT-IR (KBr) 3042, 2953, 2925, 2855, 2360, 1609, 1475, 1362, 1323, 1294, 1261, 1233, 968, 876, 809, 788 and 614 cm^{-1}; HRMS-ESI calcd for $C_{53}H_{60}BrNS_2$: *m/z* 853.3351 found 854.3693 [MH^+].

3,6-Di-*tert*-butyl-9-(7-(5-(5-(4,6-dihydropyrene-1-yl)thiophene-2-yl)thiophene-2-yl) -9,9-dihexyl-*9H*-fluoren-2-yl) -*9H*-carbazole (CFT2P)

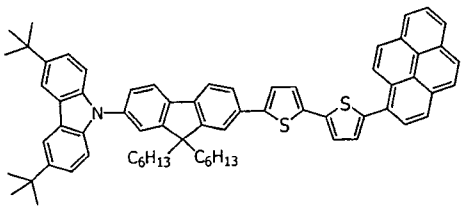

3,6-di-*tert*-butyl-9-(7-(5-(5-(4,6-dihydropyrene-1-yl)thiophene-2-yl)thiophene-2-yl-9,9-dihexyl-*9H*-fluoren-2-yl)-*9H*-carbazole was obtained from Suzuki cross coupling between 9-(7-(5-(5-bromothiophene-2-yl)thiophene-2-yl)-9,9-dihexyl-*9H*-fluoren-2-yl)-3,6-di-*tert*-butyl-*9H*-carbazole(0.6 g, 0.7 mmol) and pyreneboronic acid (0.25 g, 0.84 mmol) in the present of $Pd(PPh_3)_4$ (0.045 g, 0.035 mmol) and an aqueous sodium carbonate solution in THF (30 ml) as solvent was degassed with N_2 for 5 min. The reaction mixture was stirred at reflux under N_2 for 24 h. After being cooled to room temperature, water (50 ml) was added. The reaction mixture was extracted with dichloromethane (50 ml x 3), washed with water (100 ml), and brine solution (50 ml), dried over sodium sulfate anhydrous, filtered and the solvents were remove to dryness. Purification by column chromatography over silica gel eluting with a mixture of 7% dichloromethane : hexane afforded **CFT2P** as pale yellow solid (0.494 g, 72%); m.p. 170-172 °C; ^{1}H-NMR (300 MHz, $CDCl_3$) δ 8.64 (1H, d, J = 9.3 Hz), 8.25-8.18 (9H, m), 8.09-8.04 (1H, m), 7.91 (1H, d, J = 8.4 Hz), 7.79 (1H, d, J = 7.8 Hz), 7.70 (1H, d, J = 7.8 Hz), 7.72-7.65 (2H, m), 7.57-7.50 (4H, m), 7.42 (4H, d, J = 9.3 Hz), 7.34 (2H, d, J = 10.8 Hz), 2.09-2.07 (4H, m), 1.51 (18H, m),1.15 (12H, m) and 0.84-0.80 (10H, m) ppm; ^{13}C-NMR (75 MHz, $CDCl_3$) δ 152.66, 151.92, 143.90, 142.83, 141.55, 140.19, 139.35, 138.35, 137.02, 136.46, 133.08, 131.50, 130.98, 129.33, 129.00, 128.78, 128.21, 128.10, 127.91, 127.35, 126.22, 125.45, 125.14, 124.89, 124.81, 124.69, 124.05, 123.79, 123.57, 123.39, 121.41, 120.77, 120.27, 119.88, 116.32, 109.24, 55.51, 40.38, 34.76, 32.04, 31.55, 30.91, 29.67, 23.92, 22.60 and 14.05 ppm; FT-IR (KBr) 3042, 2952, 2926, 2855, 1609, 1583, 1477, 1363, 1324, 1294, 1262, 1233, 1033, 876, 845, 808, 756, 719 and 614 cm^{-1}; HRMS-ESI calcd for $C_{69}H_{69}NS_2$: *m/z* 975.4871 found 975.4896 [M^+].

3,6-Di-*tert*-butyl-9-(-9,9-dihexyl-7-(5-(5-(thiophene-2-yl)thiophene-2-yl)-*9H*-fluoren-2-yl)-*9H*-carbazole (6c)

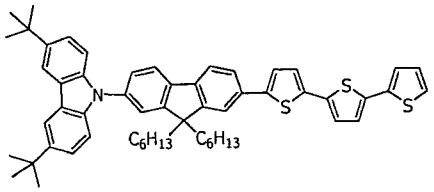

A mixture of 9-(7-(5-(5-bromothiophene-2-yl)thiophene-2-yl)-9,9-dihexyl-*9H*-fluoren-2-yl)-3,6-di-*tert*-butyl-*9H*-carbazole (1.566 g, 1.83 mmol), 2-thiopheneboronic acid (0.252 g,

141 mmol), $Pd(PPh_3)_4$ (0.0147 g, 0.127 mmol) and an aqueous sodium carbonate solution in THF (50 ml) was degassed with N_2 for 5 min. The reaction mixture was stirred at reflux under N_2 for 24 h. After the mixture was cooled to room temperature, water (50 ml) was added. The reaction mixture was extracted with dichloromethane (50 ml x 3). The combined organic phase was washed with water (50 ml), brine solution (50 ml), dried over sodium sulfate anhydrous, filtered and the solvent was remove in vacuum. Purification by column chromatography eluting with gradient solution system started with 5% dichloromethane : hexane gave **6c** as pale yellow solid (1.100 g, 70%); m.p. 92-94 °C; ^{1}H-NMR (300 MHz, $CDCl_3$) δ 8.22 (2H, s), 7.90 (1H, d, J=8.7 Hz), 7.77 (1H, d, J = 7.8 Hz), 7.67-7.63 (2H, m), 7.58-7.51 (4H, m), 7.44 (2H, d, J = 8.4 Hz), 7.35 (1H, d, J = 3.6 Hz), 7.26-7.22 (3H, m), 7.16-7.13 (2H, m), 7.07-7.04 (1H, m), 2.09-2.04 (4H, m), 1.54 (18H, m),1.15(12H, m) and 0.85-0.81 (10H, m) ppm; ^{13}C-NMR (75 MHz, $CDCl_3$) δ 152.68, 151.93, 143.91, 142.87, 140.22, 139.38, 137.17, 137.06, 136.30, 136.24, 133.03, 127.95, 125.45, 124.81, 124.64, 124.56, 124.46, 124.18, 123.75, 123.62, 123.43, 121.43, 120.81, 120.31, 119.88, 116.36, 109.28, 55.53, 40.40, 34.79, 32.08, 31.59, 29.27, 23.95, 22.64 and 14.10 ppm; FT-IR (KBr) 3042, 2952, 2925, 2855, 1609, 1477, 1362, 1324, 1294, 1262, 1233, 1033, 877, 837, 791, 690 and 614 cm^{-1} ;HRMS-ESI calcd for $C_{57}H_{63}NS_3$: *m/z* 857.4123 found 857.5636 [M^+].

9-(7-(5-(5-Bromothiophene-2-yl)thiophene-2-yl)thiophene-2-yl)-9,9-dihexyl-*9H*-fluoren-2-yl)-3,6-di-*tert*-butyl-*9H*-carbazole (7c)

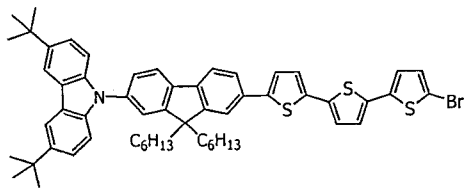

NBS (0.641 g, 3.60 mmol) was added in small portion to a stirred solution of (3,6-di-*tert*-butyl-9-(-9,9-dihexyl-7-(5-(5-(thiophene-2-yl)thiophene-2-yl)-*9H*-fluoren-2-yl)-*9H*-carbazole (2.95 g, 3.34 mmol) in THF (50 ml). After being stirred at room temperature for 30 min, water (50 ml) was added. The mixture was extracted with dichloromethane (70 ml x 3). The combined organic phase was washed with water (70 ml), brine solution (50 ml), dried over sodium sulfate anhydrous, filtered and the solvent was remove in vacuum. Purification by short column chromatography using silica gel eluting with recycle solvent gave **7c** as yellow solid (3.120 g,

100%); m.p. 104-106 °C; ^{1}H-NMR (300 MHz, $CDCl_3$) δ 8.19 (2H, s), 7.89 (1H, d, J = 8.4 Hz), 7.76 (1H, d, J = 7.8 Hz), 7.66-7.48 (6H, m), 7.40 (2H, d, J = 8.4 Hz), 7.34 (1H, d, J = 3.6 Hz), 7.20 (1H, d, J = 3.9 Hz), 7.13 (1H, d, J = 3.6 Hz), 7.05 (1H, d, J = 3.9 Hz), 6.99 (1H, d, J = 3.6 Hz), 6.94 (1H, d, J = 3.9 Hz), 2.06-2.01 (4H, m), 1.49-1.44 (18H, m), 1.12 (12H, m) and 0.82-0.78 (10H, m) ppm; ^{13}C-NMR (75 MHz, $CDCl_3$) δ 152.65, 151.91, 144.21, 142.84, 140.29, 139.33, 138.62, 137.07, 136.80, 135.89, 135.05, 132.90, 130.73, 125.43, 124.83, 124.70, 124.13, 123.75,123.56, 123.40, 121.40, 120.77, 120.26, 119.88, 116.31, 111.11, 109.22, 55.05, 40.36, 34.75, 32.03, 31.53, 29.65, 23.90, 22.58 and 14.02 ppm; FT-IR (KBr) 3042, 2926, 2953, 2855, 2361, 1609, 1476, 1362, 1324, 1294,1261, 1233, 968, 877, 809, 789 and 614 cm^{-1}; HRMS-ESI calcd for $C_{57}H_{62}BrNS_3$: *m/z* 935.3228 found 935.7048 [M$^+$].

3,6-Di-*tert*-butyl-9-(7-(5-(5-(pyrene-1-yl)thiophene-2-yl)thiophene-2-yl)thiophene-2-yl)-9,9-dihexyl-*9H*-fluoren-2-yl) -*9H*-carbazole (CFT3P)

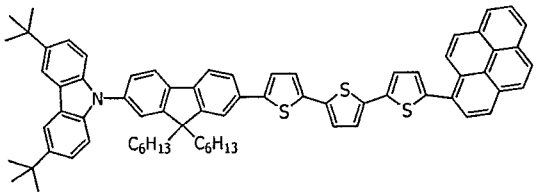

3,6-di-*tert*-butyl-9-(7-(5-(5-(4,6-dihydropyrene-1-yl)thiophene-2-yl)thiophene-2-yl)thio-phene-2-yl)-9,9-dihexyl-*9H*-fluoren-2-yl) -*9H*-carbazole was obtained from Suzuki cross coupling between 9-(7-(5-(5-bromothiophene-2-yl)thiophene-2-yl)thiophene-2-yl)-9,9-dihexyl-*9H*-fluoren-2-yl)-3,6-di-*tert*-butyl-*9H*-carbazole (0.6 g, 0.64 mmol) and pyreneboronic acid (0.19 g, 0.77 mmol) in the present of $Pd(PPh_3)_4$ (0.045 g, 0.035 mmol) and an aqueous sodium carbonate solution in THF (30 ml) as solvent was degassed with N_2 for 5 min. The reaction mixture was stirred at reflux under N_2 for 24 h. After being cooled to room temperature, water (50 ml) was added. The reaction mixture was extracted with dichloromethane (50 ml x 3), washed with water (100 ml), and brine solution (50 ml), dried over sodium sulfate anhydrous, filtered and the solvents were remove to dryness. Purification by column chromatography over silica gel eluting with a mixture of 10% dichloromethane and hexane follow by recrystallization with a mixture of dichloromethane and methanol afforded **CFT3P** as pale orange-yellow solid (0.252 g, 37%); m.p. 166-168 °C; ^{1}H-NMR (300 MHz, $CDCl_3$) δ 8.62 (1H, d, J = 9.0 Hz), 8.24-8.13 (9H, m), 8.08-

8.03 (1H, m), 7.90 (1H, d, J = 8.4 Hz), 7.78 (1H, d, J = 7.8 Hz), 7.69-7.63 (2H, m), 7.56-7.49 (4H, m), 7.43-7.34 (5H, m), 7.25-7.22 (3H, m) 2.06 (4H, m), 1.50 (18H, m),1.14 (12H, m) and 0.84-0.80 (10H, m) ppm; ^{13}C-NMR (75 MHz, $CDCl_3$) δ 152.66, 151.92, 143.98, 142.84, 141.74, 140.23, 139.34, 137.95, 137.04, 136.40, 136.23, 136.14, 132.99, 131.49, 131.15, 130.97, 129.24, 129.00, 128.80, 128.20, 128.12, 127.93, 127.35, 126.23, 125.46, 125.16. 124.85, 124.80, 124.69, 124.45, 124.30, 124.17, 123.79, 123.57, 123.39, 121.40, 120.77, 120.28, 119.88, 116.32, 109.23, 55.51, 40.37, 34.76, 32.04, 31.55, 29.67, 23.91, 22.60 and 14.04 ppm; FT-IR (KBr) 3041, 2951, 2925, 2855, 1608, 1583, 1476, 1362, 1324, 1294, 1262, 1232, 1034, 876, 844, 792, 756, 718 and 614 cm^{-1}; HRMS-ESI calcd for $C_{73}H_{71}NS_3$: *m/z* 1057.4749 found 1057.8557 [M^+].

3,6-Di-*tert*-butyl-9-(9,9-dihexyl(5-(5-(5-(thiophene-2-yl)thiophen-2-yl)thiophene-2-yl)-*9H*-fluoren-2-yl)*9H*-carbazole (6d)

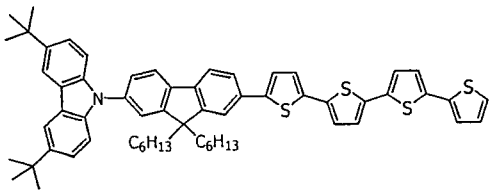

A mixture of 9-(7-(5-(5-bromothiophene-2-yl)thiophene-2-yl)thiophene-2-yl)-9,9-dihexyl-*9H*-fluoren-2-yl)-3,6-di-*tert*-butyl-*9H*-carbazole (1.7 g, 1.81 mmol), 2-thiopheneboronic acid (0.25 g, 1.40 mmol), $Pd(PPh_3)_4$ (0.0209 g, 0.018 mmol) and an aqueous sodium carbonate solution (2 M, 9 ml), in THF (45 ml) was degassed with N_2 for 5 min. The mixture was heated to reflux under N_2 for 24 h. After the mixture was cooled to room temperature water (50 ml) was added. The mixture was extracted with dichloromethane (50 ml x 3), washed with water (100 ml), and brine solution (50 ml), dried over sodium sulfate anhydrous, filtered and the solvents were remove to dryness. Purification by column chromatography over silica gel eluting with a mixture of 7% dichloromethane : hexane afforded **6d** as pale orange solid (1.380 g, 81%); m.p. 119-120 °C; ^{1}H-NMR (300 MHz, $CDCl_3$) δ 8.17 (2H, s), 7.88 (1H, d, J = 8.4 Hz), 7.76 (1H, d, J = 7.8 Hz), 7.66-7.47 (6H, m), 7.42-7.34 (3H, m), 7.26-7.20 (3H, m), 7.16-7.03 (5H, m), 2.06-2.00 (4H, m), 1.51-1.49 (18H, m), 1.12 (12H, m) and 0.82-0.78 (10H, m) ppm; ^{13}C-NMR (75 MHz, $CDCl_3$) δ 152.65, 151.90, 144.01, 142.83, 140.23, 139.33, 137.03, 136.40, 136.12, 135.88, 132.96, 135.88, 132.96, 127.93, 125.42, 124.78, 124.69, 124.61, 124.44, 124.38, 124.29, 124.23, 123.79, 123.57,

123.38, 121.39, 120.77, 120.26, 119.86, 116.31, 109.22, 55.50, 40.36, 34.76, 32.03, 31.54, 29.66, 26.92, 23.90, 22.59 and 14.04 ppm; FT-IR (KBr) 3064, 2951, 2924, 2854, 2361, 1608, 1475, 1362, 1323, 1293, 1261, 1231, 1033, 876, 834, 808, 790, 741, 688 and 614 cm^{-1}.; HRMS-ESI calcd for $C_{61}H_{65}NS_4$: *m/z* 939.4000 found 940.4363 [MH^+].

9-(7-(5-(5-(5-(5-Bromothiophene-2-yl)thiophene-2-yl)thiophene-2-yl)thiophene-2-yl)-9,9-dihexyl-*9H*-fliorene-2yl)-3,6-di-*tert*-butyl-*9H*-carbazole (7d)

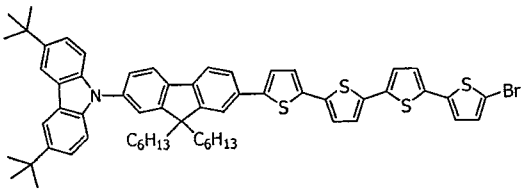

NBS (0.042 g, 0.235 mmol) was added in small portion to a stirred solution of 3,6-di-*tert*-butyl-9-(9,9-dihexyl(5-(5-(5-(thiophene-2-yl)thiophen-2-yl)thiophene-2-yl)-*9H*-fluoren-2-yl)-*9H*-carbazole (0.220 g, 0.233 mmol) in THF (50 ml). After being stirred at room temperature for 30 min, water (50 ml) was added. The mixture was extracted with dichloromethane (50 ml x 3). The combined organic phase was washed with water (50 ml), brine solution (30 ml), dried over sodium sulfate anhydrous, filtered and the solvent was remove in vacuum. Purification by short column chromatography using silica gel eluting with recycle solvent gave **7d** as orange solid (2.370 g, 100%); m.p. 112-116 °C; ^{1}H-NMR (300 MHz, $CDCl_3$) δ 8.18 (2H, s), 7.88 (1H, d, J = 8.7 Hz), 7.76 (1H, d, J = 7.8 Hz), 7.66-7.48 (6H, m), 7.41-7.33 (3H, m), 7.20 (1H, d, J = 3.6 Hz), 7.16-7.08 (3H, m), 7.04 (1H, d, J = 3.6 Hz), 6.99 (1H, d, J = 3.9 Hz), 6.93 (1H, d, J = 3.6 Hz), 2.06-2.01 (4H, m), 1.56-1.43 (18H, m), 1.12 (12H, m) and 0.82-0.77 (10H, m) ppm; ^{13}C-NMR (75 MHz, $CDCl_3$) δ 152.65, 151.91, 144.13, 142.84, 140.26, 139.32, 137.05, 136.68, 136.01, 135.21, 132.92, 130.74, 125.42, 124.77, 124.70, 124.61, 124.27, 124.24, 123.81, 123.77, 123.57, 123.39, 121.39, 120.77, 120.26, 119.88, 116.31, 111.18, 109.22, 55.50, 40.36, 34.75, 32.03, 31.54, 29.66, 26.92, 23.90, 22.59 and 14.04 ppm; FT-IR (KBr) 3064, 2952, 2924, 2854, 2361, 1609, 1476, 1362, 1323, 1294, 1261, 1232, 969, 876, 809, 788, 693 and 614 cm^{-1}; HRMS-ESI calcd for $C_{61}H_{64}BrNS_4$: *m/z* 1017.3125 found 1017.1455 [M^+].

3,6-Di-*tert*-butyl-9-(7-(5-(5-(5-(5-(pyren-1-yl)thiophene-2-yl) thiophene-2-yl) thiophene-2-yl)thiophene-2-yl)-9,9-dihexyl-*9H*-fluoren-2-yl)-*9H*-carbazole (CFT4P)

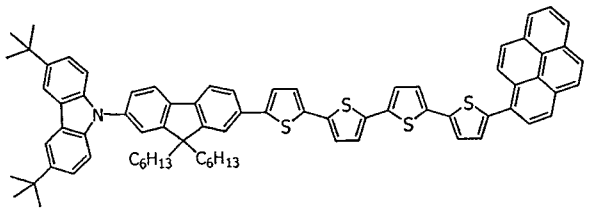

3,6-di-*tert*-butyl-9-(7-(5-(5-(5-(5-(4,6-dihydropyren-1-yl)thiophene-2-yl)thiophene-2-yl)thiophene-2-yl)thiophene-2-yl)-9,9-dihexyl-*9H*-fluoren-2-yl)-*9H*-carbazole was obtained from Suzuki cross coupling between 9-(7-(5-(5-(5-(5-bromothiophene-2-yl)thiophene-2-yl)thiophene-2-yl)thiophene-2-yl)-9,9-dihexyl-*9H*-fluoren-2-yl)-*9H*-carbazole (0.5 g, 0.422 mmol) and pyreneboronic acid (0.245 g, 0.99 mmol) in the present of $Pd(PPh_3)_4$ (0.024 g,0.02 mmol) and an aqueous sodium carbonate solution (3 ml, 4.22 mmol) in THF (30 ml) as solvent was degassed with N_2 for 5 min. The reaction mixture was stirred at reflux under N_2 for 24 h. After being cooled to room temperature, water (50 ml) was added. The reaction mixture was extracted with dichloromethane (50 ml x 3), washed with water (100 ml), and brine solution (50 ml), dried over sodium sulfate anhydrous, filtered and the solvents were remove to dryness. Purification by column chromatography over silica gel eluting with a mixture of 10% dichloromethane and hexane follow by recrystallization with a mixture of dichloromethane and methanol afforded **CFT4P** as pale orange solid (0.252 g, 37%); m.p. 220-222 °C; ^{1}H-NMR (300 MHz, $CDCl_3$) δ 8.59 (1H, d, J = 9.6 Hz), 8.19 (6H, s), 8.18-8.02 (6H, m), 7.88 (1H, d, J = 8.1 Hz), 7.76 (1H, d, J = 7.8 Hz), 7.65-7.61 (2H, m), 7.56-7.48 (5H, m), 7.41 (2H, d, J = 8.4 Hz), 7.37-7.32 (3H, m), 7.16 (4H, d, J = 12.6 Hz), 2.07-2.02 (4H, m), 1.50 (18H, m), 1.18 (12H, m) and 0.83-0.79 (10H, m) ppm; ^{13}C-NMR (75 MHz, $CDCl_3$) δ 152.68, 151.91, 142.85, 140.31, 139.34, 137.06, 136.02, 131.47, 131.17, 130.95, 128.72, 128.14, 127.95, 127.33, 126.22, 125.49, 125.42, 125.18, 124.80, 124.68, 124.45, 124.28, 123.58, 123.40, 121.39, 120.80, 120.26, 119.88, 116.33, 109.24, 55.51, 40.37, 34.77, 32.05, 31.91, 31.56, 29.68, 23.93, 22.61 and 14.06 ppm; FT-IR (KBr) 3039.17, 2923.99, 1601.42, 1582.92, 1474.87, 1361.62, 1323.38, 1293.56, 1261.08, 876.38, 843.43, 789.74, 755.90, 718.17, 681.01 and 613.59 cm^{-1}; HRMS-ESI calcd for $C_{77}H_{75}NS_4$: *m/z* 1141.4782 found 1140.4720 [M^+].

Chapter 3:

3,6-Di-*tert*-butyl-9-(5-(5-(7-(3,6-di-*tert*-9*H*-cabazyl-9-yl)-9,9-dihexyl-9*H*-fluorene-2-yl)-9*H*-carbazole (BCF)

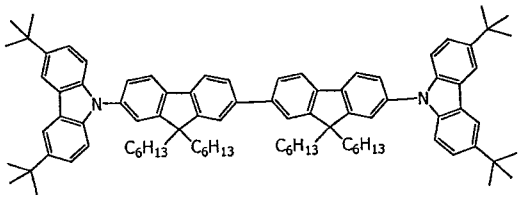

A mixture of 9-(7-bromo-9,9-dihexyl-9*H*-fluoren-2-yl)-3,6-di-*tert*-butyl-9*H*-carbazole (3.5 g, 5.16 mmol), $Pd(PPh_3)_4$ (0.042 g, 0.036 mmol) and an aqueous Na_2CO_3 solution (2 M, 25.8 ml) in THF (30 ml) was degas in with N_2 at 2 min. The mixture was heated at reflux under N_2 atmosphere for 24 h. After the mixture cooled to room temperature water (50 ml) was added. The mixture was extracted with dichloromethane (50 ml x 3). The combined organic phase was washed with water (50 ml), brine solution (50 ml) dried over anhydrous sodium sulfate, filtered and the organic solvent was remove in vacuum. Purification by column chromatography using silica gel eluting with hexane afforded **BCF** as light viscous (2.220 g, 15%); m.p. 155-156 °C; ^{1}H-NMR (300 MHz, $CDCl_3$) δ 8.19 (2H, s), 7.95 (1H, d, J = 8.7 Hz), 7.87 (1H, d, J = 8.7 Hz), 7.72 (2H, t, J = 8.4 Hz), 7.57 (2H, d, J = 6.6 Hz), 7.51 (2H, d, J = 7.8 Hz), 7.44 (2H, d, J = 8.7 Hz),2.09 (4H, m), 1.50 (18H, s), 1.16 (12H, s), 0.822 (10H, t, J = 6.6 Hz) ppm; ^{13}C-NMR (75 MHz, $CDCl_3$) δ 152.75, 151.82, 142.81, 140.63, 139.74, 139.61, 139.40, 136.90, 126.35, 125.41, 123.57, 123.39, 121.49, 120.77, 116.32, 109.27, 55.53, 40.36, 34.77, 32.05, 31.56, 30.91, 29.68, 23.96, 22.59, 14.06 ppm; FT-IR (Nujol) 2923.88, 2853.70, 1161.32, 1462.99, 1377.13, 1295.77, 1263.60, 810.13 and 744.00 cm^{-1}.

3,6-Di-*tert*-butyl-9-(5-(5-(7-(3,6-di-*tert*-9*H*-cabazyl-9-yl)-9,9-dihexyl-9*H*-fluorene-2-yl)thiophene-2-yl)thiophen-2-yl)-9*H*-carbazole (BCF2T)

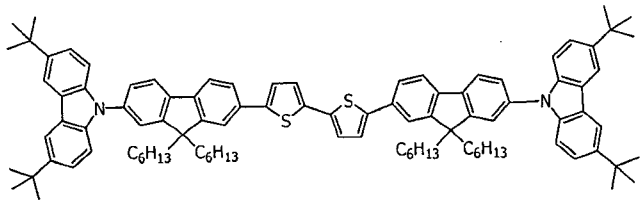

A degassed solution of the 9-(7-(5-bromothiophen-2-yl)-9,9-dihexyl-*9H*-fluoren-2-yl)-3,6-di-*tert*-butyl-*9H*-carbazole (0.244 g, 0.126 mmol), the hexabutyldistananne (0.046 g, 0.08 mmol) and $Pd(PPh_3)_4$ (0.007g, 0.0015 mmol) in toluene (25 ml) was heat at 80 °C under N_2. After 24 h the reaction mixture was cooled to room temperature, water was added. The mixture was extracted with dichloromethane (50 mlx 3). The combined organic phase was washed with water (50 ml), brine solution (50 ml), dried over anhydrous sodium sulfate, filtered and the solvent was remove in vacuum. Purification by short column chromatography using silica gel eluting with mixture of dichloromethane and methanol followed by recrystallization with methanol afforded **BCF2T** as yellow solid (0.120 g, 68%); m.p. 200-201 °C; ^{1}H-NMR (300 MHz, $CDCl_3$) δ 8.20 (4H, s), 7.90 (2H, d, J = 8.4 Hz), 7.79 (2H, d, J = 7.8 Hz), 7.70-7.64 (4H, t, J = 7.8 Hz, J = 8.7 Hz), 7.58-7.50 (8H, m), 7.45-7.38 (6H, m), 7.29-7.27 (2H, m), 2.06-2.04 (8H, m), 1.51 (36H, m), 1.15 (24H, m) and 0.90-0.80 (20H, m) ppm; ^{13}C-NMR (75 MHz, $CDCl_3$) δ 152.66, 151.92, 143.79, 142.84, 140.19, 139.35, 137.03, 136.61, 133.05, 125.44, 124.77, 123.79, 123.58, 123.40, 121.41, 120.78, 120.29, 120.08, 119.87, 116.33, 109.24, 55.01, 40.40, 34.77, 32.05, 31.57, 29.69, 23.93, 22.61 and 14.06 ppm; FT-IR (Nujol) 2923.88, 2853.70, 1161.32, 1462.99, 1377.13, 1295.77, 1263.60, 810.13 and 744.00 cm^{-1}; HRMS-ESI calcd for $C_{98}H_{116}N_2S_2$: *m/z* 1368.1130 found 1386.0360 [M$^+$].

3,6-Di-*tert*-butyl-9-(7-(5-(5-(7-(3,6-di-*tert*-butyl-9-yl)-9,9-dihexyl-*9H*-fluorene-2-yl) thiophene-2-yl)thiophene-2-yl)thiophene-2-yl)thiophene-2-yl)-9,9-dihexyl-*9H*-fluorene-2-yl)-*9H*-carbazole (BCF4T)

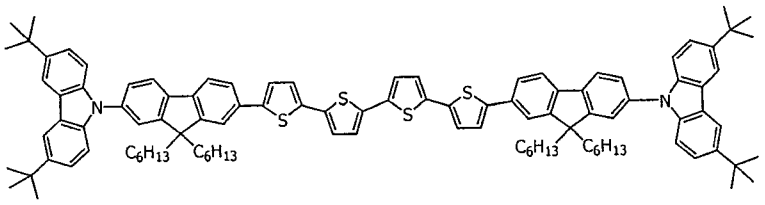

A degassed solution of the 9-(7-(5-(5-bromothiophene-2-yl)thiophene-2-yl)-9,9-dihexyl-*9H*-fluoren-2-yl)-3,6-di-*tert*-butyl-*9H*-carbazole (0.300 g, 0.167 mmol), the hexabutyldistananne (0.08 g, 0.138 mmol) and $Pd(PPh_3)_4$ (0.008 g, 0.003 mmol) in toluene (25 ml) was heat at 80^{0}C under N_2. After 24 h the reaction mixture was cooled to room temperature, water was added. The mixture was extracted with dichloromethane (50 ml x 3).

The combined organic phase was washed with water (50 ml), brine solution (50 ml), dried over anhydrous sodium sulfate, filtered and the solvent was remove in vacuum. Purification by short column chromatography using silica gel eluting with mixture of dichloromethane and methanol followed by recrystallization with methanol afforded **BCF4T** as yellow-orange solid (0.130 g, 50%); m.p. > 270 °C; ^{1}H-NMR (300 MHz, $CDCl_3$) δ 8.18 (4H, s), 7.89 (2H, d, J = 8.4 Hz), 7.77 (2H, d, J = 8.1 Hz), 7.67-7.60 (4H, t, J = 8.1 Hz, J = 10.5 Hz), 7.55-7.48 (8H, t, J = 13.2 Hz, J = 8.7 Hz), 7.41-7.34 (6H, dd, J = 8.7 Hz, J = 3.6 Hz), 7.17-7.13 (6H, q, J = 3.6 Hz), 2.07-202 (8H, m), 1.52 (36H, m), 1.13 (24H, s) and 0.82-0.78 (20H, t, J = 6 Hz, J = 6.9 Hz) ppm; ^{13}C-NMR (75 MHz, $CDCl_3$) δ 152.67, 151.87, 143.78, 142.84, 140.13, 139.34, 137.06, 136.53, 133.07, 127.90, 125.42, 124.77, 124.67, 124.38, 123.57, 123.39, 121.40, 120.78, 120.24, 119.87, 116.31, 109.23, 55.05, 40.36, 34.75, 32.04, 31.90, 31.76, 31.54, 29.66, 23.91, 22.59 and 14.04 ppm; FT-IR (Nujol) 2921.36, 2852.65, 1609.04, 1463.49, 1455.77, 1377.57, 1296.41, 1076.12, 839.32, 788.16 and 722.03 cm^{-1}; HRMS-ESI calcd for $C_{106}H_{120}N_2S_4$: *m/z* 1550.3604 found 1551.1836 [MH$^+$].

3,6-Di-*tert*-butyl-9-(7-(5-(5-(5-(5-(5-(5-(7-(3,6-di-*tert*-butyl-9-yl)-9,9-dihexyl-*9H*-fluorene-2-yl)thiophene-2-yl)thiophene-2-yl)thiophene-2-yl)thiophene-2-yl)thiophene-2-yl)thiophene-2-yl)-9,9-dihexyl-*9H*-fluorene-2-yl)-*9H*-carbazole (BCF6T)

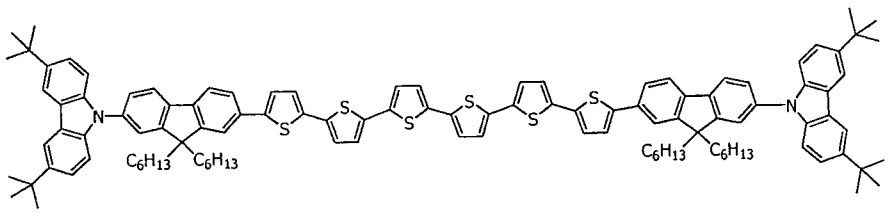

A degassed solution of the 9-(7-(5-(5-bromothiophene-2-yl)thiophene-2-yl)thiophene-2-yl)-9,9-dihexyl-*9H*-fluoren-2-yl)-3,6-di-*tert*-butyl-*9H*-carbazole (0.300 g, 0.152 mmol), the hexabutyldi-stananne (0.08 g, 0.138 mmol) and $Pd(PPh_3)_4$ (0.008 g, 0.003 mmol) in toluene (25 ml) was heat at 80°C under N_2. After 24 h the reaction mixture was cooled to room temperature, water was added. The mixture was extracted with dichloromethane (50 ml x 3). The combined organic phase was washed with water (50 ml), brine solution (50 ml), dried over anhydrous sodium sulfate, filtered and the solvent was remove in vacuum. Purification by short

column chromatography using silica gel eluting with mixture of dichloromethane and methanol followed by recrystallization with methanol afforded **BCF6T** as orange solid (0.125 g, 48%); m.p. 180-181 °C; ^{1}H-NMR (300 MHz, $CDCl_3$) δ 8.17 (4H, s), 7.89 (2H, d, J = 8.4 Hz), 7.76 (2H, d, J = 7.8 Hz), 7.66-7.47 (13H, m), 7.41-7.34 (6H, dd, J = 8.4 Hz, J = 3.6 Hz), 7.16-7.11 (9H, m), 2.04 (8H, m), 1.49 (36H, s), 1.13 (24H, m) and 0.82-0.78 (20H, t, J = 6 Hz, d, J = 6.9 Hz) ppm; ^{13}C-NMR (75 MHz, $CDCl_3$) δ 152.66, 151.92, 144.09, 142.84, 140.25, 139.34, 137.06, 136.56, 135.97, 135.76, 132.95, 125.43, 124.74, 124.50, 124.27, 123.78, 123.56, 123.40, 121.41, 120.77, 120.27, 119.88, 116.31, 109.22, 55.51, 40.36, 34.75, 32.03, 31.54, 29.66, 23.91, 22.58 and 14.02 ppm; FT-IR (Nujol) 2921.36, 2852.65, 1609.04, 1463.49, 1455.77, 1377.57, 1296.41, 1076.12, 839.32, 788.16 and 722.03 cm^{-1}; HRMS-ESI calcd for $C_{114}H_{124}N_2S_6$: *m/z* 1714.6078 found 1716.0160 [MH$^+$].

3,6-Di-*tert*-butyl-9-(7-(5-(5-(5-(5-(5-(5-(7-(3,6-di-*tert*-butyl-9-yl)-9,9-dihexyl-*9H*-fluorene-2-yl)thiophene-2-yl)thiophene-2-yl)thiophene-2-yl)thiophene-2-yl)thiophene-2-yl)thiophene-2-yl)thiophene-2-yl)thiophene-2-yl)-9,9-dihexyl-*9H*-fluorene-2-yl)-*9H*-carbazole (BCF8T)

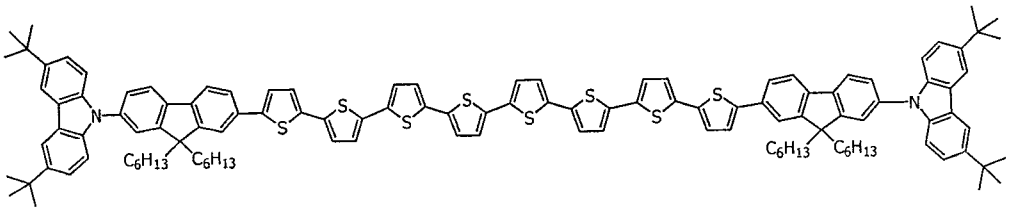

A degassed solution of the 9-(7-(5-(5-(5-(5-bromothiophene-2-yl)thiophene-2-yl)thiophene-2-yl)thiophene-2-yl)-9,9-dihexyl-*9H*-fliorene-2yl)-3,6-di-*tert*-butyl-*9H*-carbazole (0.150 g, 0.126 mmol), the hexabutyldistananne (0.036 g, 0.062 mmol) and $Pd(PPh_3)_4$ (0.0014 g, 0.002 mmol) in toluene (25 ml) was heat at 80^{0}C under N_2. After 24 h the reaction mixture was cooled to room temperature, water was added. The mixture was extracted with dichloromethane (50 ml x 3). The combined organic phase was washed with water (50 ml), brine solution (50 ml), dried over anhydrous sodium sulfate, filtered and the solvent was remove in vacuum. Purification by short column chromatography using silica gel eluting with mixture of dichloromethane and methanol followed by recrystallization with methanol afforded **BCF8T** as orange solid (0.085 g, 36%); m.p. 179-180 °C; ^{1}H-NMR (300 MHz, $CDCl_3$) δ 8.17 (4H, s), 7.89 (2H, d, J = 8.4 Hz),

7.77 (2H, d, J = 7.8 Hz), 7.66-7.47 (14H, m), 7.41-7.34 (7H, dd, J = 8.7 Hz, J = 3.9 Hz), 7.21 (2H, d, J = 3.9 Hz), 7.17-7.12 (9H, m), 2.02 (8H, m), 1.49 (36H, s), 1.13 (24H, m) and 0.81-0.77 (20H, t, J = 6.6 Hz, d, J = 6.9 Hz) ppm; ^{13}C-NMR (75 MHz, $CDCl_3$) δ 152.66, 151.91, 142.82, 139.31, 136.02, 132.94, 125.42, 124.77, 124.52, 123.80, 123.56, 123.38, 120.78, 119.84, 116.31, 109.22, 55.49, 40.36, 34.74, 32.03, 31.53, 29.66, 23.92, 22.59 and 14.04 ppm; FT-IR (Nujol) 2921.36, 2852.65, 1609.04, 1463.49, 1455.77, 1377.57, 1296.41, 1076.12, 839.32, 788.16 and 722.03 cm^{-1}; HRMS-ESI calcd for $C_{122}H_{128}N_2S_8$: *m/z* 1878.8551 found 1879.8670 [MH$^+$].

Chapter 4:

5-(7-(3,6-Di-*tert*-butyl-*9H*-carbazol-9-yl)-9,9-dihexyl-fluorene-2-yl)thiophene-2-carbaldehyde (8a)

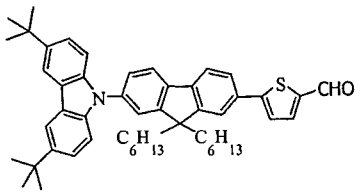

To a solution of 9-(7-bromo-9,9-dihexyl-*9H*-fluoren-2-yl)-3,6-di-*tert*-butyl-*9H*-carbazole (1.44 g, 2.06 mmol), 5-formylthiophenboronic acid (0.25 g, 1.6 mmol), $Pd(PPh_3)_4$ (0.015 g, 0.129 mmol), and 2 M Na_2CO_3 aqueous solution (8 ml, 0.21 mmol) in THF (20 ml) was degas with N_2 for 5 min. The reaction mixture was stirred at reflux under N_2 for 24 h. After being cooled to room temperature, water (50 ml) was added and extracted with dichloromethane (50 ml x 3). The combined organic phase were washed with water (50 ml) and brine solution (50 ml), dried over anhydrous Na_2SO_4, filtered, and the solvents were removed to dryness. Purification by column chromatography over silica gel eluting with a mixture of 30% dichloromethane and hexane follow by recrystallization with a mixture of dichloromethane and methanol afforded **8a** as pale yellow solid (0.520 g, 34%); ^{1}H-NMR (300 MHz, $CDCl_3$) δ 9.92 (1H,s), 8.18 (2H,s), 7.92 (1H,), 7.82-7.68 (4H, m), 7.57 (2H, d, J = 6.3 Hz) 7.51-7.48 (3H, m), 7.41 (2H, d, J = 6.3 Hz), 2.01-2.07 (4H, m), 1.49 (18H, m), 1.20-1.12 (12H, m) and 0.82-0.77 (10H, m) ppm; ^{13}C-NMR (75 MHz, $CDCl_3$) δ 182.70, 155.03, 152.90, 142.96, 142.14, 142.03, 139.25, 138.81, 137.62, 137.45, 131.93, 125.75, 125.51, 123.93, 123.61, 123.46, 121.41, 120.72, 120.45, 116.36, 109.19, 55.61, 40.28, 34.77, 32.03, 31.52, 29.62, 22.57 and 14.02 ppm;

FT-IR (KBr) 3073, 2926, 2855, 1655, 1488, 1437, 1363, 1323, 1293, 1260, 1225, 1055, 879, 806, 755 and 670 cm^{-1}.

5-(5-(7-(3,6-Di *tert*-butyl-*9H*-carbazol-9-yl)-9,9-dihexyl-fluorene-2-yl)thiophene -2-yl)thiophene-2-carbaldehyde (8b)

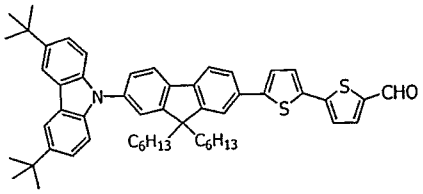

A mixture of 9-(7-(5-(5-bromothiophene-2-yl)thiophene-2-yl)-9,9-dihexyl-*9H*-fluoren-2-yl)-3,6-di-*tert*-butyl-*9H*-carbazole (2.3 g, 2.90 mmol), 5-formylthiopheneboronic acid (0.250 g, 1.6 mmol), $Pd(PPh_3)_4$ (0.016 g, 0.0138 mmol), and 2M aqueous solution (7 ml, 0.66 mmol) in THF was degassed with N_2 for 5 min. the reaction mixture was stirred at reflux under N_2 for 24 h. After being cooled to room temperature water (100 ml) was added and extracted with dichloromethane (50 ml x 3). The combined organic phase were washed with water (50 ml) and brine solution (50 ml), dried over anhydrous Na_2SO_4, filtered, and the solvents were removed to dryness. Purification by column chromatography over silica gel eluting with a mixture of dichloromethane and hexane (3:7) followed by recrystallization with a mixture of dichloromethane and methanol afforded **8b** as yellow-orange solid (1.980 g, 83 %); ^{1}H-NMR (300 MHz, $CDCl_3$) δ 9.90 (1H, s), 8.19 (2H, s), 7.90 (1H, d, J = 8.1 Hz), 7.78 (1H, d, J = 7.5 Hz), 7.72-7.66 (2H, m), 7.62-7.49 (5H, m), 7.43-7.40 (4H, m), 7.28 (1H, d, J = 12.9 Hz), 2.03 (4H, m), 1.50 (18H, m),1.13 (12H, m) and 0.90 (10H, m) ppm; ^{13}C-NMR (75 MHz, $CDCl_3$) δ 152.67, 151.93, 143.81, 142.86, 140.20, 139.38, 137.06, 136.62, 133.06, 125.45, 124.79, 124.53, 123.80, 123.59, 123.42, 121.43, 120.78, 120.30, 119.89, 116.34, 109.26, 55.52, 40.41, 34.78, 32.06, 31.93, 31.57, 29.70, 23.94, 22.62 and 14.06 ppm; FT-IR (KBr) 3073, 2926, 2855, 1655, 1488, 1437, 1363, 1323, 1293, 1260, 1225, 1055, 879, 806, 755 and 670 cm^{-1}.

5-(5-(5-(7-(3,6-Di *tert*-butyl-*9H*-carbazol-9-yl)-9,9-dihexyl-fluorene-2-yl)thiophene-2-yl)thiophene-2-yl)thiophene-2-carbaldehyde (8c)

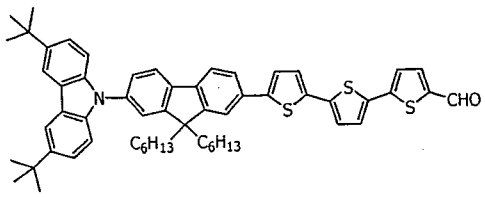

A mixture of 9-(7-(5-(5-bromothiophene-2-yl)thiophene-2-yl)-9,9-dihexyl-*9H*-fluoren-2-yl)-3,6-di-*tert*-butyl-*9H*-carbazole (1.11 g, 1.29 mmol), 5-formylthiopheneboronic acid (0.168 g, 1.07 mmol), $Pd(PPh_3)_4$ (0.0125 g, 0.011 mmol), and 2M aqueous solution (6.5 ml, 0.0129 mmol) in THF was degassed with N_2 for 5 min. the reaction mixture was stirred at reflux under N_2 for 24 h. After being cooled to room temperature water (100 ml) was added and extracted with dichloromethane (50 ml x 3). The combined organic phase were washed with water (50 ml) and brine solution (50 ml), dried over anhydrous Na_2SO_4, filtered, and the solvents were removed to dryness. Purification by column chromatography over silica gel eluting with a mixture of 40% dichloromethane and hexane followed by recrystallization with a mixture of dichloromethane and methanol afforded **8c** as pale orange solid (0.540 g, 47.%); ^{1}H-NMR (300 MHz, $CDCl_3$) δ 9.88 (1H, s), 8.18 (2H, s), 7.89 (1H, d, J = 8.4 Hz), 7.75 -7.78 (1H, m), 7.69-7.47 (8H, m), 7.41-7.30 (5H, m), 7.25 (3H, d, J = 3.3 Hz), 7.19 (1H, d, J = 6.6 Hz), 2.06-2.01 (4H, m), 1.48 (18H, m), 1.12 (12H, m) and 0.82-0.78 (10H, m) ppm; ^{13}C-NMR (75 MHz, $CDCl_3$) δ 182.37, 152.68, 151.97, 146.82, 145.00, 142.88, 141.67, 140.49, 139.35, 139.29, 139.25, 137.29, 137.17, 135.39, 134.44, 132.74, 127.02, 125.47, 124.89, 124.46, 124.03, 123.87, 123.57, 123.42, 121.43, 120.82, 120.30, 119.96, 116.32, 109.22, 55.53, 40.34, 34.75, 32.03, 31.89, 31.74, 31.53, 29.69, 29.65, 29.35, 23.91, 22.68, 22.56, 14.08 and 14.00 ppm; FT-IR (KBr) 3073, 2926, 2855, 1655, 1488, 1437, 1363, 1323, 1293, 1260, 1225, 1055, 879, 806, 755 and 670 cm^{-1}.

5-(5-(5-(5-(7-(3,6-Di *tert*-butyl-*9H*-carbazol-9-yl)-9,9-dihexyl-fluorene-2-yl) thiophene-2-yl)thiophene-2-yl)thiophene-2-yl)thiophene-2-carbaldehyde (8d)

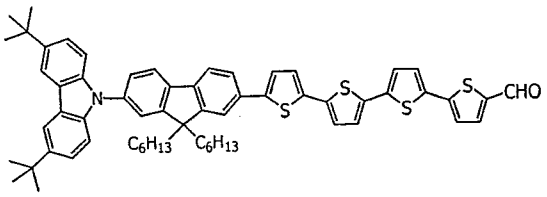

A mixture of 9-(7-(5-(5-bromothiophene-2-yl)thiophene-2-yl)thiophene-2-yl)-9,9-dihexyl-*9H*-fluoren-2-yl)-3,6-di-*tert*-butyl-*9H*-carbazole (0.813 g, 0.867 mmol), 5-formyl-thiopheneboronic acid (0.1 g, 0.64 mmol), $Pd(PPh_3)_4$ (0.0067 g, 0.0058 mmol), and 2M aqueous solution (4 ml, 8.67 mmol) in THF was degassed with N_2 for 5 min. the reaction mixture was stirred at reflux under N_2 for 24 h. After being cooled to room temperature water (100 ml) and extracted with dichloromethane (50 ml x 3). The combined organic phase were washed with water (50 ml) and brine solution (50 ml), dried over anhydrous Na_2SO_4, filtered, and the solvents were removed to dryness. Purification by column chromatography over silica gel eluting with a mixture of 40% dichloromethane and hexane followed by recrystallization with a mixture of dichloromethane and methanol afforded **8d** as orange solid. (0.420 g, 51%); ^{1}H-NMR (300 MHz, $CDCl_3$) δ 9.84 (1H, s), 8.21 (2H, s), 7.88 (1H, d, J = 7.8 Hz), 7.73 (1H, d, J = 7.5 Hz), 7.69-7.53 (7H, m), 7.45 (2H, d, J = 8.7 Hz), 7.23-7.16 (3H, m), 7.10-6.98 (4H, m), 2.03 (4H, m), 1.50 (18H, m), 1.13 (12H, m) and 0.90 (10H, m) ppm; ^{13}C-NMR (75 MHz, $CDCl_3$) δ 182.32, 152.72, 152.00, 146.67, 144.34, 142.93, 141.64, 140.36, 139.36, 139.32, 138.85, 137.37, 137.14, 135.84, 135.01, 134.55, 132.89, 129.19, 127.02, 125.45, 125.26, 125.04, 124.88, 124.55, 124.32, 124.07, 123.88, 123.67, 123.49, 121.43, 121.31, 121.13, 120.89, 120.41 119.84, 116.40, 109.32, 56.67, 55.56, 40.40, 37.65, 34.82, 32.12, 31.98, 31.63, 31.55, 30.77, 29.75, 29.63, 28.68, 24.09, 24.03, 23.20, 22.69, 22.58, 14.16 and 10.77 ppm; FT-IR (KBr) 3073, 2926, 2855, 1663, 1488, 1454, 1363, 1323, 1293, 1260, 1225, 1055, 879, 806, 755 and 670 cm^{-1}.

(*E*)-3-(5-(7-(3,6,-Di-*tert*-butyl-*9H*-carbazol-9-yl)-9,9-dihexyl-*9H*-fluoren-2-yl) thiophene-2-yl)acrylic acid (MDT)

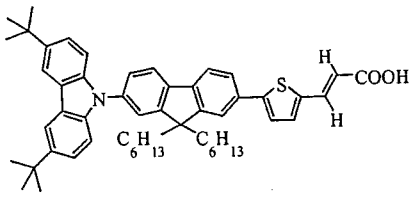

A mixture of 5-(7-(3,6-di *tert*-butyl-*9H*-carbazol-9-yl)-9,9-dihexyl-fluorene-2-yl)thiophene-2-carbaldehyde (0.358 g , 0.496 mmol) and malonic acid (0.258 g, 2.48 mmol) was vacuum-dried and added THF:acetonitrile (20 ml, 1:1 v/v) and piperidine (0.245 ml, 2.48 mmol). The solution was refluxed for 6 h. After cooling the solution, the organic layer was removed in vacuum. The pure product was obtain by silica gel chromatography to afforded **MDT** as yellow solid (0.234 g, 62%); m.p. 265-266 °C; ^{1}H-NMR (300 MHz, $CDCl_3$, DMSO-d) δ 8.17 (1H, s), 7.89-7.81 (4H, m), 7.65-7.59 (3H, m), 7.54-7.74 (4H, m),7.71-7.31 (4H, m), 7.28-7.19 (5H, m), 6.21 (1H, d, J = 4.5 Hz), 2.03 (4H, m), 1.47 (18H, m), 1.11 (12H, m) and 0.81-0.77 (10H, m) ppm; ^{13}C-NMR (75 MHz, $CDCl_3$, DMSO-d) δ 168.02, 152.41, 151.65, 143.82, 142.65, 140.00, 139.24, 139.09, 139.01, 138.21, 136.72, 136.50, 136.35, 135.56, 132.62, 131.85, 125.12, 124.69, 124.58, 124.36, 124.17, 123.74, 123.42, 123.07, 121.01, 120.71, 120.18, 119.54, 117.40, 116.04, 109.01, 68.33, 55.25, 40.70, 40.42, 40.15, 39.99, 39.87, 39.59, 39.31, 39.03, 34.51, 31.83, 31.25, 30.67, 29.32, 26.43, 23.43, 22.27 and 14.02 ppm; FT-IR (KBr) 3400, 2955, 2927, 2856, 1619, 1567, 1489, 1477, 1365, 1324, 1295, 1262, 1233, 1034, 877, 809, 742 and 614 cm^{-1}. HRMS-ESI calcd for $C_{52}H_{61}NO_2S$: *m/z* 764.4423 found 763.4760 [M$^+$].

(*E*)-3-(5-(5-(7-(3,6,-Di-*tert*-butyl-*9H*-carbazol-9-yl)-9,9-dihexyl-*9H*-fluoren-2-yl)thiophen-2-yl)thiophene-2-yl)acrylic acid (MD2T)

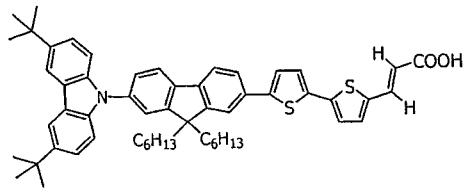

A mixture of 5-(5-(7-(3,6-di *tert*-butyl-*9H*-carbazol-9-yl)-9,9-dihexyl-fluorene-2-yl)thiophene-2-yl)thiophene-2-carbaldehyde (0.25 g, 0.346 mmol) and malonic acid (0.18 g, 1.70 mmol) was vacuum-dried and added THF:acetonitrile (20 ml, 1:1 v/v) and piperidine (0.245 ml, 2.48 mmol). The solution was refluxed for 6 h. After cooling the solution, the organic layer was removed in vacuum. The pure product was obtained by column chromatography over silica gel eluting with gradient solution system started with 1% MeOH : dichloromethane afforded **MD2T** as yellow-orange solid (0.117 g, 40%); m.p. 259-260 °C; ^{1}H-NMR (300 MHz, $CDCl_3$, DMSO-d) δ 8.17 (1H, s), 7.89-7.81 (4H, m), 7.65-7.59 (3H, m), 7.54-7.74 (4H, m),7.71-7.31 (4H, m), 7.28-7.19 (5H, m), 6.21 (1H, d, J = 4.5 Hz), 2.03 (4H, m), 1.47 (18H, m), 1.11 (12H, m) and 0.81-0.77 (10H, m) ppm; ^{13}C-NMR (75 MHz, $CDCl_3$, DMSO-d) δ 170.79, 152.67, 151.96, 145.42, 142.86, 141.28, 140.55, 139.30, 139.21, 138.91, 137.69, 137.15, 135.50, 133.03, 132.66, 128.71, 125.98, 124.92, 124.74, 12437, 124.19, 123.94, 123.57, 123.39, 120.85, 120.53, 120.31, 119.94, 116.33, 115.29, 109.21, 55.52, 40.46, 40.34, 34.76, 32.03, 31.90, 31.75, 31.53, 31.45, 29.71, 29.65, 29.53, 23.90, 22.58, 22.48 and 14.04 ppm; FT-IR (KBr) 3446, 2927, 1636, 1618, 1477, 1295 and 791 cm^{-1}. HRMS-ESI calcd for $C_{56}H_{63}NO_2S_2$: *m/z* 845.4300 found 845.6510 [M^{+}].

(*E*)-3-(5-(5-(5-(7-(3,6,-Di-*tert*-butyl-*9H*-carbazol-9-yl)-9,9-dihexyl-*9H*-fluoren-2-yl) thiophene-2-yl)thiophen-2-yl)thiophene-2-yl)acrylic acid (MD3T)

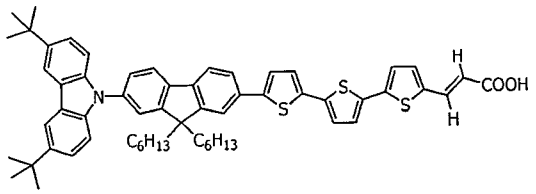

A mixture of 5-(5-(5-(7-(3,6-di *tert*-butyl-*9H*-carbazol-9-yl)-9,9-dihexyl-fluorene-2-yl)thiophene-2-yl)thiophene-2-yl)thiophene-2-carbaldehyde (0.364 g, 0.411 mmol) and malonic acid (0.213 g, 2.05 mmol) was vacuum-dried and added THF:acetonitrile (20 ml, 1:1 v/v) and piperidine (0.245 ml, 2.48 mmol). The solution was refluxed for 6 h. After cooling the solution, the organic layer was removed in vacuum. The pure product was obtain by silica gel chromatography to afforded **MD3T** as orange solid (0.190 g, 50%); m.p. 180-181 °C; ^{1}H-NMR (300 MHz, $CDCl_3$, DMSO-d) δ 8.05 (1H, s), 7.82 (1H, d, J = 8.4 Hz), 7.70-7.62 (1H,

q, J = 7.8 Hz), 7.57- 7.50 (2H, m), 7.46-7.43 (4H, m), 7.36 (2H, d, J = 8.7), 7.38 (2H, d, J = 8.4), 7.13-7.03 (7H, m), 6.06 (1H, d, J = 15.6 Hz), 2.03 (4H, m), 1.50 (18H, m),1.13 (12H, m) and 0.90 (10H, m) ppm; ^{13}C-NMR(75 MHz, $CDCl_3$, DMSO-d) δ 168.02, 152.41, 151.65, 143.82, 142.65, 140.00, 139.24, 139.09, 139.01, 138.21, 136.72, 136.50, 136.35, 135.56, 132.62, 131.85, 125.12, 124.69, 124.58, 124.36, 124.17, 123.74, 123.42, 123.07, 121.01, 120.71, 120.18, 119.54, 117.40, 116.04, 109.01, 68.33, 55.25, 40.70, 40.42, 40.15, 39.99, 39.87, 39.59, 39.31, 39.03, 34.51, 31.83, 31.25, 30.67, 29.32, 26.43, 23.43, 22.27 and 14.02 ppm; FT-IR (KBr) 3446, 2927, 1636, 1618, 1477, 1295 and 791 cm^{-1}.

(*E*)-3-(5-(5-(5-(5-(7-(3,6-Di-*tert*-buthyl-*9H*-carbazol-9-yl)-9,9-dihexyl-*9H*-fluoren-2-yl)thiophene-2-yl)thiophen-2-yl)thiophene-2-yl)thiophene-2-yl)acrylic acid (MD4T)

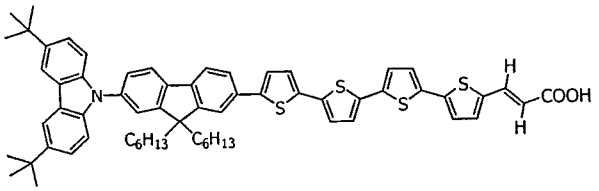

A mixture of 5-(5-(5-(5-(7-(3,6-di-*tert*-butyl-*9H*-carbazol-9-yl)-9,9-dihexyl-fluorene-2-yl)thiophene-2-yl)thiophene-2-yl)thiophene-2-yl)thiophene-2-carbaldehyde (0.450 g, mmol) and malonic acid (0.213 g, 2.05 mmol) was vacuum-dried and added THF : acetonitrile (20 ml, 1:1 v/v) and piperidine (0.245 ml, 2.48 mmol). The solution was refluxed for 6 h. After cooling the solution, the organic layer was removed in vacuum. The pure product was obtain by silica gel chromatography to afforded **MD4T** as orange solid (0.190 g, 50%); m.p. 240-241 °C; ^{1}H-NMR (300 MHz, $CDCl_3$, DMSO-d) δ 8.05 (1H, s), 7.82 (1H, d, J = 8.4 Hz), 7.70-7.62 (1H, q, J = 7.8 Hz), 7.57- 7.50 (2H, m), 7.46-7.43 (4H, m), 7.36 (2H, d, J = 8.7), 7.38 (2H, d, J = 8.4), 7.13-7.03 (7H, m), 6.06 (1H, d, J = 15.6 Hz), 2.03 (4H, m), 1.50 (18H, m),1.13 (12H, m) and 0.90 (10H, m) ppm; ^{13}C-NMR (75 MHz, $CDCl_3$, DMSO-d) δ 168.02, 152.41, 151.65, 143.82, 142.65, 140.00, 139.24, 139.09, 139.01, 138.21, 136.72, 136.50, 136.35, 135.56, 132.62, 131.85, 125.12, 124.69, 124.58, 124.36, 124.17, 123.74, 123.42, 123.07, 121.01, 120.71, 120.18, 119.54, 117.40, 116.04, 109.01, 68.33, 55.25, 40.70, 40.42, 40.15, 39.99, 39.87, 39.59, 39.31, 39.03, 34.51, 31.83, 31.25, 30.67, 29.32, 26.43, 23.43, 22.27, 13.83 ppm; FT-IR (KBr) 3446, 2927, 1636, 1618, 1477, 1295, 791 cm^{-1}. HRMS-ESI calcd for $C_{64}H_{67}NO_2S_4$: *m/z* 1009.4056 found 1009.7150 [M$^+$]

(*E*)-2-Cyano-3-(5-(7-(3,6,-di-*tert*-butyl-*9H*-carbazol-9-yl)-9,9-dihexyl-*9H*-fluoren-2-yl)thiophene-2-yl)acrylic acid (CAT)

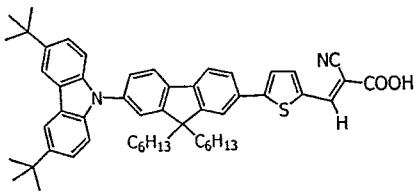

A mixture of 5-(7-(3,6-di *tert*-butyl-*9H*-carbazol-9-yl)-9,9-dihexyl-fluorene-2-yl)thiophene-2-carbaldehyde (0.228 g , 0.317 mmol) and cyanoacetic acid (0.125 g, 1.58 mmol) was vacuum-dried and added THF:acetonitrile (20 ml, 1:1 v/v) and piperidine (0.156 ml, 1.58 mmol). The solution was refluxed for 6 h. After cooling the solution, the organic layer was removed in vacuum. The pure product was obtain by silica gel chromatography to afforded **CAT** as yellow solid (0.130 g, 52%); m.p. 259-260 °C; ^{1}H-NMR (300 MHz, $CDCl_3$, DMSO-d) δ 8.19 (1H, s), 8.05 (1H, s), 7.84 (1H, d, J = 8.4 Hz), 7.71-7.59 (5H, m), 7.42 (3H, m), 7.25 (3H, dd, J = 8.7 Hz), 1.97 (4H, m), 1.36 (18H, m),1.00 (12H, m) and 0.65 (10H, m) ppm; ^{13}C-NMR (75 MHz, $CDCl_3$, DMSO-d) δ 152.75, 151.92, 150.88, 142.89, 142.66, 139.10, 139.05, 137.15, 136.26, 136.09, 132.29, 125.59, 125.33, 124.11, 123.70, 121.31, 121.14, 120.60, 120.22, 118.95, 116.27, 109.23, 55.55, 44.26, 40.81, 40.53, 40.25, 39.97, 39.69, 39.41, 39.13, 34.70, 32.05, 31.39, 29.42, 23.84, 22.69, 22.41 and 14.05 ppm; FT-IR (KBr) 3429, 2954, 2927, 2865, 2212, 1613, 1582, 1489, 1477, 1454, 1363, 1324, 1295, 1263, 1145, 877, 840, 792, 762, 742 and 614 cm^{-1}. HRMS-ESI calcd for $C_{53}H_{60}N_2O_2S$: *m/z* 788.4375 found 788.7350 [M^{+}].

(*E*)-2-Cyano-3-(5-(5-(7-(3,6,-di-*tert*-butyl-*9H*-carbazol-9-yl)-9,9-dihexyl-*9H*-fluoren-2-yl)thiophene-2-yl)thiophene-2-yl)acrylic acid (CA2T)

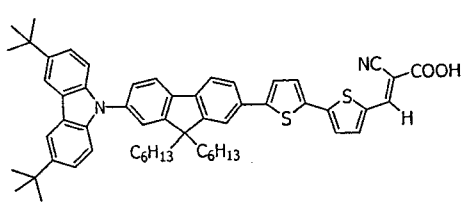

A mixture of 5-(5-(7-(3,6-di *tert*-butyl-*9H*-carbazol-9-yl)-9,9-dihexyl-fluorene-2-yl)thiophene-2-yl)thiophene-2-carbaldehyde (0.150 g, 0.207 mmol) and cyanoacetic acid (0.088 g, 1.03 mmol) was vacuum-dried and added THF : acetonitrile (20 ml, 1:1 v/v) and piperidine (0.017 ml, 1.03 mmol). The solution was refluxed for 6 h. After cooling the solution, the organic layer was removed in vacuum. The pure product was obtained by column chromatography over silica gel eluting with gradient solution system started with 10% MeOH : dichloromethane afforded **CA2T** as yellow-orange solid (0.285 g, 87%); m.p. 258-259 °C; ^{1}H-NMR (300 MHz, $CDCl_3$, DMSO-d) δ 9.17 1H, s), 8.85 (2H, s), 8.46 (1H, d, J = 6.9 Hz), 8.30 (2H, s), 8.23-8.03 (8H, m), 7.94 (2H, s), 7.86 (1H, s), 2.74 (4H, s), 2.15 (18H, s), 1.79 (12H, s), and (10H, t, J = 6.5 Hz) ppm; ^{13}C-NMR (75 MHz, $CDCl_3$, DMSO-d) δ 153.42, 152.64, 146.46, 143.59, 141.17, 139.91, 139.87, 137.82, 136.15, 136.04, 133.34, 124.35, 124.07, 117.01, 109.92, 56.25, 41.71, 41.44, 41.16, 40.88, 40.60, 40.32, 40.05, 35.44, 32.76, 32.21, 30.32, 24.69, 23.26 and 14.79 ppm; FT-IR (KBr) 3436, 2955, 2927, 2856, 2212, 1610, 1490, 1476, 1365, 1295, 1263 and 809 cm^{-1}. HRMS-ESI calcd for $C_{57}H_{62}N_2O_2S_2$: *m/z* 870.4252 found 871.0330 [M^{+}].

(*E*)-2-Cyano-3-(5-(5-(5-(7-(3,6,-di-*tert*-butyl-*9H*-carbazol-9-yl)-9,9-dihexyl-*9H*-fluoren-2-yl)thiophene-2-yl)thiophene-2-yl)thiophene-2-yl)acrylic acid (CA3T)

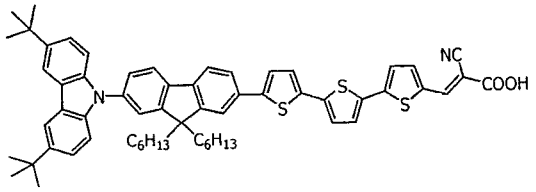

A mixture of 5-(5-(5-(7-(3,6-di *tert*-butyl-*9H*-carbazol-9-yl)-9,9-dihexyl-fluorene-2-yl)thiophene-2-yl)thiophene-2-yl)thiophene-2-carbaldehyde (0.294 g, 0.332 mmol) and cyanoacetic acid (0.145 g, 1.70 mmol) was vacuum-dried and added THF : acetonitrile (20 ml, 1:1 v/v) and piperidine (0.140 ml, 1.70 mmol). The solution was refluxed for 6 h. After cooling the solution, the organic layer was removed in vacuum. The pure product was obtain by silica gel chromatography to afforded **CA3T** as orange solid (0.234 g, 74%); m.p. 257-258 °C; ^{1}H-NMR (300 MHz, $CDCl_3$, DMSO-d) δ 8.02 (1H, s), 7.66 (1H, d, J = 7.8 Hz), 7.39-7.53 (6H, m), 7.23 (4H, d, J = 9.6 Hz), 6.97 (1H, d, J = 8.1 Hz), 1.94 (4H, m), 1.22 (18H, m), 0.97 (12H, m) and 0.64 (10H, m) ppm; ^{13}C-NMR (75 MHz, $CDCl_3$, DMSO-d) δ 152.58, 144.15, 144.03, 140.04,

139.04, 138.16, 137.01, 135.67, 135.29, 134.64, 132.72, 125.16, 124.86, 124.35, 123.81, 123.48, 123.26, 121.22, 120.74, 120.43, 119.47, 116.16, 109.03, 55.41, 40.51, 40.23, 39.95, 39.67, 39.39, 39.12, 34.56, 31.87, 31.59, 39.67, 39.39, 34.56, 31.87, 31.59, 30.84, 29.49, 23.90, 22.41 and 13.92 ppm; FT-IR (KBr) 3429, 2954, 2927, 2856, 2212, 1613, 1582, 1489, 1477, 1454, 1363, 1324, 1295, 1263, 1145, 877, 840, 792, 762, 742 and 614 cm^{-1}. HRMS-ESI calcd for $C_{61}H_{64}N_2O_2S_3$: *m/z* 952.4129 found 953.8260 [MH^+].

(*E*)-2-Cyano-3-(5-(5-(5-(5-(7-(3,6,-di-*tert*-butyl-*9H*-carbazol-9-yl)-9,9-dihexyl-*9H*-fluoren-2-yl)thiophene-2-yl)thiophene-2-yl)thiophene-2-yl)thiophene-2-yl)acrylic acid (CA4T)

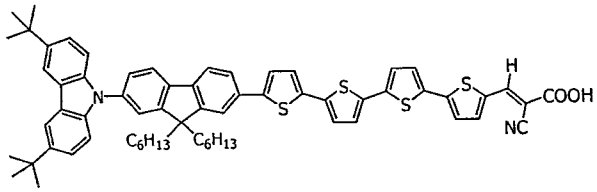

A mixture of 5-(5-(5-(5-(7-(3,6-di *tert*-butyl-*9H*-carbazol-9-yl)-9,9-dihexyl-fluorene-2-yl)thiophene-2-yl)thiophene-2-yl)thiophene-2-yl)thiophene-2-carbaldehyde (0.167 g, 0.172 mmol) was vacuum-dried and added THF : acetonitrile (20 ml, 1:1 v/v) and piperidine (0.062 ml, 0.863 mmol). The solution was refluxed for 6 h. After cooling the solution, the organic layer was removed in vacuum. The pure product was obtain by silica gel chromatography to afforded **CA4T** as orange solid (0.115 g, 65%); m.p. > 270 °C; ^{1}H-NMR (300 MHz, $CDCl_3$, DMSO-d) δ 8.03 (1H, s), 7.66 (1H, d, J = 7.8 Hz), 7.39-7.53 (6H, m), 7.23 (4H, d, J = 9.6 Hz), 6.97 (1H, d, J = 8.1 Hz), 2.01 (4H, m), 1.22 (18H, m), 0.97 (12H, m) and 0.64 (10H, m); ^{13}C-NMR (75 MHz, $CDCl_3$, DMSO-d) δ 152.49, 151.74, 143.67, 142.71, 142.63, 140.04, 139.09, 138.93, 138.00, 136.84, 135.72, 135.30, 132.71, 131.86, 125.18, 124.64, 124.37, 124.20, 123.77, 123.47, 123.17, 121.13, 120.73, 119.61, 116.12, 109.08, 60.17, 55.33, 40.79, 40.51, 40.23, 40.10, 39.67, 39.39, 39.12, 34.59, 34.44, 31.89, 31.81, 31.34, 31.23, 29.34, 26.47, 23.75, 22.75, 22.31, 13.90 and 13.84 ppm; FT-IR (KBr) 3414, 2955, 2362, 1638, 1617, 1512, 1477, 1443, 1366, 1295, 1263, 793 and 614 cm^{-1}. HRMS-ESI calcd for $C_{65}H_{66}N_2O_2S_4$: *m/z* 1035.4917 found 1036.2740 [MH^+].

Chapter 5:

2-((5-(7-(3,6,-Di-*tert*-butyl-*9H*-carbazol-9-yl)-9,9-dihexyl-*9H*-fluoren-2-yl) thiophene-2-yl)methylene)-2H-indene-1,3-dion (InT)

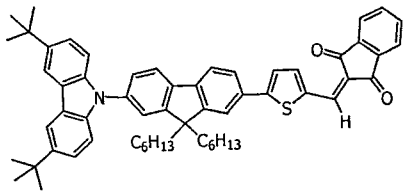

A mixture of 5-(7-(3,6-di *tert*-butyl-*9H*-carbazol-9-yl)-9,9-dihexyl-fluorene-2-yl)thiophene-2-carbaldehyde (0.265 g, 0.367 mmol) and 1,3-indandion (0.268 g, 1.83 mmol) was vacuum-dried and added piperidine (0.182 ml, 1.835 mmol), and acetic acid (0.5 ml, 7.34 mmol) in the solvent mixture of THF:acetonitrile (20 ml, 1:1 v/v). After stirring for 6 h at room temperature, water (50 ml) was added and extracted with dichloromethane (50 ml x 3). The combined organic phase were washed with water (50 ml) and brine (50 ml) solution, dried over anhydrous Na_2SO_4, filtered, and the solvents were removed to dryness. Purification by column chromatography over silica gel eluting with a mixture of Dichloromethane and hexane (2:3) followed by recrystallization with hexane afforded **InT** as red-violet solid (0.215 g, 69%); m.p. 159-160 °C; ^{1}H-NMR (300 MHz, $CDCl_3$) δ 8.18 (2H, s), 8.01-7.97 (4H, m), 7.92 (1H, d, J = 8.7 Hz), 7.86-7.78 (5H, m), 7.58 (3H, d, J = 3.9 Hz), 7.51-7.40 (4H, dd, J = 8.7 Hz), 2.01-2.05 (4H, m), 1.49 (18H, m), 1.12 (12H, m) and 0.81-0.77 (10H, m) ppm; ^{13}C-NMR (75 MHz, $CDCl_3$) δ 190.42, 189.92, 158.16, 153.00, 152.17, 143.83, 142.95, 142.22, 142.07, 140.56, 139.25, 138.89, 137.64, 136.50, 135.05, 134.86, 132.21, 125.95, 125.49, 124.77, 123.77, 123.61, 123.46, 123.04, 122.82, 121.39, 121.21, 120.79, 120.46, 116.35, 109.22, 55.72, 40.31, 34.76, 32.03, 31.57, 29.63, 23.94, 22.59 and 14.03 ppm; FT-IR (KBr) 2953, 2927, 2857, 1723, 1682, 1598, 1581, 1490, 1475, 1429, 1369, 1347, 1325, 1294, 1262, 1237, 1155, 1094, 993, 878, 734, 661 and 614 cm^{-1}. HRMS-ESI calcd for $C_{59}H_{63}NO_2S$: *m/z* 849.4579 found 850.1800 [MH^+].

2-((5-(5-(7-(3,6,-Di-*tert*-butyl-*9H*-carbazol-9-yl)-9,9-dihexyl-*9H*-fluoren-2-yl) thiophene-2-yl)thiophene-2-yl)methylene)-2H-indene-1,3-dion (In2T)

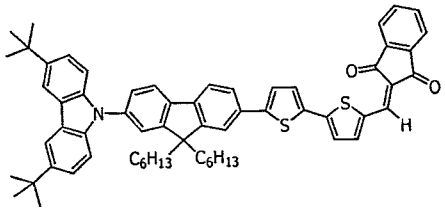

A mixture of 5-(5-(7-(3,6-di *tert*-butyl-*9H*-carbazol-9-yl)-9,9-dihexyl-fluorene-2-yl)thiophene-2-yl)thiophene-2-carbaldehyde(0.250 g, 0.310 mmol) and 1,3-indandion (0.227 g, 1.55 mmol) was vacuum-dried and added piperidine (0.132 ml, 1.55 mmol), and acetic acid (0.1 ml, 1.55 mmol) in the solvent mixture of THF : acetonitrile (20 ml, 1:1 v/v). After stirring for 6 h at room temperature, water (50 ml) was added and extracted with dichloromethane (50 ml x 3). The combined organic phase were washed with water (50 ml) and brine (50 ml) solution, dried over anhydrous Na_2SO_4, filtered, and the solvents were removed to dryness. Purification by column chromatography over silica gel eluting with a mixture of dichloromethane and hexane (2:3) followed by recrystallization with hexane afforded **In2T** as violet solid (0.172 g, 59%); m.p. 168-169 °C; ^{1}H-NMR (300 MHz, $CDCl_3$) δ 8.18 (2H, s), 8.00-7.95 (3H, m), 7.91-7.88 (2H, t, J = 4.3 Hz), 7.80-7.77 (3H, d, J = 3.9 Hz), 7.69-7.63 (2H, t, J = 8.8 Hz), 7.57-7.48 (5H, m), 7.43-7.35 (4H, m), 2.07-2.02 (4H, m), 1.49 (18H, m), 1.13 (12H, s) and 0.82-0.78 (10H, t, J = 6.6 Hz) ppm; ^{13}C-NMR (75 MHz, $CDCl_3$) δ 190.35, 189.83, 152.76, 152.04, 150.42, 147.33, 143.74, 142.89, 142.04, 140.90, 140.55, 139.30, 139.14, 137.27, 135.99, 135.86, 135.28, 135.00, 134.81, 132.46, 127.54, 125.46, 125.02, 124.56, 124.37, 123.59, 123.42, 122.99, 122.81, 121.41, 120.93, 120.37, 120.09, 116.34, 109.22, 55.56, 40.35, 34.76, 32.03, 31.90, 31.77, 31.55, 29.66, 23.93, 22.59 and14.04 ppm; FT-IR (KBr) 2953, 2926, 2856, 1722, 1681, 1597, 1579, 1540, 1489, 1475, 1432, 1379, 1347, 1325, 1295, 1262, 1203, 1154, 1094, 1018, 992, 980, 877, 808, 734, 649 and 614 cm^{-1}.

2-((5-(5-(5-(7-(3,6,-Di-*tert*-butyl-*9H*-carbazol-9-yl)-9,9-dihexyl-*9H*-fluoren-2-yl) thio-phene-2-yl)thiophene-2-yl)thiophene-2-yl)methylene)-2H-indene-1,3-dion (In3T)

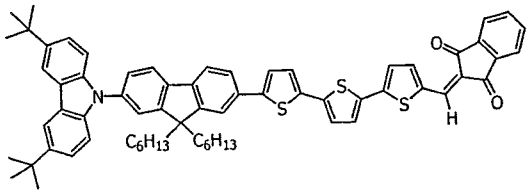

A mixture of 5-(5-(5-(7-(3,6-di *tert*-butyl-*9H*-carbazol-9-yl)-9,9-dihexyl-fluorene-2-yl)thiophene-2-yl)thiophene-2-yl)thiophene-2-carbaldehyde (0.240 g, 0.271 mmol) and 1,3-indandion (0.197 g, 1.34 mmol) was vacuum-dried and added piperidine (0.23 ml, 2.80 mmol), and acetic acid (0.18 ml, 2.80 mmol) in the solvent mixture of THF : acetonitrile (20 ml, 1:1 v/v). After stirring for 6 h at room temperature, water (50 ml) was added and extracted with dichloromethane (50 ml x 3). The combined organic phase were washed with water (50 ml) and brine (50 ml) solution, dried over anhydrous Na_2SO_4, filtered, and the solvents were removed to dryness. Purification by column chromatography over silica gel eluting with a mixture of dichloromethane and hexane (2:3) followed by recrystallization with hexane afforded **In3T** as violet solid (0.172 g, 59%); m.p. 155-156 °C; ^{1}H-NMR (300 MHz, $CDCl_3$) δ 8.18 (2H, s), 7.95-7.86 (5H, m), 7.76 (3H, d, J = 7.5 Hz), 7.65-7.60 (2H, m), 7.56-7.48 (4H, m), 7.42-7.39 (3H, m), 7.35 (1H, m), 7.42-7.23 (3H, m), 7.20 (1H, d, J = 3.9 Hz), 2.07-2.02 (4H, m), 1.49 (18H, m), 1.13 (12H, s) and 0.82-0.78 (10H, t, J = 6.6 Hz) ppm; ^{13}C-NMR (75 MHz, $CDCl_3$) δ 190.31, 189.74, 152.69, 151.96, 149.92, 145.03, 143.63, 142.87, 142.02, 140.51, 140.48, 139.68, 139.32, 139.25, 135.70, 139.25, 137.14, 136.11, 135.70, 135.52, 134.98, 134.86, 134.78, 132.73, 125.53, 125.44, 124.89, 123.94, 123.58, 123.41, 122.97, 122.80, 121.40, 120.84, 120.32, 119.91, 116.33, 109.23, 55.52, 40.36, 34.76, 32.04, 31.56, 29.67, 23.93, 22.60 and 14.05 ppm; FT-IR (KBr) 2952, 2925, 2855, 1720, 1678, 1597, 1578, 1524, 1489, 1475, 1430, 1366, 1346, 1324, 1294, 1261, 1234, 1202, 1154, 1017, 991, 979, 940, 876, 839, 808, 791, 732, 652, 663 and 614 cm^{-1}. HRMS-ESI calcd for $C_{67}H_{67}NO_2S_3$: *m/z* 1013.4333 found 1013.7360 [M^+].

2-((5-(5-(5-(5-(7-(3,6,-Di-*tert*-butyl-9*H*-carbazol-9-yl)-9,9-dihexyl-9*H*-fluoren-2-yl) thiophene-2-yl)thiophene-2-yl)thiophene-2-yl)thiophene-2-yl)methylene)-2H-indene-1,3-dion (In4T)

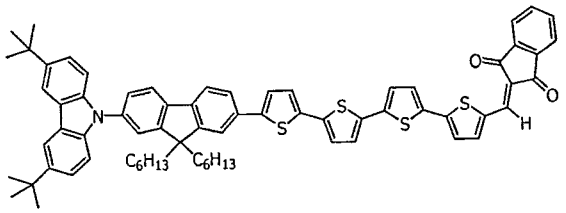

A mixture of 5-(5-(5-(5-(7-(3,6-di *tert*-butyl-9*H*-carbazol-9-yl)-9,9-dihexyl-fluorene-2-yl)thiophene-2-yl)thiophene-2-yl)thiophene-2-yl)thiophene-2-carbaldehyde (0.240g, 0.248 mmol) and 1,3-indandion (0.18 g, 1.23 mmol) was vacuum-dried and added piperidine (0.21 ml, 2.48 mmol), and acetic acid (0.15 ml, 2.48 mmol) in the solvent mixture of THF : acetonitrile (20 ml, 1:1 v/v). After stirring for 6 h at room temperature, water (50 ml) was added and extracted with dichloromethane (50 ml x 3). The combined organic phase were washed with water (50 ml) and brine (50 ml) solution, dried over anhydrous Na_2SO_4, filtered, and the solvents were removed to dryness. Purification by column chromatography over silica gel eluting with a mixture of dichloromethane and hexane (2:3) followed by recrystallization with hexane afforded **In4T** as violet solid (0.215 g, 69%); m.p. 169-170 °C; ^{1}H-NMR (300 MHz, $CDCl_3$, DMSO-d) δ 8.17 (2H, s), 7.98-7.84 (5H, m), 7.76-7.74 (3H, m), 7.64-7.59 (2H, m), 7.55-7.47 (4H, m), 7.39 (3H, d, J = 8.7 Hz), 7.32 (1H, m), 7.19-7.13 (3H, m), 2.07 (4H, m), 1.51 (18H, m), 1.13 (12H, m) and 0.82-0.78 (10H, t, J = 6.6 Hz) ppm; ^{13}C-NMR (75 MHz, $CDCl_3$) δ 190.26, 189.71, 152.66, 151..93, 149.78, 144.38, 143.57, 142.85, 142.01, 140.50, 140.32, 139.32, 139.29, 139.26, 137.47, 137.08, 136.16, 135.97, 135.82, 135.63, 135.14, 134.96, 135.14, 135.00, 134.96, 134.76, 132.85, 127.32, 125.43, 125.29, 125.00, 124.78, 124.68, 124.35, 123.82, 123.67, 123.58, 123.40, 122.96, 122.78, 121.40, 120.80, 120.29, 119.85, 116.32, 109.23, 55.51, 40.36, 34.76, 32.04, 31.91, 31.78, 31.55, 29.67, 23.93, 22.60, 22.50, 19.63 and 14.05 ppm; FT-IR (KBr) 2952, 2925, 2855, 1720, 1678, 1597, 1578, 1524, 1489, 1475, 1430, 1366, 1346, 1324, 1294, 1261, 1234, 1202, 1154, 1017, 991, 979, 940, 876, 839, 808, 791, 732, 652, 663 and 614 cm^{-1}. HRMS-ESI calcd for $C_{71}H_{69}NO_2S_4$: *m/z* 1095.4211 found 1096.1950 [MH^+].

2-((5-(7-(3,6,-Di-*tert*-butyl-9*H*-carbazol-9-yl)-9,9-dihexyl-9*H*-fluoren-2-yl) thiophene-2-yl)methylene)malononitrile (DMT)

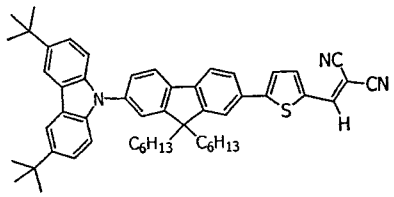

A mixture of 5-(7-(3,6-di- *tert*-butyl-9*H*-carbazol-9-yl)-9,9-dihexyl-fluorene-2-yl)thiophene-2-carbaldehyde (0.225 g, 0.311 mmol) and malononitrile (0.103 g, 1.55 mmol) was vacuum-dried and added piperidine (0.30 ml, 3.11 mmol), and acetic acid (0.252 ml, 3.11 mmol) in the solvent mixture of THF : acetonitrile (20 ml, 1:1 v/v). After stirring for 6 h at room temperature, water (50 ml) was added and extracted with dichloromethane (50 ml x 3). The combined organic phase were washed with water (50 ml) and brine (50 ml) solution, dried over anhydrous Na_2SO_4, filtered, and the solvents were removed to dryness. Purification by column chromatography over silica gel eluting with a mixture of dichloromethane and hexane (2:3) followed by recrystallization with hexane afforded **DMT** as yellow solid (0.038 g, 16%); m.p. 210-211 °C; ^{1}H-NMR (300 MHz, $CDCl_3$) δ 8.07 (2H, s), 7.84-7.78 (1H, d, J = 8.7 Hz), 7.71 (1H, d, J = 7.8 Hz), 7.60-7.54 (3H, m), 7.51 (2H, s), 7.41 (3H, d, J = 8.7 Hz), 7.33 (3H, d, J = 8.7 Hz), 1.97-1.95 (4H, m), 1.41 (18H, s), 1.05 (12H, s), 0.73-0.69 (10H, t, J = 6.0 Hz) ; ^{13}C-NMR (75 MHz, $CDCl_3$) δ 152.70, 152.01, 150.30, 149.38, 148.23, 142.88, 142.81, 141.12, 140.56, 139.23, 139.19, 138.96, 137.29, 133.86, 133.32, 132.04, 133.86, 133.32, 132.04, 128.63, 128.36, 125.38, 125.09, 124.77, 124.46, 124.26, 123.56, 123.35, 121.28, 120.99, 120.79, 120.40, 120.26, 120.05, 119.83, 116.36, 113.58, 55.51, 55.44, 40.63, 40.35, 40.22, 40.07, 39.79, 39.51, 34.69, 31.98, 31.85, 31.68, 31.45, 29.55, 23.84, 22.49, 13.98 ppm; FT-IR (KBr) 3041, 2954, 2926, 2856, 2222, 1609, 1571, 1490, 1475, 1428, 13363, 1324, 1294, 1261, 1233, 1201, 1139, 1105, 1067, 1033, 1006, 921, 877, 840, 808, 741, 666, 653 and 609 cm^{-1}.

2-((5-(5-(7-(3,6,-Di-*tert*-butyl-*9H*-carbazol-9-yl)-9,9-dihexyl-*9H*-fluoren-2-yl) thiophene-2-yl)thiophene-2-yl)methylene)malononitrile (DM2T)

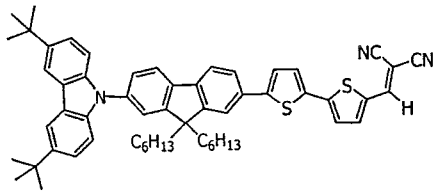

A mixture of 5-(5-(7-(3,6-di *tert*-butyl-*9H*-carbazol-9-yl)-9,9-dihexyl-fluorene-2-yl)thiophene-2-yl)thiophene-2-carbaldehyde (0.290 g, 0.360 mmol) and malononitrile (0.12 g, 1.81 mmol) was vacuum-dried and added piperidine (0.177 ml, 1.81 mmol), and acetic acid (0.145 ml, 1.81 mmol) in the solvent mixture of THF : acetonitrile (20 ml, 1:1 v/v). After stirring for 6 h at room temperature, water (50 ml) was added and extracted with dichloromethane (50 ml x 3). The combined organic phase were washed with water (50 ml) and brine (50 ml) solution, dried over anhydrous Na_2SO_4, filtered, and the solvents were removed to dryness. Purification by column chromatography over silica gel eluting with a mixture of dichloromethane and hexane (2:3) followed by recrystallization with hexane afforded **DM2T** as yellow-orange solid (0.055 g, 18%); m.p. 150-151 °C; ^{1}H-NMR (300 MHz, $CDCl_3$) δ 8.18 (2H, s), 7.90 (1H, d, J = 8.7 Hz), 7.79 (2H, d, J = 8.1 Hz), 7.68-7.65 (2H, m), 7.61 (1H, s), 7.57-7.55 (2H, m), 7.50-7.47 (3H, dd, J = 7.5 Hz), 7.42-7.38 (3H, m), 7.33 (1H, d, J = 4.2 Hz), 2.07-2.02 (4H, m), 1.48 (18H, m), 1.12 (12H, m) and 0.82-0.77 (10H, t, J = 6.8 Hz) ppm; ^{13}C-NMR (75 MHz, $CDCl_3$) δ 152.76, 152.11, 150.03, 148.40, 142.93, 141.25, 140.23, 139.27, 138.99, 137.42, 133.89, 133.33, 132.07, 128.39, 125.48, 125,14, 124.46, 124.24, 123.59, 123.44, 121.40, 121.01, 120.42, 120.15, 116.35, 114.32, 113.53, 109.19, 55.58, 40.32, 34.76, 32.02, 31.89, 31.53, 29.63, 23.91, 22.57 and 14.01 ppm; FT-IR (KBr) 2953, 2927, 2856, 2222, 1610, 1572, 1538, 1489, 1475, 1432, 1363, 1324, 1295, 1262, 1231, 1057, 878, 809 and 614 cm^{-1}. HRMS-ESI calcd for $C_{57}H_{61}N_3S_2$: *m/z* 851.4306 found 852.5640 [MH$^+$].

2-((5-(5-(5-(7-(3,6,-Di-*tert*-butyl-*9H*-carbazol-9-yl)-9,9-dihexyl-*9H*-fluoren-2-yl)thio-phene-2-yl)thiophene-2-yl)thiophene-2-yl)methylene)malononitrile (DM3T)

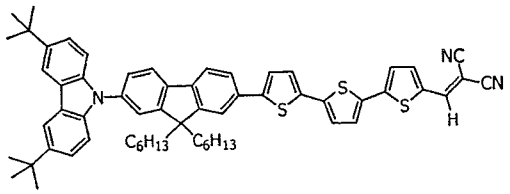

A mixture of 5-(5-(5-(7-(3,6-di *tert*-butyl-*9H*-carbazol-9-yl)-9,9-dihexyl-fluorene-2-yl)thiophene-2-yl)thiophene-2-yl)thiophene-2-carbaldehyde (0.174g, 0.196mmol) and malononitrile (0.065g, 0.984 mmol) was vacuum-dried and added piperidine (0.197 ml, 1.96 mmol), and acetic acid (0.161 ml, 1.96 mmol) in the solvent mixture of THF : acetonitrile (20 ml, 1:1 v/v). After stirring for 6 h at room temperature, water (50 ml) was added and extracted with dichloromethane (50 ml x 3). The combined organic phase were washed with water (50 ml) and brine (50 ml) solution, dried over anhydrous Na_2SO_4, filtered, and the solvents were removed to dryness. Purification by column chromatography over silica gel eluting with a mixture of dichloromethane and hexane (2:3) followed by recrystallization with hexane afforded **DM3T** as orange solid (0.025 g, 14%); m.p. 165-166 °C; ^{1}H-NMR (300 MHz, $CDCl_3$) δ 8.19 (2H, s), 7.91-7.87 (2H, m), 7.80 (2H, m), 7.66-7.61 (4H, m), 7.57-7.49 (5H, m), 7.43 (2H, d, J = 8.7 Hz), 7.38-7.36 (2H, d, J = 3.8 Hz), 7.28-7.25 (3H, t, J = 4.4 Hz), 7.21 (1H, d, J = 3.9 Hz), 2.07-2.02 (4H, m), 1.48 (18H, m), 1.12 (12H, m) and 0.82-0.77 (10H, t, J=6.8 Hz) ppm; ^{13}C-NMR (75 MHz, $CDCl_3$) δ 152.67, 151.98, 151.06, 149.97, 149.05, 145.55, 142.88, 140.73, 140.64, 140.24, 139.27, 139.16, 138.12, 137.18, 136.88, 135.02, 133.40, 132.56, 129.03, 128.27, 125.93, 125.44, 124.92, 124.75, 124.32, 124.00, 123.59, 123.40, 121.37, 120.89, 120.35, 119.94, 116.35, 114.33, 113.53, 109.21, 55.52, 40.35, 34.77, 32.04, 31.91, 31.78, 31.55, 30.49, 29.72, 29.66, 29.38, 23.91, 22.60, 22.50, 14.14 and 14.07 ppm; FT-IR (KBr) 2953, 2927, 2856, 2222, 1610, 1572, 1538, 1489, 1475, 1432, 1363, 1324, 1295, 1262, 1231, 1057, 878, 809 and 614 cm^{-1}. HRMS-ESI calcd for $C_{61}H_{63}N_3S_3$: *m/z* 933.4184 found 933.9030 [M$^+$].

2-((5-(5-(5-(5-(7-(3,6,-Di-*tert*-butyl-*9H*-carbazol-9-yl)-9,9-dihexyl-*9H*-fluoren-2-yl)thio-phene-2-yl)thiophene-2-yl)thiophene-2-yl)thiophene-2-yl)methylene)malononitrile (DM4T)

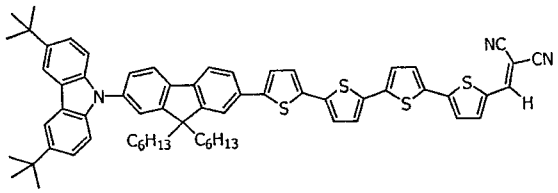

A mixture of 5-(5-(5-(5-(7-(3,6-di *tert*-butyl-*9H*-carbazol-9-yl)-9,9-dihexyl-fluorene-2-yl)thiophene-2-yl)thiophene-2-yl)thiophene-2-yl)thiophene-2-carbaldehyde (0.250g, 0.258 mmol) and malononitrile (0.085 g, 1.29 mmol) was vacuum-dried and added piperidine (0.197 ml, 1.29 mmol), and acetic acid (0.103 ml, 1.29mmol) in the solvent mixture of THF : acetonitrile (20 ml, 1:1 v/v). After stirring for 6 h at room temperature, water (50 ml) was added and extracted with dichloromethane (50 ml x 3). The combined organic phase were washed with water (50 ml) and brine (50 ml) solution, dried over anhydrous Na_2SO_4, filtered, and the solvents were removed to dryness. Purification by column chromatography over silica gel eluting with a mixture of dichloromethane and hexane (2:3) followed by recrystallization with hexane afforded **DM4T** as orange solid (0.025 g, 14%); m.p. 219-220 °C; ^{1}H-NMR (300 MHz, $CDCl_3$) δ 8.14 (2H, s), 7.85 (1H, d, J = 8.7 Hz), (2H, d, J = 8.1 Hz), 7.61-7.56 (3H, m), 7.50-7.44 (4H, m), 7.36 (2H, d, J = 8.7 Hz), 7.32-7.30 (2H, t, J = 1.8 Hz), 7.22-7.18 (2H, q, J = 3.6 Hz), 7.12 (3H, d, J = 4.2 Hz), 2.03-1.98 (4H, m), 1.46 (18H, m), 1.09 (12H, m) and 0.78-0.74 (10H, t, J = 6.6 Hz) ppm; ^{13}C-NMR (75 MHz, $CDCl_3$) δ 152.67, 152.09, 151.96, 149.84, 148.87, 144.64, 142.89, 140.42, 140.29, 140.10, 139.32, 139.25, 137.99, 137.13, 135.62, 134.63, 133.55, 133.43, 132.77, 128.20, 125.70, 125.43, 124.85, 124.81, 124.37, 123.86, 123.60, 123.43, 121.39, 120.83, 119.88, 116.35, 114.28, 113.50, 109.24, 55.52, 40.36, 34.77, 32.05, 31.92, 31.78, 31.56, 29.68, 23.94, 22.61,22.61, 22.50 and 14.06 ppm; FT-IR (KBr) 2953, 2927, 2856, 2222, 1610, 1572, 1538, 1489, 1475, 1432, 1363, 1324, 1295, 1262, 1231, 1057, 878, 809 and 614 cm^{-1}. HRMS-ESI calcd for $C_{65}H_{65}N_3S_4$: *m/z* 1015.4061 found 1016.6160 [MH^+].

(*E*)-Methyl-2-cyano-3-(5-(7-(3,6,-di-*tert*-butyl-*9H*-carbazol-9-yl)-9,9-dihexyl-*9H*-fluoren-2-yl)thiophene-2-yl)acrylate (MCT)

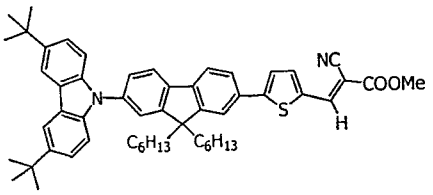

A mixture of 5-(7-(3,6-di- *tert*-butyl-*9H*-carbazol-9-yl)-9,9-dihexyl-fluorene-2-yl)thiophene-2-carbaldehyde (0.200g, 0.277 mmol) and methyl-2-cyanoacetate (0.137 g, 1.38 mmol) was vacuum-dried and added piperidine (0.30 ml, 2.76 mmol), and acetic acid (0.252 ml, 2.76 mmol) in the solvent mixture of THF : acetonitrile (20 ml, 1:1 v/v). After stirring for 6 h at room temperature, water (50 ml) was added and extracted with dichloromethane (50 ml x 3). The combined organic phase were washed with water (50 ml) and brine (50 ml) solution, dried over anhydrous Na_2SO_4, filtered, and the solvents were removed to dryness. Purification by column chromatography over silica gel eluting with a mixture of dichloromethane and hexane (2:3) followed by recrystallization with hexane afforded as yellow-orange solid **MCT** (0.188 g, 85%); m.p. 139-140 °C; ^{1}H-NMR (300 MHz, $CDCl_3$) δ 8.28 (1H, s), 8.10 (1H, s), 7.86-7.83 (1H, m), 7.73-7.67 (3H, m), 7.61 (1H, m), 7.49-7.46 (3H, m), 7.43-7.31 (4H, dd, J = 8.7 Hz, J = 8.4 Hz), 1.99 (4H, m), 1.46 (18H, m), 1.09 (12H, m) and 0.78-0.74 (10H, t, J = 6.6 Hz) ppm; ^{13}C-NMR (75 MHz, $CDCl_3$) δ 163.47, 155.55, 152.95, 152.89, 152.13, 146.82, 143.13, 142.92, 142.23, 139.67, 139.14, 138.71, 137.60, 137.32, 137.60, 137.32, 134.54, 131.62, 131.53, 130.88, 128.73, 125.88, 125.69, 125.65, 125.40, 124.35, 123.84, 123.57, 123.37, 123.10, 121.50, 121.27, 120.59, 120.48, 119.78, 116.42, 116.27, 116.09, 68.08, 55.63, 53.14, 40.15, 38.67, 34.69, 31.97, 31.68, 31.68, 31.45, 30.85, 30.30, 29.61, 29.50, 28.86, 23.94, 23.84, 23.69, 22.90, 22.60, 22.48 and 13.96 ppm; FT-IR (KBr) 2953, 2926,, 2855, 2215, 1724, 1585, 1491, 1475, 1445, 1428, 1389, 1363, 1325, 1265, 1215, 1119, 1090, 1064, 1019, 879, 808, 746, 670, 635 and 615 cm^{-1}. HRMS-ESI calcd for $C_{54}H_{62}N_2O_2S$: *m/z* 802.4532 found 802.5360 [M^+].

(*E*)-Methyl-2-cyano-3-(5-(5-(7-(3,6,-di-*tert*-butyl-9*H*-carbazol-9-yl)-9,9-dihexyl-9*H*-fluoren-2-yl)thiophene-2-yl0thiophene-2-yl)acrylate (MC2T)

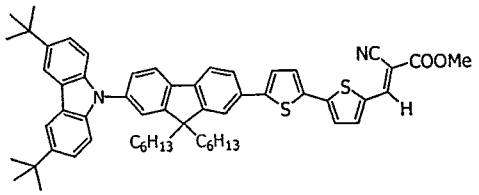

A mixture of 5-(5-(7-(3,6-di *tert*-butyl-9*H*-carbazol-9-yl)-9,9-dihexyl-fluorene-2-yl)thiophene-2-yl)thiophene-2-carbaldehyde (0.250g, 0.311 mmol) and methyl-2-cyanoacetate (0.153 g, 1.55 mmol) was vacuum-dried and added piperidine (0.153 ml, 1.55 mmol), and acetic acid (0.251 ml, 1.55 mmol) in the solvent mixture of THF : acetonitrile (20 ml ,1:1 v/v). After stirring for 6 h at room temperature, water (50 ml) was added and extracted with dichloromethane (50 ml x 3). The combined organic phase were washed with water (50 ml) and brine (50 ml) solution, dried over anhydrous Na_2SO_4, filtered, and the solvents were removed to dryness. Purification by column chromatography over silica gel eluting with a mixture of dichloromethane and hexane (2:3) followed by recrystallization with hexane afforded **MC2T** as yellow-orange solid (0.215 g, 78%); m.p. 188-189 °C; ^{1}H-NMR (300 MHz, $CDCl_3$) δ 8.30 (1H, s), 8.18 (2H, s), 7.88 (1H, d, J = 8.5 Hz), 7.88 (1H, d, J = 8.5 Hz), 7.77 (1H, d, J = 7.9 Hz), 7.74-7.45 (8H, m), 7.43-7.39 (4H, m), 7.31 (1H, d, J = 4 Hz), 3.94 (3H, s), 2.07-2.01 (4H, m), 1.49 (18H, m), 1.12 (12H, m) and 0.81-0.77 (10H, m) ppm; ^{13}C-NMR (75 MHz, $CDCl_3$) δ 163.54, 152.75, 152.06, 147.86, 147.40, 146.43, 142.90, 140.98, 139.50, 139.30, 139.10, 137.31, 134.51, 134.08, 132.31, 127.63, 125.46, 125.04, 124.30, 124.11, 123.58, 123.42, 121.41, 120.94, 120.37, 121.41, 116.34, 109.21, 97.04, 55.56, 53.19, 40.33, 34.76, 32.03, 31.54, 29.64, 23.91, 22.58 and 14.02 ppm; FT-IR (KBr) 2952, 2927, 2856, 2222, 1721, 1583, 1541, 1489, 1475, 1430, 1364, 1324, 1294, 1261, 1222, 1206, 1054, 878, 796, 758 and 614 cm^{-1}. HRMS-ESI calcd for $C_{58}H_{64}N_2O_2S_2$: *m/z* 884.4409 found 885.4250 [MH^+].

(*E*)-Methyl-2-cyano-3-(5-(5-(5-(7-(3,6,-di-*tert*-butyl-*9H*-carbazol-9-yl)-9,9-dihexyl-*9H*-fluoren-2-yl)thiophene-2-yl)thiophene-2-yl0thiophene-2-yl)acrylate (MC3T)

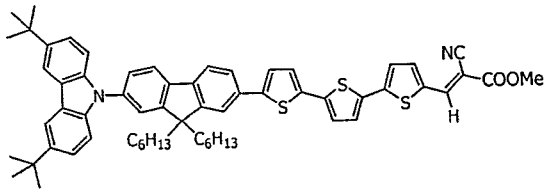

A mixture of 5-(5-(5-(7-(3,6-di *tert*-butyl-*9H*-carbazol-9-yl)-9,9-dihexyl-fluorene-2-yl)thiophene-2-yl)thiophene-2-yl)thiophene-2-carbaldehyde (0.290g, 0.327mmol) and methyl-2-cyanoacetate (0.162 g, 1.63 mmol) was vacuum-dried and added piperidine (0.323 ml, 3.27 mmol), and acetic acid (0.264 ml, 3.27 mmol) in the solvent mixture of THF : acetonitrile (20 ml ,1:1 v/v). After stirring for 6 h at room temperature, water (50 ml) was added and extracted with dichloromethane (50 ml x 3). The combined organic phase were washed with water (50 ml) and brine (50 ml) solution, dried over anhydrous Na_2SO_4, filtered, and the solvents were removed to dryness. Purification by column chromatography over silica gel eluting with a mixture of dichloromethane and hexane (2:3) followed by recrystallization with hexane afforded **MC3T** as orange solid (0.180 g, 57%); m.p. 200-201 °C; ^{1}H-NMR (300 MHz, $CDCl_3$) δ 8.27 (1H, s), 8.19 (2H, d, J = 1.5 Hz), 7.89 (1H, d, J = 8.7 Hz), 7.76 (1H, d, J = 7.8 Hz), 7.67-7.61 (3H, dd, J = 3.9 Hz, J = 5.1 Hz), 7.56-7.51 (4H, m), 7.41 (2H, d, J = 8.7 Hz) 7.36-7.33 (2H, t, J = 4.2 Hz), 7.26-7.23 (2H, t, J = 3.6 Hz), 3.92 (3H, s), 2.07-2.02 (4H, m), 1.50 (18H, m), 1.13 (12H, m) and 0.83-0.78 (10H, t, J = 6.75 Hz) ppm; ^{13}C-NMR (75 MHz, $CDCl_3$) δ 163.48, 152.69, 151.98, 147.36, 146.28, 145.15, 142.88, 140.52, 139.76, 139.38, 139.33, 139.23, 137.17, 135.33, 134.18, 134.07, 132.70, 134.18, 134.07, 132.70, 127.47, 125.62, 125.45, 124.90, 124.62, 124.22, 123.94, 123.59, 123.43, 121.41, 120.41, 120.86, 120.34, 119.94, 116.34, 116.10, 55.53, 53.19, 40.36, 34.77, 32.05, 31.56, 29.67, 23.94, 22.60 and 14.05 ppm; FT-IR (KBr) 2952, 2926, 2217, 1723, 1610, 1580, 1526, 1489, 1476, 1430, 1364, 1324, 1294, 1261, 1233, 1211, 1093, 1050, 878, 839, 809, 791, 757, 742, 665 and 614 cm^{-1}. HRMS-ESI calcd for $C_{62}H_{66}N_2O_2S_3$: *m/z* 966.4286 found 967.3810 [MH$^+$].

(*E*)-Methyl-2-cyano-3-(5-(5-(5-(7-(3,6,-di-*tert*-butyl-*9H*-carbazol-9-yl)-9,9-dihexyl-*9H*-fluoren-2-yl)thiophene-2-yl)thiophene-2-yl0thiophene-2-yl)acrylate (MC4T)

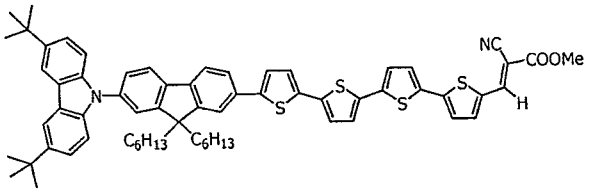

A mixture of 5-(5-(5-(5-(7-(3,6-di *tert*-butyl-*9H*-carbazol-9-yl)-9,9-dihexyl-fluorene-2-yl)thiophene-2-yl)thiophene-2-yl)thiophene-2-yl)thiophene-2-carbaldehyde (0.250 g, 0.258 mmol) and methyl-2-cyanoacetate (0.143 g, 1.41 mmol) was vacuum-dried and added piperidine (0.290 ml, 2.94 mmol), and acetic acid (0.238 ml, 2.94 mmol) in the solvent mixture of THF : acetonitrile (20 ml ,1:1 v/v). After stirring for 6 h at room temperature, water (50 ml) was added and extracted with dichloromethane (50 ml x 3). The combined organic phase were washed with water (50 ml) and brine (50 ml) solution, dried over anhydrous Na_2SO_4, filtered, and the solvents were removed to dryness. Purification by column chromatography over silica gel eluting with a mixture of dichloromethane and hexane (2:3) followed by recrystallizatio with hexane afforded **MC4T** as orange solid (0.178 g, 66%); m.p. 160-161 °C; ^{1}H-NMR (300 MHz, $CDCl_3$) δ 8.28 (1H, s), 8.17 (2H, s), 7.88 (1H, d, J = 8.5 Hz), 7.76 (1H, d, J = 7.9 Hz), 7.68-7.60 (3H, m), 7.55-7.47 (4H, m), 7.40 (1H, d, J = 8.6 Hz), 7.35-7.33 (2H, t, J = 3.2 Hz), 7.25 (1H, d, J = 5.4 Hz), 7.22 (1H, d, J = 3.6 Hz), 7.17 (2H, s), 3.92 (3H, s), 2.05 (4H, m), 1.48 (18H, m), 1.12 (12H, m) and 0.82-0.78 (10H, t, J = 6.6 Hz) ppm; ^{13}C-NMR (75 MHz, $CDCl_3$) δ 163.48, 152.65, 151.93, 146.31, 144.46, 142.85, 140.35, 139.32, 137.61, 137.09, 135.75, 134.93, 134.22, 132.83, 127.47, 125.42, 125.06, 124.83, 124.74, 124.36, 124.29, 123.83, 123.57, 123.39, 121.39, 120.81, 120.29, 119.88, 116.09, 109.22, 97.18, 55.50, 53.20, 40.36, 34.76, 32.03, 31.54, 29.66, 23.91, 22.59 and 14.04 ppm; FT-IR (KBr) 3413, 2952, 2217, 1724, 1638, 1617, 1579, 1551, 1529, 1477, 1431, 1366, 1324, 1261, 1233, 1051, 809, 786 and 614 cm^{1}. HRMS-ESI calcd for $C_{66}H_{68}N_2O_2S_4$: *m/z* 1048.4164 found 1049.5460 [MH^+].

Chapter 6:

***N*-(2-Ethylhexyl)-*N*-phenylbenzenenamine (A2)**

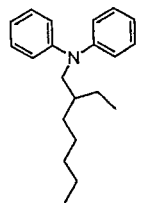

To a mixture of diphenylamine (5 g, 29.5 mmol) in DMSO (100 ml) was added an aqueous NaOH (9.88 g, 0.247 mol) follow by 2-ethylhexylbromide (6.3 ml). After being stirred at room temperature for 24 h, the reaction mixture was extracted with ethyl acetate (100 ml x 3). The combined organic phase was washed with water (100 ml), HCl solution (1 M, 50 ml), brine solution (100 ml), dried over sodium sulfate anhydrous, filtered and the organic phase was removed in vacuum. Purification by column chromatography using silica gel eluent with hexane gave **A2** as a colorless viscous (3.100 g, 36%); ^{1}H-NMR (300 MHz, $CDCl_3$) δ 7.29 (4H, t, J = 8.1 Hz), 7.05 (4H, d, J = 7.8 Hz), 6.97 (2H, t, J = 7.5 Hz), 3.66 (2H, d, J = 7.2 Hz), 1.91 (1H, m), 1.40 (4H, m), 1.29 (5H, m) and 1.23 (7H, m) ppm; ^{13}C-NMR (75 MHz, $CDCl_3$) δ 147.92, 143.27, 137.68, 135.64, 127.84, 126.52, 124.64, 124.11, 123.37, 122.59, 121.46, 56.50, 37.65, 30.79, 28.70, 24.12, 23.16, 14.10 and 10.79 ppm.

4-Bromo-*N*-(4-bromophenyl)-*N*-2-ethylhexylbenzenenamine (A3)

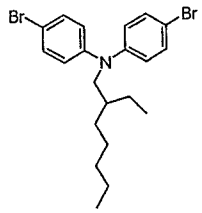

N-bromosuccinamide (3.8 g, 0.021 mmol) was added in small portions to a stirred solution of *N*-(2-ethylhexyl)-*N*-phenylbenzenenamine (5.74 g, 0.019 mmol)and ammoniumacetate in acetonitrile (30 ml). After being stirred at room temperature for 1 h, water was added. The mixture was extracted with dichloromethane (50 ml x 3). The combined organic phase was washed with water (50 ml), brine solution (50 ml), dried over anhydrous sodium sulfate, filtered

and the solvent was remove in vacuum. Purification by short column chromatography using silica gel eluting with Hexane gave **A3** as colorless viscous (5.500 g,64%); ^{1}H-NMR (300 MHz, $CDCl_3$) δ 7.26 (4H, d, J = 8.1 Hz), 6.08 (4H, d, J=8.1 Hz), 3.48 (2H, d, J = 6.9 Hz), 1.73 (1H, m), 1.28(9H, m) and 0.88 (7H, m) ppm; ^{13}C-NMR (75 MHz, $CDCl_3$) δ 147.60, 132.23, 122.96, 114.00, 56.76, 37.52, 30.78, 30.78, 28.70, 24.12, 23.14, 14.10 and 10.77 ppm.

N-(4-Bromophenyl)-N-(2-ethylhexyl)-4-(thiophene-2-yl)benzenenamine (A4)

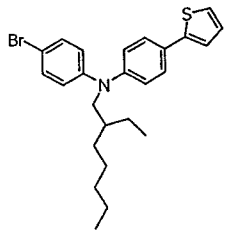

A mixture of 4-bromo-N-(4-bromophenyl)-N-(2-ethylhexylbenzenenamine (2.89 g, 6.37 mmol), 2-thiopheneboronic acid (0.9g, 7.03 mmol), $Pd(PPh_3)_4$ (0.366 g, 0.316 mmol) and an aqueous sodium carbonate solution (2 M, 32 ml), in THF (40 ml) was degassed with N_2 for 5 min. The mixture was heated to reflux under N_2 for 24 h. After the mixture was cooled to room temperature water (100 ml) was added. The mixture was extracted with dichloromethane (100 ml x 3), washed with water (100 ml), and brine solution (100 ml), dried over sodium sulfate anhydrous, filtered and the solvents were remove to dryness. Purification by column chromatography over silica gel eluting with hexane afforded **A4** as colorless viscous (1.05 g, 36%); ^{1}H-NMR (300 MHz, $CDCl_3$) δ 7.51 (2H, d, J = 8.4 Hz), 7.35 (2H, d, J = 9 Hz), 7.22 (2H, m), 7.08 (1H, m), 6.99 (2H, d, J = 8.7 Hz), 6.89 (2H, d, J = 9 Hz), 3.60 (2H, d, J = 6.9 Hz), 1.73 (1H, m), 1.28 (9H, m) and 0.88 (7H, m) ppm; ^{13}C-NMR (75 MHz, $CDCl_3$) δ 147.80, 147.70, 144.36, 132.12, 131.71, 131.55, 128.26, 127.97, 127.89, 126.89, 126.89, 126.18, 125.75, 124.02, 123.88, 122.82, 122.10, 121.58, 115.84, 113.59, 56.64, 38.31, 37.57, 30.77, 28.69, 24.10, 23.13, 14.08 and 10.76 ppm; FT-IR (Nujol) 2920.20, 2853.64, 1694.45, 1596.07, 1556.91, 1456.20, 1377.15, 1306.44, 1214.58, 1193.81, 1168.17, 872.71, 833.20, 794.09 and 721.47 cm^{-1}.

N-(2-Ethylhexyl)-4-(thiophene-2-yl)-N--4-(thiophene-2-yl)benzenenamine (A5)

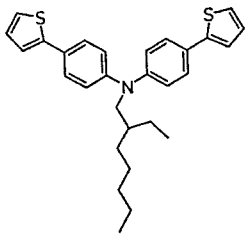

A mixture of 4-bromo-N-(4-bromophenyl)-N-(2-ethylhexylbenzenenamine (2.89 g, 6.37 mmol), 2-thiopheneboronic acid (0.9 g, 7.03 mmol), $Pd(PPh_3)_4$ (0.366 g, 0.316 mmol) and an aqueous sodium carbonate solution (2 M, 32 ml), in THF (40 ml) was degassed with N_2 for 5 min. The mixture was heated to reflux under N_2 for 24 h. After the mixture was cooled to room temperature water (100 ml) was added. The mixture was extracted with dichloromethane (100 ml x 3), washed with water (100 ml), and brine solution (100 ml), dried over sodium sulfate anhydrous, filtered and the solvents were remove to dryness. Purification by column chromatography over silica gel eluting with hexane afforded **A5** as light yellow viscous (0.379 g, 14%); ^{1}H-NMR (300 MHz, $CDCl_3$) δ 7.60 (4H, dd, J = 3.6 Hz), 7.28 (4H, m), 7.13 (6H, m), 3.73 (2H, d, J = 6.9 Hz), 1.91 (1H, m), 1.39 (9H, m) and 0.99 (7H, m) ppm; ^{13}C-NMR (75 MHz, $CDCl_3$) δ 147.77, 147.67, 144.34, 132.11, 131.69, 127.97, 127.85, 126.88, 123.88, 122.80, 122.09, 121.55, 121.28, 115.79, 113.57, 56.61, 37.53, 30.74, 28.67, 24.07, 23.13, 14.08 and 10.74 ppm; FT-IR (Nujol) 2920.20, 2853.64, 1694.45, 1596.07, 1556.91, 1456.20, 1377.15, 1306.44, 1214.58, 1193.81, 1168.17, 872.71, 833.20, 794.09 and 721.47 cm^{-1}.

4-(-5-Bromothiophen-2-yl)-N-(4-(5-bromothiophen-2-yl)phenyl-N-(2-ethylhexyl) benzenenamine (A6)

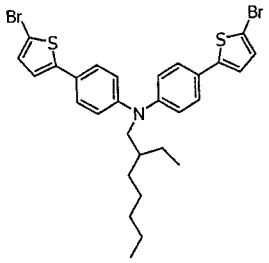

N-bromosuccinamide(0.40g, 2.24 mmol) was added in small portions to a stirred solution of *N* -(4-bromophenyl)-*N*-(2-ethylhexyl)-4-(thiophene-2-yl)benzenenamine(0.52g, 1.13 mmol) in THF (20 ml). After being stirred at room temperature for 30 min, water was added. The mixture was extracted with dichloromethane (30 ml x 3). The combined organic phase was washed with water (30 ml), brine solution (30 ml), dried over anhydrous sodium sulfate, filtered and the solvent was remove in vacuum. Purification by short column chromatography using silica gel eluting with Hexane gave **A6** as colorless viscous (0.7 g, 100%); ^{1}H-NMR (300 MHz, $CDCl_3$) δ 7.40 (4H, d, J = 8.4 Hz), 7.04-7.01 (6H, t, J = 6.9 Hz, J = 3 Hz), 6.97 (2H, d, J = 3.9 Hz), 3.63 (2H, d, J = 7.5 Hz), 1.78 (1H, m), 1.28 (9H, m) and 0.86 (7H, m) ppm; ^{13}C-NMR (75 MHz, $CDCl_3$) δ 148.08, 145.92, 130.79, 126.83, 126.54, 122.10, 121.47, 110.15, 56.48, 37.61, 30.73, 28.65, 24.07, 23.11, 14.05 and 10.74 ppm; FT-IR (Nujol) 2920.20, 2853.64, 1694.45, 1596.07, 1556.91, 1456.20, 1377.15, 1306.44, 1214.58, 1193.81, 1168.17, 872.71, 833.20, 794.09 and 721.47 cm^{-1}.

_N_-(4-(5-Bromothiophen-2-yl)phenyl)-_N_-(2-ethylhexyl)-4-(thiophene-2-yl) thiophene-2-yl)benzenenamine (A7)

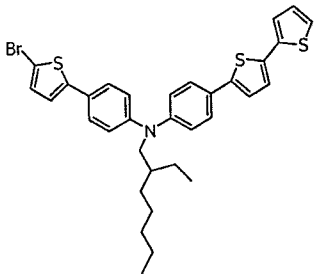

A mixture of 4-(-5-bromothiophen-2-yl)-*N*-(4-(5-bromothiophen-2-yl)phenyl-*N*-(2-ethylhexyl)benzenenamine (0.800 g, 1.29 mmol), 2-thiopheneboronic acid (0.178 g, 1.40 mmol), $Pd(PPh_3)_4$ (0.075 g, 0.064 mmol) and an aqueous sodium carbonate solution (2 M, 2 ml), in THF (40 ml) was degassed with N_2 for 5 min. The mixture was heated to reflux under N_2 for 24 h. After the mixture was cooled to room temperature water (100 ml) was added. The mixture was extracted with dichloromethane (100 ml x 3), washed with water (100 ml), and brine solution (100 ml), dried over sodium sulfate anhydrous, filtered and the solvents were remove to dryness. Purification by column chromatography over silica gel eluting with hexane afforded **A7** as light yellow viscous

(0.32 g, 40%); ^{1}H-NMR (300 MHz, $CDCl_3$) δ 7.53 (2H, d, J = 8.4 Hz), 7.42 (2H, d, J = 8.7 Hz), 7.28-7.22 (2H, m), 7.16 (2H, s), 7.02-7.09 (6H, m), 6.97 (1H, d, J=3.6 Hz), 3.67 (2H, d, J=7.5 Hz), 1.82 (1H, m), 1.32(9H, m), 0.9 (7H, m) ppm; ^{13}C-NMR (75 MHz, $CDCl_3$) δ 148.24, 147.76, 146.02, 143.17, 137.64, 135.73, 130.79, 127.84, 127.52, 126.53, 124.64, 124.14, 123.39, 122.67, 122.02, 121.89, 121.04, 110.05, 56.49, 37.63, 30.92, 30.77, 29.73, 28.68, 24.10, 23.14, 14.09 and 10.77 ppm; FT-IR (Nujol) 2923.03, 2853.67, 1694.45, 1500.15, 1462.96, 1377.33, 1018.17 and 721.26 cm^{-1}.

N-(2-Ethylhexyl)-N-(4-(5-thiophen-2-yl)thiophen-2-yl)-N-(4-(5-(thiophene-2-yl) thiophene-2-yl)phenyl)benzenenamine (A8)

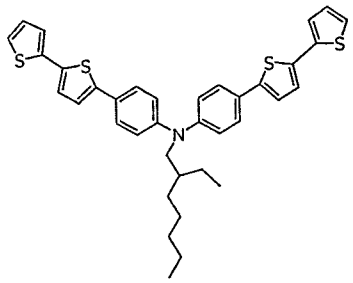

A mixture of 4-(-5-bromothiophen-2-yl)-N-(4-(5-bromothiophen-2-yl)phenyl-N-(2-ethylhexyl)benzenenamine (0.8 g, 1.29 mmol), 2-thiopheneboronic acid (0.178g, 1.40 mmol), $Pd(PPh_3)_4$ (0.075 g, 0.064 mmol) and an aqueous sodium carbonate solution (2 M, 2 ml), in THF (40 ml) was degassed with N_2 for 5 min. The mixture was heated to reflux under N_2 for 24 h. After the mixture was cooled to room temperature water (100 ml) was added. The mixture was extracted with dichloromethane (100 ml x 3), washed with water (100 ml), and brine solution (100 ml), dried over sodium sulfate anhydrous, filtered and the solvents were remove to dryness. Purification by column chromatography over silica gel eluting with hexane afforded **A8** as light yellow viscous yield was (0.32 g, 12%); ^{1}H-NMR (300 MHz, $CDCl_3$) δ 7.48 (2H, d, J = 8.1 Hz), 7.38 (2H, d, J = 8.4 Hz), 7.26 (1H, s), 7.17-7.12 (4H, m), 7.03-6.94 (7H, m), 3.67 (2H, d, J = 7.5 Hz), 1.70 (1H, m), 1.25 (9H, m), 0.85 (7H, m) ppm; ^{13}C-NMR (75 MHz, $CDCl_3$) δ 147.91, 143.27, 137.67, 135.63, 127.84, 127.20, 126.51, 124.64, 123.36, 122.59, 121.46, 56.48, 37.65, 30.90, 30.79, 29.74, 28.70, 24.12, 23.16, 14.10 and 10.79 ppm; FT-IR (Nujol) 2920.20, 2853.64, 1694.45, 1596.07,

1556.91, 1456.20, 1377.15, 1306.44, 1214.58, 1193.81, 1168.17, 872.71, 833.20, 794.09 and 721.47 cm^{-1}.

N-(4-(5-Bromothiophen-2-yl)phenyl)-4-(5-bromothiophene-2-yl)-N-(2-ethyl hexylbenzenenamine (A9)

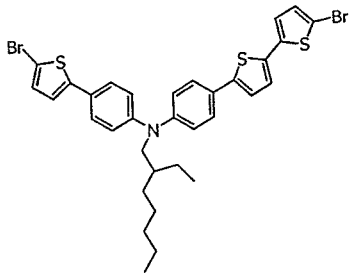

NBS (0.102 g, 0.573 mmol) was added in small portion to a stirred solution of *N*-(4-(5-bromothiophen-2-yl)phenyl)-*N*-(2-ethylhexyl)-4-(thiophene-2-yl)thiophene-2-yl)benzene-namine (0.350 g, 0.531 mmol) in THF (20 ml). After being stirred at room temperature for 30 min, water (30 ml) was added. The mixture was extracted with dichloromethane (50 ml x 3). The combined organic phase was washed with water (50 ml), brine solution (50 ml), dried over sodium sulfate anhydrous, filtered and the solvent was remove in vacuum. Purification by short column chromatography using silica gel eluting with recycle solvent gave **A9** as light yellow viscous (0.371 g, 100%); ^{1}H-NMR (300 MHz, $CDCl_3$) δ 7.54 (2H, d, J = 8.4 Hz), 7.44 (2H, d, J = 8.7 Hz), 7.24 (2H, d, J = 4.8 Hz), 7.17 (1H, s), 7.09-7.02 (6H, m), 6.98 (1H, d, J = 3.6 Hz), 3.68 (2H, d, J = 6.6 Hz), 1.84 (1H, m), 1.56-1.32 (9H, m), 0.92 (7H, d, J = 7.2Hz) ppm; ^{13}C-NMR (75 MHz, $CDCl_3$) δ 147.91, 143.27, 137.67, 135.63, 127.84, 127.20, 126.51, 124.64, 123.36, 122.59, 121.46, 56.48, 37.65, 30.90, 30.79, 29.74, 28.70, 24.12, 23.16, 14.10 and 10.79 ppm; FT-IR (Nujol) 1919.85, 2852.28, 1654.23, 1598.59, 1590.21, 1500.36, 1462.79, 1377.20, 1017.59, 783.47 and 721.90 cm^{-1}.

N-(2-Ethylhexyl)-N-(4-(5-formylphenylthiophen-2-yl)phenyl)-4-(5-(5-formyl phenylthiophene-2-yl)thiophene-2-yl)benzenamine (A10)

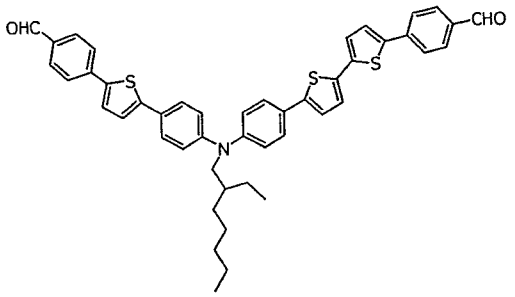

A mixture of *N*-(4-(5-bromothiophen-2-yl)phenyl)-4-(5-bromothiophene-2-yl)-*N*-(2-ethylhexylbenzenenamine (0.310 g, 0.443 mmol), 4-formylphenylboronic acid (0.140 g, 0.933 mmol), $Pd(PPh_3)_4$ (0.026 g, 0.022 mmol) and an aqueous sodium carbonate solution (2 M, 3 ml), in THF (20 ml) was degassed with N_2 for 5 min. The mixture was heated to reflux under N_2 for 24 h. After the mixture was cooled to room temperature water (50 ml) was added. The mixture was extracted with dichloromethane (50 ml x 3), washed with water (50 ml), and brine solution (50 ml), dried over sodium sulfate anhydrous, filtered and the solvents were remove to dryness. Purification by column chromatography over silica gel eluting with hexane afforded **A10** as yellow solid (0.290 g, 87%); ^{1}H-NMR (300 MHz, $CDCl_3$) δ 9.95 (2H, s), 7.89 (2H, d, J = 8.4 Hz), 7.59 (2H, d, J = 8.4 Hz), 7.54 (2H, d, J = 8.4 Hz), 7.44 (2H, d, J = 8.7 Hz), 7.24 (2H, d, J = 4.8 Hz), 7.17 (1H, s), 7.09-7.02 (6H, m), 6.98 (1H, d, J = 3.6 Hz), 3.68 (2H, d, J = 6.6 Hz), 1.84 (1H, m), 1.56-1.32 (9H, m), 0.92 (7H, d, J = 7.2Hz) ppm; ^{13}C-NMR (75 MHz, $CDCl_3$) δ 191.36, 191.31, 148.29, 147.94, 146.12, 144.03, 140.81, 140.50, 140.18, 139.77, 139.22, 135.06, 135.03, 134.85, 130.51, 128.03, 127.22, 126.79, 126.61, 126.14, 125.91, 125.60, 125.49, 125.19, 124.48, 123.24, 122.85, 122.85, 121.80, 121.17, 56.49, 37.65, 30.76, 29.70, 28.67, 24.10, 23.13, 14.07 and 10.76 ppm; FT-IR (KBr) 3073, 2964, 1698, 1596, 1494, 1448, 1374, 1214, 1168, 830, 796 cm^{-1}.

N-(2-Ethylhexyl)-N-(4-(5-phenylthiophen-2-yl)phenyl)-4-(5-(5-phenylthiophene-2-yl)thiophene-2-yl)-2-cyano-3-phenylacrylic acid (PTA2TP)

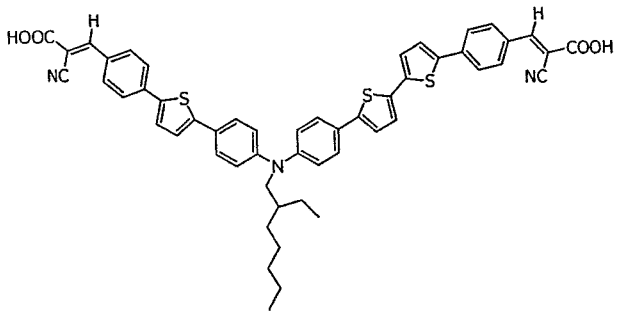

A mixture of *N*-(2-ethylhexyl)-*N*-(4-(5-formylphenylthiophen-2-yl)phenyl)-4-(5-(5-formylphenylthiophene-2-yl)thiophene-2-yl)benzenamine (0.290 g , 3.86 mmol) and cyanoacetic acid (0.164 g, 1.92 mmol) was vaccum-dried and added THF:acetonitrile (20 ml ,1:1 v/v) and piperidine (0.190 ml, 1.92 mmol). The solution was refluxed for 6 h. After cooling the solution, the organic layer was removed in vacuum. The pure product was obtain by silica gel chromatography eluting with dichloromethane-methanol gradient to afforded **PTA2TP** as orange solid (0.204 g, 60%); m.p. 260-261°C; ^{1}H-NMR (300 MHz, $CDCl_3$) δ 8.14 (2H, s), 7.90-7.85 (3H, m), 7.78 (2H, d, J = 5.1 Hz), 7.70 (2H, d, J = 8.1 Hz), 7.55 (3H, d, J = 8.4 Hz), 7.04 (1H, d, J = 8.1 Hz), 3.68 (2H, d, J = 6.6 Hz), 1.71 (1H, m), 1.19 (9H, s), 0.81 (7H, s) ppm; ^{13}C-NMR (75 MHz, $CDCl_3$) δ 191.36, 191.31, 148.29, 147.94, 146.12, 144.03, 140.81, 140.50, 140.18, 139.77, 139.22, 135.06, 135.03, 134.85, 130.51, 128.03, 127.22, 126.79, 126.61, 126.14, 125.91, 125.60, 125.49, 125.19, 124.48, 123.24, 122.85, 122.85, 121.80, 121.17, 56.49, 37.65, 30.76, 29.70, 28.67, 24.10, 23.13, 14.07 and 10.76 ppm; FT-IR (Nujol) 3393, 3073, 2964, 2215, 1698, 1596, 1494, 1448, 1374, 1214, 1168, 830, 796 cm^{-1}.

4-(5-(5-Brothiophen-2-yl)-*N*-(4-(5-(5-bromothiophen-2-yl)thiophen-2-yl)-*N*-(2-ethylhexyl)benzenenamine (A11)

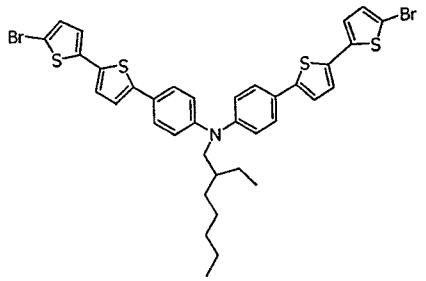

NBS (0.244 g, 0.688 mmol) was added in small portion to a stirred solution of *N*-(4-(5-bromothiophen-2-yl)phenyl)-*N*-(2-ethylhexyl)-4-(thiophene-2-yl)thiophene-2-yl)-benzenenamine (0.410 g, 1.37 mmol) in THF (20 ml). After being stirred at room temperature for 30 min, water (30 ml) was added. The mixture was extracted with dichloromethane (50 ml x 3). The combined organic phase was washed with water (50 ml), brine solution (50 ml), dried over sodium sulfate anhydrous, filtered and the solvent was remove in vacuum. Purification by short column chromatography using silica gel eluting with recycle solvent gave **A11** as light yellow viscous (1.07 g, 100%); ^{1}H-NMR (300 MHz, $CDCl_3$) δ 7.50 (4H, d, J = 8.4 Hz), 7.39 (2H, d, J = 3.6 Hz), 7.21-7.16 (6H, m), 7.04 (4H, d, J = 8.7 Hz), 3.66 (2H, d, J = 7.5 Hz), 1.57 (1H, m), 1.25 (9H, m), 0.88 (7H, m) ppm; FT-IR (Nujol) 2925.46, 2853.28, 1654.15, 1598.78, 1522.26, 1462.98, 1377.21, 1017.90, 971.67, 794.39, 786.50 and 721.80 cm^{-1}.

***N*-(2-Ethylhexyl)-4-(5-(5-formylphenylthiophen-2-yl)thiophen-2-yl)-*N*-(4-(5-(5-formylphenyl)thiophen-2-yl))-*N*-(2-ethylhexyl)benzenenamine (A12)**

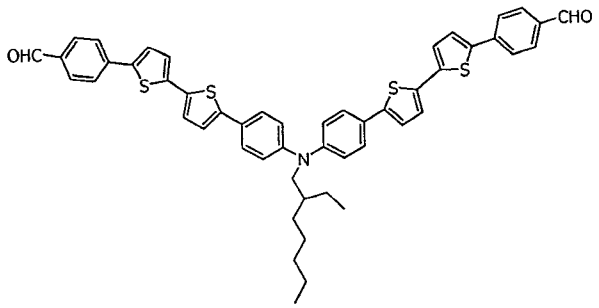

A mixture of 4-(5-(5-brothiophen-2-yl)-*N*-(4-(5-(5-bromothiophen-2-yl)thiophen-2-yl)-*N*-(2-ethylhexyl)benzenenamine(0.315 g, 0.403 mmol), 5-formylphenylboronic acid (0.127g, 0.846 mmol), $Pd(PPh_3)_4$ (0.024 g, 0.020mmol) and an aqueous sodium carbonate solution (2 M, 4 ml), in THF (20 ml) was degassed with N_2 for 5 min. The mixture was heated to reflux under N_2 for 24 h. After the mixture was cooled to room temperature water (50 ml) was added. The mixture was extracted with dichloromethane (50 ml x 3), washed with water (50 ml), and brine solution (50 ml), dried over sodium sulfate anhydrous, filtered and the solvents were remove to dryness. Purification by column chromatography over silica gel eluting with hexane afforded **A12** as yellow solid (0.236 g, 60%); ^{1}H-NMR (300 MHz, $CDCl_3$) δ 10.00 (2H, s), 7.88 (4H, d, *J*=8.4 Hz), 7.74 (4H, d, *J* = 8.4 Hz), 7.50 (4H, d, *J* = 8.4 Hz), 7.39 (2H, d, *J* = 3.6 Hz), 7.21-7.16(6H, m), 7.04 (2H, d, *J* = 8.7 Hz), 3.66 (2H, d, *J* = 7.5 Hz), 1.57 (1H, m), 1.25 (9H, m), 0.88 (7H, m) ppm; ^{13}C-NMR (75 MHz, $CDCl_3$) δ 207.15, 191.28, 148.04, 144.09, 140.78, 139.78, 135.04, 134.99, 130.84, 130.49, 128.79, 127.01, 126.58, 125.90, 125.17, 124.45, 122.78, 121.47, 68.15, 56.49, 38.75, 37.65, 30.76, 30.62, 30.37, 30.11, 29.85, 29.67, 29.34, 28.92, 28.67, 24.10, 23.76, 23.10, 22.96, 14.03, 10.93, 10.74 ppm; FT-IR (KBr) 3073, 2924, 1692, 1636, 1597, 1493, 1454, 1379, 1213, 1166, 830 and 796 cm^{-1}.

N-(2-Ethylhexyl)-4-(5-(5-phenylthiophen-2-yl)thiophen-2-yl)-N-(4-(5-(5-phenyl thiophen-2-yl) -N-(2-ethylhexyl)benzenenamyl-2-cyano-3-acrylic acid (P2TA2TP)

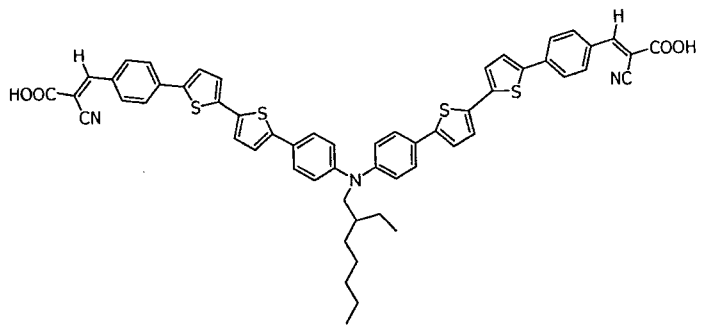

A mixture of *N*-(2-ethylhexyl)-4-(5-(5-formylphenylthiophen-2-yl)thiophen-2-yl)-*N*-(4-(5-(5-formylphenyl)thiophen-2-yl))-*N*-(2-ethylhexyl)benzenenamine (0.236 g , 0.007 mmol) and cyanoacetic acid (0.104 g, 1.22 mmol) was vaccum-dried and added THF:acetonitrile (20 ml, 1:1 v/v) and piperidine (0.120 ml, 1.22 mmol). The solution was refluxed for 6 h. After cooling

the solution, the organic layer was removed in vacuum. The pure product was obtain by silica gel chromatography to afforded **PTTP** as yellow solid (0.204 g, 65%); m.p. 245-246 °C; ^{1}H-NMR (300 MHz, $CDCl_3$+DMSO) δ 7.91-7.85 (6H, t, J = 8.4 Hz, J = 9.9 Hz), 7.77 (4H, d, J = 8.4 Hz), 7.64-7.58 (6H, d, J = 3.9 Hz, J = 8.4 Hz), 7.41-7.37 (4H, d, J = 3.9 Hz, J = 2.1 Hz), 7.07 (4H, d, J = 8.4 Hz), 5.74 (2H, s), 3.66 (2H, d, J = 7.5 Hz), 2.07 (1H, m), 1.30 (9H, m), 0.82 (7H, m) ppm; FT-IR (Nujol) 3393, 3073, 2964, 2215, 1698, 1596, 1494, 1448, 1374, 1214, 1168, 830, 796 cm^{-1}.

4-(5-(4-((4-(5-(4-Phenyl)thiophen-2-yl)phenyl)(2phylheptyl)amino)phenyl) thiophene-2-yl)benzaldehyle (A13)

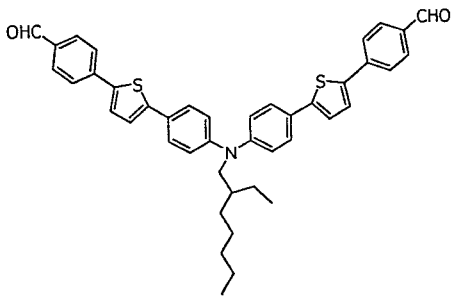

A mixture of 4-(-5-bromothiophen-2-yl)-*N*-(4-(5-bromothiophen-2-yl)phenyl-*N*-(2-ethylhexyl)benzenenamine (0.556 g, 0.90 mmol),4-formylphenylboronic acid (0.146 g, 0.976 mmol), $Pd(PPh_3)_4$ (0.052 g, 0.044 mmol) and an aqueous sodium carbonate solution (2 M, 9 ml), in THF (40 ml) was degassed with N_2 for 5 min. The mixture was heated to reflux under N_2 for 24 h. After the mixture was cooled to room temperature water (100 ml) was added. The mixture was extracted with dichloromethane (100 ml x 3), washed with water (100 ml), and brine solution (100 ml), dried over sodium sulfate anhydrous, filtered and the solvents were remove to dryness. Purification by column chromatography over silica gel eluting with hexane afforded **A13** as orange solid (0.360 g, 60%); ^{1}H-NMR (300 MHz, $CDCl_3$) δ 9.99 (2H, s), 7.89-7.74 (7H, m), 7.57-7.35 (6H, m), 7.26-6.99 (7H, m), 3.67 (2H, d, J = 6.9 Hz), 1.82 (2H, s), 1.26 (9H, m), 0.88 (6H, m) ppm; ^{13}C-NMR (75 MHz, $CDCl_3$) δ 191.35, 148.18, 146.05, 140.55, 140.14, 134.85, 130.50, 130.36, 128.02, 127.00, 126.69, 126.51, 126.15, 125.48, 124.30, 123.30, 123.14, 122.81, 121.48, 120.69, 56.47, 37.65, 30.91, 30.76, 29.71, 28.67, 24.10, 23.13, 14.08, 10.77 ppm.

4-(4-((2-Ethylhexyl)-4-(thiophen-2-yl)phenyl)amino)phenylthiophen-2-yl)2-cyano -3-phenylacrylic acid (PTATP)

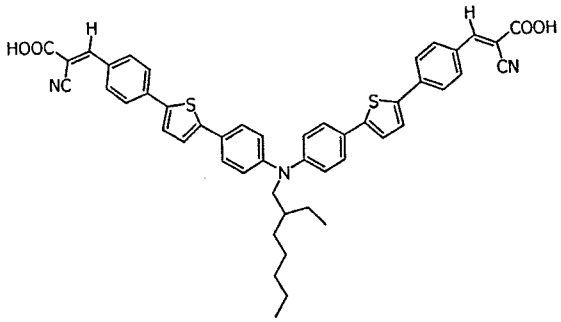

A mixture of 4-(5-(4-((4-(5-(4-phenyl)thiophen-2-yl)phenyl)(2-thylheptyl) amino)phenyl)thiophene-2-yl)benzaldehyle (0.250 g , 0.382 mmol) and cyanoacetic acid (0.162 g, 1.91 mmol) was vacuum-dried and added THF:acetonitrile (20 ml, 1:1 v/v) and piperidine (0.188ml, 1.91 mmol). The solution was refluxed for 6 h. After cooling the solution, the organic layer was removed in vacuum. The pure product was obtain by silica gel chromatography to afforded **PTATP** as yellow solid (0.130 g, 52%); m.p. 258-259 °C; ^{1}H-NMR (300 MHz, $CDCl_3$) δ 8.01 (2H, d, J = 6.9 Hz), 7.94 (1H, s), 7.86 (3H, d, J = 8.1 Hz), 7.66 (3H, d, J = 8.1 Hz),7.53-7.45 (5H, dd, J = 8.7 Hz, J = 4.8 Hz), 7.21 (3H, s), 7.01 (d, J = 8.1 Hz), 5.49 (2H, s), 3.67 (2H, d, J = 6.9 Hz), 2.05 (2H, s), 1.28 (9H, m), 0.82 (6H, m) ppm; FT-IR (Nujol) 3393, 3073, 2964, 2215, 1698, 1596, 1494, 1448, 1374, 1214, 1168, 830, 796 cm^{-1}.

5-(4-((4-Bromophenyl)(2-ethylhexyl)amino)phenyl)thiophene-2-carbaldehyde (A14)

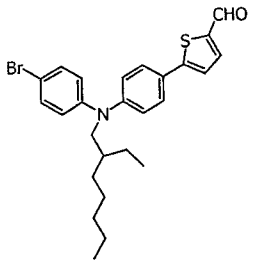

A mixture of 4-bromo-*N*-(4-bromophenyl)-*N*-2-ethylhexylbenzenenamine (1.839 g, 4.05 mmol), 5-formylthiopheneboronic acid (1.3g, 8.33 mmol), $Pd(PPh_3)_4$ (0.235 g, 0.203 mmol)

and an aqueous sodium carbonate solution (2 M, 20 ml), in THF (40 ml) was degassed with N_2 for 5 min. The mixture was heated to reflux under N_2 for 24 h. After the mixture was cooled to room temperature water (100 ml) was added. The mixture was extracted with dichloromethane (100 ml x 3), washed with water (100 ml), and brine solution (100 ml), dried over sodium sulfate anhydrous, filtered and the solvents were remove to dryness. Purification by column chromatography over silica gel eluting with hexane afforded **A14** as light yellow viscous (0.473 g, 15%); ^{1}H-NMR (300 MHz, $CDCl_3$) δ 9.83 (1H, s), 7.68 (1H, s), 7.50 (2H, d, J = 7.8 Hz), 7.41 (2H, d, J = 7.8 Hz), 7.27 (1H, s), 6.99 (2H, d, J = 8.4 Hz), 6.88 (2H, d, J = 7.8 Hz), 3.59 (2H, d, J = 6.9 Hz), 1.75 (2H, s), 1.45 (9H, m) and 0.86 (6H, m) ppm; FT-IR (KBr) 3073, 2926, 2855, 1655, 1488, 1437, 1363, 1323, 1293, 1260, 1225, 1055, 879, 806, 755 and 670 cm^{-1}.

5-(4-((2-Ethylhexyl)-4-(formylthiophen-2-yl)phenyl)amino)phenylthiophen-2-carbaldehyde (A15)

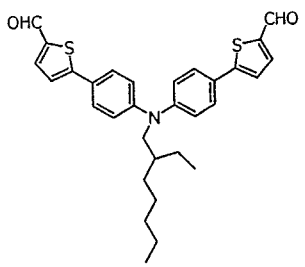

A mixture of 4-bromo-*N*-(4-bromophenyl)-*N*-2-ethylhexylbenzenenamine (1.839 g, 4.05 mmol), 5-formyl-2-thiopheneboronic acid (1.3g, 8.33 mmol), $Pd(PPh_3)_4$ (0.235 g, 0.203 mmol) and an aqueous sodium carbonate solution (2 M, 20 ml), in THF (40 ml) was degassed with N_2 for 5 min. The mixture was heated to reflux under N_2 for 24 h. After the mixture was cooled to room temperature water (100 ml) was added. The mixture was extracted with dichloromethane (100 ml x 3), washed with water (100 ml), and brine solution (100 ml), dried over sodium sulfate anhydrous, filtered and the solvents were remove to dryness. Purification by column chromatography over silica gel eluting with hexane afforded **A15** as light yellow viscous (0.302 g, 15%); ^{1}H-NMR (300 MHz, $CDCl_3$) δ 9.85 (2H, s), 7.70 (2H, d, J = 3.9 Hz), 7.58 (2H, d, J = 8.7 Hz), 7.32 (2H, d, J = 3.9 Hz), 7.08 (2H, d, J = 8.7 Hz), 3.69 (2H, d, , J = 7.2 Hz), 1.75 (2H, s), 1.45 (9H, m) and 0.86 (6H, m) ppm; ^{13}C-NMR (75 MHz, $CDCl_3$) δ 182.58, 154.42, 149.04, 141.43, 137.74, 137.68, 127.48, 126.50, 126.29, 122.96, 121.51, 56.42, 37.67, 30.67,

30.73, 29.69, 28.64, 24.08, 23.08 and 14.04 ppm; FT-IR (KBr) 3073, 2924, 1665, 1588, 1444, 1361, 1223, 1187, 1056, 802 and 668 cm^{-1}.

5-Cyano-3-(4-((2-ethylhexyl)-4-(thiophen-2-yl)phenyl)amino)phenylthiophen-2-acrylic acid (TAT)

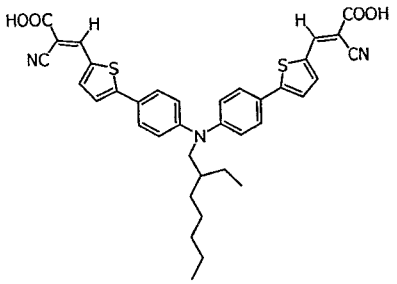

A mixture of 5-(4-((2-ethylhexyl)-4-(formylthiophen-2-yl)phenyl)amino)phenyl thiophe-2-carbaldehyde(0.302 g, 0.585 mmol) and cyanoacetic acid (0.248 g, 2.92 mmol) was vacuum-dried and added THF:acetonitrile (20 ml,1:1 v/v) and piperidine (0.287 ml, 2.92 mmol). The solution was refluxed for 6 h. After cooling the solution, the organic layer was removed in vacuum. The pure product was obtain by silica gel chromatography to afforded **TAT** as orange solid (0.234 g, 74%); m.p. 239-240 °C; ^{1}H-NMR (300 MHz, $CDCl_3$) δ 8.06 (1H, s), 7.49 (6H, s), 7.20 (2H, s), 6.97 (3H, s), 5.18 (2H, s), 3.59 (2H, s), 1.71 (2H, s), 1.15 (9H, m) and 0.77 (6H, m) ppm; FT-IR (Nujol) 3393, 3073, 2964, 2215, 1698, 1596, 1494, 1448, 1374, 1214, 1168, 830, 796 cm^{-1}.

4-(4-(5-(2-Ethylhexyl)-4-(formylphenyl)phenyl)amino) phenylthiophen-2-carbaldehyde (A16)

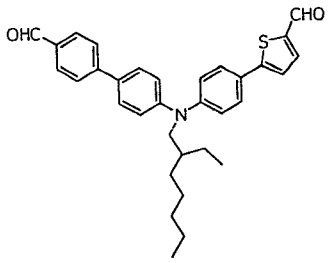

A mixture of 5-(4-((4-bromophenyl)(2-ethylhexyl)amino)phenyl)thiophene-2-carbaldehyde (0.473 g, 0.976 mmol), 5-formylphenylboronic acid (0.160g, 1.06 mmol), $Pd(PPh_3)_4$ (0.056 g, 0.048 mmol) and an aqueous sodium carbonate solution (2 M, 5 ml), in THF (30 ml) was degassed with N_2 for 5 min. The mixture was heated to reflux under N_2 for 24 h. After the mixture was cooled to room temperature water (50 ml) was added. The mixture was extracted with dichloromethane(50 ml x 3), washed with water (100 ml), and brine solution (100 ml), dried over sodium sulfate anhydrous, filtered and the solvents were remove to dryness. Purification by column chromatography over silica gel eluting with hexane afforded **A16** as yellow solid (0.260 g, 52%); ^{1}H-NMR (300 MHz, $CDCl_3$) δ 10.5 (1H, s), 9.85 (1H, s), 7.90 (2H, d), 7.75 (3H, dd), 7.60 (4H, dd), 7.30 (3H, dd), 7.10 (2H, d), 3.75 (2H, d), 1.75 (2H, s), 1.45 (9H, m) and 0.86 (6H, m) ppm; FT-IR (KBr) 2940, 1698, 1596, 1494, 1448, 1374, 1214, 1168, 830 and 796 cm^{-1}.

(*E*)-(4-Cyano-3-(4(5-(4-((2-ethylhexyl)phenyl)amino)phenylthiophene-2-cyanoacrylic acid (PAT)

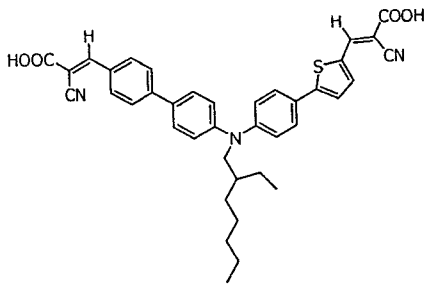

A mixture of 4-(4-(5-(2-ethylhexyl)-4-(formylphenyl)phenyl)amino) phenylthiophen-2-carbaldehyde (0.258 g , 0.506 mmol) and cyanoacetic acid (0.301g, 3.54 mmol) was vaccum-dried and added THF:acetonitrile (20 ml ,1:1 v/v) and piperidine (0.350 ml, 3.54 mmol). The solution was refluxed for 6 h. After cooling the solution, the organic layer was removed in vacuum. The pure product was obtain by silica gel chromatography to afforded **PAT** as yellow solid (0.175 g, 54%); m.p. 219-220 °C; ^{1}H-NMR (300 MHz, $CDCl_3$) δ 8.05-7.86 (4H, m), 7.65-7.28 (9H, m), 7.03 (3H, s), 3.63 (2H, s), 205 (1H, s),1.75 (1H, s), 1.40-1.04 (9H, m) and 0.80 (6H, m) ppm; FT-IR (Nujol) 3393, 3073, 2964, 2215, 1698, 1596, 1494, 1448, 1374, 1214, 1168, 830, 796 cm^{-1}.

REFERENCES

REFERENCES

REFERENCES

[1] P. F. Baude and et al. (2003). "A lithographic process for integrated organic field-effect transistors", Appl. Phys. Lett. 82: 3964-3966.

[2] V. Sunder and et al. (2004). "Elastomeric Transistor Stamps: Reversible Probing of Charge Transport in Organic Crystals", Science. 303: 1644-1646.

[3] S. Wakim and et al. (2004). "Organic Microelectronics: Design, Synthesis, and Characterization of 6,12-Dimethylindolo [3,2-*b*]Carbazoles", Chem Mater. 16: 4386.

[4] S. Wakim and et al. (2004). "Synthesis of diindolo-carbazoles by Ullmann reaction: a rapid route to ladder oligo(p-aniline)s", Org Lett. 6: 3413-3416.

[5] Y. Li, Y. Wu, S. Gardnera and B. S. Ong. (2005). "Novel peripherally substituted indolo [3, 2-b]carbazoles for high-mobility organic thin-film transistors", Adv. Mater. 17: 849-853.

[6] Y. Wu and et al. (2005). "High-Performance, Stable Organic Thin-Film Field-Effect Transistors Based on Bis-5'-alkylthiophen-2'-yl-2,6-anthracene Semiconductors", J. Am. Chem. Soc. 127: 614-618.

[7] D. Adam and et al (1994). "Fast photoconduction in the highly ordered columnar phase of a discotic liquid crystal", Nature. 371: 141-143.

[8] A. M. Van De Craats and et al. (1999). "Record Charge Carrier Mobility in a Room-Temperature Discotic Liquid-Crystalline Derivative of Hexabenzocoronene", Adv. Mater. 11: 1469-1472.

[9] A. Fechtenkotter and et al. (1999). "Highly Ordered Columnar Structures from Hexa-*peri*-hexabenzocoronenes-Synthesis, X-ray Diffraction, and Solid-State Heteronuclear Multiple-Quantum NMR Investigations", Angew Chem Int. Ed. 38: 3039-3042.

[10] M. Funahashi and J. Hanna. (2000). "High ambipolar carrier mobility in self-organizing terthiophene derivative", Appl. Phys. Lett. 76: 2574-2576.

[11] H. Sirringhaus and et al. (2000). "Mobility enhancement in conjugated polymer field-effect transistors through chain alignment in a liquid-crystalline phase", Appl. Phys. Lett. 77: 406.

REFERENCES (CONTINUED)

[12] I. McCulloch and et al (2006). "Liquid-crystalline semiconducting polymers with high charge carrier mobility", Nature Materials. 5: 328-333.

[13] Kallmann, H. and M. Pope. (1960). "Positive Hole Injection into Organic Crystals", J. Chem. Phys. 32: 300. doi:10.1063/1.1700925.

[14] W. Helfrich and W. G. Schneidere. (1965) "Recombination radiation in anthracene Crystals", Phys. Rev. Lett. 14: 229 .

[15] L. J. Rothberg and A. J. Lovinger. (1996). "Electrically Active Organic and. Polymeric Materials for Thin-Film-Transistor Technologies", J. Mater. Res. 12: 3174-3186.

[16] Sheats, J. R. and et al. (1996). "Organic Electroluminescent Devices", Science. 273: 884-888.

[17] D. D. C. Bradley. (1992). "Electroluminescence: a bright future for conjugated polymers", Adv. Mater. 4: 756-758.

[18] S. R. Forrest and et al. (1997). "Organic electroluminescent elements", El. Mater. Dev. 415-458.

[19] M. Deussen and H. Bässler. (1997). "Organic light emitting diodes", Chiuz. 31: 76-86.

[20] M. Sonntag. (2005). "New Carbazole Based Materials for Optoelectronic Applications", Doctor of Natural Science: University of Bayreuth, 147-178.

[21] Y. Shirota and et al. (2005). "Amorphous electron-accepting materials for organic optoelectronics", J. Mater. Chem. 15: 75-93.

[22] Y. Kishigami and et al. (2005). "Conjugated polymers: theory, synthesis, properties, and characterization", Synth. Met. 153: 241-244.

[23] J. H. Burroughes and et al (1990). "Light-emitting-diodes based on conjugated polymers", Nature. 347: 539-541.

[24] S. S. Raint and et al (2010). "Increased Luninesence of MEH-PPV and PFO based PELDs by using salmon DNA as an electron blocking layer", J. Lumin. 30: 331-333.

[25] D.Y. Kim and et al. (2000). "Blue light emitting polymers", Prog. Polym. Sci. 25: 1089-1139;.

[26] L. Romarner and et. al. (2003). "The Influence of keto defected on photoexcitation dynamics in polyfluorene", 139: 851-854.

REFERENCES (CONTINUED)

[27] M. Sonntag and P. Strohriegl. (2006). "Synthesis and Characterization of Novel conjugated bisindenocabazoles", 62: 8103-8108.

[28] M. Kodomari, H. Satoh and S. Yoshitomi. (1988). "Selective halogenations of aromatic hydrocarbons with alumina-supported copper(II) halides", 53: 2093-2094.

[29] A. D. Schluter. (2001). "The tenth anniversary of Suzuki polycondensation (SPC)", 39: 1533-1556.

[30] I. Kymissis. (2009). "Organic Field Effect: Theory, Fabrication and Characterization", Springe.

[31] N. Herbert. (2002). "Polymers, Electrically Conducting" in Ullmann's Encyclopedia of Industrial Chemistry" Wiley-VCH, Weinheim, doi:10.1002/14356007.a21_429

[32] H.S. Nalwa. (2000). "Handbook of Nanostructured Materials and Nanotechnology" Academic Press, 5: 501–575.

[33] R. Parashkovand et. a (2004). "All-organic thin-film transistors made of poly(3-butylthiophene) semiconducting and various polymeric insulating layers", J. Appl. Phys. 95:1594-96.

[34] G. Horowitz and et al. (1999). "Theory of Organic FieldEffect Transistors", Synth. Met. 101:401

[35] G. Horowitz and et al. (1998). " Organic Field-Effect Transistors", Adv. Mater. 10:36

[36] O. Katz et al. (2005). "Charge carrier mobility in field effect transistors: analysis of capacitance–conductance measurements", Semicond. Sci. Technol. 20: 90.

[37] G. Horowitz and et al. (1998). "Gate voltage dependent mobility of oligothiophene field-effect transistors", J. of appl. Phys. 85: 3202-3206.

[38] C. Xiaoyang and et al. (2012). "Downscaling of n-channel organic field-effect transistors with inkjet-printed electrodes", Org. elec. 13: 320-328.

[39] Y. Zhang and et al. (2007). "Poly (3,3"-didodecylquarterthiophene) field effect transistors with single-walled carbonnanotube based source and drain electrodes". Appl. Phys. Lett. 91, 223512-223514.

REFERENCES (CONTINUED)

[40] K. P. Pernstich. (2004). "Organic Field-Effect Transistors: Towards Molecular Scale. Proceedings of Symposium E. E-MRS Spring Meeting", Chem. Mater., 146: 325-328.

[41] A. Zen and et al. (2005). "Improving the Performance of Organic Field Effect Transistor by Optimizing the Gate Insulator Surface", Jap. J.Appl. Phys. 44: 3721-3727.

[42] J. Veres and et al. (2003). "Synthesis, Functional Properties and Applications of Nanostructures",Adv. Funct. Mater., 13:199-204.

[43] J. Veres and et al. (2004). "Gate Insulators in Organic Field-Effect Transistors", Chem. Mater. 16: 4543-4555.

[44] C. D. Dimitrakopoulos and P. R. L. Malenfant. (2002). "Organic Thin Film Transistors for Large Area Electronics", Adv. Mater. 14: 99-117.

[45] C. D. Dimitrakopoulos and D. J. Mascaro. (2001). "Organic thin-film transistors: A review of recent advances", J. Res. & Dev. 45: 11-28.

[46] N. Karl. (2003). "Charge carrier transport in conjugate polymers". Synth. Met.133-134: 649-657.

[47] H. Sirringhaus. (2005). "Device Physics of Solution-Processed Organic Field-Effect Transistors", Adv. Mater.17: 2411-2425.

[48] C. Sundar Vikram and et al. (2004). "Basic and Applied Aspects of Single and polycrystalline Organic Transistors", Science. 303: 1644-1646.

[49] T. W. Kelley. (2003). "High Performance Organic Thin Film Transistors", Mat. Res. Soc Symp . Proc. 771: 169-179.

[50] H. Meng and et al. (2003). "Oligofluorene-Thiophene Derivatives as High Performance Semiconductors for Organic Thin Film Transistors", Chem. Mater. 15: 1778-1787.

[51 Q. Miao and et al. (2003). "Synthesis, assembly, and thin film transistors of dihydrodiazapentacene: an isostructural motif for pentacene", J. Am. Chem. Soc. 125: 10284-10287.

[52] J. G. Laquindanum and et al. (1998). "Synthesis, Morphology and Field-Effect Mobility of Anthradithiophenes", J. Am. Chem. Soc. 120: 664-672.

REFERENCES (CONTINUED)

[53] H. E. Katz and et al. (2001). "Synthetic Chemistry for Ultrapure, Processable, and High-Mobility Organic Transistor Semiconductors", Acc. Chem. Res. 34: 359-369.

[54] F. Garnier and et al. (1993). "Molecular Engineering of Organic Semiconductors: Design of Self-Assembly Properties in Conjugated Thiophene Oligomers", J. Am. Chem. Soc. 115: 8716-8721.

[55] A. Dodabalapur, L. Torsi and H. E. Katz. (1995). "Organic Transistors: Two-Dimensional Transport and Improved Electrical Characteristics", Science. 268: 270-271.

[56] H. Meng and et al. (2001). "High Field Effect Mobility Oligofluorene Derivatives with High Environmental Stability", J. Am. Chem. Soc. 123: 9214-9215.

[57] Z. Bao, A. Dodabalapur, A. Lovinger. (1996). "Soluble and processable reioregular poly (3-hexylthiophene) for thin film field-effect transistor applications with high moblity", J. Appl. Phys. Lett. 69: 4108

[58] H. Sirringhaus, N. Tessler and R. H. Friend. (1998). "Integrated Optoelectronic Devices Based on Conjugated Polymers", Science. 280: 1741-1744.

[59] H. Sirringhaus and et al. (1999). "Two-dimensional charge transport in self-organised, high-mobility conjugated polymers", Nature. 401: 685.

[60] W. Yu, H. Meng, J. Pei and W. Huang. (1998). "Tuning Redox Behavior and Emissive Wavelength of Conjugated Polymers by p-n Diblock Stuctures", J. Am. Chem. Soc. 120: 11808-11809.

[61] J. Ficker, H. von Seggern and et al. (2004). "Influence of intensive light exposure on polymer field-effect transistors", Appl. Phys. Lett. 85: 1377.

[62] H. Fuchigami, A. Tsumura and H. Koezuka. (1993). "Polythienylenevinylene Thin-Film Transistor With High Carrier Mobility", Appl. Phys. Lett. 63: 1372-1374.

[63] I. McCulloch and et al. (2006). "Liquid-crystalline semiconducting polymers with high charge-carrier mobility", Nature. Mat. 5: 328-333.

REFERENCES (CONTINUED)

[64] H. Sirringhaus and et al. (2000). "Mobility enhancement in conjugated polymer field-effect transistors through chain alignment in a liquid-crystalline phase", Appl. Phys. Lett. 77: 406.

[65] D. J. Broer, J. Lub and G. N. Mol. (1995). "Wide-band reflective polarizers from cholesteric polymer networks with a pitch gradien", Nature.378: 467-469.

[66] I. McCulloch and et al. (2003). "Polymerisable liquid crystalline organic semiconductors and their fabrication in organic field effect transistors", J. Mater. Chem. 13: 2436-2444.

[67] M. Gratzel. (2005). "Solar energy conversion by dye-sensitized photovoltaic cells", Inorg. Chem. 44: 6841-6851.

[68] D. Hagberg. (2008). "Synthesis of Organic Chromophores for Dye-Sensitized Solar Cells", Doctoral Thesis: Rutgers University, New York.

[69] M. Gratzel and et al. (2003). "Dye-sensitized solar cells", Photochem. Photobiol. C. 4 : 145-153.

[70] X. Li and et al. (2008). "A new carbazole-based phenanthrenyl ruthenium complex as sensitizer for a dye-sensitized solar cell", Inorg. Chim. Acta. 361: 2835–2840.

[71] K. Hara and et al. (2003). "Dye-sensitized nanocrystalline TiO_2 solar cells based on novel coumarin dyes", Solar Energy Mat. Sol. Cells. 77: 89–103.

[72] K. Hara and et al. (2005). "Oligothiophene-Containing Coumarin Dyes for Efficient Dye-Sensitized Solar Cells", J. Phys. Chem. B. 109: 15476-15482.

[73] S. Ito and et al. (2006). "High-Efficiency Organic-Dye- Sensitized Solar Cells Controlled by Nanocrystalline-TiO_2 Electrode Thickness", Adv. Mater. 18: 1202-1205.

[74] S. Kim and et al. (2007). "Novel conjugated organic dyes containing bis-dimethylfluorenyl amino phenyl thiophene for efficient solar cell", Tetrahedron. 63: 9206–9212.

[75] D. Kim and et al. (2007). "Molecular engineering of organic dyes containing *N*-aryl carbazole moiety for solar cell", Tetrahedron. 63: 1913–1922.

[76] E. Galoppini (2004). "Linker for anchoring to semiconductor nanoparticle", Coord. Chem. Rev. 248 : 1283-1297.

REFERENCES (CONTINUED)

[77] W. M. Capbell and et al. (2004). "Porphyrins as light harvesters in the dye-sensitised TiO_2 solar cell", Coor. Chem. Rev. 248: 1363-1379.

[78] K. Brunner, A. Van Dijken and et al. (2004). J. Am. Chem. Soc. 126: 6035–6042.

[79] J. H. Schon and et al. (2000). "Efficient organic photovoltaic diodes based on doped pentacene"Nature. 403: 408–410.

[80] U. Mitschke, P. BaE` uerle. (2000). "The electroluminescence of organic materials", J. Mater. Chem. 10: 1471–1507.

[81] V. Promarak, and et al. (2007). "Synthesis and characterization of *N*-carbazole end-capped oligofluorene-thiophenes", Tetrahedron. 63: 8881- 8890.

[82] K.-T. Wong, T. H. Hung and et al. (2001). "Synthesis and properties of novel bis (triarylamines) based on a 3,3A-diphenyl-2,2A-bithiophene core", Chem. Com. 628–1629.

[83] J. Pei and et al. (2003). "Star-Shaped Polycyclic Aromatics Based on Oligothiophene-Functionalized Truxene: Synthesis, Properties, and Facile Emissive Wavelength Tuning", J. Am. Chem. Soc. 125:9944–9945.

[84] F. Silvia and et al. (2007). "Opto-Electronic Properties of Fluorene-Based Derivatives as Precursors for Light-Emitting Diodes", J. Phys. Chem. C. 111: 5812-5820.

[85] P. C. Bevilacqua and et al. (2009). "Pyrene-cored dendrimer with carbazole derivatives as dendrons: synthesis, properties and application in white light-emitting diode", J. Phys. Chem. C. 113: 4641.

[86] K-C. Wu and et al. (2008). "High-Efficiency Deep-Blue Light-Emitting Diodes Based on Phenylquinoline/Carbazole-Based Compounds", Adv. Funct. Mater. 18: 67.

[87] J.. Bäckvall. (2010) . "Paladium-catalyzed cross couplings in organic synthesis". The Royal Swedish Academy of Sciences. 1-13.

[88] K. Maruoka and T. Oo. (2007). "Recent Advances in Asymmetric Phase-Transfer Catalysis" Angew. Chem. Int. Ed. 46; 4222 – 4266.

REFERENCES (CONTINUED)

[89] F. Liu and et al. (2009). "Solutionprocessable red-emission organic materials containing triphenylamine and benzothiodiazole units: Synthesis and applications in organic light-emitting diodes", J. Phys. Chem. C. 113: 4641.

[90] C. Tang and et al. (2006). "Synthesis and Characterization of Pyrene-Centered Starburst Oligofluorenes", J. Mater. Chem. 16: 4074.

[91] K. Brunner and et al. (2004). "Carbazole Compounds as Host Materials for Triplet Emitters in organic Light-Emitting Diodes: Tuning the HOMO Level without Influencing the Triplet Energy in Small Molecules", J. Am.Chem. Soc. 126: 6035–6042.

[92] V. Promarak and et al. (2008). "Thermally and electrochemically stable amorphous hole transporting materials based on carbazole dendrimers for electroluminescent devices", Thin Sol. Films. 516; 2881-2888.

[93] U. Mitschke, P. BaE` uerle. (2000). "The electroluminescence of organic materials", J. Mater. Chem. 10: 1471-1507.

[94] H. E. Katz, Z. Bae and S. L. Gilat. (2001). "Synthetic Chemistry for Ultrapure, Processable, and High-Mobility Organic Transistor Semiconductors", Acc. Chem. Res. 34: 359–369.

[95] M. Mazzeo and et al. (2003). "Bright oligothiophene-based light emitting diodes", Synth. Met. 139: 671–673.

[96] V. Promarak, and et al. (2007). "Synthesis, optical, electrochemical, and thermal properties of α,α'-bis(9,9-bis-n-hexylfluorenyl)-substituted oligothiophenes", Tetrahedron. 63: 8881- 8890.

[97] A. Galal and et al. (1994). Proc. Electrochem. Soc. "Development of the methotrexate-nanogold complex for cancer therapeutics in animal models", 90-2. 179.

[98] Md. K. Nazeeruddin and et al. (1993). "conversion of light to electricity by cis-X2bis-(2,2'-bipyridyl-4,4'-dicarboxylate) ruthenium(II) charge-transfer sensitizers (X = Cl-, Br-, I-, CN-, and SCN-) on nanocrystalline TiO2 electrodes", J. Am. Chem. Soc. 155: 6382-6390.

REFERENCES (CONTINUED)

[99] Z. S. Wang and et al. (2000). "Photoelectric conversion properties of nanocrystalline TiO_2 electrodes sensitized with hemicyanine derivatives", J. Phys Chem. B. 104: 9676-9682.

[100] M. Tsuyoshi and et al. (2010). "Synthesis and Properties of 1,8-Carbazole-Based Conjugated Copolymers", Polymers. 2: 159-173.

[101] Z. Huaqiang and et al. (2010). "Selective Tuning of the HOMO–LUMO Gap of Carbazole-Based Donor–Acceptor–Donor Compounds toward Different Emission Colors", Eur. J. Org. Chem. 1681–1687.

[102] M. Lequan and et al. (1992). "Synthesis of Organic Chromophores for Dye Sensitized Solar Cells", Adv. Mater. Opt. Electron. 1: 243-248.

[103] K. Hara and et al. (2003). "Design of new coumarin dyes having thiophene moieties for highly efficient organic-dye-sensitized solar cell", J. Chem. 27: 783-785.

[104] Md. K. Nazeeruddin and et al. (1999). "Acid-base equilibria of (2,2'-bipyridyl-4,4'-dicarboxylic acid)ruthenium (II)complexes and the effect of protonation of charge-transfer sensitization off nanocrystalline titania", Inorg. Chem. 38 : 6298-6305.

[105] I. Tsutomu and K. Hiroyuki (2005) "*E*- or *Z*-Selective Knoevenagel Condensation of Acetoacetic Derivatives: Effect of Acylated Substituent, that is, TEMPO and Amines, as an Auxiliary, and New Accesses to Trisubstituted *E*- and *Z*-2-Alkenals and Furans", J. Org.Chem. 71; 947-953.

[106] J. Kenyon and W. A. Ross. (1951). "The mechanism of the decarboxylation of substituted malonic acid derivatives". J. Chem. Soc. 3407-3411.

[107] N. Sekar and V. Y. Gehlot. (2010). "Metal Complex Dyes for Dye-Sensitized Solar Cells: Recent Developments", Resonance. 819-831.

[108] R. Chen and et al. (2007). "Effect of Tetrahydroquinoline Dyes Structure on the Performance of Organic Dye-Sensitized Solar Cells", Chem. Mate. 19: 4007- 4015.

[109] V. Promarak and et al. (2006). "synthesis and properties of stable amorphous hole-transporting molecules for electroluminescent devices", Tetrahedron Lett. 47: 8949- 8952.

REFERENCES (CONTINUED)

[110] V. Promarak and et al. (2007). "Synthesis of electrochemically and thermally stable amorphous hole-transporting carbazole dendronized fluorene", Synth. Met. 157: 17–22.

[111] P. I. Shih and et al. (2006). "Novel Carbazole/Fluorene Hybrids: Host Materials for Blue Phosphorescent OLEDs", Org. Lett. 8: 2799- 2802.

[112] V. Promarak and et al. (2007). "Synthesis and characterization of *N*-carbazole end-capped oligofluorenes", Tetrahedron Lett. 48: 89- 93.

[113] V. Promarak, and et al. (2007). "Synthesis and characterization of *N*-carbazole end-capped oligofluorene-thiophenes", Tetrahedron. 63: 8881- 8890.

[114] T. P. I. Saragi and et al. (2004). "Organic phototransistor based on intramolecular charge transfer in a bifunctional spiro compound", J. Appl. Phys. Lett. 84: 2334.

[115] C. Ego and et al. (2002). "Triphenylamine- Substituted Polyfluorene- A Stable Blue-Emitter with Improved Charge Injection for Light-Emitting Diodes", Adv Mater. 14: 809.

[116] S. L. Tao and et al. (2005). "Efficient blue and white organic light-emitting devices based on a single bipolar emitter" Adv. Funct. Mater. 15: 1716- 1721.

[117] Z.H. Li and et al. (2006). "Synthesis and Light-Emitting Properties of Bipolar Oligofluorenes Containing Triarylamine and 1,2,4-Triazole Moieties", Org. Lett. 8: 4271- 4274.

[118] F. Freeman. (1969). "The Chemistry of Malononitrile", Chem.Rev. 69: 591- 624.

[119] M. Lapkowski and et al. (2006). "Electrochemical study of 1,3-indandione derivatives of terthiophenes", e-Polymers. 111: 1618- 7229.

[120] J. Chan and et al. (2000). "Morphology of electrodeposited WO_3 stuided by atomic force microscopy", J. Mater. Chem.10: 55.

[121] T. J. Chow and et al. (2005). "Photoinduced electron transfer across linearly fused oligo-norbornyl structures", Tetrahedron. 61 :6967.

[122] J. C. Yuan and J. C. Tahsin. (2009). "Dye-sensitized solar cell utilizing organic dyards containing triaryamine conjugates" Tetrahedron. 65: 4726-4734.

S2-P47

Synthesis and Characterization of Luminescence Materials Based on Pyrene-Oligothiophenes

Janeeya Khunchalee, Taweesak Sudyoadsuk, Tinagon Keawin, Sayant Saengsuwan, Narid Prachumrak and Vinich Promarak

Advance Organic Materials and Devices Laboratory, Department of Chemistry and Center for Innovation in Chemistry, Faculty of Science, Ubon Ratchathani University, Warinchumrap, Ubon Ratchathani 34190, Thailand.

Objective

To synthesize a series of novel luminescence organic materials based on pyrene-oligothiophenes with the thiophene unit up to 4 for use as emissive layers in organic light-emitting diodes (OLEDs).

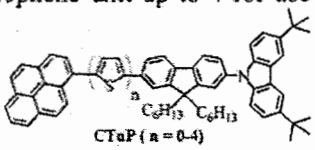

CTnP (n = 0-4)

Methods

7-Bromo-9,9-dihexyl-*9H*-fluorenyl-3,6-di-tert-butyl-*9H*-carbazole was synthesized by using Ullmann coupling reaction between 2,7-dibromo-9,9-dihexyl-*9H*-fluorene and 3,6-di-tert-butyl carbazole in the presence of CuI as catalyst, potassium phosphate as base and (±)-*trans*-1,2-diaminocyclohexane as co-catalyst in toluene at 170°C. Suzuki cross-coupling reaction of 2-thiophenboronic acid and the corresponding bromo-compound with $Pd(PPh_3)_4$ as catalyst in the presence of aqueous sodium carbonate solution in THF at reflux was employed to increase the number of thiophene units in the molecules. Finally, the final products **CTnP (n = 0-4)** were obtained by using Suzuki cross-coupling reaction of pyrene boronic acid and bromo-compounds.

Results

Pyrene-oligothiophenes were synthesized by using Suzuki cross-coupling reaction of pyrene boronic acid and the corresponding bromo-compounds to give **CTnP (n = 0-4)** in 10%, 11%, 72%, 37%, and 70% yields, respectively. The absorption and emission spectra of target molecules showed red shift depending on the number of thiophene units within molecules. The solid state emission is largely red shift from the solution state. Pyrene-oligothiophenes exhibited the blue to orange emission. DSC measurements revealed that **CTP**, **CT1P** and **CT2P** form amorphous while **CT3P** and **CT4P** usually form semi-crystalline with T_g increasing as the number of thiophene units increase. The CV curves of target molecules demonstrated two reversible oxidations and no distinct reduction process was observed in each case. The increased thiophene unit results in a decrease of the potentials of the first oxidations process. The fluorescence quantum yields (Φ_F) of the fluorescence oligomers **CTnP (n = 0-4)** in dilute CH_2Cl_2 solution range from 0.84 to 0.078 and decrease as the conjugation in molecule increase. The OLED devices using these materials as emissive layers will be discussed.

Conclusion

A series of novel pyrene-oligothiophenes were synthesized. Their electronic properties are variable depending on a number of thiophene units. They have good electrochemical stability and thermal stability. The OLED devices using **CTnP (n = 0-4)** as emissive layers were fabricated.

Keywords: OLED, oligothiophene, thiophene

Selected References:

1. Promarak, V.; *et al. Tetrahedron Lett.* **2007**, *48*, 1151-1154.
2. Promarak, V.; *et al. Tetrahedron Lett.* **2007**, *48*, 89-93.

* Ph.D. Student

Synthesis and Chacterization of Luminascence Materials Based on Pyrene-Oligothiophene

Janeeya Khunchalee, Taweesak Sudyoadsuk, Tinagon Keawin, Sayan Saengsuwan, Narid Prachumrak and Vinich Promarak

Advance Organic Materials and Devices Laboratory, Department of Chemistry and Center of Excellence for Innovation in Chemistry, Faculty of Science, Ubonratchatani University, Warinchumrap, Ubon Ratchatani, 34190, Thailand

Introduction

Oligothiophenes have some very investigating electronic and optical properties and have been lately investigation as advanced molecular optoelectronic materials. Advantages of oligothiophenes include cheap precursers, high thermal and photochemical stabilities. In this work, a series of novel pyrene-oligothiophene derivatives with the thiophene unit up to 4 for use as emissive layers in organic light-emitting diodes (OLED).

Result and Discussion

Synthesis and Characterization : Ullman coupling reaction, Suzuki coupling reaction and Bromination

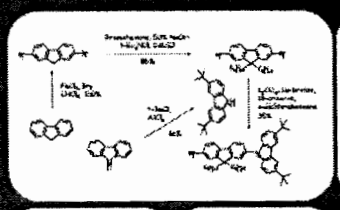

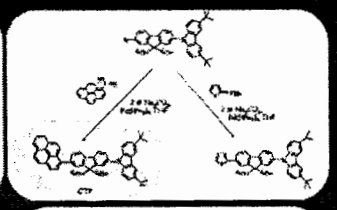

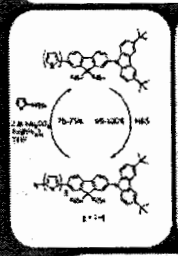

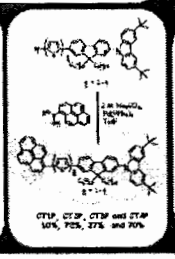

Computer Calculation : TDDFT/B3LYP

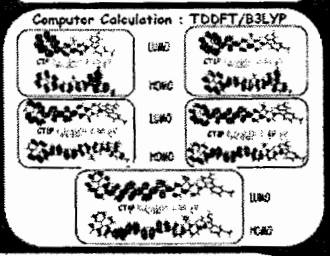

Optical Properties : UV-Vis, PL and EL

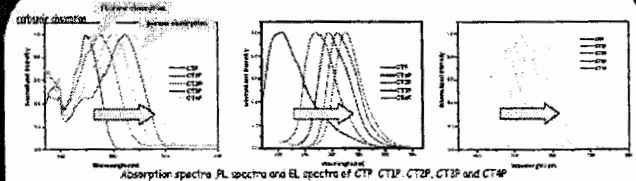

Absorption spectra PL spectra and EL spectra of CTP, CT1P, CT2P, CT3P and CT4P

Table : Summery of OLED device performance

[illegible]	[illegible]	[illegible]	[illegible]	[illegible]	[illegible]	[illegible]	[illegible]	[illegible]
CTP	[illegible]	[illegible]	[illegible]	[illegible]	[illegible]	[illegible]	[illegible]	[illegible]
CT1P	[illegible]	[illegible]	[illegible]	[illegible]	[illegible]	[illegible]	[illegible]	[illegible]
CT2P	[illegible]	[illegible]	[illegible]	[illegible]	[illegible]	[illegible]	[illegible]	[illegible]
CT3P	[illegible]	[illegible]	[illegible]	[illegible]	[illegible]	[illegible]	[illegible]	[illegible]
CT4P	[illegible]	[illegible]	[illegible]	[illegible]	[illegible]	[illegible]	[illegible]	[illegible]

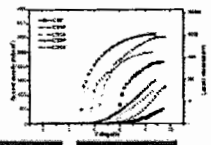

Optical Properties : CV using Glassy carbon working electrode, Pt counterelectrode, SCN reference electrode, DCM solution, n-Bu_4NPF_6 electrolyte, Scan rate 50 mV/s

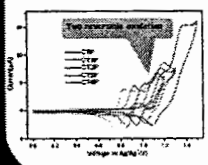

[illegible]	[illegible]	[illegible]	[illegible]	[illegible]
CTP	[illegible]	[illegible]	[illegible]	[illegible]
CT1P	[illegible]	[illegible]	[illegible]	[illegible]
CT2P	[illegible]	[illegible]	[illegible]	[illegible]
CT3P	[illegible]	[illegible]	[illegible]	[illegible]
CT4P	[illegible]	[illegible]	[illegible]	[illegible]

Thermal Properties : DSC and TGA measurements

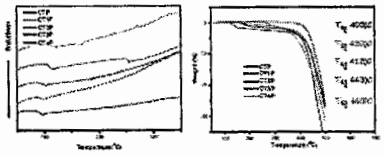

DSC (2nd scan) and TGA Curves; under N_2 at heating rate of 10°C/min

Conclusion

A series of novel pyrene-oligothiophene were synthesized by using Suzuki cross-coupling reaction of pyrene boronic acid and corresponding bromo-compounds to give CTnP (n=0-4). Their electronic properties are variable depending on a number of thiophene units. The presence of thiophene unit decreases the fluorescence quantum yield. pyrene-oligothiophene derivatives have good electrochemical stability and thermal stability. The OLED devices using CTnP (n=0-4) as emissive layers were fabricated.

Reference

V. Promarak, A. Pankvuang ans S. Ruchirawat. Tetrahedrol Lett. 2007. 48, 7, 1151-1154.

V. Promarak, S. saengsuwan, S. Jungsuttiwong, T. Sudyoadsuk and T. Keawin. Tetrahedrol Lett. 2007. 48, 89-93.

Ackowledgements

This work was supported by PERCH-CIC

Abstracts

34th Congress
on Science and Technology of Thailand (STT 34)

SCIENCE AND TECHNOLOGY FOR GLOBAL CHALLENGES

• To Celebrate the 60th Anniversary of the Science Society of Thailand under the Patronage of His Majesty the King

• To Celebrate the 20th Anniversary of Faculty of Science, King Mongkut's Institute of Technology Ladkrabang

October 31 – November 2, 2008
Venue: Queen Sirikit National Convention Center
Bangkok, Thailand

Organized by :
The Science Society of Thailand under the Patronage of His Majesty the King
In association with Faculty of Science, King Mongkut's Institute of Technology Ladkrabang, Bangkok, Thailand

Supported by the National Research Council of Thailand

C3_C0184 SYNTHESIS AND CHARACTERIZATION OF A NOVEL *N*-CARBAZOLE END-CAPPED OLIGOFLUORENE-THIOPHENE DERIVATIVES AS COLOUR TURNABLE LIGHT-EMITTING MATTERIALS FOR OLEDs

Janeeya Khunchalee, Taweesak Sudyoadsuk, Tinnagon Keawin, Siriporn Jungsuttiwong and Vinich Promarak
Advanced Organic Materials and Devices Laboratory, Department of Chemistry, Faculty of Science, Ubon Ratchathani University, Warinchumrap, Ubon Ratchathani, 34190;
e-mail: janeeyainjumpa@hotmail.com

Abstract: In this work, to develop a series of novel organic materials based on *N*-carbazole end-capped oligofluorene-thiophene derivatives as color tunable light-emitting for OLEDs. *N*-carbazole end-capped oligofluorene-thiophene derivatives was synthesized by Ullmann coupling reaction, Suzuki cross coupling reaction, bromination and the final products were synthesized by using palladium catalyzed cross-coupling reaction of 2,5-dithiopheneboronic acid and the corresponding bromo-compounds afforded **CFTn** (n = 1, 3, 5, 7 and 9) or nickel catalyzed reductive dimerization of corresponding bromo-compounds in the present of triphenylphosphine, bipyridyl and zinc power as co-catalyst in DMAc as solvent afforded **CFTn** (n = 2, 4, 6 and 8). The **CFTn** (n = 1-9) were characterized by ^{1}H, ^{13}C NMR, FTIR, UV-Vis and fluorescence spectroscopy. Thermal properties were studied by DSC and TGA. Electrochemical properties were measured using three electrode system cyclic voltammetry.

VITAE

NAME	Miss Janeeya Khunchalee
BORN	2 November 1976, Ubonratchathani, Thailand
EDUCATION	1996-1999,
	Bachelor of Science Chemistry,
	Ubon Ratchathani University
	2000-2003,
	Master of Science Chemistry,
	Kasetsart University
SCHOLARSHIPS	Research Prize from Center for Innovation
	in Chemistry: Postgraduate Education
	and Research Program in Chemistry
	(PERCH-CIC), 2007